COMPONENT BASED SEISMIC VULNERABILITY ASSESSMENT
PROCEDURE FOR RC BUILDINGS

A THESIS SUBMITTED TO
THE GRADUATE SCHOOL OF NATURAL AND APPLIED SCIENCES
OF
MIDDLE EAST TECHNICAL UNIVERSITY

BY

EMRAH ERDURAN

IN PARTIAL FULFILLMENT OF THE REQUIREMENTS
FOR
THE DEGREE OF DOCTOR OF PHILOSOPHY
IN
CIVIL ENGINEERING

JULY 2005

Approval of the Graduate School of Natural and Applied Sciences

_____
Prof. Dr. Canan ÖZGEN
Director

I certify that this thesis satisfies all the requirements as a thesis for the degree of Doctor of Philosophy.

_____
Prof. Dr. Erdal ÇOKÇA
Head of Department

This is to certify that we have read this thesis and that in our opinion it is fully adequate, in scope and quality, as a thesis for the degree of Doctor of Philosophy.

_____
Assoc. Prof. Dr. Ahmet Yakut
Supervisor

Prof. Dr. Polat Gülkan	(METU,CE)	_____
Assoc. Prof. Dr. Ahmet Yakut	(METU,CE)	_____
Prof. Dr. Güney Özcebe	(METU,CE)	_____
Asst. Prof. Dr. Murat Altuğ Erberik	(METU,CE)	_____
Asst. Prof. Dr. Burcu Güneş	(Atılım University, CE)	_____

I hereby declare that all information in this document has been obtained and presented in accordance with academic rules and ethical conduct. I also declare that, as required by these rules and conduct, I have fully cited and referenced all material and results that are not original to this work.

Name, Last name : Emrah Erduran

Signature   :

ABSTRACT

COMPONENT BASED SEISMIC VULNERABILITY ASSESSMENT PROCEDURE FOR RC BUILDINGS

Emrah Erduran

Ph.D., Department of Civil Engineering

Supervisor: Assoc. Prof. Dr. Ahmet Yakut

July 2005, 207 pages

A detailed seismic performance assessment procedure has been developed for reinforced concrete frame buildings with masonry in-fill walls and reinforced concrete frames including shear walls. The procedure uses member damage functions, in terms of inter-story drift ratios, developed for the primary components: columns, beams, in-fill walls and shear walls. Analytical investigations carried out to determine the influence of a number of parameters on the damageability of components were combined with existing experimental data to develop component damage functions. A new approach has been developed to combine component damage states to determine the story and building level performance states. The procedure has been calibrated and compared with other procedures by predicting the observed performance of seven buildings exposed to recent earthquakes in Turkey. It was observed that the damage experienced by most of the components of these buildings was predicted satisfactorily, and that the observed building damage states were captured. The procedure can be used for a reliable performance assessment as well as performance-based design of the RC frame structures.

Keywords: reinforced concrete, vulnerability, damage curves, damage index

ÖZ

BETONARME BİNALAR İÇİN ELEMAN BAZLI SİSMİK
DEĞERLENDİRME YÖNTEMİ

Emrah Erduran

Doktora, İnşaat Mühendisliği Bölümü

Tez Yöneticisi: Doç. Dr. Ahmet Yakut

Temmuz 2005, 207 Sayfa

Tuğla dolgulu betonarme çerçeveler ve perde duvarlı çerçeve sistemleri için detaylı bir sismik değerlendirme yöntemi geliştirilmiştir. Bu yöntem, kolon, kiriş, tuğla dolgu ve betonarme perde duvarlar için geliştirilmiş olan hasar fonksiyonlarını kullanmaktadır. Her bir eleman tipinin davranışlarını etkileyen parametrelerin belirlenmesi için yürütülen analitik çalışmaların sonuçları mevcut deneysel verilerle birleştirilmiş ve her bir eleman tipi için hasar fonksiyonları oluşturulmuştur. Eleman hasar değerlerinin birleştirilerek kat ve bina düzeyinde hasar değerleri elde edilebilmesi için yeni bir yöntem geliştirilmiştir. Geliştirilen sismik değerlendirme yöntem Türkiye'de son zamanlarda meydana gelmiş çeşitli depremlerde hasar görmüş binalar üzerinde uygulanmış ve yöntemin güvenilirliği test edilmiştir. Bu analizler sonucunda elemanlarda gözlenen hasarlarla önerilen hasar eğrilerinin öngördüğü hasarlarının büyük çoğunluğunun uyumlu olduğu ve genel bina davranışının da büyük ölçüde tutturulabildiği görülmüştür. Geliştirilmiş olan yöntem mevcut binaların sismik performanslarının değerlendirilmesinin yanı sıra yeni binaların performansa dayalı tasarım ilkeleri ile tasarımında da kullanılabilir.

Anahtar Kelimeler: Betonarme, hasar görebilirlik, hasar eğrileri, hasar indeksi

to my mother…

for dedicating your life to me…

ACKNOWLEDGMENT

This study was carried out under the supervision of Assoc. Prof. Dr. Ahmet Yakut. I gratefully appreciate his guidance, criticism, support, encouragement and friendship throughout this study.

I want to thank Prof. Dr. Güney Özcebe and Asst. Prof. Dr. Burcu Güney for their invaluable suggestions that improved the quality of this dissertation.

My home mate Musa Yilmaz helped me a lot during this study with his understanding and patience in our house life. Thank you very much being such a patient home mate.

My dear friends Dr. Arda Şorman and Dr. Aynur Şensoy Şorman were always with me when I was exhausted and upset. I thank you for being alongside with me throughout these years. You were the ones who guided me throughout the difficulties of life in the last couple of years.

My beloved Özgü... Thank you for your love and peace you had given me in the most stressful and difficult period of this study. It is a privilege for me to walk alongside with you. I wish you will always be nearby with the light, peace and love in your eyes.

My deepest thanks and love go to my family for their endless love, support and encouragement throughout my whole life.

TABLE OF CONTENTS

LIST OF FIGURES

LIST OF TABLES

CHAPTER 1

INTRODUCTION

1.1 GENERAL

In the last fifteen years, Turkey has lost tens of thousands of its citizens and huge amounts of economic properties in moderate and severe earthquakes. Moreover, most of the population and industry of Turkey is under the threat of a possible major earthquake since they are located in earthquake prone regions. The current seismic code of Turkey [1] was rewritten in 1998 to enable the satisfactory performance of the structures and thus to reduce loss after a major earthquake. However, a vast majority of the structures in Turkey had been constructed before the adaptation of the 1998 Turkish Earthquake Code [1]. Moreover, new structures are not generally designed and/or constructed according to the provisions of this code resulting in a huge number of deficient structures. As a result the engineers in Turkey, like most of their colleagues in the world, are faced with a critical question which must be answered immediately: Which buildings are safe and which must be strengthened or even demolished?

For decades researchers have been studying on developing seismic vulnerability assessment procedures to overcome this problem. These vulnerability assessment procedures can be categorized in three according to the level of complexity they contain. The first level of seismic assessment procedures is known as the walk-down survey or street survey and is the quickest and simplest way of ranking the buildings in a building stock relative to each other based on their certain attributes. The typical parameters used in this type of assessment procedures are the number of stories, the age of the building, vertical

and plan irregularities, location of the building and the apparent material and workmanship quality. The procedures of FEMA 154 [2] and FEMA 310 Tier 1 [3] and the one developed by Sucuoğlu and Yazgan [4] fall into this category.

Preliminary assessment techniques are employed when a more detailed assessment than the walk-down survey is needed. The preliminary assessment procedures generally require data on the dimensions of the structural components and material properties in addition to the data that had been collected for the walk-down survey procedures. In general, the capacity of the system is computed by some approximate means and it is compared with the demand to decide whether the building is safe or not. The well-known preliminary assessment procedure is the FEMA 310 Tier 2 [3] procedure. The procedures developed by Özcebe et. al. [5], Yücemen et. al. [6] and Yakut [7] are also some examples of the preliminary assessment procedures developed mainly for the reinforced concrete structures in Turkey.

The last type of the assessment procedures is the detailed vulnerability assessment procedures which require the detailed analysis of the building. The additional information needed for the detailed vulnerability assessment procedures generally include the as-built dimensions and the reinforcement details of the structural components and mechanical properties of the materials. These procedures require the linear or non-linear analysis of the building to determine the response quantities which are compared with the prescribed values to assess the performance of the components and/or building. Detailed vulnerability assessment procedures are either forced based [8, 9, 10] or displacement based [8, 9, 11, 12]. The displacement based detailed vulnerability assessment procedures will be discussed briefly in the following paragraphs.

The displacement based detailed assessment procedures summarized in the following paragraphs had been calibrated for the buildings which reflect the construction practice in the developed countries which has considerable differences from the practice in Turkey. The observed earthquake damage in Turkey during past earthquakes generally arose from certain problems in the construction such as:

- Improper configuration of structural and architectural system

- Inadequate detailing
- Poor material and construction quality

These problems are generally not that severe in the developed countries; hence they might not be reflected in these displacement procedures. Based on this fact, research had been undertaken to develop a displacement based vulnerability assessment procedure that mainly aims to predict the behavior of the buildings both in Turkey and the other countries.

1.2 PREVIOUS STUDIES

The general tendency in most of the assessment procedures is to determine an index that reflects vulnerability or damageability of the structure. In their State–of–the-Art review Williams and Sexsmith [13] grouped the damage indices as global and local. The local damage indices [11, 14, 15, 16] are defined for individual elements, whereas global damage indices are given for the entire structure. The global damage indices were further classified into two as weighted average damage indices [11, 16] and the damage indices based on the variation of the modal parameters due to damage [17, 18]. In the following paragraphs, the well known and most widely used local and weighted average damage indices will be summarized briefly.

1.2.1 Park & Ang Damage [11] Index

Park & Ang [11] damage index is the best-known and most widely used local damage index and weighted average global damage index. The local damage index is defined as:

$$D = \frac{\delta_m}{\delta_u} + \beta_e \frac{\int dE}{F_y \delta_u} \tag{1.1}$$

The first term in Eq. 1.1 is the ratio of the maximum attained deformation to the ultimate deformation capacity of the member under static loading (δ_u). The second term accounts for the effect of the dissipated hysteretic energy on the accumulated damage. The term $\int dE$ is the total hysteretic energy absorbed by the element of interest; F_y is the calculated yield strength and β_e is a coefficient

3

for cyclic loading effect. Williams and Sexsmith [13] states that the advantages of this model are its simplicity and the fact that it has been calibrated against a significant amount of observed seismic damage including some instances of shear and bond failures. Park, Ang and Wen [19] suggested the following classification for the thresholds between damage states:

D<0.1   No damage or localized minor cracking

0.1≤D<0.25   Minor damage – light cracking throughout

0.25≤D<0.40   Moderate damage – severe cracking, localized spalling

0.40≤D<1.00   Severe damage – crushing of concrete

D≥1.00   Collapsed

This model can also be used to assess the damage of the entire building. The global damage index was defined as the weighted average of the damage indices of all the elements (Eq. 1.2), where the weighing coefficient of an element is equal to the ratio of the energy absorbed by that element to the sum of the energy absorbed by all of the elements (Eq. 1.3).

$$D_T = \sum \lambda_i D_i \qquad\qquad (1.2)$$

$$\lambda_i = \frac{E_i}{\sum E_i} \qquad\qquad (1.3)$$

Eqs. 1.2 and 1.3 can also be used to compute the damage index of each story of the building. However, this index has certain drawbacks. The major drawback of this index is that both the component damage and the component weighing coefficient are proportional to the energy dissipated by that component which results in a direct relationship between the damage score and the weighing coefficient of the component. In other words, the elements that suffer more damage turn out to be more important in the seismic behavior of the building. This may lead to misleading results if the damage distribution in the building is non-uniform since the building damage level may be governed by a single heavily damaged component.

1.2.2   ATC-40 [9] & FEMA-356 [8]

The guidelines for the assessment of existing structures published by the Applied Technology Council (ATC-40 [9]) and the Federal Emergency

Management Agency (FEMA-356 [8]) have similar detailed vulnerability assessment procedures. These procedures are similar in the sense that they propose plastic rotation limits for the three limit states, namely Immediate Occupancy (IO), Life Safety (LS) and Collapse Prevention (CP) (Structural Stability, SS, in case of ATC-40). The maximum plastic rotation attained by a member under the given ground motion is compared with these plastic rotation limits and the performance of that member under that earthquake is assessed. The plastic rotation limits differ according to the type, predominant failure mode and ductility level of the member. For flexure controlled beams, different plastic rotation limits are proposed for different combinations of amount of longitudinal reinforcement, shear force and transverse reinforcement amount. For columns, the axial load level is used to determine the ductility level of the member instead of the amount of longitudinal reinforcement. The plastic rotation limits for beams and columns proposed in ATC-40 [9] and FEMA-356 [8] are given in Tables 1.1 to 1.4.

Table 1.1 – ATC-40 plastic hinge rotation limits for reinforced concrete beams

$\dfrac{\rho - \rho'}{\rho_{bal}}$	Trans. Rein.	$\dfrac{V}{b_w d \sqrt{f_c{}'}}$	IO (Immediate Occupancy)	LS (Life Safety)	SS (Structural Stability)
≤0.0	C (Conforming)	≤0.25	0.005	0.02	0.025
≤0.0	C	≥0.50	0.005	0.01	0.02
≥0.5	C	≤0.25	0.005	0.01	0.02
≥0.5	C	≥0.50	0.005	0.005	0.015
≤0.0	NC (Non-Conforming)	≤0.25	0.005	0.01	0.02
≤0.0	NC	≥0.50	0.000	0.005	0.01
≥0.5	NC	≤0.25	0.005	0.01	0.01
≥0.5	NC	≥0.50	0.000	0.005	0.005

Table 1.2 - ATC-40 plastic hinge rotation limits for reinforced concrete columns

$\dfrac{P}{A.f_c{}'}$	Trans. Rein.	$\dfrac{V}{b_w d\sqrt{f_c{}'}}$	IO (Immediate Occupancy)	LS (Life Safety)	SS (Structural Stability)
≤0.1	C (Conforming)	≤0.25	0.005	0.01	0.02
≤0.1	C	≥0.50	0.005	0.01	0.015
≥0.4	C	≤0.25	0.0	0.005	0.015
≥0.4	C	≥0.50	0.000	0.005	0.01
≤0.1	NC (Non-Conforming)	≤0.25	0.005	0.005	0.01
≤0.1	NC	≥0.50	0.005	0.005	0.005
≥0.4	NC	≤0.25	0.000	0.0	0.005
≥0.4	NC	≥0.50	0.000	0.0	0.0

Table 1.3 – FEMA-356 plastic hinge rotation limits for reinforced concrete beams

$\dfrac{\rho - \rho'}{\rho_{bal}}$	Trans. Rein.	$\dfrac{V}{b_w d\sqrt{f_c{}'}}$	IO (Immediate Occupancy)	LS (Life Safety)	CP (Collapse Prevention)
≤0.0	C (Conforming)	≤0.25	0.010	0.02	0.025
≤0.0	C	≥0.50	0.005	0.01	0.02
≥0.5	C	≤0.25	0.005	0.01	0.02
≥0.5	C	≥0.50	0.005	0.005	0.015
≤0.0	NC (Non-Conforming)	≤0.25	0.005	0.01	0.02
≤0.0	NC	≥0.50	0.0015	0.005	0.01
≥0.5	NC	≤0.25	0.005	0.01	0.01
≥0.5	NC	≥0.50	0.0015	0.005	0.005

Table 1.4 - FEMA-356 plastic hinge rotation limits for reinforced concrete columns

$\dfrac{P}{A.f_c{'}}$	Trans. Rein.	$\dfrac{V}{b_w d \sqrt{f_c{'}}}$	IO (Immediate Occupancy)	LS (Life Safety)	SS (Collapse Prevention)
≤0.1	C (Conforming)	≤0.25	0.005	0.015	0.02
≤0.1	C	≥0.50	0.005	0.012	0.016
≥0.4	C	≤0.25	0.003	0.012	0.015
≥0.4	C	≥0.50	0.003	0.01	0.012
≤0.1	NC (Non-Conforming)	≤0.25	0.005	0.005	0.006
≤0.1	NC	≥0.50	0.005	0.005	0.005
≥0.4	NC	≤0.25	0.002	0.002	0.003
≥0.4	NC	≥0.50	0.002	0.002	0.002

1.2.3   EUROCODE 8 [12]

Eurocode 8 [12] defines three limit states similar to the ATC-40 [9] and FEMA-356 [8] documents. These limit states are Damage Limitation (DL), Significant Damage (SD) and Near Collapse (NC). It can be stated that these limit states roughly correspond to the Immediate Occupancy, Life Safety and Collapse Prevention limit states of ATC-40 [9] and FEMA-356 [8], respectively.

In Eurocode 8 [12], it is stated that the assessment of the buildings may be carried out using one of the following procedures: Linear lateral force analysis, linear multi-modal response spectrum analysis, non-linear static analysis and non-linear time history analysis. Of these methods, the non-linear methods will be summarized here since the procedure developed in this study also utilizes non-linear procedures.

Eurocode 8 [12] proposes a displacement based assessment procedure for flexure critical members, whereas a force based procedure is imposed for shear critical members.

The damage levels of all of the flexure critical members were assessed according to the chord rotation values that the member undergoes at the performance point of the building under the given ground motion. The chord

rotation values obtained from the structural analysis were compared with the capacities for each limit state defined in the Eurocode 8 [12].

For the damage limitation limit state, the chord rotation capacity is given by the chord rotation at yielding, θ_y (Eq. 1.4)

$$\theta_y = \phi_y \frac{L_v}{3} + \alpha_{el} + \alpha_{sl} \frac{0.2\varepsilon_{sy}d_b f_y}{(d-d')\sqrt{f_c}} \tag{1.4}$$

In this equation the first two terms account for the flexural and shear contributions, respectively and the third for anchorage slip of bars. In the first term, φ_y is the curvature at yielding obtained from the section analysis, L_v is the shear span (=M/V) which can be taken to be equal to the half of the length of the member. In the document, it is stated that α_{el} can be taken as 0.00275 for beams and columns and 0.0025 for rectangular walls. In the third term, d and d' are the depth of the tension and compression reinforcement, respectively and f_y and f_c are the estimated values of the steel tensile and concrete compressive strength, respectively. α_{sl} is a variable that is associated with the slip condition of the longitudinal reinforcement. If it is known that slip occurs in the longitudinal reinforcement, α_{sl} is taken as 1. Otherwise it is taken to be equal to 0.

If the chord rotation of a member remains below the chord rotation capacity at the yield computed using Eq. 1.4, then the damage limit state of this member is computed to be damage limitation (DL) (immediate occupancy (IO) according to ATC-40 [9] and FEMA-356 [8]).

The chord rotation capacity for the near collapse (NC) damage state was taken as the ultimate chord rotation capacity of the member computed according to Eq. 1.5:

$$\theta_u = \theta_y + (\phi_u - \phi_y)L_{pl}\left(1 - \frac{0.5L_{pl}}{L_v}\right) \tag{1.5}$$

In this equation θ_y is the yield chord rotation computed according to Eq. 1.4, φ_u and φ_y are the curvature at ultimate and yield, L_{pl} is the plastic hinge length, which can be taken as the half of the depth of the member. In the original document an alternative formulation for the computation of the ultimate rotation

which is based on the work by Panagiotakos and Fardis [20] is given. This formulation is summarized in section 2.4.5 of this study.

According to Eurocode 8 [12], the chord rotation related to the severe damage state can be assumed as the 75% of the ultimate chord rotation θ_u given in Eq. 1.5.

For the shear critical members, the limit states of severe damage (SD) and damage limitation (DL) is not required to be checked. The only limit state that needs to be checked is the near collapse (NC) limit state. To check the exceedance of this limit state, the maximum shear force attained by a member is compared with the shear capacity of the member computed according to Eq.1.6:

$$V_R = \frac{h-x}{2L_v}\min(N, 0.55A_c f_c) + 0.16\left(1 - 0.055\min\left(5, \mu_\Delta^{pl}\right)\right)$$

$$\left[\max(0.5, 100\rho_{tot})\left(1 - 0.16\min\left(\frac{L_v}{h}, 5\right)\right)\sqrt{f_c}\, A_c + V_w\right] \tag{1.6}$$

where h: depth of cross-section (equal to the diameter D for circular sections); x: compression zone depth; N: compressive axial force (positive, taken as being zero for tension); L_v: shear span; A_c: cross-section area, taken as $b_w d$ for a web of thickness b_w and depth, d; μ_Δ^{pl} is the displacement ductility ratio, ρ_{tot}: total longitudinal reinforcement ratio, V_w contribution of transverse reinforcement to shear resistance which can be computed using Eq. 1.7 for rectangular members:

$$V_w = \rho_w b_w z f_{yw} \tag{1.7}$$

ρ_w is the transverse reinforcement ratio, z is the internal lever arm (taken as being equal to d-d′ in beam-columns, or to 0.75h in walls) and f_{yw} is the yield stress of the transverse reinforcement.

1.3 OBJECT AND SCOPE OF THE STUDY

Reinforced concrete structures are amongst the most widely used construction types in Turkey as well as elsewhere in the world. Although the seismic codes of the countries are revised or rewritten to enable the satisfactory performance of reinforced concrete structures, there are still a huge number of seismically deficient structures throughout the world which are not conforming

to these codes. Identifying deficient structures is of critical importance for both reliable loss estimation in case of a possible major future earthquake and setting priority criterion for strengthening of these structures.

The main objective of this study is to develop a detailed displacement based vulnerability assessment procedure for reinforced concrete building type structures. The methodology developed herein is mainly based on the estimation of the damage level of the components of the assessed structure resulting from a given ground motion. For this purpose, damage functions were developed for each component type that contributes to the lateral load resisting capacity of the structures. Columns, beams, masonry infills and shear walls are the components that were considered in this study. The main damage inducing parameters were chosen as the inter-story drift ratio for the column, brick infills and shear walls and the chord rotation for the beams, which are believed to be strongly correlated with the damage observed during earthquakes. The component damage scores are then combined to compute story and finally building damage scores. According to the classification by Williams and Sexsmith [13], this procedure can be classified as a weighted average global index type.

In addition to assessing the building performance, the developed procedure can also be used for performance based design of reinforced concrete buildings.

1.4 OUTLINE OF THE PROCEDURE

1.4.1 General

The procedure developed within the scope of this study is a detailed vulnerability assessment procedure carried out for a single building under a given ground motion or design spectrum. The assessment procedure is a weighted average global index type which depends on the computation of the damage scores for each member in the structure and taking the weighted average of these member damage scores to compute the story and building damage scores. The performance of the building under the given ground motion is

determined based on the story and building damage scores. This part is devoted to summarize the general outline of the procedure.

1.4.2 General Outline of the Developed Procedure

Figure 1.1 schematically summarizes the outline of the developed procedure. The steps involved in this procedure are explained in detail next.

Step 1. Data Collection: The developed methodology requires the nonlinear analysis, either static or dynamic, of the given building. For this, as required in most detailed assessment procedures, some data must be collected about the building at hand. This data includes the design drawings, as-built dimensions of the building, the condition of the building, the material properties preferably obtained from in-situ tests and the reinforcement detailing of the members.

Step 2. Nonlinear Analysis and the Determination of the Member End Deformations: The computer model developed may be a two dimensional or a three dimensional model based on the choice of the user. Similarly, the user chooses the type of the nonlinear analysis (nonlinear static analysis or nonlinear time history analysis) that will be used. If a nonlinear static analysis is carried out, the capacity curve obtained as a result of this analysis must be used to determine the performance point of the building under the prescribed ground motion or design spectrum using the procedures available in literature such as the Capacity Spectrum Method summarized in ATC-40 [9], the Displacement Coefficient Method of FEMA-356 [8] or the Constant Ductility Spectrum Method [21]. The member end deformations at this performance point will be recorded and used in the forthcoming steps. If a nonlinear time history analysis is carried out, then the maximum member end deformations will be recorded.
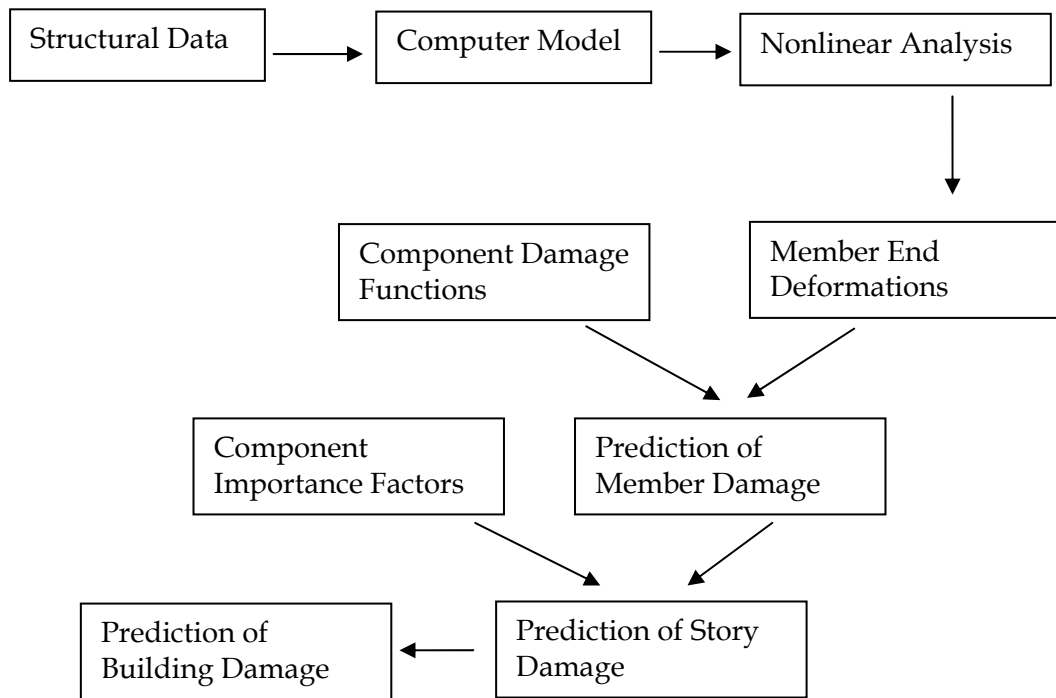
Figure 1.1 – Flowchart of the Developed Procedure

Step 3. Determination of the Member Damage Scores: The maximum member end deformations obtained as a result of the nonlinear analysis will be used in the damage functions developed to compute the damage score of each member.

Step 4. Determination of the Story and Building Damage Scores: Once the damage score for each member is determined, then the weighted average of these damage scores is computed to determine the damage score of each story and finally the entire building. The weighing coefficients used here depend on the contribution of each member in resisting the seismic forces and named as *component importance factors*. Approximate values for the component importance factors were developed for both brick infilled reinforced concrete frame structures

and reinforced concrete wall-frame structures and are given in the sixth chapter of this dissertation.

The final step of the procedure is the determination of the performance of the building based on the computed building damage score.

The first two steps of this procedure are familiar to the engineers, hence these parts will not be elaborated in this dissertation and the last two steps will be discussed in the forthcoming chapters.

1.5 OUTLINE OF THE THESIS

The structure of this dissertation closely follows the order in which the work was undertaken in response to the aims as they were initially conceived. It consists of seven further chapters.

Chapter 2 summarizes the work undertaken to develop drift based damage functions for reinforced concrete columns. The results of the parametric studies and the most significant parameters that were found to affect the behavior of reinforced concrete columns were discussed. The developed damage functions are summarized and their validity is tested through the application to the column test data available in the literature.

In the third chapter, the development of the damage functions for the reinforced concrete beams is discussed. The damage curves of the reinforced concrete beams are defined in terms of the chord rotation. This chapter mainly follows the organization of the previous one.

Chapter 4 describes the drift based damage curves for brick infills. In the development of these curves equivalent strut models for brick infills were studied and used. The damage curves for brick infills were also calibrated using the test results available.

Chapter 5 is devoted to discuss the damage curves developed for shear walls. As in the case of chapters 2 and 3, this chapter starts with the discussion of the numerical studies carried out and the significant parameters that influence the behavior of the shear walls. The developed damage curves are then reviewed and these curves were validated via the application of them to the available test results.

Chapter 6 describes the methodology to develop component importance factors which enables the combination of the component damage scores to determine the story level and building level damage scores. This methodology uses the energy dissipation capacity of the undamaged and damaged frames to determine the relative importance of each component. Approximate values developed for the component importance factors of brick infilled reinforced concrete frames and wall-frame systems were also discussed.

In the seventh chapter, the application of the developed procedure on seven case study buildings which were damaged in the recent earthquakes occurred in Turkey is discussed. The component, story and building level damage scores predicted by the developed procedure were compared with the observed damage states to calibrate and validate the procedure developed herein. The application of the procedure to the 10 buildings located in the Zeytinburnu district of Istanbul was also discussed at the end of this chapter.

Finally, Chapter 8 summarizes the work done within the scope of this dissertation and discusses the conclusions drawn from the work carried out. It also addresses the recommendations for the similar works that are intended to be done in the future.

CHAPTER 2

DRIFT BASED DAMAGE FUNCTIONS FOR COLUMNS

2.1 GENERAL

Of the structural components of reinforced concrete structures, columns are amongst the most important ones as far as seismic behavior and vulnerability is concerned. Thus, predicting the damage level of columns is of great importance in predicting the damage level of the overall structure. This chapter summarizes the studies carried out to develop drift based damage curves for reinforced concrete columns.

2.2 A BRIEF REVIEW OF THE EXPERIMENTAL BEHAVIOR AND PREVIOUS RESEARCH

The deformation capacity of reinforced concrete columns is affected by various parameters including axial load level, confinement, and concrete strength; this has been investigated both experimentally and numerically in the past.

Numerous studies carried out on the deformation capacity of columns dealt with two important terms: the yield displacement and ultimate ductility of the columns. In 1992 Azizinamini et. al. [22] tested 12 reinforced concrete columns to investigate the effects of transverse reinforcement on the seismic performance of the columns. At the end of these tests, it was observed that for a constant amount of confinement, flexural capacity of a column increase with axial load, but displacement ductility was reduced substantially.

In their work, Priestly and Kowalsky [23] aimed to develop dimensionless yield, serviceability and damage control curvatures for structural walls and

columns; they proved that all of the three curvature limit states were largely independent of amount and distribution of longitudinal reinforcement.

Paulay [24] stated that the amount of reinforcement used in a section and the gravity induced axial compression do not affect the nominal yield curvature in a significant way. The two important terms affecting column yield displacements are the yield strain of the longitudinal reinforcement (ε_y) and the slenderness ratio of the column. The yield displacement is essentially independent of the strength of the section.

Although the conclusions drawn are useful for better understanding of the behavior of the reinforced concrete columns, most of them were qualitative. In this study, the aim is to develop damage functions for reinforced concrete columns based on the drift ratio, defined as the ratio of the difference between the displacements of the two ends of the column to the column height. These damage functions take all the related parameters into account quantitatively. The results of many experimental studies of reinforced concrete columns were compiled in a database [25] that presents observed damage and the corresponding level of measured drift ratio. Although, the observed damage states were expressed verbally referring to various types of concrete failure such as spalling and crushing, the explicit definitions of damage states were not given. To develop consistent and reliable damage-drift relations, a number of finite element analyses were carried out for reinforced concrete columns and the results of these analyses were used together with the experimental data.

2.3   METHOD OF ANALYSIS

The behavior of reinforced concrete columns are affected by various parameters. The damage functions developed should take the effect of all these parameters into account quantitatively. Thus, as the first step, the effect of these parameters, namely concrete strength (f_{ck}), axial load level (N/N_o), slenderness of the column (L/i; L is the length of the column and i is the radius of gyration in the direction of loading), amount of longitudinal reinforcement (ρ), yield strength of longitudinal reinforcement (f_y), amount of transverse reinforcement (ρ_s), was

investigated by carrying out several finite element analyses. In the numerical analyses carried out, the finite element software ANSYS was used.

The first step of these numerical analyses was the verification of the finite element model used. For this purpose, a column which was tested previously by Azizinamini et. al. [22] was modeled first. Upon verifying that the finite element model used represents the actual behavior adequately, the effects of the pre-mentioned parameters on the damageability of reinforced concrete columns were investigated. When a database of sufficient size was obtained, least-squares curve fitting technique was used to develop the drift based damage functions taking the effect of all the significant parameters into account.

2.4   FLEXURE CRITICAL COLUMNS

2.4.1   Numerical Analyses

In the finite element analyses, 8 node brick elements were used to model the reinforced concrete. The element used can take the cracking and crushing of concrete into account. The longitudinal reinforcement was modeled as smeared throughout the section. In their work, Barbosa and Ribeiro [26] stated that, the difference between modeling the longitudinal reinforcement as discrete or smeared has no significant effect in the nonlinear analyses of reinforced concrete members.

In order to take the confinement into account, Modified Kent and Park model [27] was used to model the stress-strain relationship of concrete used. Figure 2.1 shows a schematic sketch of the finite element model of a column.

All the capacity curves were obtained by carrying out pushover analyses, which is a one-way static procedure. Thus, the problems which rise during cyclic loading such as bond and lap splice problems could not be taken into account in these analyses. Hence, it was assumed that the detailing of the longitudinal reinforcement was properly done so that no significant bond and/or lap splice problems occur.

17
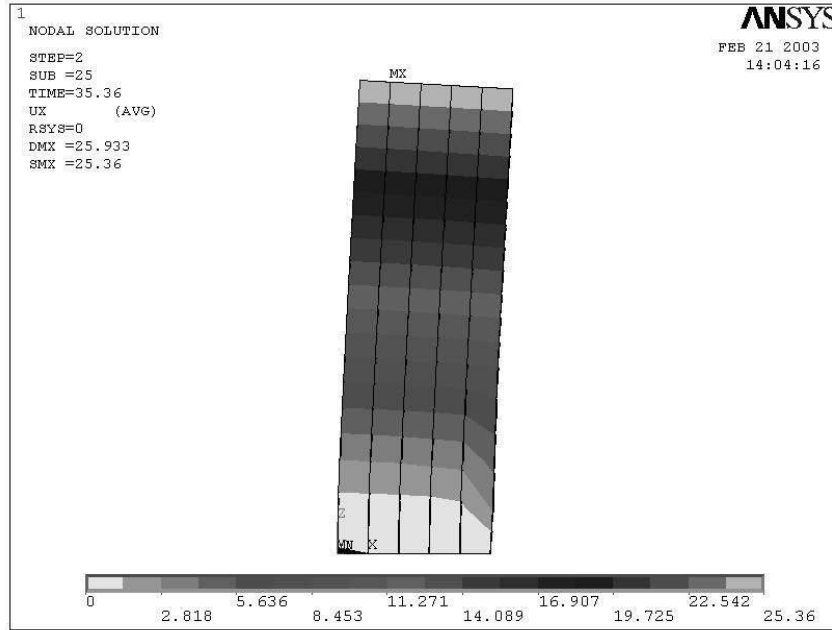
Figure 2.1 – Schematic Sketch of the Finite Element Model

2.4.2 Verification of the Finite Element Model used

To validate the finite element model used, a column tested by Azizinamini et. al. [22] was modeled and analyzed. Hereafter, this column will be referred as the *reference column*. The cross-section of the column was 457 mm by 457 mm and characteristic concrete strength was 39.3 MPa. The half height of the column, i. e. the distance from the point of inflection to the base of the column was 1372 mm. The axial load level on the column (N/N_o) was 20%. The properties of the reference column are shown in Figure 2.2.

A displacement-controlled nonlinear static analysis was performed by applying incremental displacements at the tip of the column. The load was then calculated in each step.

Figure 2.3 presents the experimental and numerical load-displacement curves of the reference column. The numerical and experimental results match fairly well up to a displacement level of 30 mm. When the displacement level exceeds 30 mm, the numerical model overestimates the lateral load capacity of the column. The main reason for this is the difference in the types of loading of the

18

experiment and numerical simulation. The numerical capacity curve was obtained through a pushover analysis, which is a one-way static procedure. On the other hand, the experimental curve was obtained under cyclic loading. Since, the numerical model can not take the strength degradation due to cyclic loading into account; it overestimates the strength of the member beyond a certain drift level.

Transverse Reinforcement:
ϕ12 / 102 mm (fywk=454 MPa)

$N/N_0=0.20$

P

330

457

330

457

All dimensions are in mm

1372 mm

Longitudinal Reinforcement:
8 ϕ25.4 mm (fy=439 MPa)
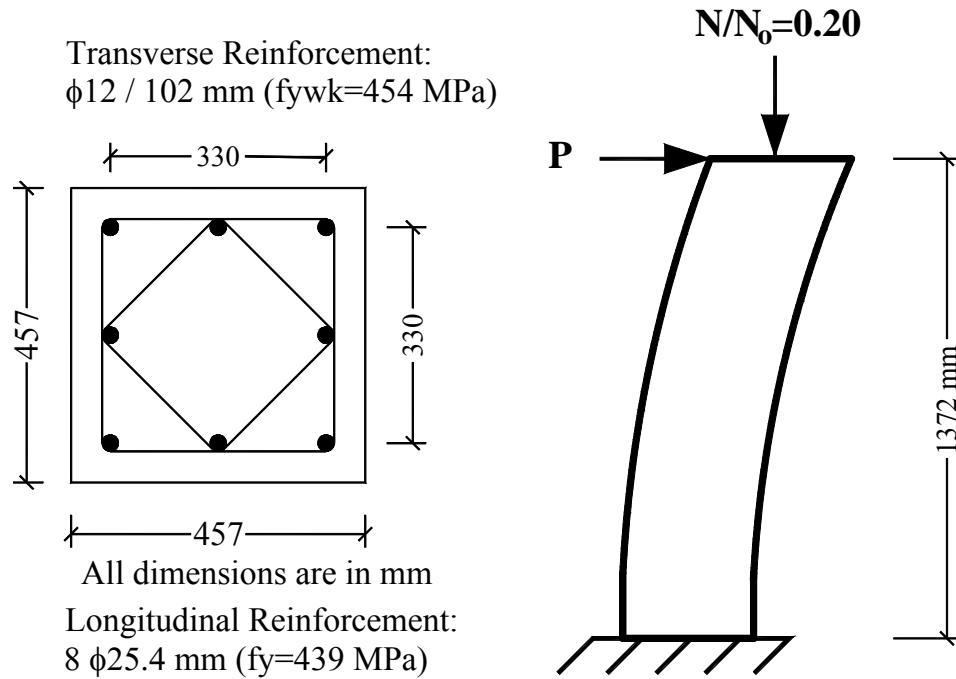
Figure 2.2 Properties of the Reference Column

2.4.3   Parametric Studies

Once the finite element model used was proven to reflect the actual response of the reinforced concrete member accurately, further analyses were carried out to see the effect of the parameters on the capacity curve of the columns. In each analysis, only one parameter of the reference column was changed and the others were kept constant. The range of the parameters used in the analyses is summarized in Table 2.1.
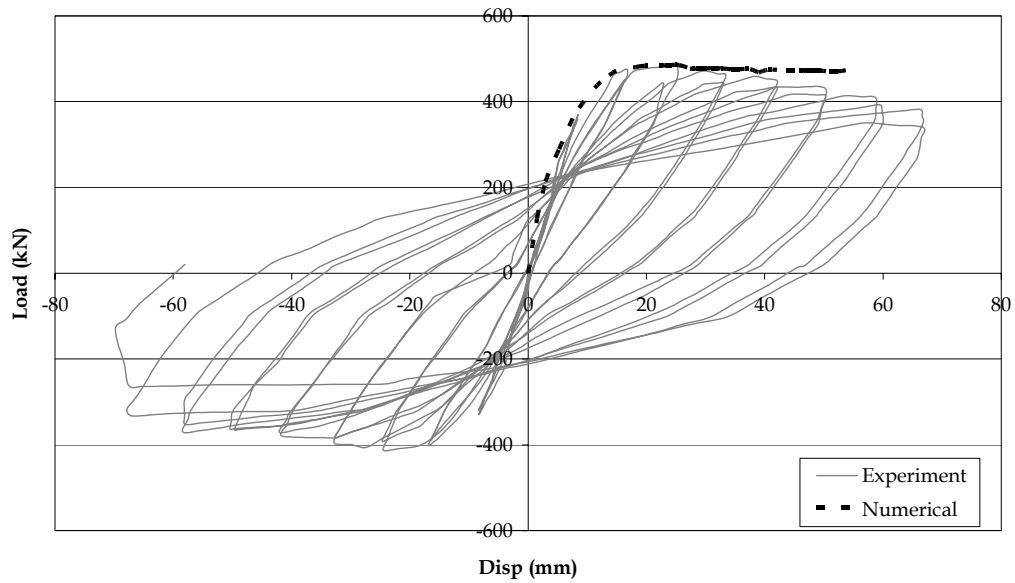
Figure 2.3 – Experimental and Numerical Load-Deflection Behavior of the
Reference Column

Table 2.1 – Range of Parameters used

| f_{ck} (MPa) | N/N_o | Longitudinal Reinforcement | | Transverse Reinforcement | | L/i |
		ρ	f_y (MPa)	ρ_s	f_{ywk} (MPa)	
10	0.1	0.0075	220	0.01	454	12.7
14	0.2	0.0100	300	0.02		15.9
16	0.3	0.0195	375	0.03		21.1
20	0.4	0.0300	439	0.04		24.4
25	0.5	0.0400	525			28.6
39.3	0.6		600			32.3
						37.0

The damage criterion used in this study mainly depends on drift levels. Basically four damage levels were defined in terms of the drift corresponding to the maximum load carrying capacity of the column, which is the point that the slope of the capacity curve becomes 0.0 or the point where the slope of the capacity curve changes significantly. In all of the analyses carried out in this study, the post-elastic slope was nearly 0.0. Although this point is slightly

different than the yield point, it will be referred to as the yield drift ratio, (δ_y). The other major term used to investigate the damageability of reinforced concrete columns is the ultimate ductility of the member, defined as the ratio of the ultimate drift ratio to the yield drift ratio. The ultimate drift ratio was taken as the point where the lateral load capacity of a column decreases by 15%. The damage criterion will be discussed in detail in section 2.4.4.2.

The effect of each parameter on the damageability of reinforced concrete columns will be discussed according to their influence on the yield drift and the ultimate ductility of columns.

2.4.3.1   Effect of Concrete Strength, fc_k

In order to investigate the effect of concrete strength on the deformation capacities of reinforced concrete columns, six pushover analyses were carried out for concrete strengths of 10, 14, 16, 20, 25, and 39.3 MPa. The capacity curves obtained from these analyses (Figure 2.4) indicate that, although the lateral load capacity of the columns increase significantly with increasing concrete strength, the yield drift ratio (δ_y) is not significantly affected by the variations in f_{ck}. Moreover, as long as the axial load level and confinement are kept constant, ultimate ductility of the columns is also not affected by the concrete strength significantly. Recalling that the damage criterion used mainly depends on the yield drift ratio and ultimate ductility, it can be stated that the concrete strength has no significant effect on the damage level of the reinforced concrete columns provided that all other parameters are constant. Although, the maximum f_{ck} value used in the analyses was 39.3 MPa, and no analyses were carried out for higher strengths, it is assumed that the trend observed in the analyses carried out may be generalized for higher f_{ck} values.

2.4.3.2   Axial Load Level, N/N_o

Six analyses were carried out to see the effect of the axial load level on the behavior of columns. In these analyses N/N_o varied between 10% and 60%. Figure 2.5 shows that, although the yield drift ratio was almost constant for different axial load levels, the ultimate ductility decreases significantly with the

increasing axial load level. This indicates that columns with high axial load level do not show ductile behavior and hence may experience high damage beyond yield drift ratio.

2.4.3.3   *Slenderness Ratio, L/i*

The slenderness ratio of the column is defined as the ratio of the length of the column (L) to the radius of gyration (i). Seven analyses were carried out to see the effect of slenderness ratio on the damageability of columns. The slenderness ratio of the reference column was 21.122. In Figure 2.6 it can be observed that the yield drift ratio increases with increasing slenderness ratio indicating that slender columns suffer less damage for a given drift level. The slenderness ratio has no significant effect on the ultimate ductility of the columns.
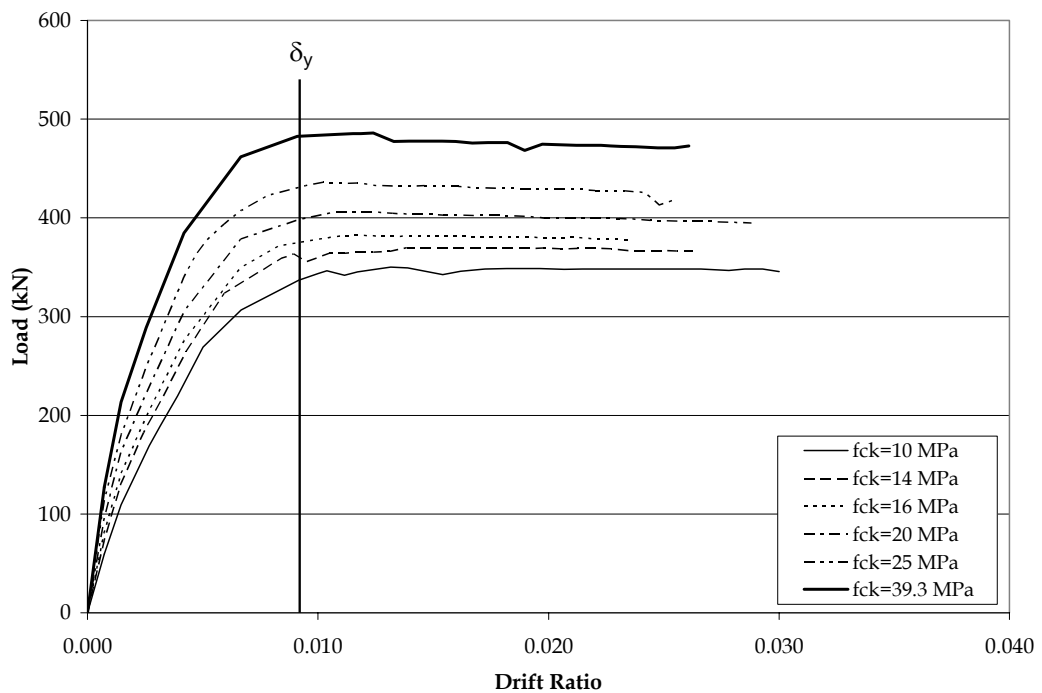
Figure 2.4 – Effect of Concrete Strength on Capacity Curves

2.4.3.4   *Amount of Longitudinal Reinforcement,(ρ)*

The pushover analyses carried out for five different ρ values (ranging from 0.75% to 4%) indicate that (Figure 2.7) the amount of longitudinal reinforcement has no significant effect on either yield drift ratio or ultimate ductility of the columns. Thus, based on the damage criterion explained before, it can be stated that amount of longitudinal reinforcement do not have significant effect on the drift - damage relationship of reinforced concrete columns.
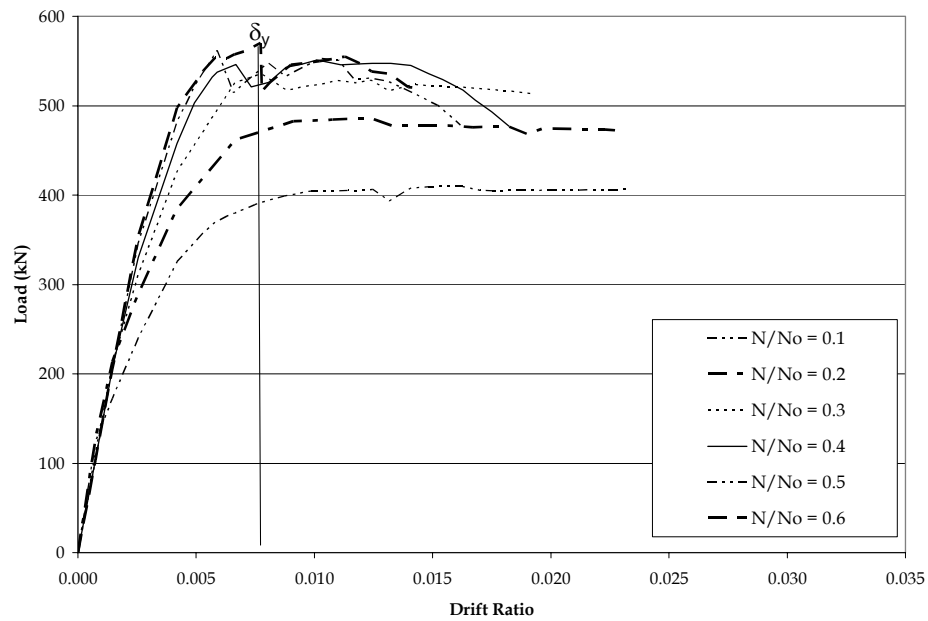
Figure 2.5 – Effect of Axial Load Level on Capacity Curves
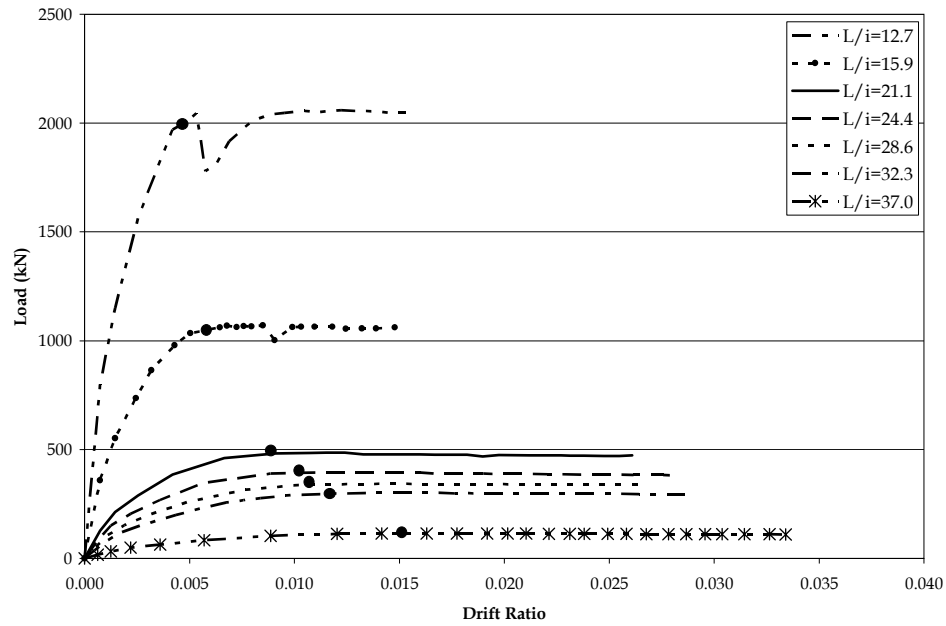
Figure 2.6 - Effect of Slenderness Ratio on Capacity Curves

2.4.3.5 Yield Strength of Longitudinal Reinforcement (f_y)

The results of the analyses carried out for different steel grades show that the yield drift ratio increases with increasing f_y (Figure 2.8). Thus, the damage level of the reinforced concrete columns is significantly affected by the variation in the yield strength of the longitudinal reinforcement.

2.4.3.6 Amount of Transverse Reinforcement, ρ_s

The capacity curves obtained for four different ρ_s values, ranging from 1% to 4%, indicate that (Figure 2.9) the ultimate ductility increases significantly with increasing ρ_s value, whereas the amount of transverse reinforcement has no significant effect on the yield drift ratio, δ_y.
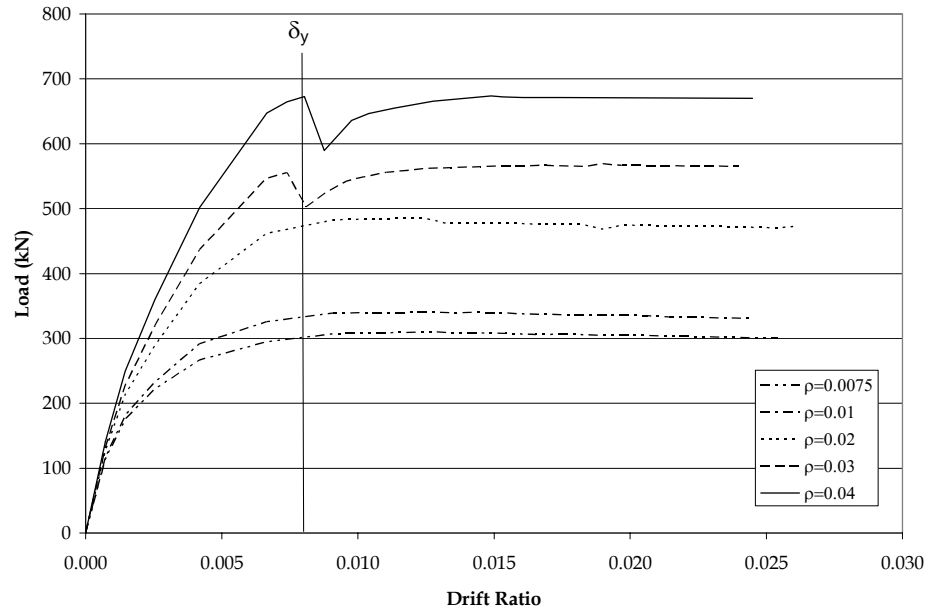
Figure 2.7 – Effect of Amount of Longitudinal Reinforcement on

Capacity Curves

2.4.4   Development of Damage Curves

After the investigation of the effect of different parameters on the damageability of reinforced concrete columns was completed and a database of sufficient size was formed, the damage curves were developed. For this purpose, firstly the significant parameters and the way they will affect the damage curves were determined. Then, the damage criterion was defined and the certain damage scores were assigned to certain drift levels for all of the columns. As the last step least – squares curve fitting technique was used to develop the drift based damage functions for reinforced concrete columns.
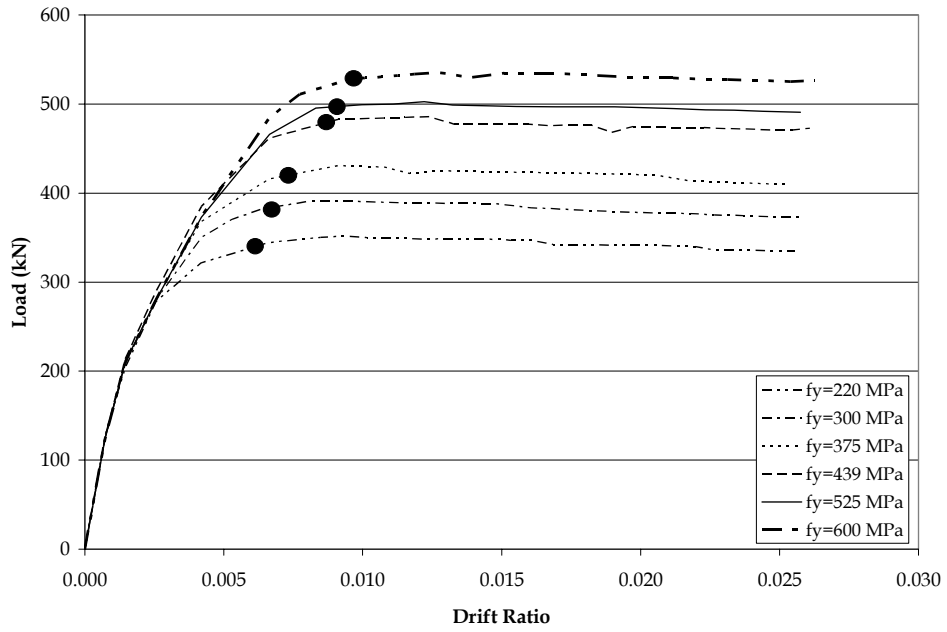
Figure 2.8 – Effect of Yield Strength on Longitudinal Reinforcement on
Capacity Curves
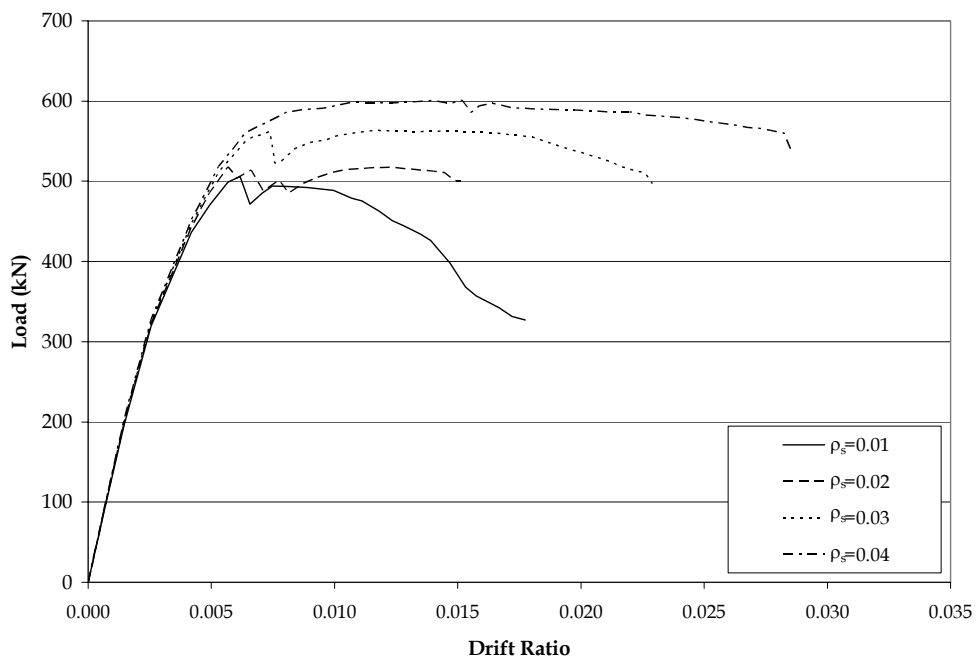
Figure 2.9 – Effect of Amount of Transverse Reinforcement on Capacity
Curves

2.4.4.1 Significant Parameters

The parametric study carried out revealed that the most important parameters that affect the deformation limits of columns are the yield strength of longitudinal reinforcement (f_y), slenderness ratio (L/i), amount of transverse reinforcement (ρ_s) and the axial load level (N/N_o), whereas concrete strength (f_{ck}) and amount of longitudinal reinforcement (ρ) were determined to be insignificant parameters. Of the significant parameters, the first two, i.e. f_y and slenderness ratio affect the yield drift ratio significantly. On the other hand the axial load level and amount of transverse reinforcement have significant effects on the ultimate ductility of columns. If Figures 2.5 and 2.9 are examined carefully, it will be observed that axial load level and amount of transverse reinforcement have similar effect on the deformation capacities of the columns. Increase (or decrease) in the amount of transverse reinforcement and decrease (or increase) in the axial load level has the same effect on the capacity curves (lateral load versus tip displacement) of the reinforced concrete columns. In light of this discussion, a new term, which is defined as the ratio of amount of longitudinal reinforcement to the axial load level ($\rho_s/(N/N_o)$) is introduced. This term is believed to represent the ductility level of the columns satisfactorily. In order to take the effect of amount of transverse reinforcement and axial load level into account, the columns were divided into three groups according to their ductility. The columns with a $\rho_s/(N/N_o)$ value less than 5% are considered to be of low ductility. The columns with moderate ductility have a $\rho_s/(N/N_o)$ value between 5% and 10%. If the $\rho_s/(N/N_o)$ value of a column exceeds 10%, then this column is considered to have high ductility. Based on this discussion, three different damage curves were developed; one curve for each ductility level.

Since the other two parameters, the yield strength of the longitudinal reinforcement (f_{yk}) and slenderness ratio (L/i) affect directly the yield drift ratio, which is the major parameter in the damage criterion used herein; these two parameters will affect the damage level of the columns at every stage. In the damage curves, the effects of these two parameters were not reflected; instead adjustments were applied to the calculated drift ratio by the introduction of correction factors, which will be discussed in detail later on.

2.4.4.2 *Damage Criterion*

The damage criterion used for columns in this study mainly depends on the ductility index (ratio of given drift ratio to the yield drift ratio), hence on the yield drift ratio. Basically four damage states were defined: Negligible, light, moderate, and heavy. The first three damage states, i.e negligible, light and moderate, were expressed quantitatively and related to the crack width as summarized in Table 2.2. Heavy damage, on the other hand, was assigned a damage score of 90% (upper limit) and was determined from the test results since crack width is not a proper criterion for the detection of heavy damage.

In order to establish the ductility indices for negligible to moderate levels of damage, four columns under low axial load level ($N/N_o=0.1$) were analyzed. These four columns had the same sectional and material properties except the amount of longitudinal reinforcement (ρ). When the axial load level is low, the behavior is close to pure flexural behavior and the main parameter that determines the damage level is the amount of longitudinal reinforcement. The volumetric longitudinal reinforcement ratios for these columns varied from 1% to 4%. The other parameters were the same as those of the reference column. In the case of high axial load level, the cracks observed on the column surface may be closed. However, if the axial load level is low, this closure will be minimal and insignificant. Therefore, the crack width may be a good indicator of damage for columns under low axial load level.

Table 2.2 – Damage Scores

Crack Width (mm)	Damage Score suggested by Japanese [28]	Damage Score used in this Study	Damage States
0.2<	0.00-0.01*	0.005	Negligible
0.2-1.0	0.05-0.10	0.075	Light
1.0-2.0	0.10-0.50	0.300	Moderate

* this value was modified form the original value of 5%

The damage score for a crack width of 0.2 mm was originally 5% and it was modified to 1%. This modification was done to be able to obtain a damage score of 0.00 for very low drift ratio values, which could not be possible when a

damage score of 5% was assigned as the upper limit of the negligible damage state.

In the literature, there are various relationships for the calculation of the crack widths. Almost all of these relationships are based on the tensile strain in the tension steel and the arrangement of longitudinal reinforcement. In this study, the crack width formula proposed by Frosch [29] was used. According to Frosch the maximum crack width can be calculated by the relationship given in Eq. 2.1.

$$w = 2\varepsilon_s d^*$$
(2.1)

In this equation w is the maximum crack width, ε_s is the strain in tensile reinforcement and d^* is the controlling cover distance given in Eq. 2.2.

$$d^* = \sqrt{d_c^2 + (\frac{s}{2})^2}$$
(2.2)

where d_c is the clear cover and s is the spacing between two longitudinal bars. In the analyses a constant value of 100 mm was used for the controlling over distance in order to eliminate the effect of variations in the reinforcement arrangement.

Based on Equations 2.1 and 2.2, the crack widths for each displacement level for all of the four columns were determined. Then, damage scores to different levels of crack widths were assigned. In assigning these scores, the criterion used by the Japanese Government was used [28]. In Japanese approach, the range of damage scores presented in Table 2.2 for different crack widths were recommended; of these scores, the average values were used in damage calculations. After the assignment of the damage scores, the ductility indices corresponding to these damage levels were determined for each of the four columns analyzed under low axial load (Table 2.3). If the values given in Table 2.3 were examined carefully, it will be noted that the variation of ductility indices for the corresponding crack widths is insignificant for different longitudinal reinforcement ratios. Therefore, the average values of the ductility indices for the assigned damage levels were used. In the light of the above discussion, the ductility indices corresponding to 0.5%, 7.5%, 30% damage levels were

determined as 0.2, 0.6 and 1.0, respectively. In the development of the damage curves, these ductility indices were used instead of the crack width to locate the drift ratio – damage data points for all axial load levels.

The ductility index corresponding to the heavy damage level was determined using the hysteretic load-displacement curves of the columns tested under cyclic loading. This is mainly due to the fact that the capacity curves obtained from the pushover analysis may overestimate the ultimate ductility of the columns since the pushover analysis can not take strength degradation due to cyclic loading into account. To determine the ultimate ductility (defined as the ultimate drift ratio divided by the yield drift ratio) of the columns, the test data of 32 reinforced concrete columns obtained from the NISTIR report [25] was used. The data for these columns are given in Appendix A. The ultimate drift ratio is defined as the drift ratio where the lateral load capacity of the column decreases by 15%.

Table 2.3 – Ductility Indices for Columns under an

Axial Load of N/N_o=0.1

		Ductility Level		
Specimen	ρ	w=0.2 mm	w=1.0 mm	w=2.0 mm
SP-8	0.0195	0.189	0.564	0.949
SP-69	0.010	0.166	0.576	0.933
SP-70	0.030	0.262	0.703	1.079
SP-71	0.040	0.213	0.620	0.918
AVERAGE		**0.208**	**0.616**	**0.970**

As mentioned before, the axial load level and the amount of transverse reinforcement significantly affect the ultimate ductility of a column. To take these two parameters into account, the columns with a wide range of $\rho_s/(N/N_o)$ value were selected. In Figure 2.10 the ultimate ductility indices for corresponding $\rho_s/(N/N_o)$ values were plotted. A curve was fitted to develop a relationship between $\rho_s/(N/N_o)$ and ultimate ductility index (μ_u) by using least squares approach (Equation 2.3).

$$\mu_u = 0.6 \ln\left[\left(\frac{\rho_s}{N/N_o}\right)^2\right] + 7.25 \qquad (2.3)$$

After the relationship between μ_u and $\rho_s/(N/N_o)$ was developed, the ratio of observed (μ_{u_obs}) and predicted (μ_{u_ult}) ultimate ductility index was calculated for each of the 32 columns. The mean value for $\mu_{u\_obs}/\ \mu_{u\_ult}$ ratio was calculated to be 0.95 and the coefficient of variation was 19%. The high variation is mainly due to the fact that the columns were tested by different researchers and under different loading histories and the ultimate ductility is significantly affected by the variations in the loading history.
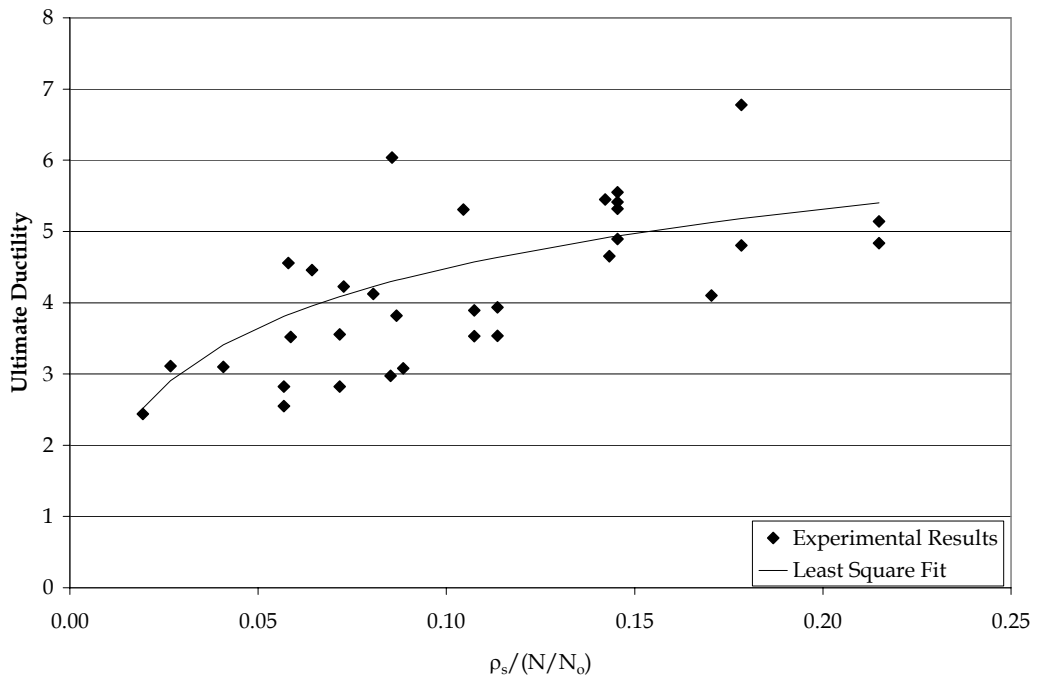
Figure 2.10 – Variation of Ultimate Ductility with $\rho_s/(N/N_o)$

The damage level corresponding to the ultimate ductility index was chosen as the upper limit of heavy damage and assigned a damage score of 90% as mentioned earlier.

2.4.4.3 Damage Curves

After the parametric study was completed and the damage criterion was established, damage curves for three different ductility levels were obtained. First of all, the columns were grouped according to their ductility levels. Then, the capacity curves for all of the seventy-one columns were analyzed and the drift ratios corresponding to the negligible (0.5%), light (7.5%), and moderate (30%) damage levels were calculated using the yield drift ratio and the ductility indices for the corresponding damage levels. Then, the ultimate ductility index for each column was computed using Equation 2.3 and the $\rho_s/(N/N_o)$ of the column and the drift ratio corresponding to the heavy damage level of each column was computed by multiplying the ultimate ductility index by the yield drift ratio. So a damage database involving seventy-one columns was formed. Then, these damage scores and corresponding drift ratios were plotted. It must be noted that, in these plots the columns with yield strength of longitudinal reinforcement and slenderness ratio different than those of the reference column were excluded. In other words, f_y of every column was 439 MPa and the slenderness ratio of all the columns was 21.1. The effect of these two parameters were included later by the introduction of correction factors which will be discussed in detail in section 2.5.1

When the damage score – drift ratio plots (Figure 2.11) were examined, it was observed that the most suitable functional form for these is the exponential function given in Equation 2.4.

$$f(\delta) = 1 - e^{-\left(\frac{\delta}{a}\right)^b} \tag{2.4}$$

Nevertheless, the function given in Equation (2.4) may give damage larger than zero for very small deformations. In order to prevent this, the function $f(\delta)$ is further multiplied with another function given in Equation 2.5.

$$g(\delta) = 0.5\left[1 - \cos\left(\frac{\pi\delta}{c}\right)\right] \qquad \text{if } \delta \leq c$$

$$g(\delta) = 1 \qquad\qquad\qquad \text{if } \delta > c \tag{2.5}$$

In Equations 2.4 and 2.5, δ represents the interstory drift ratio and a, b, c are the equation parameters.

Then, the damage of a column is given by:

Damage (δ) = f(δ) g(δ) (2.6)

The values of the equation parameters a, b, and c vary according to the ductility levels. These parameters were determined by least squares curve fitting technique using mean and extreme values at each damage state. The values of these parameters are given in Table 2.4. The data points and the corresponding damage functions for all three ductility levels are presented in Figures 2.11 to 2.13 for mean drift ratios as well as upper and lower bounds. Figure 2.14 presents the mean damage functions for all ductility levels.

Table 2.4 – Values of Equation Parameters

Par.	Low Ductility			Moderate Ductility			High Ductility		
	Upper	Mean	Lower	Upper	Mean	Lower	Upper	Mean	Lower
a	0.0065	0.0119	0.0170	0.0145	0.0170	0.0202	0.0155	0.0205	0.0271
b	1.3578	1.4206	1.2507	1.1264	1.1021	1.0571	1.0023	0.9859	0.9995
c	0.0110	0.0093	0.0128	0.0106	0.0123	0.0145	0.0118	0.0144	0.0191
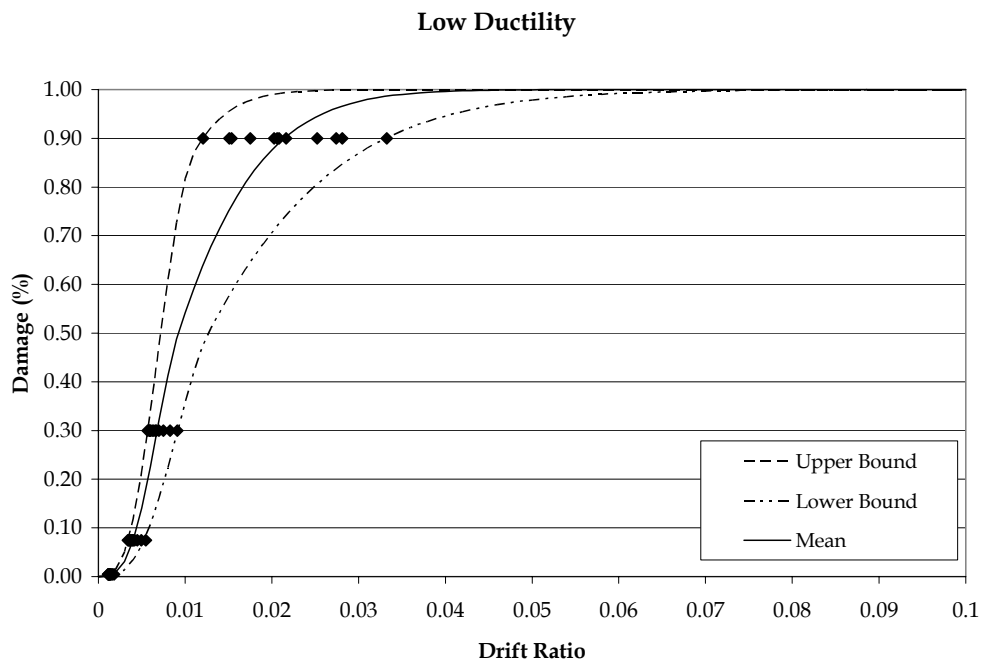
Low Ductility

Figure 2.11 – Developed Damage Curve and the Corresponding Data Points for Low Ductility

33
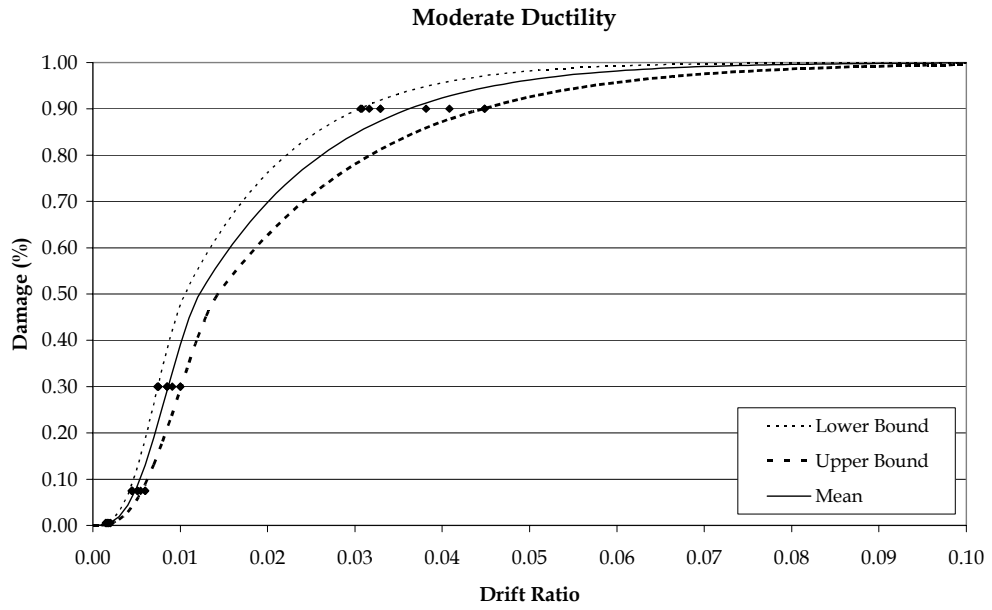
Figure 2.12 - Developed Damage Curve and the Corresponding Data
Points for Moderate Ductility
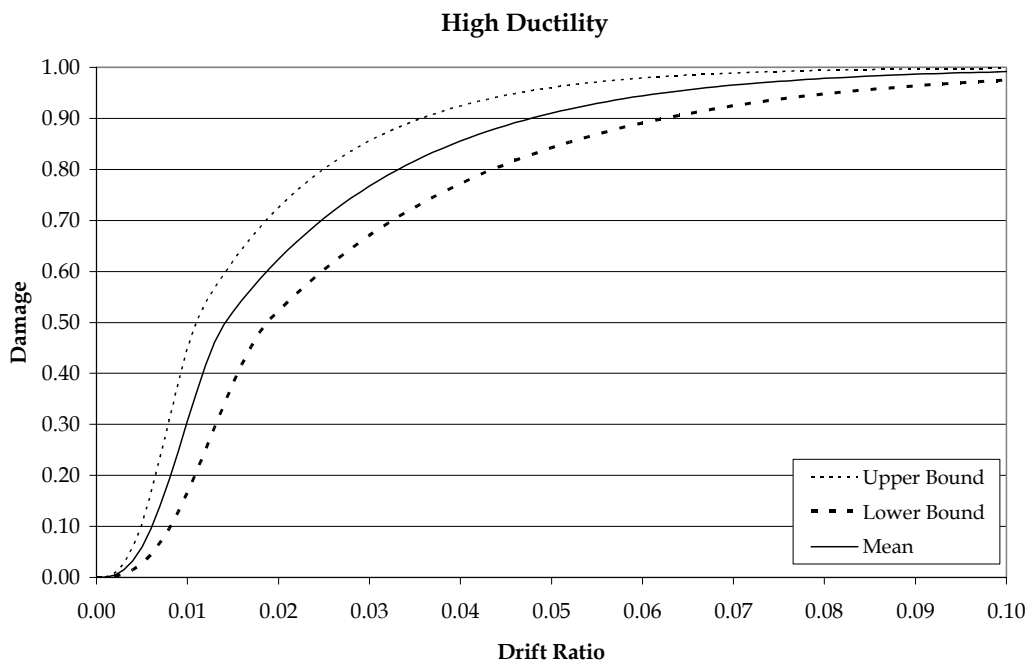
Figure 2.13 - Developed Damage Curve and the Corresponding Data
Points for High Ductility
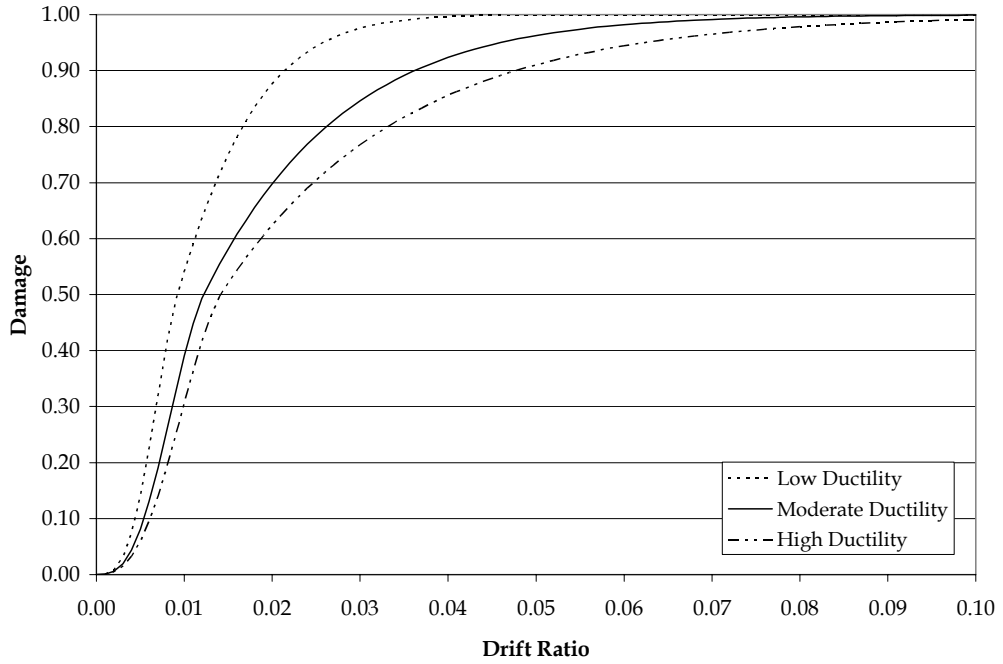
Figure 2.14 – Developed Mean Damage Curves for all Ductility Levels

2.4.4.4 Correction Factors for Yield Strength of Longitudinal Reinforcement and Slenderness Ratio

As mentioned before, both the yield strength of longitudinal reinforcement and the slenderness ratio of the columns affect the yield drift ratio. Since the damage criterion used herein depends directly on the yield drift ratio, the damage level of the columns is directly affected by the variations in these two parameters at every stage. Thus, the effect of these parameters must be reflected in the damage curves. For this purpose, correction factors were developed for both of them.

In Figure 2.15, the slenderness ratio of the columns and the corresponding yield drift ratios, both normalized to the corresponding values of the reference column, are plotted. To see the effect of slenderness ratio of the column on the yield drift ratio numerically, a curve was fit to the plotted data. The expression given in Equation 2.7 seemed to represent the general trend in a good manner.

$$\delta_y = 0.95 \frac{(L/i)}{(L/i)_{ref}} (\delta_y)_{ref} \tag{2.7}$$

35

where,

$(L/i)_{ref}$: slenderness ratio of the reference column and is equal to 21.123

$(\delta_y)_{ref}$: yield drift ratio of the reference column and is equal to 0.0091

(L/i) and (δ_y) : slenderness and the yield drift ratio of the considered column.

The effect of the slenderness on the yield drift ratio will directly be reflected on the damage levels since these are obtained through the ductility indices that depend on δ_y. Thus the interstory drift obtained for a column of slenderness (L/i) should be modified by the correction factor for slenderness, C_s given in Equation 2.8.

$$C_s = 0.045\left(\frac{L}{i}\right) \tag{2.8}$$
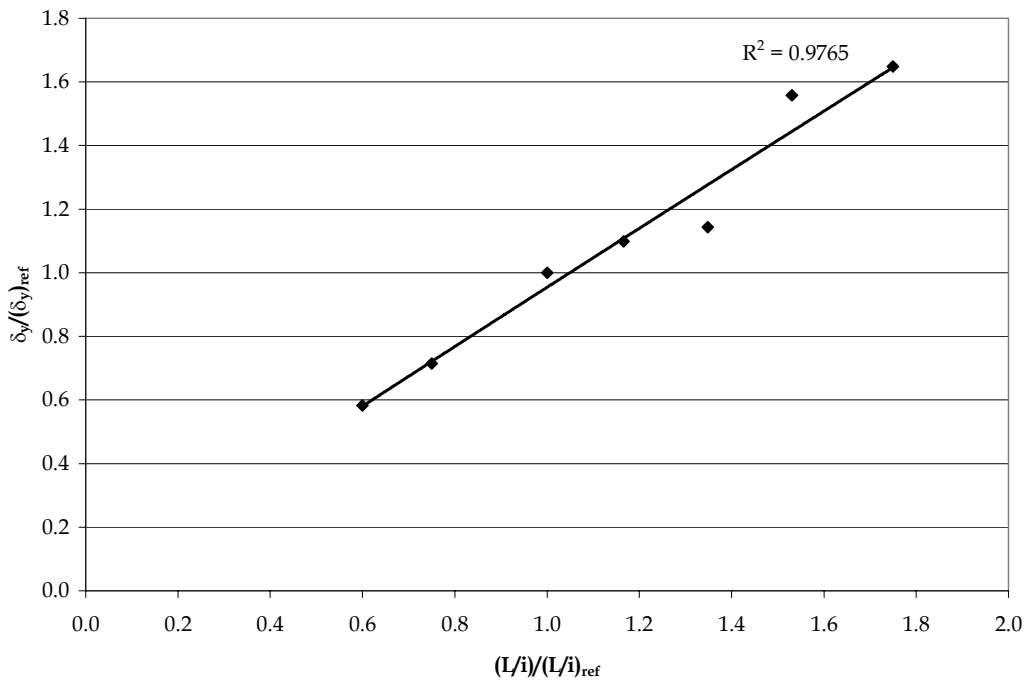
Figure 2.15 – Variation of Yield Drift Ratio with Slenderness Ratio

In Figure 2.16 yield drift ratios for columns with different f_y values (both normalized with respect to the corresponding values of the reference column) were plotted. When the data points were examined, it was observed that the trend was linear and can be represented by a straight line (Equation 2.9).

36

$$\delta_y = \left\{ 0.4 \left(\frac{f_y}{(f_y)_{ref}} \right) + 0.6 \right\} (\delta_y)_{ref} \qquad \text{for fy} \geq 220 \text{ MPa} \qquad (2.9)$$

where,

$(f_y)_{ref}$: yield strength of the longitudinal reinforcement of the reference column and is equal to 439 MPa.

(f_y) and (δ_y) : yield strength of the longitudinal reinforcement and the yield drift ratio of the considered column respectively.
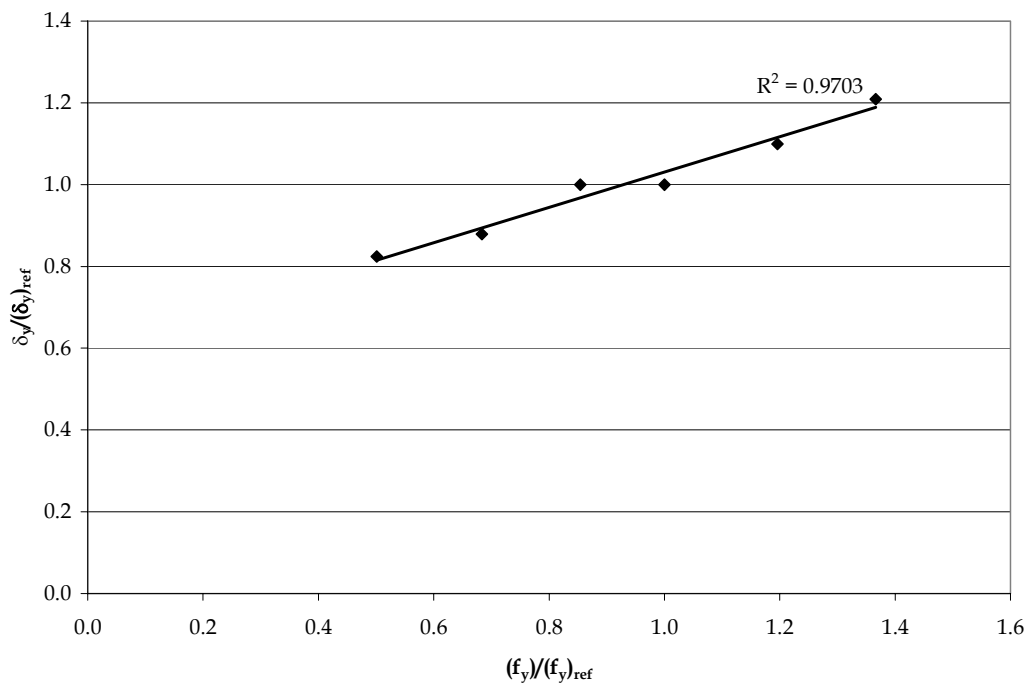
Figure 2.16 – Variation of Yield Drift Ratio with f_y

The discussion on the effect of slenderness ratio on the damage levels also holds for the effect of f_y on the damage levels. Thus, another correction factor for the yield strength of longitudinal reinforcement, C_{fy} is introduced (Equation 2.10).

$$C_{fy} = 0.4 \left(\frac{f_y}{439} \right) + 0.6 \qquad (2.10)$$

Taking the effect of both yield strength of longitudinal reinforcement and slenderness ratio of the column, the expression for the damage curves developed takes its final form:

$$f(\delta) = 1 - e^{-\left(\frac{\delta}{a(C_s)(C_{fy})}\right)^b} \tag{2.11}$$

$$g(\delta) = 0.5\left[1 - \cos\left(\frac{\pi\delta}{c(C_s)(C_{fy})}\right)\right] \qquad \text{if } \frac{\delta}{C_s C_{fy}} \leq c$$

$$g(\delta) = 1 \qquad \text{if } \frac{\delta}{C_s C_{fy}} > c \tag{2.12}$$

$$Damage(\delta) = f(\delta)g(\delta) \tag{2.13}$$

where,

δ: interstory drift

C_s, C_{fy}: correction factors for slenderness ratio and yield strength of longitudinal reinforcement respectively (Equations 2.8 and 2.10)

a, b, c: equation parameters given in Table 2.4 for different ductility levels.

2.4.5 Comparison with Experimental Data

In order to validate the damage curves developed for reinforced concrete columns, forty-two columns, of which cyclic lateral load-drift ratio curves were available, were analyzed and predicted damage levels were compared with the observed ones. The experimental data and the properties of the columns were obtained from NISTIR report [25]. The comparison made depends on mainly two critical damage states; namely the yield level and the ultimate level. The yield drift ratio predicted by the damage curves developed (corresponding to a damage score of 30%) was compared with the yield drift ratio observed from the cyclic-load deformation curves. Here it may be useful to repeat that the yield drift ratio is defined as the drift ratio corresponding to the maximum load capacity of the columns or the point where the slope decreases drastically. Similarly, the ultimate drift ratio predicted by the damage curves (corresponding to a damage score of 90%) was compared with the ultimate drift ratio, defined as the drift ratio corresponding to a 15% decrease in the lateral load capacity of the column.

Furthermore, the observed data were also compared with the yield and ultimate drift ratios proposed by Panagiotakos and Fardis [20] and Priestly [30]. These two studies will be summarized in the following paragraphs briefly.

2.4.5.1 *Panagiotakos & Fardis Method*

In their work, Panagiotakos and Fardis [20] used a database of 1000 tests (mainly cyclic) to develop expressions for the deformations of reinforced concrete members at yielding and ultimate.

To calculate the yield drift ratio, δ_y the expression given 2.14 was statically fitted to the results of 963 tests.

$$\delta_y = \phi_y \frac{L_s}{3} + 0.0025 + a_{sl} \frac{0.25\varepsilon_y d_b f_y}{(d-d')\sqrt{f_c{}'}} \tag{2.14}$$

In equation 2.14,

Φ_y: yield curvature

L_s: Shear span

a_{sl}: zero – one variable according to the occurrence of slip of longitudinal reinforcement. Zero means no slip occurs.

ε_y: yield strain of longitudinal reinforcement

d_b: diameter of compression reinforcement

f_y: yield strength of longitudinal reinforcement

d: effective depth of cross-section

d': distance of center of compression reinforcement from extreme compression fiber

$f_c{}'$: compressive strength of concrete

The second term on the right hand side of Equation 2.14 can be considered as the (average) shear distortion of the shear span at flexural yielding.

For the ultimate drift ratio, the authors suggested three different expressions. One of these is for monotonic loading, one for cyclic loading and the last is the combination of the first two accounting for both monotonic and cyclic loading. Of these three expressions, the one, which was developed for cyclic loading by fitting a curve to 633 cyclic test data, was used in this particular study,

since all the columns used for comparison had been tested under cyclic loading. The resulting expression is given in Equation 2.15.

$$\delta_u (\%) = \alpha_{st,cyc}\left(1 + \frac{a_{sl}}{2}\right)(1 - 0.4 a_{wall})(0.2^\upsilon)(f_c')^{0.175}\left(\frac{L_s}{h}\right)^{0.4}1.1^{\left(100\alpha\rho_{sx}\frac{f_{yh}}{f_c'}\right)}$$

$$(1.3^{100\rho_d}) \tag{2.15}$$

where,

$\alpha_{st,cyc}$: coefficient for the type of steel equal to 1.125 for hot-rolled steel, 1.0 for heat-treated steel, and 0.8 for cold-worked steel

ρ_{sx}: ratio of transverse steel parallel to the direction of loading

f_{yh}: yield stress of transverse steel

ρ_d: steel ratio of diagonal reinforcement in each diagonal direction

a_{wall}: coefficient equal to 1.0 for shear walls and 0.0 for columns

υ: axial load ratio ($\upsilon = N/(A_g f_c')$)

α: confinement effectiveness factor given by:

$$\alpha = \left(1 - \frac{s_h}{2b_c}\right)\left(1 - \frac{s_h}{2h_c}\right)\left(1 - \frac{\sum b_i^2}{6b_c h_c}\right) \tag{2.16}$$

In Equation 2.16, b_c and h_c denotes the width and depth of confined core, respectively, and b_i the distances of successive longitudinal bars laterally restrained at stirrup corners or by 135° hooks. s_h is the spacing of transverse reinforcement. In this study, the reinforcement of all the columns that were used in the comparison was assumed to be hot-rolled; thus $\alpha_{st,cyc}$ was equal to 1.125. The wall coefficient, a_{wall} automatically turns out to be zero. No diagonal reinforcement was present in the columns; hence ρ_d was also zero. Making these simplifications the expression for the ultimate drift ratio becomes:

$$\delta_u (\%) = 1.4625\left(1 + \frac{a_{sl}}{2}\right)(0.2^\upsilon)(f_c')^{0.175}\left(\frac{L_s}{h}\right)^{0.4}1.1^{\left(100\alpha\rho_{sx}\frac{f_{yh}}{f_c'}\right)} \tag{2.17}$$

2.4.5.2 Priestly [30] Method

Priestly [30] suggested simple expressions for yield and ultimate drift ratios. The yield drift ratio of concrete member can be calculated by:

$$\delta_y = 0.5\varepsilon_y\left(\frac{l}{h}\right) \tag{2.18}$$

where,

ε_y: yield strain of longitudinal reinforcement

l: length of the member

h: depth of cross-section

The ultimate drift ratio proposed by Priestly [30] depends on the sectional response and given as:

$$\delta_u = \delta_y + (\phi_u - \phi_y)l_p \tag{2.19}$$

In Equation 2.19 ϕ_u and ϕ_y are the curvatures at ultimate and yield, respectively and l_p is the plastic hinge length. Although empirical expressions were proposed by the author for ultimate and yield curvatures, the exact values computed from section analyses were used in this study for the sake of accuracy. The plastic hinge length was taken to be equal to the section depth.

2.4.5.3 Discussion of Results

The yield and ultimate drift ratios observed in the cyclic tests of forty-two reinforced concrete columns were compared with the corresponding values predicted by using the damage curves developed in this study, the method proposed by Panagiotakos and Fardis [20] and Priestly [30]. The columns were selected so that the significant properties varied in a broad range.

The predicted and observed yield drift ratios are presented together with a line indicating correct estimations in Figure 2.17. Moreover, the results are also summarized in Table 2.5. This table and Figure 2.17 show that Panagiotakos and Fardis method overestimates the yield drift ratio by 17% in the average with a coefficient of variation (cov) of 18%, if it is assumed that slipping of the longitudinal bars occurs in all of the columns. If the third term in Equation is ignored, i. e. it is assumed that no slippage occurs, then the same method

41

underestimates δ_y by 10% with a cov of 19%. On the other hand the formula proposed by Priestly (Eq. 2.18) underestimates the yield drift ratio by 21%. The coefficient of variation of this method is 21%. The damage curves proposed in this study underestimates the yield drift ratio by 6%. Although the damage curves developed gives the best predictions as far as mean value is concerned, the variation is slightly higher than that of the relationship proposed by Panagiotakos and Fardis. In the light of the above discussion, it can be stated that this study and Panagiotakos and Fardis method neglecting slippage yields the best results as far as yield drift ratio is concerned.
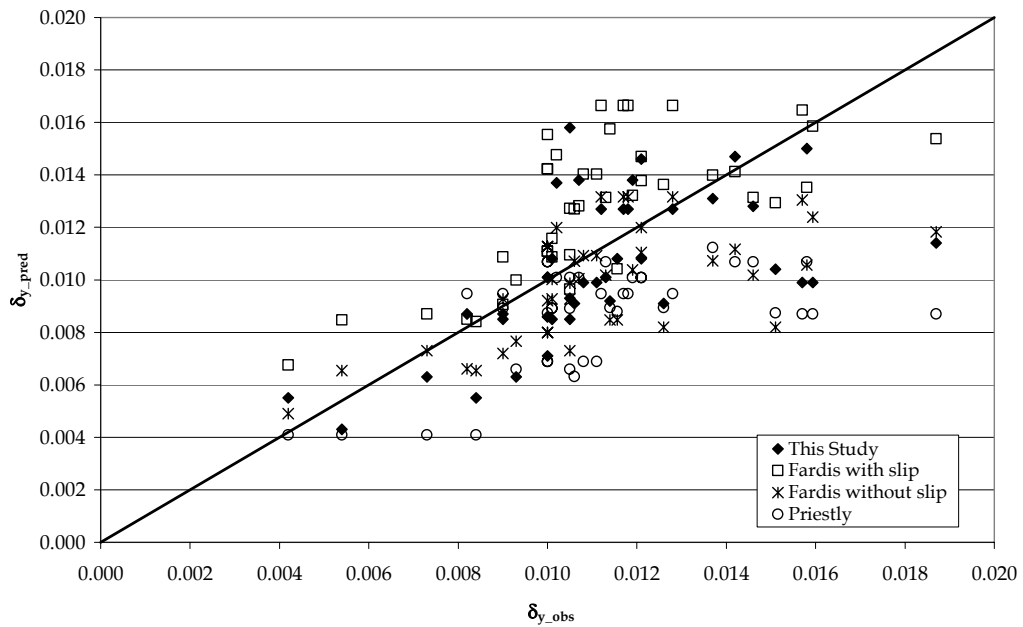
Figure 2.17 – Observed and Predicted Yield Drift Ratios

For the ultimate drift ratio, Panagiotakos and Fardis method overestimates the ultimate yield drift ratio by 86% on the average with a cov of 27% (Figure 2.18, Table 2.5) if full slippage of longitudinal reinforcement is assumed. When, perfect bond between concrete and reinforcement is assumed, the average value of $\delta_{u\_pred}/\delta_{u\_obs}$ decreases to 1.24 indicating a 24% overestimation of the ultimate drift ratio. In both cases Panagiotakos and Fardis method gives highly unconservative results. Similarly Priestly method also yields unconservative results since it

overestimates the ultimate drift ratio by 61%. The method proposed in this study yields very accurate results on the average with a mean value of 1.02 for $\delta_{u\text{-pred}}/\delta_{u\_obs}$. The variation in all the three methods is almost the same (between 27% and 28%). Thus, it can be concluded that the damage curves developed in this study yields the best results as far as ultimate drift ratio is concerned.

Table 2.5 – Observed and Predicted Values for Yield and Ultimate Drift Ratios

		$\delta_{y\text{-pred}}/\delta_{y\_obs}$	$\delta_{u\text{-pred}}/\delta_{u\_obs}$
This Study	Mean	0.94	1.02
	cov	0.22	0.27
Panagiotakos & Fardis	Mean	1.17	1.86
	cov	0.18	0.27
Panagiotakos & Fardis (w/o slip)	Mean	0.90	1.24
	cov	0.19	0.27
Priestly	Mean	0.79	1.61
	cov	0.21	0.28
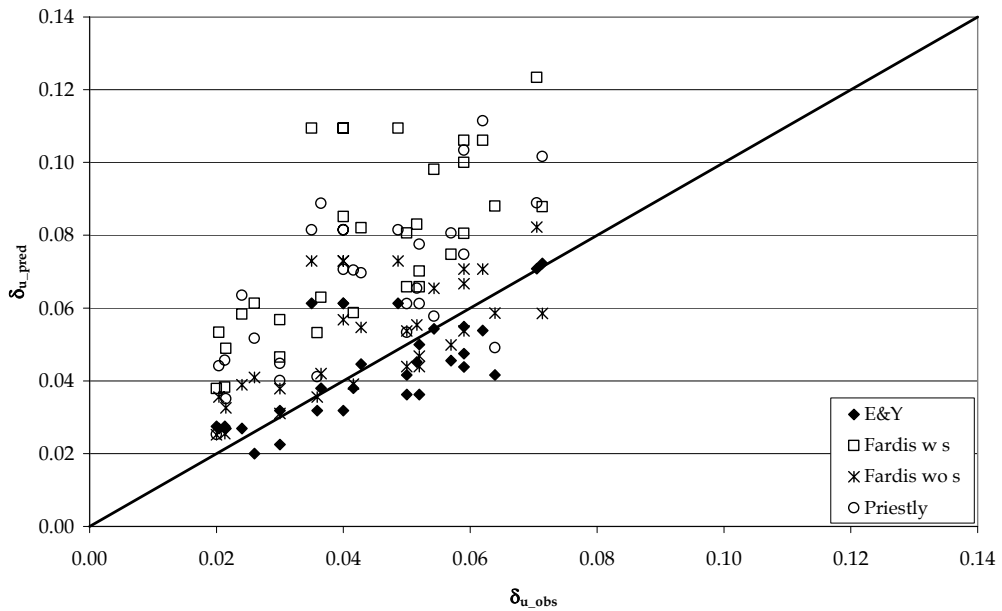
Figure 2.18 - Observed and Predicted Ultimate Drift Ratios

2.4.6   Comparison with ATC-40 Acceptance Criteria

ATC-40 [9] gives a set of acceptance criteria for reinforced concrete components based on certain levels of desired performance. For reinforced concrete columns, acceptance criteria is based on plastic rotation limits assigned to three levels of performance; Immediate Occupancy, Life Safety and Structural Stability. These rotation limits depend on the level of axial load on the column and the two categories of confining reinforcement, Conforming (C) or Nonconforming (NC). The performance levels given in ATC-40 and elsewhere have similar definitions of physical damage to be expected in the structures. Immediate occupancy, Life Safety and Structural Stability performance levels generally correspond to the light, moderate and heavy damage states described in this study. In this context, the rotation limits of ATC-40 were converted to respective drift limits (Equation 2.20) for several columns with different material and geometric properties and compared with the damage curves developed herein.

$$\delta = \phi_y \frac{L}{3} + \theta_p (L - l_p) \qquad (2.20)$$

where,

ϕ_y : Yield Curvature

L: Length of the columns

θ_p : Plastic rotation given in ATC-40

l_P: plastic hinge length

The first term in Equation 2.20 accounts for the elastic drift occurring till the yielding of the member and the second term is the plastic drift as a result of the plastic rotation, θ_p .

The purpose is both to check the reliability of ATC-40 acceptance limits and recommend more reasonable ranges for drift limits when necessary. The comparison is depicted in Figure 2.19. In order to obtain these curves, drift ratios corresponding to the immediate occupancy, life safety and collapse prevention limit states were computed using the plastic rotation limits given in the ATC-40

document. Then, the damage scores for the three limit states were computed using the developed damage curves and the projections of these drift limits on the developed damage curves were plotted. ATC-40 conditions of $N/N_o \leq 0.1$ with C transverse reinforcement detail corresponds to high ductility, $N/N_o \leq 0.1$ with NC and $N/N_o \geq 0.4$ with C correspond to moderate ductility and $N/N_o \geq 0.1$ with NC is equivalent to low ductility levels defined in this study.
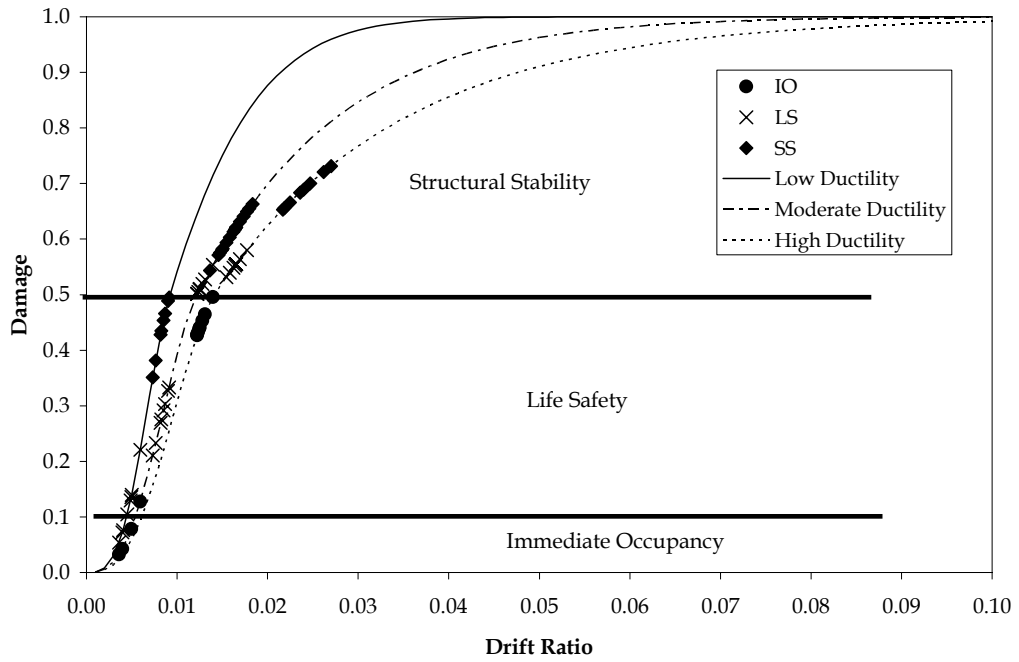
Figure 2.19 – Comparison of Damage Curves with ATC-40 Limits

These results indicate that for low and moderate ductility levels ATC-40 limits look reasonable, whereas for columns with high ductility, deformation limits suggested for immediate occupancy are too high thus unconservative. Even if the lower bound for columns with high ductility were used, the ATC-40 limits yield unconservative values (Figure 2.20). A drift ratio of approximately 1.3 % is attributed to a negligible or light damage of reinforced concrete columns; this drift would lead to, in average, a physical damage of approximately 40% according to this study. In the columns investigated, this damage level

45

corresponded to a drift beyond the yield drift. Sozen [31] indicated that a drift limit of 0.5% is acceptable for reinforced concrete buildings and 2% had been found to be acceptable only for a few frames of a series tested.
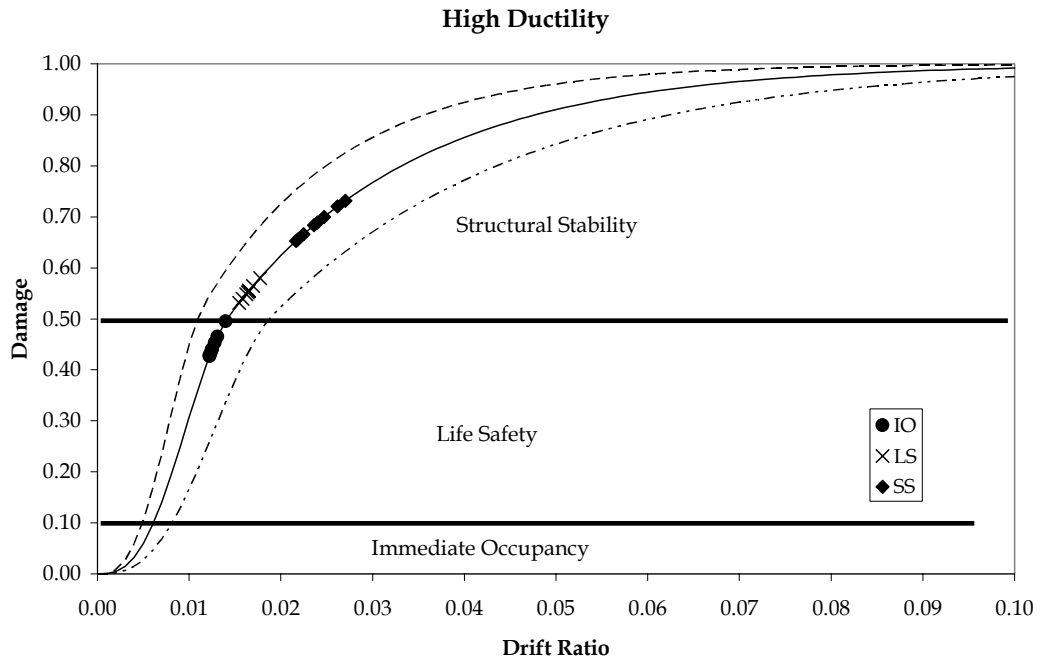
High Ductility

Figure 2.20 – Comparison of ATC-40 Limits with Upper and Lower Bounds for High Ductility Columns

2.5 SHEAR CRITICAL COLUMNS

The behavior and the displacement capacity of a reinforced concrete member completely changes when the predominant failure mode of the member changes from flexure to shear. To be able to reflect this change in the damage curves a new set of finite element analyses were carried out on columns whose predominant failure mode is expected to be shear. In order to differentiate shear and flexure critical columns, a capacity based approach was utilized.

In this approach, firstly the nominal shear capacity of the column is computed according to the TS-500 [32] formulation. According to TS-500, the

nominal shear strength of a member (V_r) can be computed by adding the concrete (V_c) and web reinforcement contributions (V_w):

$$V_r = V_c + V_w \tag{2.21}$$

The concrete strength, V_c can be taken to be 80% of the diagonal cracking strength of concrete, which is computed as:

$$V_{cr} = 0.65 f_{ctk} b_w d \left(1 + \gamma \frac{N_d}{A_c} \right) \tag{2.22}$$

In Eq. 2.22 f_{ctk} is the tensile strength of concrete, which is equal to $0.35\sqrt{f_{ck}}$, b_w is the width of the column section, d is the distance from the compression face of the section to the centroid of the tension reinforcement, N_d is the axial load on the column and A_c is the area of the column. γ is a dimensionless parameter which takes a value of 0.07 if the column is in compression. If the column is in tension, then γ is equal to -0.30. If the axial stress on the column is less than 0.5 MPa, then γ should be taken as 0.00.

The contribution of web reinforcement to the shear strength of a member can be computed as:

$$V_w = \frac{A_{sw}}{s} f_{ywk} d \tag{2.23}$$

In Eq. 2.23, A_{sw} is the total cross sectional area of shear reinforcement, s is the spacing of the stirrups and f_{ywk} is the yield strength of the shear reinforcement.

To be able to decide on the predominant failure mode of the column, the nominal shear capacity of the column computed using Eqs. 2.21 to 2.23 is compared with the flexural shear capacity of the column (V_f), which is equal to:

$$V_f = \frac{M_i + M_j}{L} \tag{2.24}$$

In Eq. 2.24, M_i and M_j are the moment capacities of the i and j ends of the column and L is the length of the column. If the nominal shear capacity of the column is greater than the flexural shear capacity ($V_r > V_f$), then the predominant failure mode of the column is flexure and the damage curves developed in section 2.3 of this chapter should be used for these columns. However, if the nominal

shear capacity of a column is less than the flexural shear capacity of the column ($V_f < V_r$), this indicates that the column will fail in shear rather than flexure. For these columns, the damage functions, which will be presented in the forthcoming paragraphs, should be used.

In order to be able to develop damage functions for shear critical reinforced concrete columns a series of finite element analyses were carried out in ANSYS [33]. However, at the first stage, two columns tested by Lynn [34] and Arakawa et. al. [35], both of which were reported to have failed in shear, were modeled and analyzed in order to investigate the effectiveness of ANSYS in predicting the force-deformation behavior of shear critical columns. The first column used for the verification of the finite element model was a 457.2 mm x 457.2 mm column with a shear span of 1.473 m and was tested by Lynn [34]. The concrete strength was 27.6 MPa and the yield strength of longitudinal and transverse reinforcement was 331 MPa and 400 MPa, respectively. The shear reinforcement consisted of 9.5 mm diameter stirrups spaced at 457.2 mm. The axial load was 1512 kN corresponding to the 33% of the nominal axial load capacity. The V_r/V_f ratio was computed to be 0.89 with a V_r value of 327.9 kN and V_y value of 368.9 kN. Figure 2.21 shows the experimental and numerical force-displacement curves for this column. The column tested by Arakawa et. al was a 180 mm x 180 mm column with a shear span of 225 mm. The concrete strength was 33 MPa and the yield strength of the longitudinal reinforcement was 340 MPa. 4 mm diameter bars were used as stirrups spaced at 64.3 MPa. The axial load was 476 kN which is equal to the 52% of the nominal axial load capacity of the column. The nominal shear capacity of the column was computed to be 87.1 kN, whereas the flexural shear capacity was 166.7 kN resulting in a V_r/V_f value of 0.52. The experimental and numerical force-deformation curves of the members are shown in Figure 2.22.

Figures 2.21 and 2.22 show that the finite element model used can predict the behavior of shear critical column in a quite satisfactory manner. After verifying the finite element model, 54 additional finite element analyses with various values for concrete strength, yield strength and amount of longitudinal reinforcement, yield strength and amount of shear reinforcement and slenderness

ratio were carried out using ANSYS. In these analyses, the V_r/V_f ratio ranged from 0.57 to 1.00. In addition to these analyses, in order to be able to compute the corresponding flexural yield drift ratio of the shear critical column (the drift ratio at which the column would yield if the predominant failure mode was flexure), the nominal shear strength of the shear critical columns were increased significantly by changing the amount and yield strength of the shear reinforcement and the columns were re-analyzed. The ultimate drift ratio of (δ_u) of each shear critical column was recorded and the ratio of δ_u to the yield drift ratio of the corresponding flexure critical column (δ_y) was plotted against the V_r/V_f ratio. Figure 2.23 presents the δ_u/δ_y vs. V_r/V_f data points and the line fitted (Eq. 2.23) to these data points.

The ratio of the δ_u/δ_y values predicted by the line fitted to the data points (Eq.2.23) and the observed δ_u/δ_y values is 1.01 for the 55 shear critical columns analyzed with a coefficient of variation of 0.11.

The results of the finite element analyses show that, for a shear critical column with a V_r/V_f value very close to 1.00, the ultimate drift ratio capacity is practically equal to the yield drift ratio of the corresponding flexure critical column. The acceptance criterion given in ATC-40 and FEMA-356 is also in accordance with this observation and the plastic rotation limits given in these documents for the collapse prevention limit state are both 0.0, which means that, once a shear critical member is found to be yielding in flexure in the nonlinear analysis, then this member is heavily damaged. In the light of this discussion, the damage curves for shear critical columns were developed by modifying the damage curve for the flexure critical columns (Figure 2.14). Recalling that the flexural yield point of flexure critical members corresponds to a damage score of 30% in the damage curves developed for these members, the damage curve for shear critical members was formed by modifying the damage curve for low ductility columns in such a way that the flexural yield point now corresponds to a damage score of 90% instead of 30% (Figure 2.24). In this modification, the damage curve for low ductility columns is selected for the sake of being conservative in the prediction of the damage score of shear critical columns, which display a very brittle behavior. The damage curve developed for shear

critical members is presented in Figure 2.25 together with the damage curves for flexure critical members.
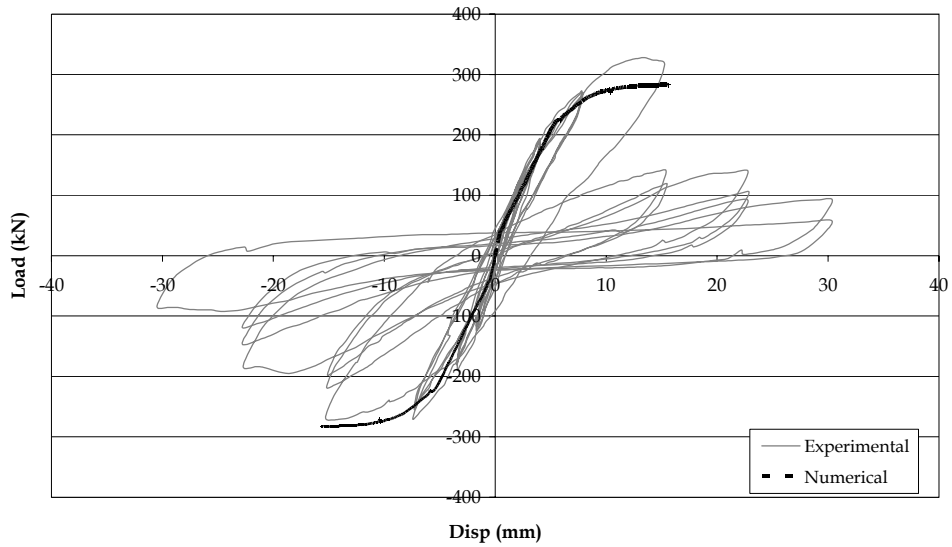
Figure 2.21 – Experimental and Numerical Capacity Curves for the Column tested by Lynn [34].
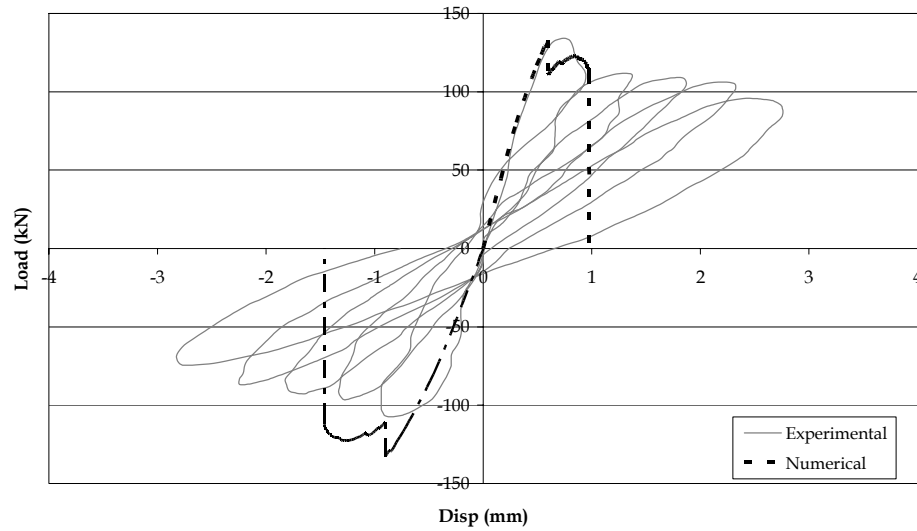
Figure 2.22 - Experimental and Numerical Capacity Curves for the Column tested by Arakawa et. al [35].

50
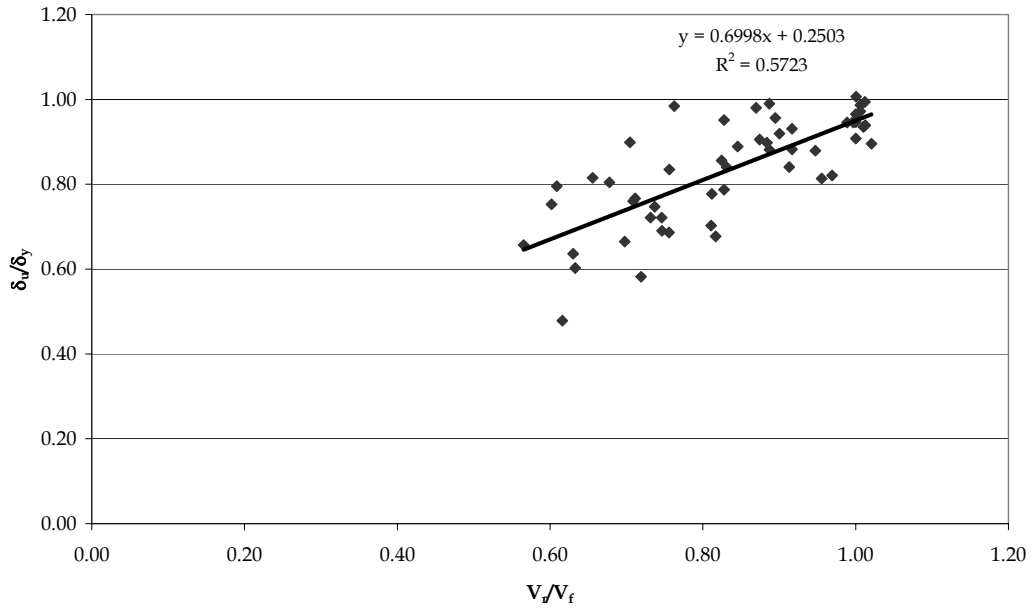
Figure 2.23 – δ_u/δ_y vs. V_r/V_f data points

$$\frac{\delta_u}{\delta_y} = 0.70 \times \frac{V_r}{V_f} + 0.25 \qquad\qquad \text{for} \quad \frac{V_r}{V_f} \leq 1.00 \qquad\qquad (2.23)$$
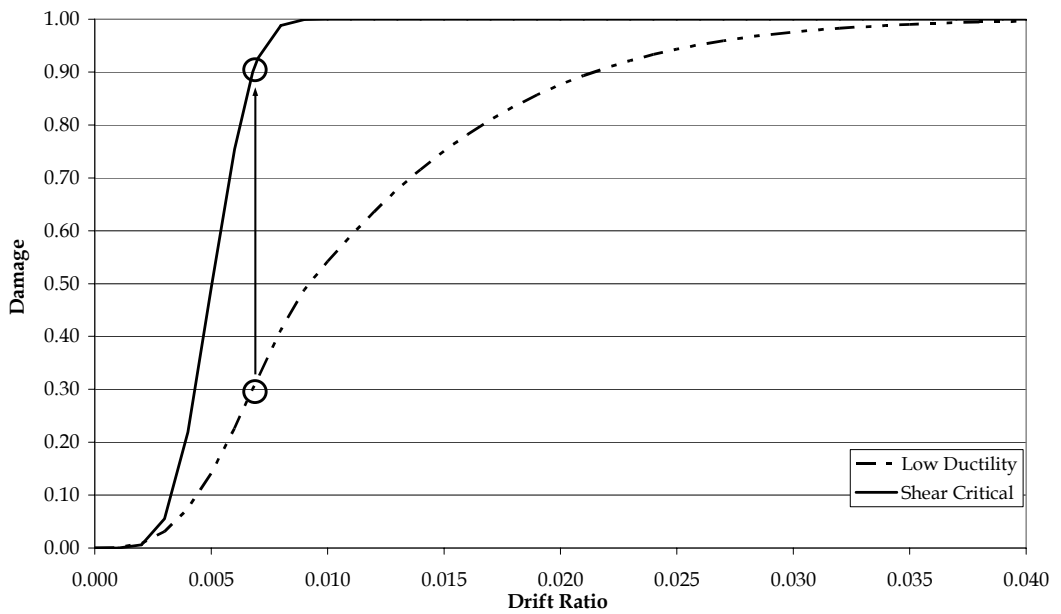
Figure 2.24 – Formation of the damage curves for shear critical columns
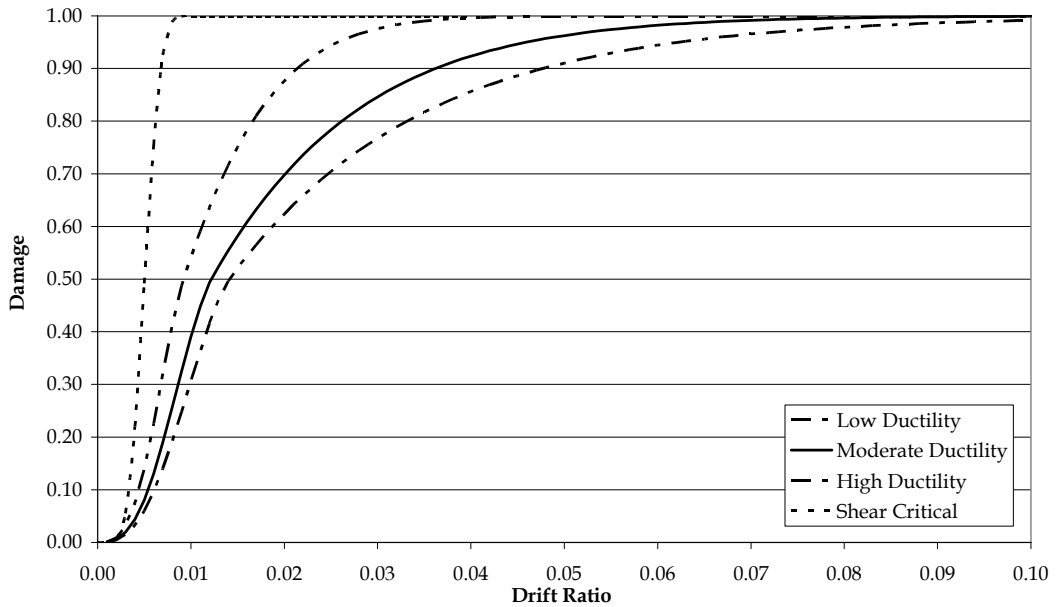
Figure 2.25 – Damage curves for shear and flexure critical columns

The equation parameters for shear critical columns are given in Table 2.6.

Table 2.6 –Values of equation parameters for shear critical columns

Parameter	
a	0.0063
b	4.0000
c	0.0050

The damage curve for the shear critical columns given in Figures 2.22 and 2.23 are for columns of which V_r/V_f ratio is equal to 1.00. However, as the Figure 2.21 implies, the ultimate drift capacity of a shear critical column decreases with a decrease in V_r/V_f ratio. To take this into account, a correction factor must be applied to the drift ratio computed for a shear critical column as a result of the structural analysis. The correction factor for the shear strength of the column (C_V) should be applied together with the correction factors for the slenderness ratio (C_s) and for the yield strength of longitudinal reinforcement (C_{fy}) which is known to affect the yield drift ratio, the parameter that the damage curve for shear

52

critical columns is based on. From Figure 2.21 and Eq. 2.23, the correction factor for the shear strength of the column is:

$$C_v = 0.70 \times \frac{V_r}{V_f} + 0.25 \qquad\qquad \text{for} \quad \frac{V_r}{V_f} \leq 1.00 \qquad\qquad (2.24)$$

The drift ratio computed from the structural analysis for a shear critical column should be corrected by $1/(C_v.C_s.C_{fy})$ before it is used in the corresponding damage function. Hence, the final form of the damage function for shear critical columns becomes:

$$f(\delta) = 1 - e^{-\left(\frac{\delta}{a(C_s)(C_{fy})(C_V)}\right)^b} \qquad\qquad (2.25)$$

$$g(\delta) = 0.5\left[1 - \cos\left(\frac{\pi\delta}{c(C_s)(C_{fy})(C_V)}\right)\right] \qquad \text{if} \quad \frac{\delta}{C_s C_{fy} C_V} \leq c$$

$$g(\delta) = 1 \qquad\qquad\qquad\qquad \text{if} \quad \frac{\delta}{C_s C_{fy} C_V} > c \qquad (2.26)$$

CHAPTER 3

ROTATION BASED DAMAGE FUNCTIONS FOR BEAMS

3.1 GENERAL

The performance of the beams of a structure is one of the critical factors that affect the seismic vulnerability of that structure. One of the most important issues in the seismic performance of buildings is the damageability of the beams relative to the columns of that building, which can alter the behavior of the building totally. In order to be able to evaluate the damage level of the beams as a result of a certain seismic excitation, damage curves based on chord rotation were developed.

3.2 EXPERIMENTAL BEHAVIOR

The behavior of reinforced concrete beams had been investigated by various researchers in the past. These researchers shared the objective of understanding the cyclic behavior and identifying the parameters affecting the ductility of beams.

Scribner and Wight [36] grouped the reinforced concrete beams they tested into three based on the maximum shear stress. Shear stress values of $0.24\sqrt{f_c'}$ and $0.48\sqrt{f_c'}$ were used as the points of separation for the three groups. They stated that the overall performance of the beams was governed most significantly by the maximum shear stress. Shear span to depth ratio and reinforcement ratio were also important, but only to the extent that they influenced maximum shear stress. Specimens with a shear stress less than $0.24\sqrt{f_c'}$ showed ductile behavior. When the shear stress level exceeded

$0.48\sqrt{f_c'}$, it was observed that the specimens suffered severe stiffness and strength deterioration during repeated cyclic loading due to the planes of shear slippage. Moreover, Scribner and Wight [36] observed that buckling of compression reinforcement was a major cause of the severe loss of flexural strength and concluded that the closely spaced ties may delay reinforcement buckling only slightly unless they are as nearly as large as the longitudinal bars themselves.

Nmai and Darwin [37] tested seven lightly reinforced concrete beams under cyclic load. The flexural reinforcement ratio, ρ, was either 0.69% or 1.03%. Based on these tests they stated that the performance of reinforced concrete beams subjected to cycling loading will improve with a decrease in maximum shear stress. Since a decrease in the flexural reinforcement ratio, ρ, reduces both the maximum shear stress and compressive stress in the concrete, it reduces the rate of strength degradation. Moreover, a reduced stirrup spacing can improve cyclic performance, even with some reduction in nominal stirrup capacity. Finally, they stated that, an increased ratio of positive to negative steel at the face of the support improves the performance of a cantilever specimen.

In 1994 Xie et al. [38] stated that increasing the shear reinforcement ratio has an insignificant effect on the shear ductility of beams with a shear span to depth (a/d) ratio of 1. For beams with a/d of 2 and 3, increasing the shear reinforcement ratio increases the shear ductility significantly. This indicates the difficulty of preventing shear failure of beams with an a/d of 1.

3.3 METHOD OF ANALYSIS

It is easier and more appropriate to relate the damage in the beams to the rotations at the end of the members rather than to the interstory drift ratio directly. This is due to the fact that, the interstory drift ratio – damage relations can significantly vary with the variations in the structural system, relative performance of the beams with respect to the columns, etc… However, it can be stated that, the rotation damage relationship is unique for a certain beam and is not related to the parameters stated above. Hence, the damage curves for the

reinforced concrete beams developed were based on the end rotations. After the development of the rotation based damage curves, studies were carried out on several frames to develop interstory drift ratio – rotation relationships. By this way the damage in the beams were related to the interstory drift ratio indirectly.

In the development of the rotation based damage curves, numerical analyses were carried out using the finite element software ANSYS. Using the results of the numerical analyses, the effect of certain parameters on the damageability of reinforced concrete beams was investigated. These parameters are concrete strength (f_{ck}), depth of the beam (d), amount of tension reinforcement (ρ), amount of compression reinforcement (ρ'/ρ), and yield strength of longitudinal reinforcement (f_{yk}). Upon the completion of the parametric study, the damage curves were developed.

3.4 FLEXURE CRITICAL MEMBERS

3.4.1 Numerical Analyses

In the finite element analyses carried out, a portal frame was modeled rather than a single beam in order to be able to impose the boundary conditions and the deflected configuration of the beams during seismic action in a better manner. The columns of this portal frame were assumed to remain elastic in all stages of the loading. Reinforced concrete was modeled in the same manner it had been modeled in the analyses of columns. The finite element model of the portal frame is shown in Figure 3.1.

In this study, the rotation was defined as the chord rotation between two sections of the beam. The first of these sections is at the face of the column and the second one is at a distance of d/2 units (d being the depth of the beam) away from the face of the column. Figure 3.2 presents the definition of the chord rotation used in this study.
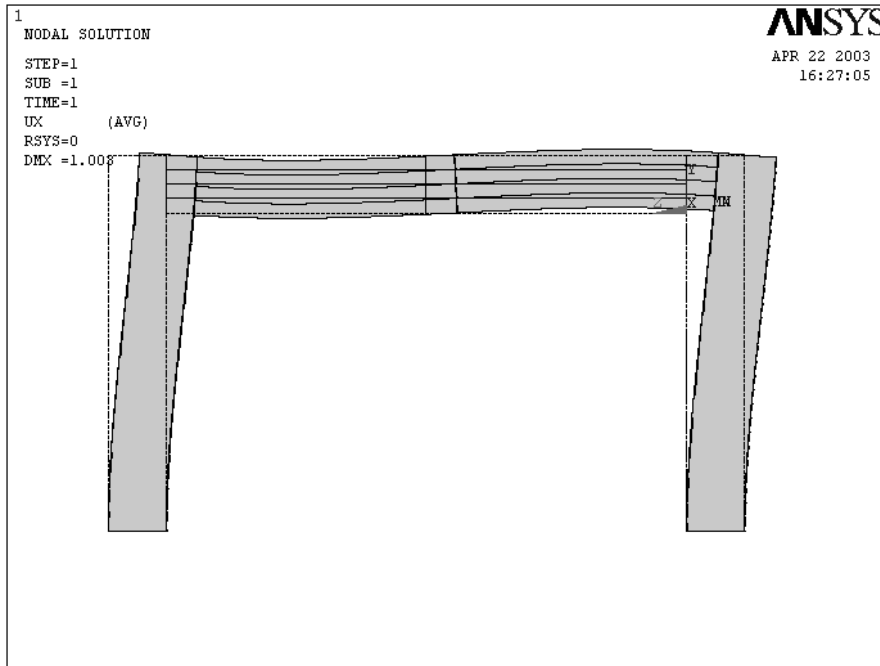
Figure 3.1 – Finite element of the portal frame

3.4.2 Damage Criterion

For reinforced concrete beams, two different damage criteria were adopted. The first criterion was for the negligible, light and moderate damage levels and was based on the width of the cracks occurring in the beams. The second criterion was for the heavy damage. As in the case of columns, it was thought that using crack widths for the detection of the heavy damage was not appropriate. Instead, the moment rotation curves derived from classical section analyses were used to detect heavy damage.

In the case of beams, in which the axial load level is negligibly small, the crack width is a good indicator for damage. In the calculation of the crack width, the expression proposed by Frosch [29] and given in Equations 2.1 and 2.2 were used. The damage scores corresponding to certain crack widths were assigned according to the criterion adopted by the Ohkubo [28]. Accordingly, the damage state of a beam is considered to be negligible for a crack with of 0.2 mm and this value was assigned a damage score of 0.5% (the damage score range for negligible

damage is 0%-1%). For the light damage state (5%-10%), a crack width of 1 mm was chosen as the indicator and assigned a damage score of 7.5%. The damage score range for the moderate damage is 10%-50%. In the document published by Ohkubo, it was stated that a crack width of 2 mm can be assumed to be an average value for the detection of moderate damage. Based on this discussion, a damage score of 30% was assigned to a crack width of 2 mm.
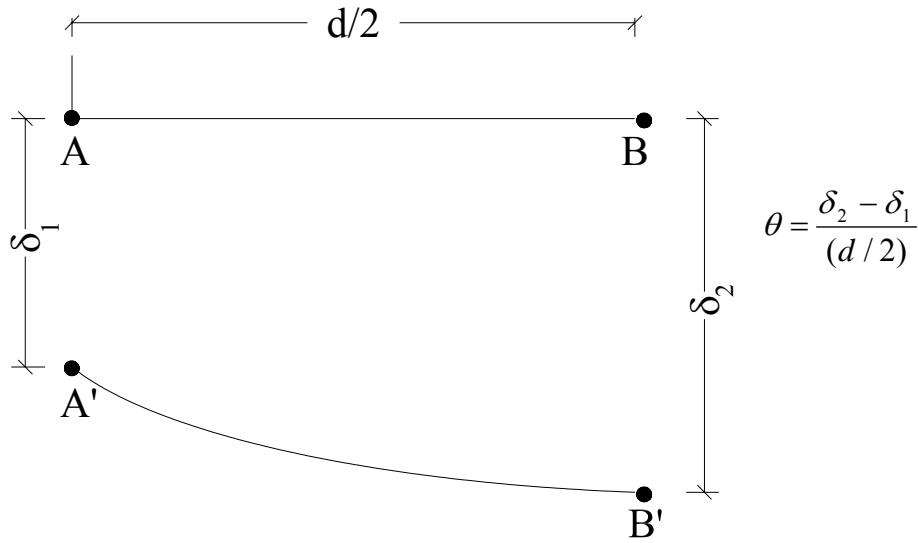
Figure 3.2 – Definition of chord rotation

For the detection of the heavy damage, the moment – curvature and, in turn, moment – rotation curves of the beam sections were developed. The expressions proposed in ATC-40 and given in Equations 3.1 and 3.2 were used to compute the yield rotation and ultimate rotation from the corresponding curvature values.

$$\theta_y = \phi_y \frac{L}{6}$$ (3.1)

$$\theta_u = \theta_y + (\phi_u - \phi_y)\frac{L_p}{2}$$ (3.2)

where, θ_y and θ_u are the rotations at yield and ultimate, φ_y and φ_u are the curvatures at yield and ultimate, respectively. L is the length of the member and L_p is the plastic hinge length which was taken to be equal to the half of depth of

the member. After the moment-rotation relationship for the beam was obtained, the rotation at which the beam reaches 75% of its plastic rotation capacity was determined and was assigned a damage score of 75% (Figure 3.3).

3.4.3   Parametric Studies

The effect of several parameters on the damageability of reinforced concrete beams was investigated to determine the significant parameters and reflect their effect on the damage curves that would be developed. For this, finite element analyses were carried out along with section analyses. In each analysis, only one parameter was changed and the others were kept constant. The range of the parameters investigated is given in Table 3.1.

As explained in detail in the above paragraphs, two different criteria were used for different damage levels. One of these was the crack width that had been used for none to moderate damage levels. To investigate the effect of the parameters on the damageability of beams in this damage range crack width – rotation curves were compared. In the case of heavy damage, the damage criterion depends on the plastic rotation capacity; hence rotation ductility of the beams. In this range, variation of ductility with the variations in the parameters indicated was monitored to see the effect of the indicated parameter on the behavior of the beams.
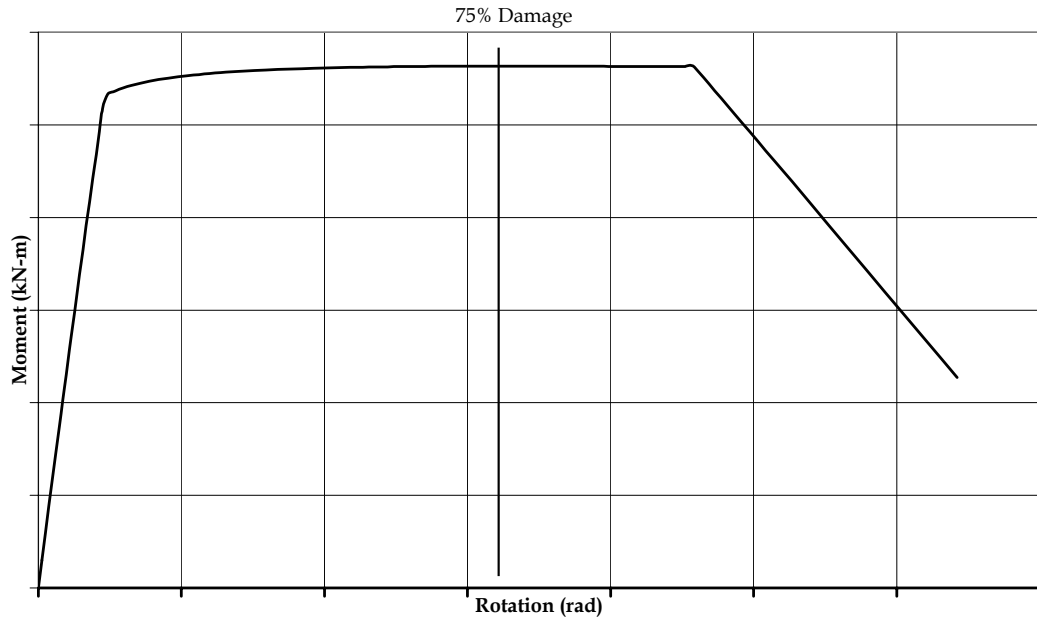
Figure 3.3 – Sample Moment – Rotation Diagram and Damage Criterion

Table 3.1 – Range of parameters used

f_{ck} (MPa)	ρ_s	d(mm)	Longitudinal Reinforcement		
			f_{yk} (MPa)	ρ	ρ'/ρ
10	0.000	375	220	0.0075	0.30
14	0.001	500	330	0.0100	0.50
16	0.003	625	420	0.0125	0.70
20	0.005	750	530	0.0150	0.85
25			650	0.0175	1.00
				0.0200	

3.4.3.1 *Effect of Concrete Strength, f_{ck}*

Five analyses were carried out for different concrete strengths ranging from 10 MPa to 25 MPa. Crack width – rotation curves given in Figure 3.4 show that f_{ck} influence the damageability of RC beams in none to moderate damage range to some extent. Moreover this curve reveals that the effect of concrete strength is less pronounced as f_{ck} increases. The variation of ultimate ductility with concrete strength is presented in Figure 3.5. This curve shows that the plastic rotation capacity of a beam increases with the increase in concrete

strength. Thus, f_{ck} influences the behavior of the beams in the heavy damage range significantly.
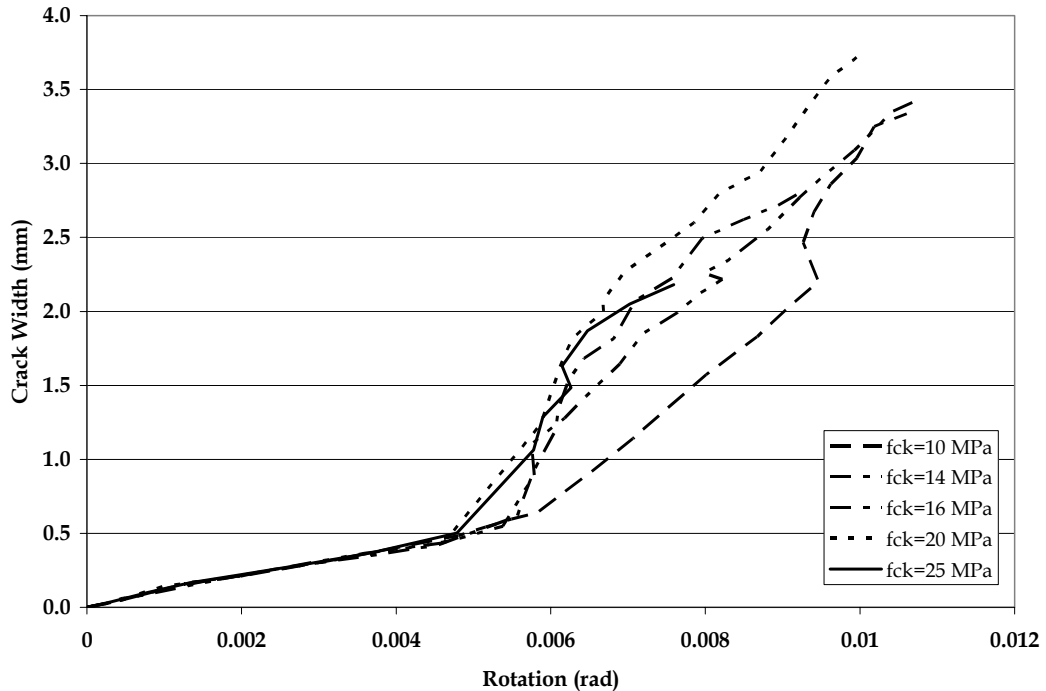
Figure 3.4 – Rotation – crack width curves for different fck values

3.4.3.2 *Yield Strength of Longitudinal Reinforcement, f_{yk}*

The crack width – rotation curves for different f_{yk} given in Figure 3.6 indicate that, for a given rotation, the beam with a lower f_{yk} suffer significantly higher damage than the one with a higher f_{yk}. Moreover, Figure 3.7 reveals that the plastic rotation capacity of the beams vary significantly by the variations in the yield strength of the longitudinal reinforcement. Thus, yield strength of longitudinal reinforcement affects the damageability of reinforced concrete in all damage ranges.
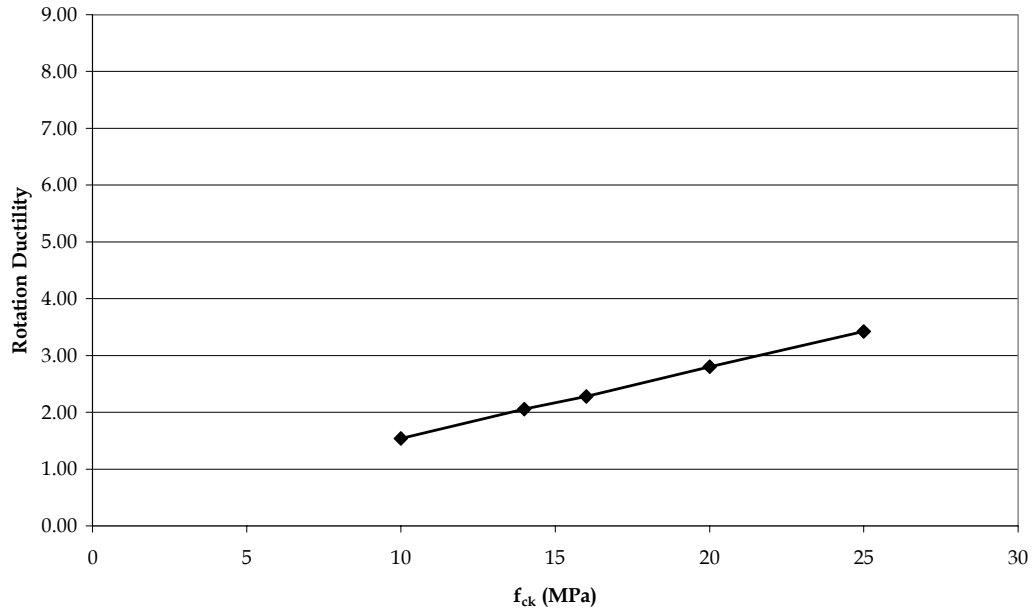
Figure 3.5 – Variation of ultimate rotational ductility with concrete strength

3.4.3.3 Amount of Tension Reinforcement, ρ

As it can be seen from the rotation – crack width curves given in Figure 3.8 and ρ – ultimate rotational ductility relationship shown in Figure 3.9, the amount of tension reinforcement affect the damageability of RC beams in the heavy damage range and it has no significant effect in the other ranges.

3.4.3.4 Amount of Compression Reinforcement, ρ'/ρ

The effect of amount of compression reinforcement on the damageability of RC beams is very similar to that of amount of tension reinforcement. In other words, amount of compression reinforcement influence the damage curves only in the heavy damage range (Figures 3.10 and 3.11).
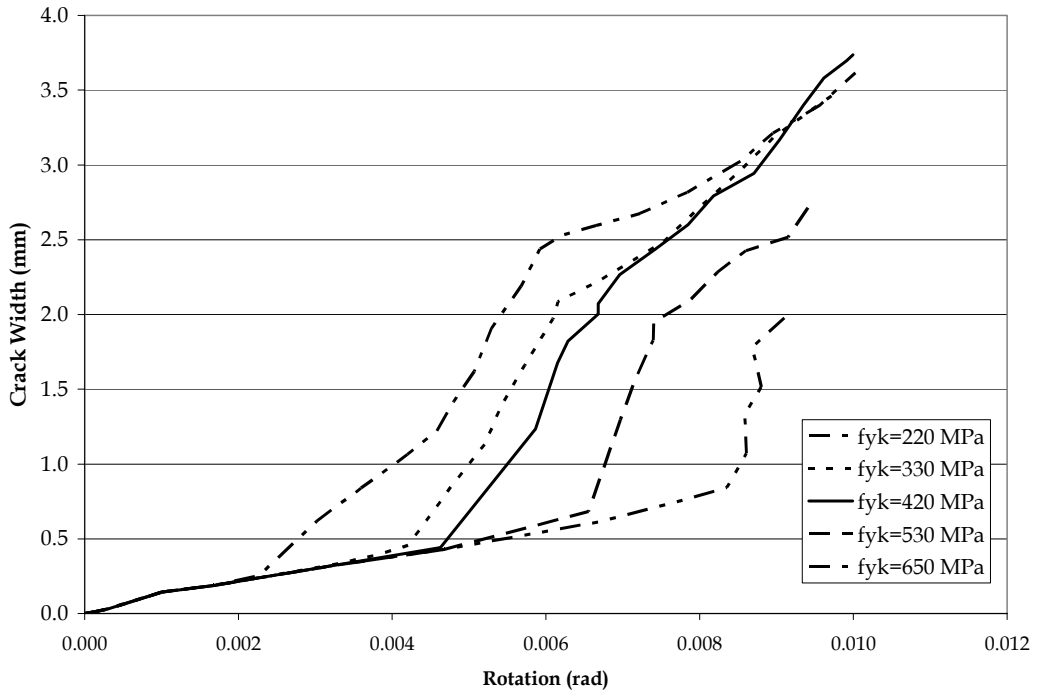
Figure 3.6 - Rotation – crack width curves for different f_{yk} values
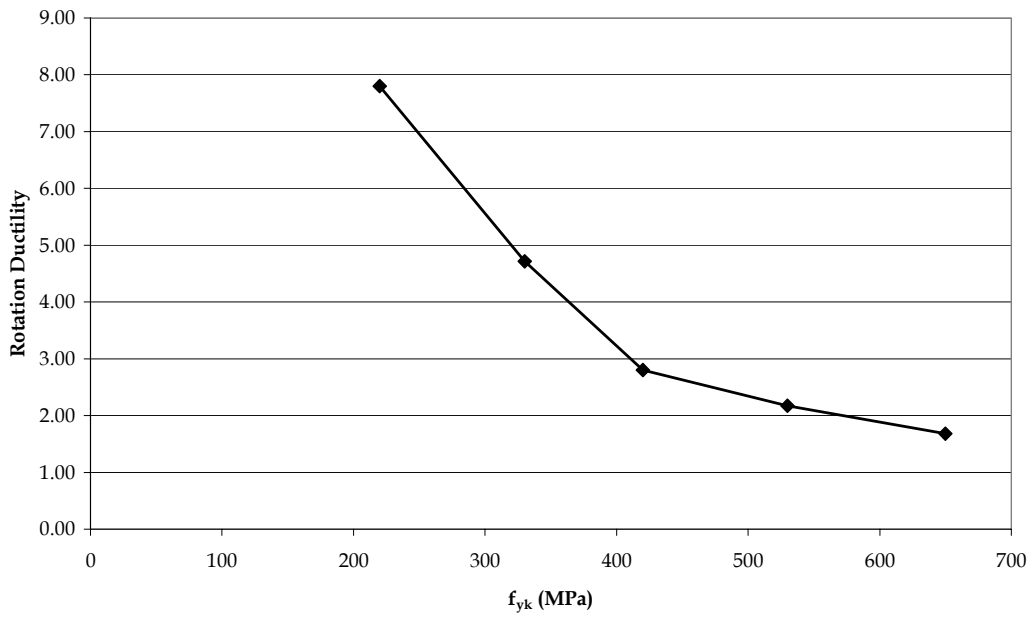
Figure 3.7 - Variation of ultimate rotational ductility with yield strength of longitudinal reinforcement
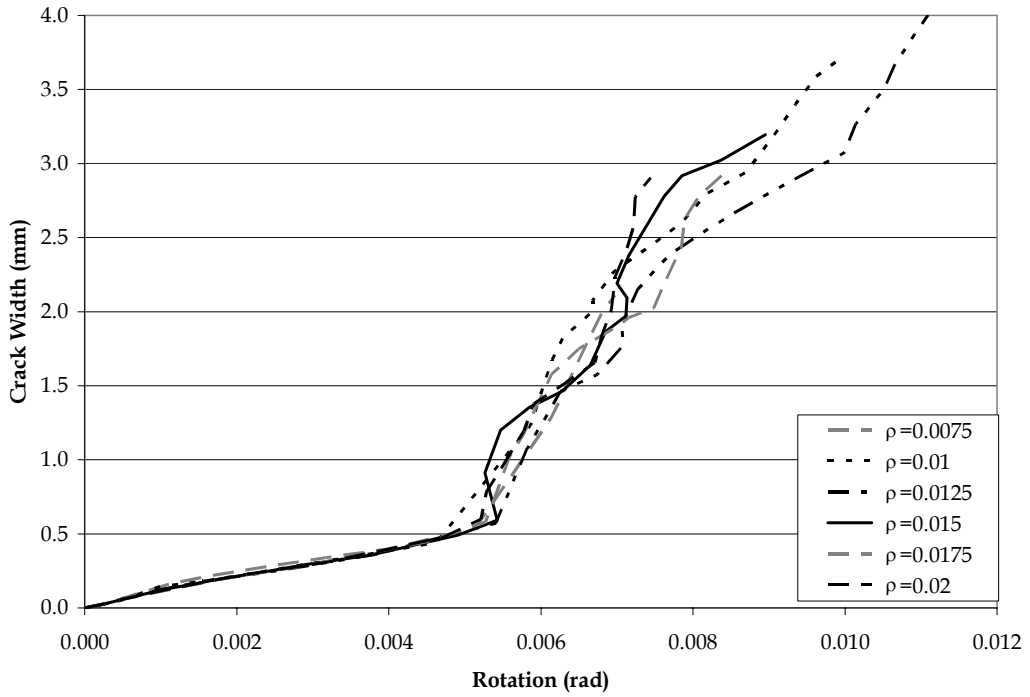
Figure 3.8 - Rotation – crack width curves for different tension
reinforcement amounts
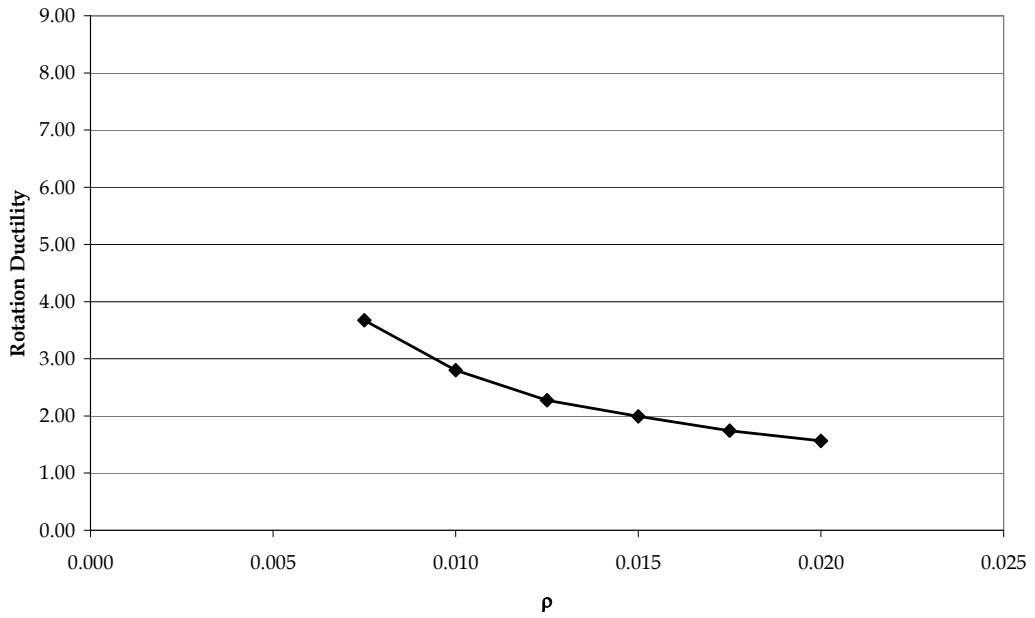
Figure 3.9 - Variation of ultimate rotational ductility with amount of
tension reinforcement
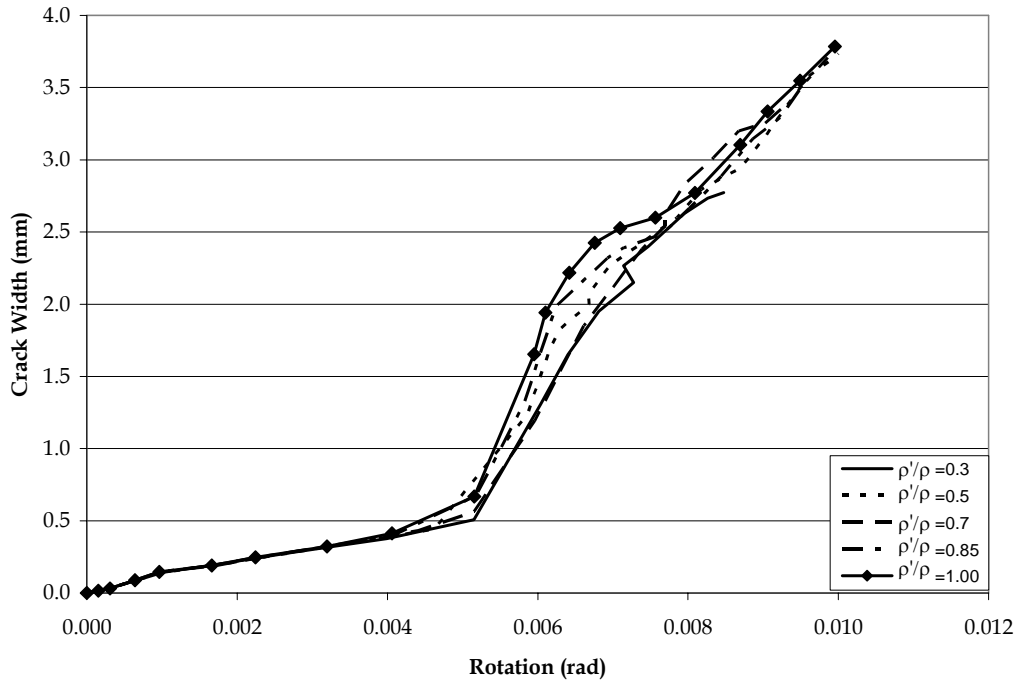
Figure 3.10 - Rotation – crack width curves for different compression reinforcement amounts
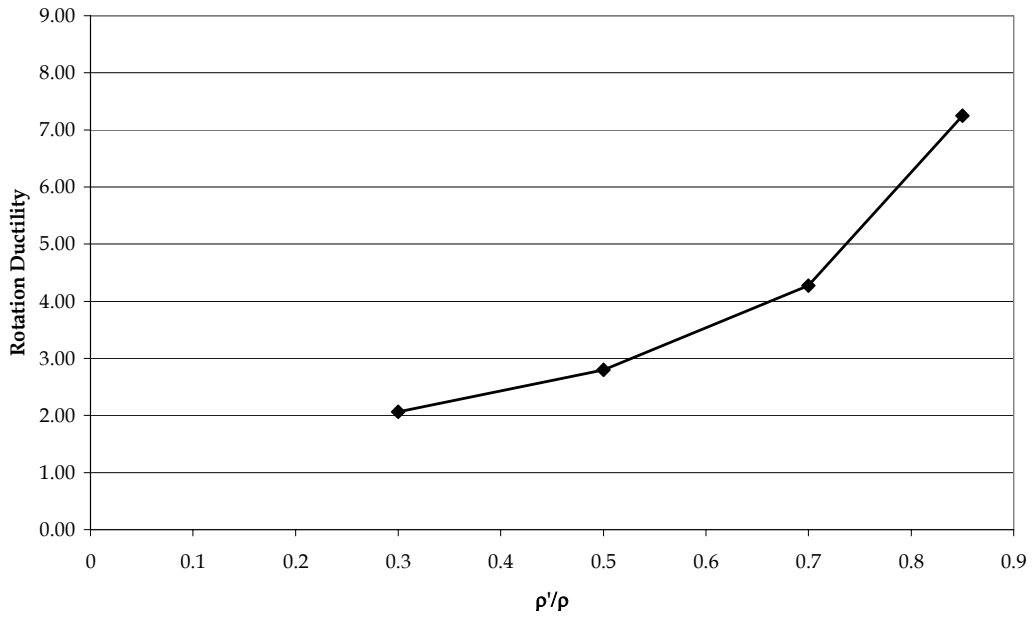
Figure 3.11 - Variation of ultimate rotational ductility with amount of compression reinforcement

3.4.3.5 *Depth of Beam, d*

The crack width – rotation curves plotted for different d values (Figure 3.12) show that these curves are significantly influenced by the variations in d. The ultimate rotational ductility of the beams is also affected by the variations in the depth of the beam (Figure 3.13). However, this variation is very limited compared to the variation in the plastic rotation capacity due to the other parameters.
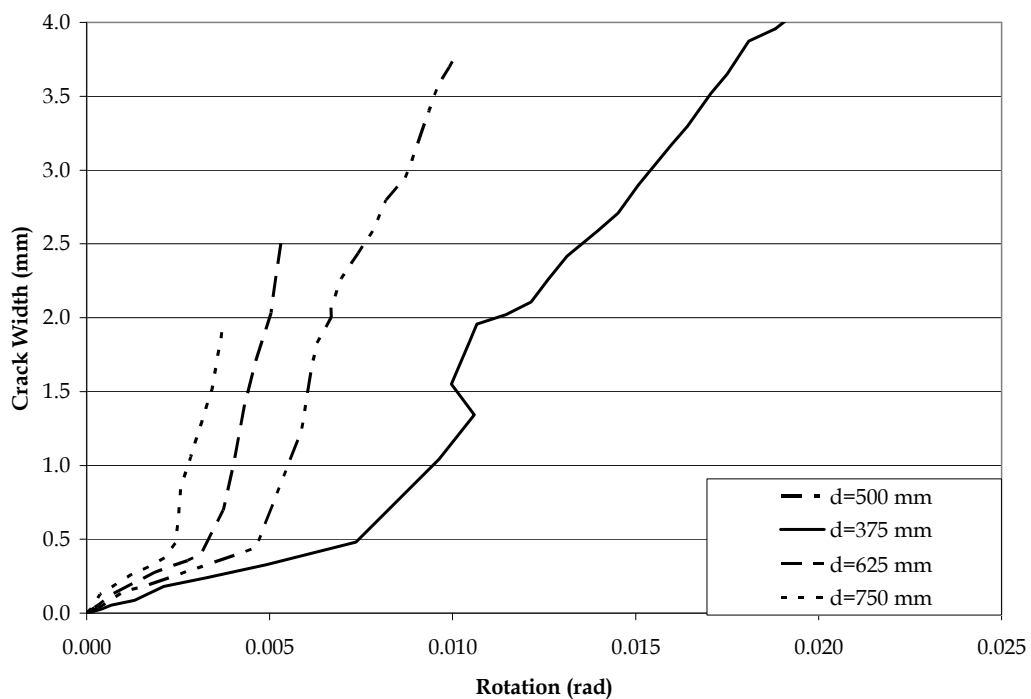
Figure 3.12 – Crack Width – rotation curves for different d values

3.4.3.6 *Amount of Transverse Reinforcement, ρ_s*

Lastly, the effect of amount of transverse reinforcement on the ultimate ductility of reinforced concrete beams was investigated. Figure 3.14 shows that the ultimate rotational ductility of beams increases significantly with the increase in the amount of transverse reinforcement.

66
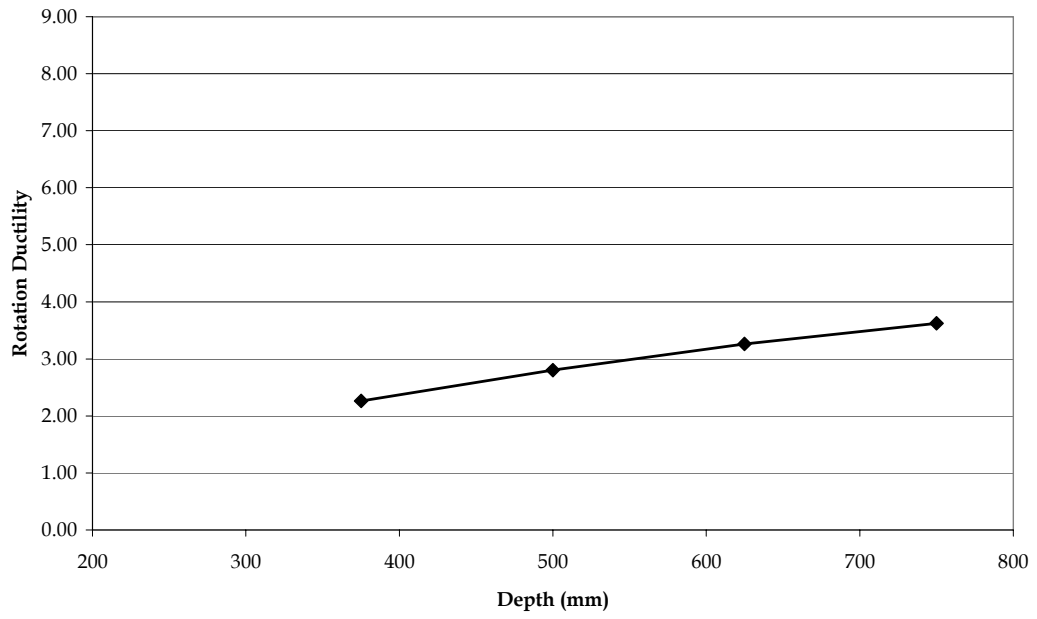
Figure 3.13 - Variation of ultimate rotational ductility with depth
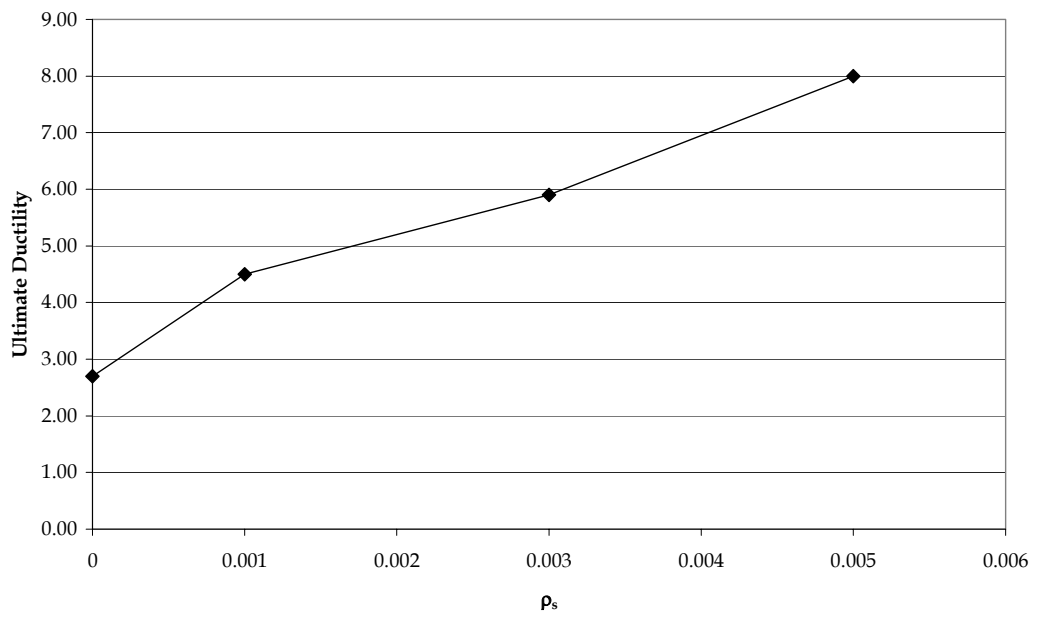
Figure 3.14 - Variation of ultimate rotational ductility with amount of

transverse reinforcement

3.4.4   Development of Damage Curves

Upon the completion of the parametric study, the damage curves based on rotation were developed using the least squares curve fitting technique.

3.4.4.1   *Significant Parameters*

The effect of the parameters on the damageability of reinforced concrete beams was investigated at two stages. In none to moderate damage levels, rotation – crack width relationships were used. In this range, the main parameters that affect the behavior of RC beams were found to be the depth of the beam and the yield strength of the longitudinal reinforcement. Amount of both compression and tension reinforcement has no effect on the rotation – crack width curves. Concrete strength influences the rotation – crack width curves to some extent. However, the influence of this parameter is not as significant as the influence of the parameters mentioned above.

For the heavy damage case, the criterion that had been used to evaluate the significance of the effect of the parameters was the ultimate rotational ductility of the beams. Of the parameters investigated, all but depth of the beam affect the plastic rotation capacity of the beams. Although the depth of the beam also affects the ultimate rotational ductility of the beams, its influence can be neglected with respect to the effect of the other parameters. From the discussion in the above paragraphs, it is observed that the rotational ductility of RC beams increases with increasing values of concrete strength, amount of compression reinforcement and amount of transverse reinforcement. Moreover, decrease in the amount of tension reinforcement and yield strength of longitudinal reinforcement results in an increase in the plastic rotation capacity of the beams. In light of this discussion, a new term, defined as the ratio of product of amount of transverse reinforcement, concrete strength and amount of compression reinforcement to the product of yield strength of longitudinal reinforcement and amount of tension reinforcement $\left(\rho_s \, \dfrac{f_{ck}(\rho'/\rho)}{f_{yk}\rho} \right)$. Then, the beams analyzed

were grouped into three according to their $\left(\rho_s \dfrac{f_{ck}(\rho'/\rho)}{f_{yk}\rho} \right)$ values. If the

$\left(\rho_s \dfrac{f_{ck}(\rho'/\rho)}{f_{yk}\rho} \right)$ value of a beam is smaller than or equal to 0.25%, then the

ductility level of this beam was considered to be low. If the $\left(\rho_s \dfrac{f_{ck}(\rho'/\rho)}{f_{yk}\rho} \right)$

value of a beam is between 0.25% and 1.0%, then this beam is considered to be moderately ductile. The ductility of a RC beam is considered to be high if its

$\left(\rho_s \dfrac{f_{ck}(\rho'/\rho)}{f_{yk}\rho} \right)$ value exceeds 1.0%.

The depth of the beam affects the damageability of RC beams at every stage. To reflect the influence of these parameters, adjustments to the rotation were applied via the introduction of correction factor.

3.4.4.2 Damage Curves

Upon the completion of the parametric study, the damage curves for reinforced concrete beams of three ductility level were established. Firstly, the damage data points obtained from the finite element and section analyses were plotted. In these plots the depth of the beam, which affects the damage level of the beams at every stage, was kept constant as 500 mm. Then, the damage function similar to the one adopted for the columns was fit to these damage points (Equation 3.3).

$$damage(\theta) = \left[1 - e^{-\left(\frac{\theta}{a} \right)^b} \right] g(\theta) \tag{3.3}$$

where g(θ) is given as:

$$g(\theta) = 0.5 \left[1 - \cos\left(\frac{\pi\theta}{c} \right) \right] \qquad \text{if } \theta \leq c$$

$$g(\theta) = 1 \qquad \text{if } \theta > c \tag{3.4}$$

In Equations 3.3 and 3.4, θ is the rotation at the beam end and a, b and c are the equation parameters. These parameters were determined using least squares curve fitting technique. The damage curves obtained for the three ductility levels are shown in Figures 3.15 to 3.18.

Table 3.2 – Values of Equation Parameters

Par.	Low Ductility			Moderate Ductility			High Ductility		
	Upper	Mean	Lower	Upper	Mean	Lower	Upper	Mean	Lower
a	0.0160	0.0118	0.0090	0.0230	0.0172	0.0130	0.0450	0.034	0.0030
b	3.00	2.80	2.50	1.60	1.50	1.40	0.95	1.05	1.10
c	0.012	0.010	0.008	0.016	0.014	0.012	0.015	0.014	0.011
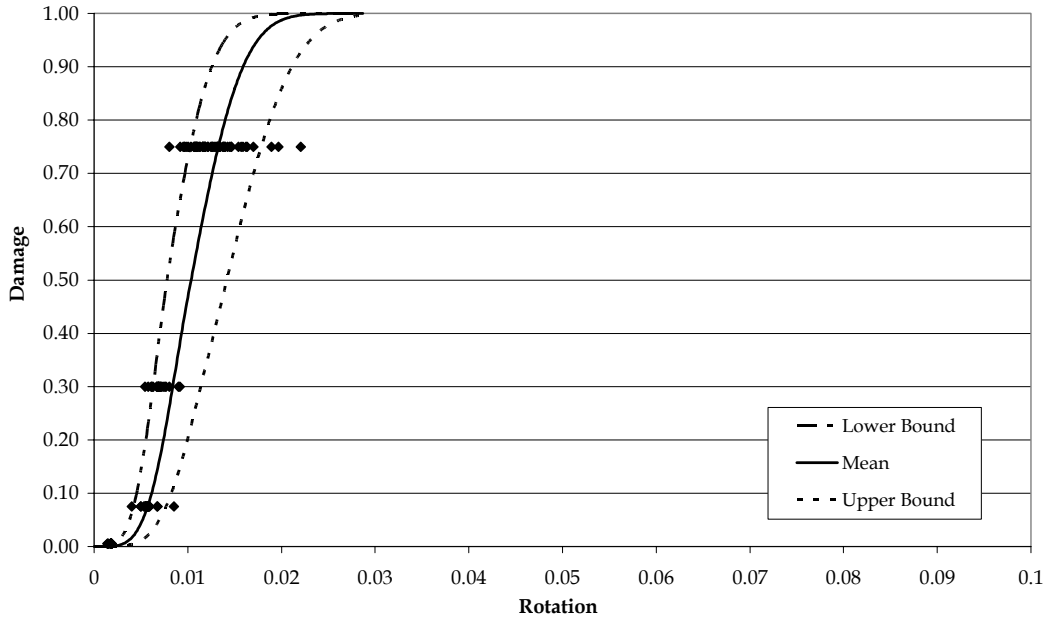
Figure 3.15 – Damage curves for low ductility level

3.4.4.3 *Correction Factor for the Depth of the Beam*

As a result of the parametric study carried out, it was observed that, the depth of the beam affects the damageability of RC beams at none to moderate damage level. To reflect the effect of d on the damage curves, correction to the computed rotation value will be applied. The major assumption here is that, the

effect of d on the damage curves in the none to moderate damage levels is reflected to the heavy damage level.
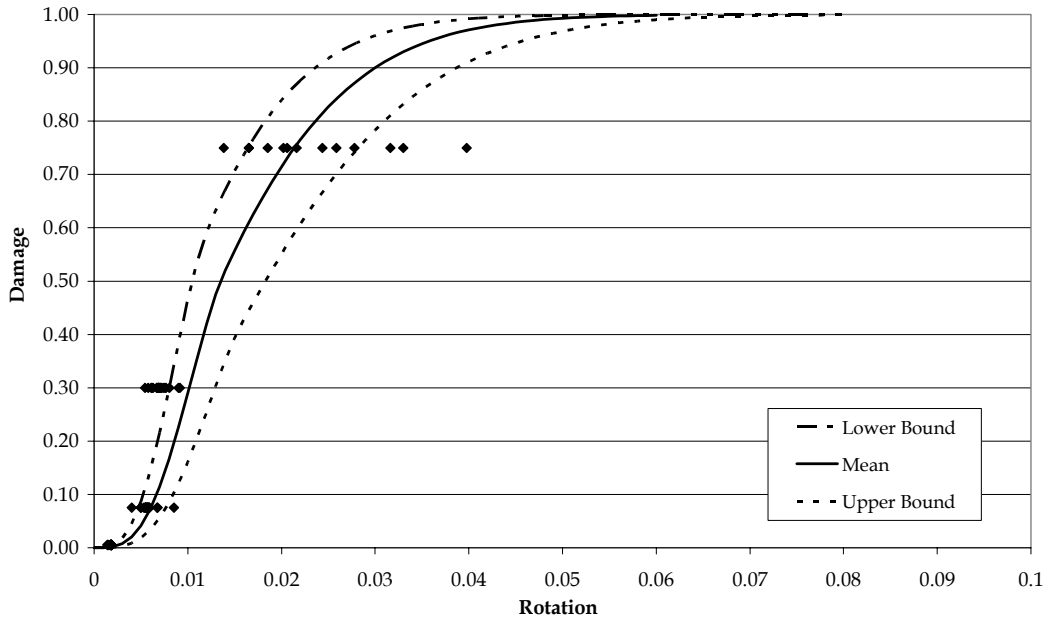
Figure 3.16 - Damage curves for moderate ductility level
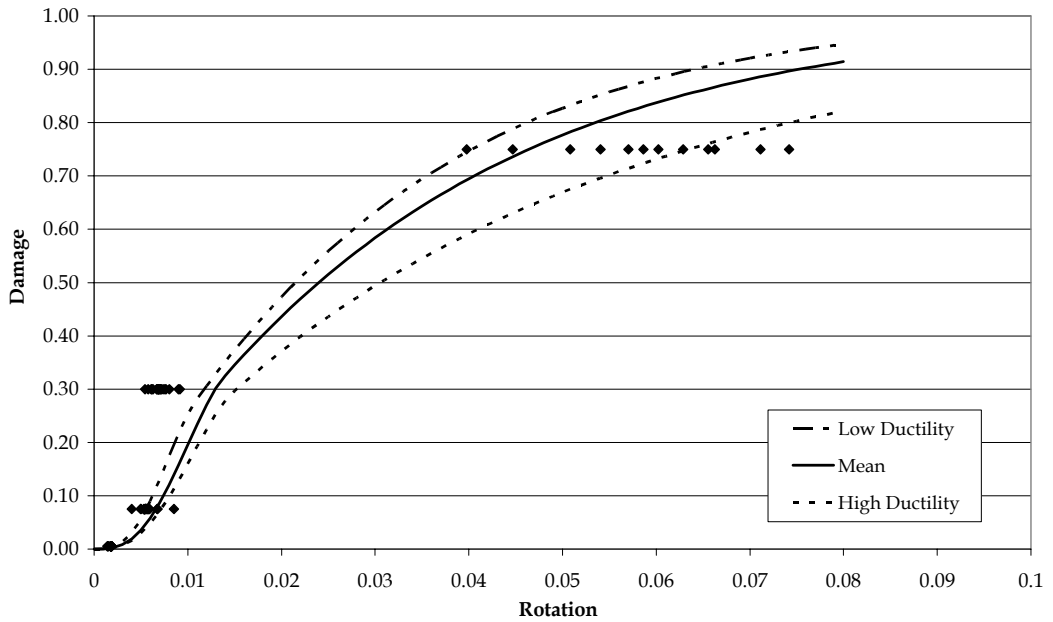
Figure 3.17 - Damage curves for high ductility level

71
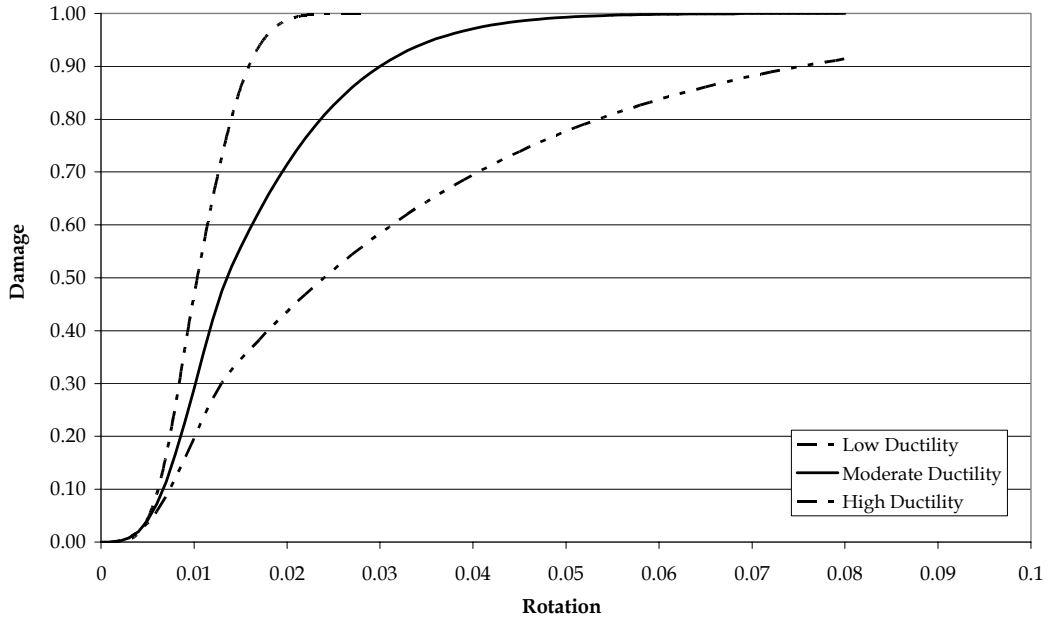
Figure 3.18 – Mean damage curves for all ductility levels

In Figure 3.19 variation of the rotation at which a crack width of 0.2, 1 and 2 mm was observed with the depth of the beam. All the rotation values in this figure were normalized with the corresponding values for a beam of 500 mm depth, for which the damage curves had been developed. The variation in the crack width and hence in the damage level was not so significant for the cases investigated. Then, the curve shown in Figure 3.19 and given in Equation 3.5 was fit.

$$C_d = \left(\frac{d}{500}\right)^{-1.0}$$ (3.5).

where d is the depth of the beam in mm.
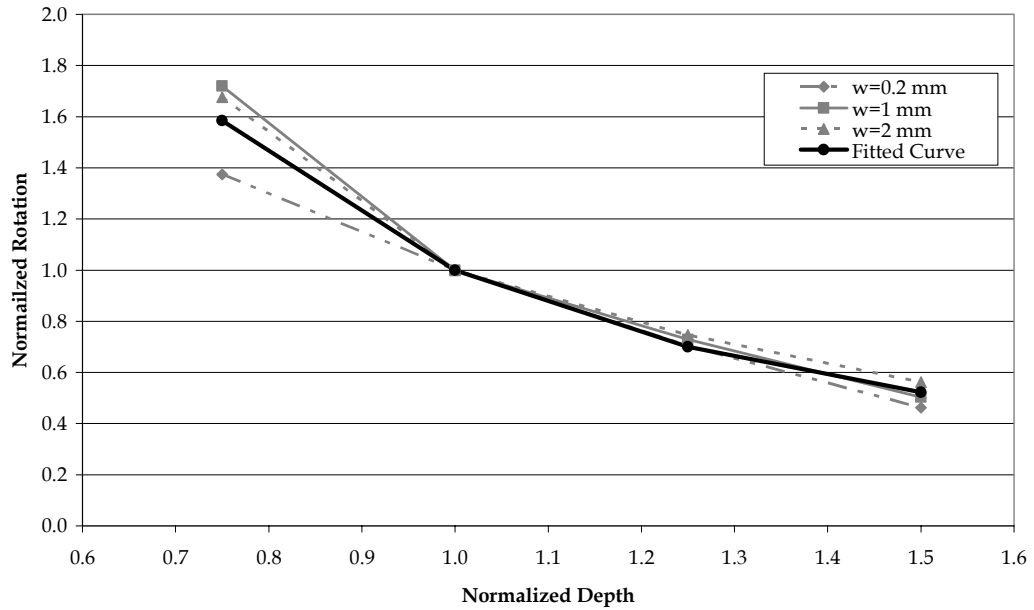
Figure 3.19 – Variation of rotation with depth

If the depth of the beam analyzed is different from 500 mm, then the rotation computed should be divided by the correction factor C_d before entering the damage curves proposed.

3.4.5   Comparison with Experimental Data and Discussion of Results

The developed damage curves for flexure critical reinforced concrete beams were compared with the results of the 25 beams tested by various researchers. The comparison was carried out at the yield and ultimate points as in the case of columns. The test results were also compared with the yield and ultimate chord rotation values computed using the expressions developed by Panagiotakos and Fardis [20] and Priestly [30], which were summarized in section 2.4.5.

The results of this comparison are shown in Table 3.3 and Figures 3.20 and 3.21. In these figures and table, the θ_{y_obs} and $\theta_{y\text{-pred}}$ denotes the observed and predicted yield rotation, respectively, whereas $\theta_{u\text{-obs}}$ and $\theta_{u\text{-pred}}$ are the observed and the predicted ultimate rotation values.

Table 3.3 – Observed and Predicted Yield and Ultimate Rotation Values

		$\theta_{y\text{-obs}}/\theta_{y\_pred}$	$\theta_{u\text{-obs}}/\theta_{u\_pred}$
This Study	Mean	0.89	1.20
	cov	0.25	0.30
Panagiotakos & Fardis (with slip)	Mean	0.64	0.92
	cov	0.32	0.61
Panagiotakos & Fardis (without slip)	Mean	0.77	1.38
	cov	0.38	0.61
Priestly	Mean	0.88	1.54
	cov	0.48	0.45
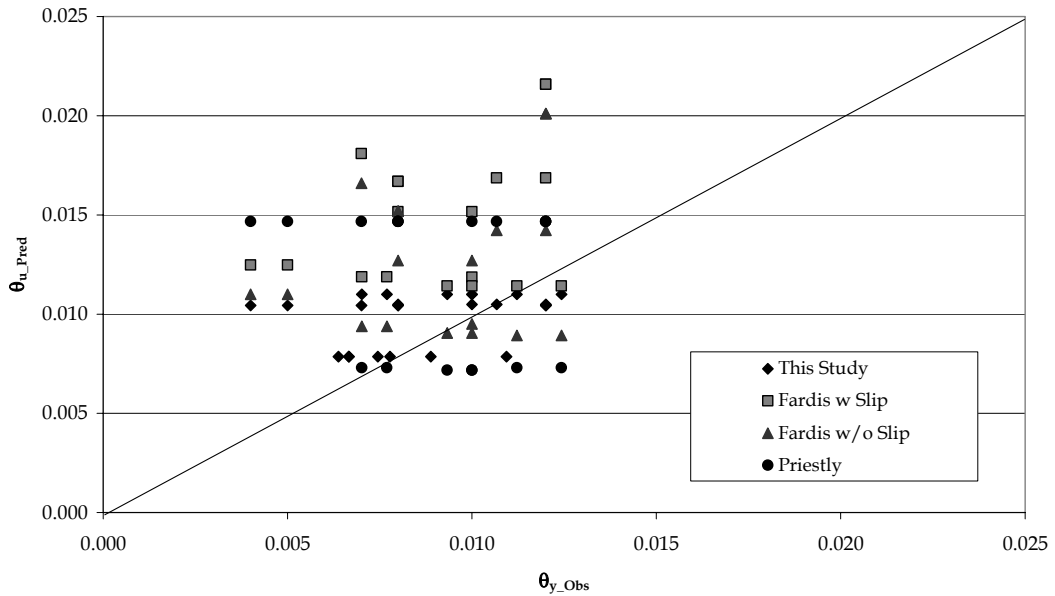
Figure 3.20 – Comparison of observed and predicted yield rotation values

Table 3.3 and Figure 3.20 reveal that all of the methods investigated overestimate the yield rotation values for flexure critical beams. The expression proposed by Panagiotakos and Fardis [20] considering slippage of the reinforcement overestimates the yield rotation value by 36% with a coefficient of variation (cov) of 32%. The developed damage curves and the expression by Priestly [30] give the best estimates for the yield rotation value by an overestimation of 11% and 12%, respectively. However, the variation in case of

Priestly's method is very high with a coefficient of variation of 48%. The coefficient of variation for the developed damage curves is 25%.
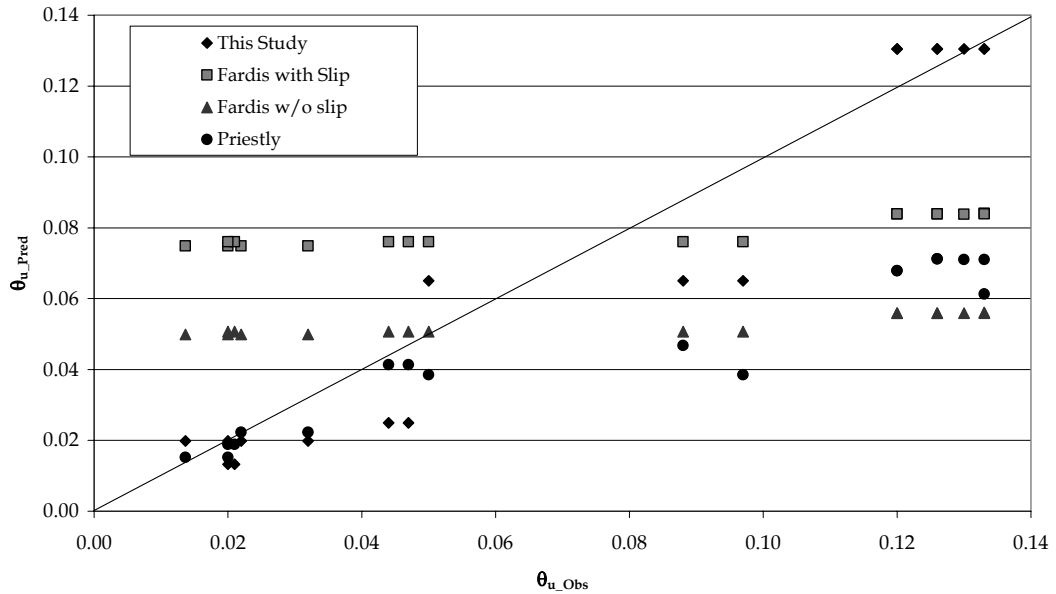
Figure 3.21 - Comparison of observed and predicted ultimate rotation values

For the ultimate rotation value (Figure 3.21), it can be stated that the expression by Panagiotakos and Fardis considering slip [20] gives the best estimate with an overestimation of 8%. However, the coefficient of variation is too high for this expression as well as for the expression neglecting slip (cov=61% in both cases). The developed damage curves underestimate the ultimate rotation value by 20%. The coefficient of variation for the ratio of the observed ultimate rotation to the ultimate rotation predicted by the developed damage curves is 30%, which is considerably less then the coefficient of variation values for the other expressions.

In the light of these discussions, it can be stated that the developed damage curves for the flexure critical beams gives the best estimates for the yield and ultimate rotation values.

3.5 SHEAR CRITICAL BEAMS

3.5.1 Development of the Damage Curve

In the development of the damage curve for shear critical beams, a very similar methodology used in the development of the damage curve for shear critical columns (section 2.4) was used. The nominal shear capacity (V_r) of the beams is computed using the expressions given in TS-500/2000 and summarized in Eqs. 2.21 to 2.23 were used. However, the effect of the gravity loads on the beams must be taken into account in the computation of the flexural shear capacity (V_f) of the beams. As Figure 3.22 implies the flexural shear capacity of a beam is equal to the shear force coming from the gravitational forces (V_g) and sum of the moment capacities of the two ends of the beam divided by the length of the beam (Eq. 3.6)
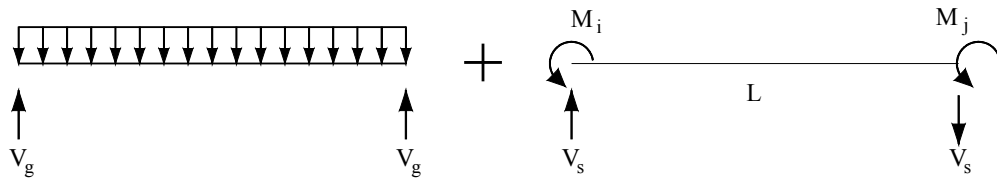
Figure 3.22 – Nominal shear capacity for beams

$$V_f = \frac{M_i + M_j}{L} + V_g \qquad (3.6)$$

As in the case of columns, it was assumed that the ultimate rotation capacity of a beam with a V_r/V_f ratio equal to 1.00 is equal to the yield rotation of the corresponding flexure critical beam. Hence, the damage curve for the low ductility beams were modified so that a damage score of 30% (corresponding to the yield rotation of a beam) now corresponds to a damage score of 90% and the damage curve for the shear critical beams was obtained. Moreover, based on the finite element analyses carried out on the columns, it was assumed that the ultimate rotation capacity of a beam decreases with a decrease in the V_r/V_f ratio

76

of the beam. To be able to take this into account, a correction factor was developed similar to the one developed for the columns (Eq. 2.24). However, in this case the correction factor was taken to be equal to V_r/V_f ratio in order to be conservative since no analyses had been carried out for the shear critical beams (Eq. 3.7).

$$C_v = \frac{V_r}{V_f} \qquad\qquad \frac{V_r}{V_f} \le 1.00 \qquad\qquad (3.7).$$

The final form of the damage function for the shear critical beams is given in Eqs. 3.8 and 3.9 and is shown in Figure 3.23 together with the damage curves for flexure critical beams. The values of the equation parameters for shear critical beams are given in Table 3.3.

$$damage(\theta) = \left[1 - e^{-\left(\frac{\theta}{aC_d C_V}\right)^b} \right] g(\theta) \qquad\qquad (3.8)$$

$$g(\theta) = 0.5 \left[1 - \cos\left(\frac{\pi\theta}{c}\right) \right] \qquad\qquad \text{if } \frac{\theta}{C_d C_V} \le c$$

$$g(\theta) = 1 \qquad\qquad \text{if } \frac{\theta}{C_d C_V} > c \qquad\qquad (3.8)$$
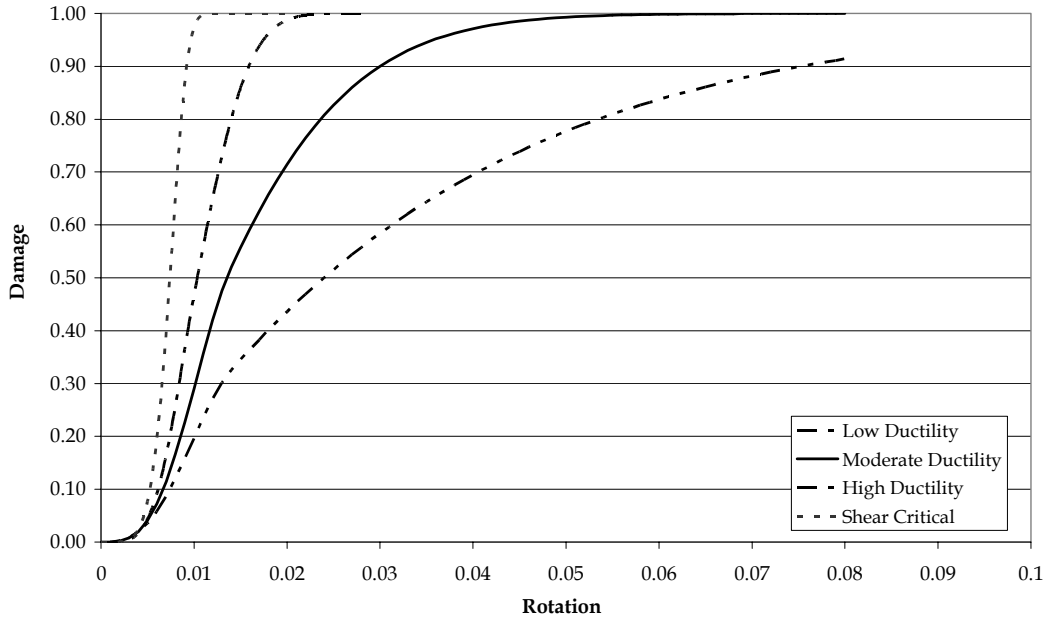
Figure 3.23 – Damage curves for reinforced concrete beams

Table 3.4 – Values of equation parameters for shear critical beams

Parameter	
a	0.0079
b	5.5000
c	0.0010

3.5.2   Comparison with Experimental Data

The ultimate rotation capacity of 9 shear critical beams tested previously by various researchers was compared with the developed damage curves. The comparison was made at the ultimate level which corresponds to a damage score of 90%. The results of this comparison are given in Figure 3.24 and Table 3.5.
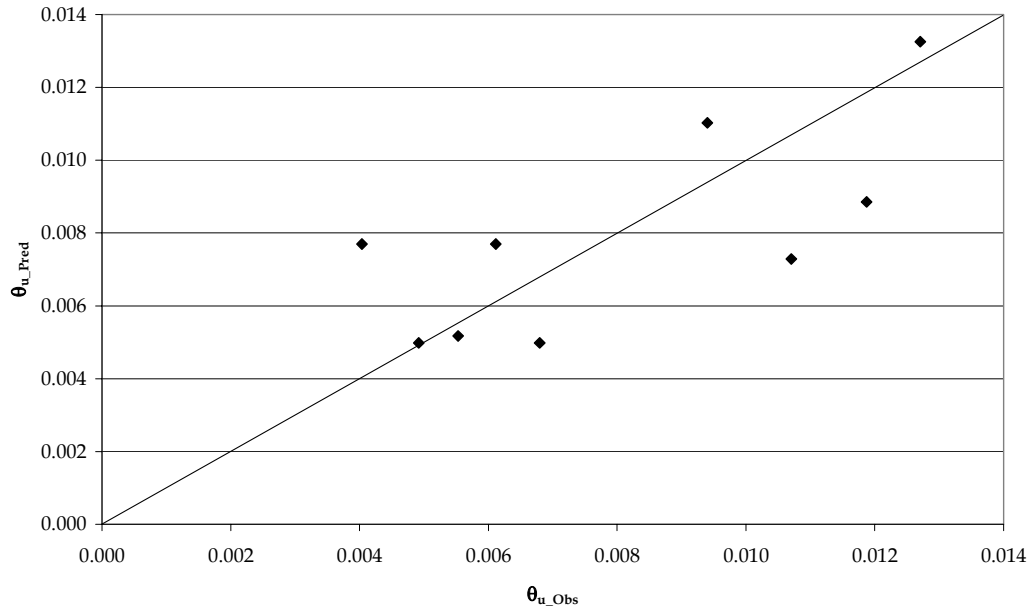
Figure 3.24 – Observed and predicted ultimate rotation values for shear critical beams

Table 3.5 – Comparison of observed and predicted ultimate rotation values for shear critical beams

	$\theta_{u\text{-obs}}/\theta_{u\_pred}$
Mean	1.04
cov	0.29

3.6 ROTATION – DRIFT RELATIONSHIP

In this study, the independent parameter that had been chosen to relate the damage was the drift ratio. However, as explained at the beginning of this chapter, the damage – drift ratio relationship for reinforced concrete beams may vary depending on the structural system, damageability of columns, etc. Thus, the damage curves were developed in terms of the end rotation. Then, rotation – drift relationship of several frames were investigated to relate the damage to the drift ratio. The effect of several parameters on the rotation – drift relationship was investigated by carrying out pushover analyses for each case.   The investigated parameters were the concrete strength, yield strength of longitudinal

79

reinforcement, bay width, story height and beam column capacity ratio (BCCR). Of these parameters only the last one (BCCR) influence the rotation - drift relationship significantly. The other parameters had no significant effect. In this study, beam column capacity ratio is defined as the ratio of the moment capacities of the beams to the moment capacities of the columns adjoining at a joint. In computing the moment capacities of the columns, the axial load on the columns was taken as the one imposed by the gravity loading only.

At the end of the analyses, mainly three curves for the rotation – drift ratio relationship were observed. The first relationship observed was a linear relationship and it was observed for the cases where BCCR value is less than or equal to 0.75 (Figure 3.25). If the BCCR value of a joint is between 0.75 and 1.00, the rotation – drift ratio relationship is bilinear with a certain slope for the second portion (Figure 3.26). If the beam column capacity ratio exceeds 1.00, this relationship is again bilinear, but this time the slope of the second portion is 0.00 (Figure 3.27). Figure 3.28 presents all three relationships derived.
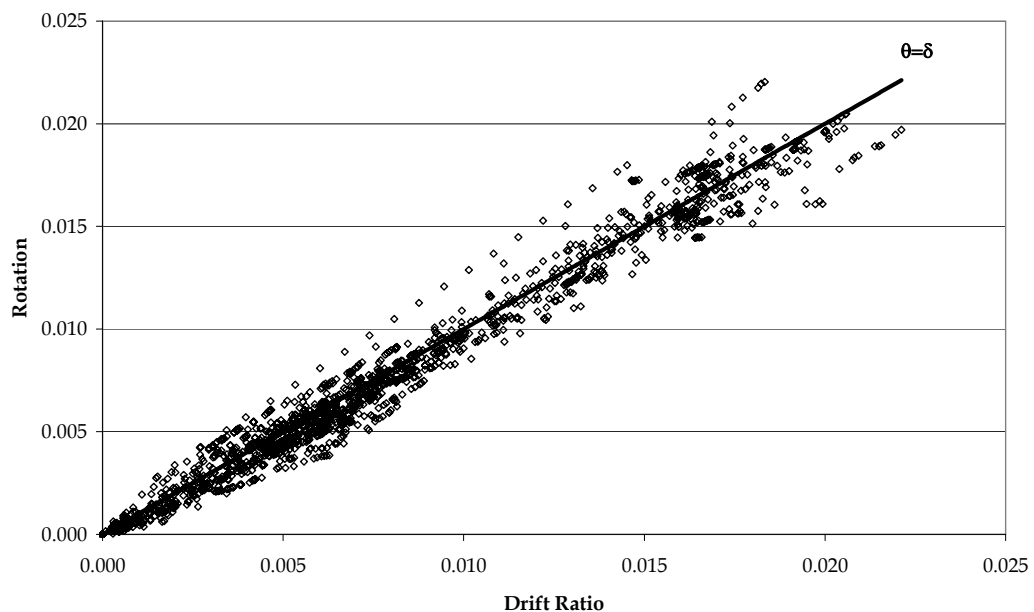
Figure 3.25 – Drift Ratio – Rotation Relationship for BCCR≤0.75
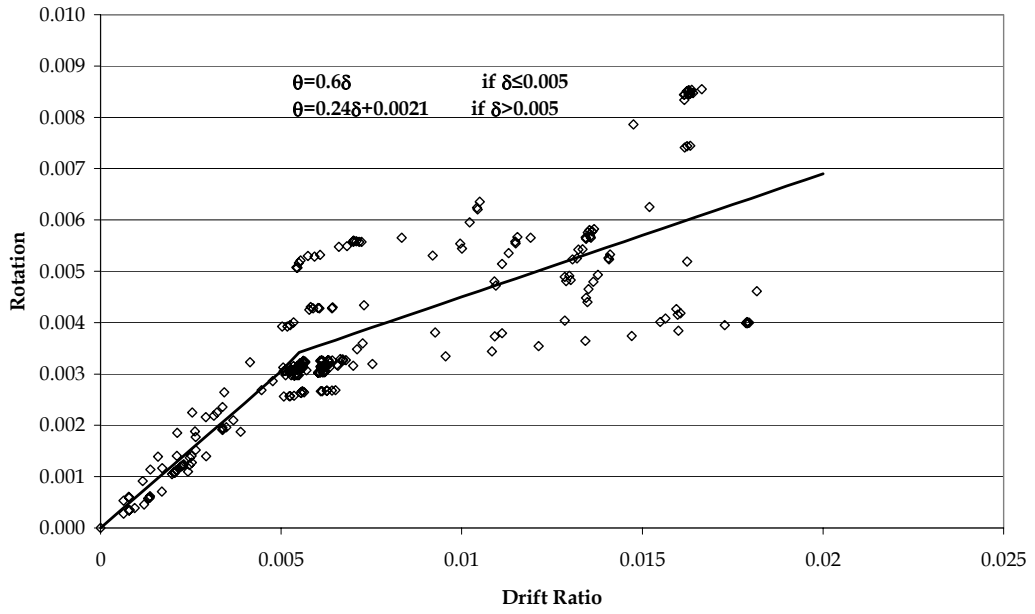
Figure 3.26 - Drift Ratio – Rotation Relationship for 0.75<BCCR≤1.00
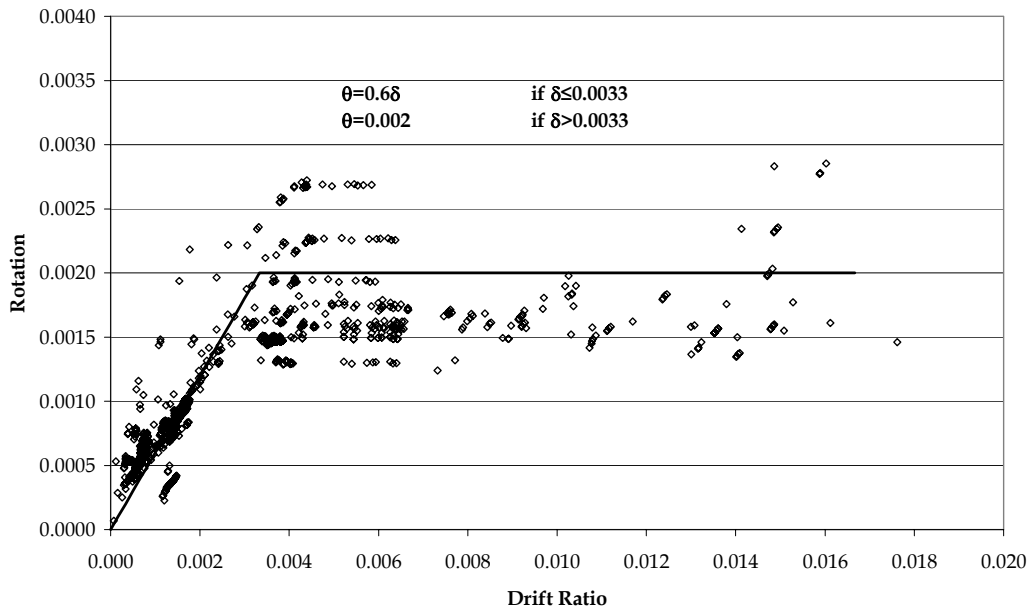
Figure 3.27 - Drift Ratio – Rotation Relationship for BCCR>1.00
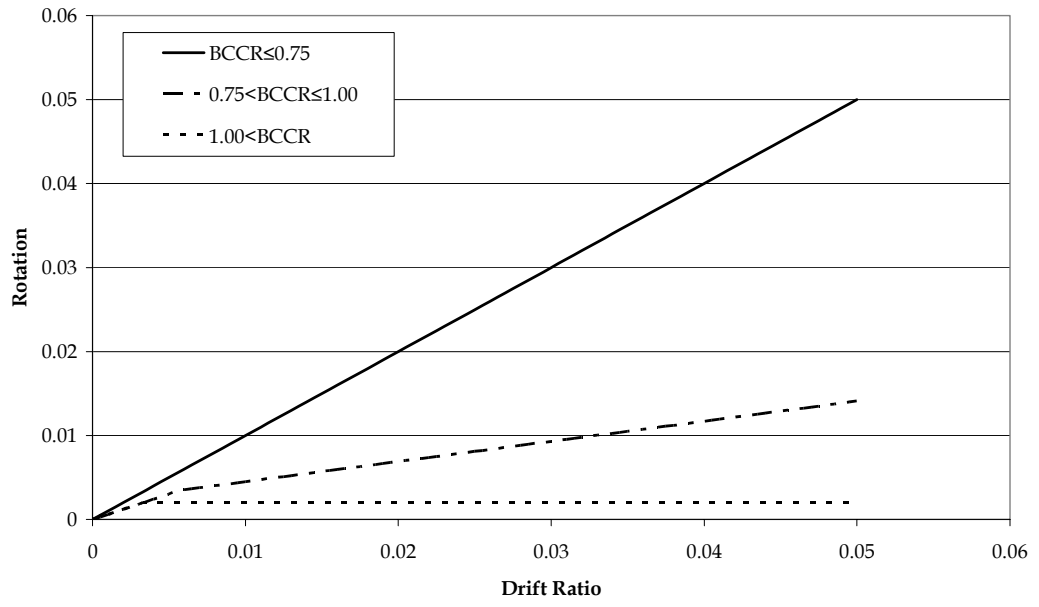
Figure 3.28 – Drift Ratio – Rotation Relationship for all groups

CHAPTER 4

DRIFT BASED DAMAGE FUNCTIONS FOR BRICK INFILLS

4.1 GENERAL

Brick infills are generally treated as non-structural elements and their contribution is neglected in practical design applications. However, intensive research carried out on this subject has revealed that the existence or non-existence of brick infills has significant influence on the seismic behavior of reinforced concrete structures. Hence, in evaluating the seismic vulnerability of brick infilled reinforced concrete structures, the contribution of brick infills must be taken into account. For this purpose, the behavior of brick infills was investigated and damage function for brick infills based on drift ratio were developed.

4.2 EQUIVALENT STRUT MODELS

Modeling of brick infills for seismic analysis is a challenging engineering problem that had been investigated for decades. In 1961 Holmes [39] proposed that the strength and stiffness of a brick infill panel can best be modeled using diagonal compression struts with modulus of elasticity and thickness equal to that of the infill material, and the width equal to one-third of the infill's diagonal length as depicted in Figure 4.1. After this pioneering work, several researchers proposed different expressions for the width of the equivalent compression strength [40, 41, 42]. In this study two of these models, Sucuoglu & McNiven [41]

and Smith [42] models were used. These models will be discussed briefly in the following sections.
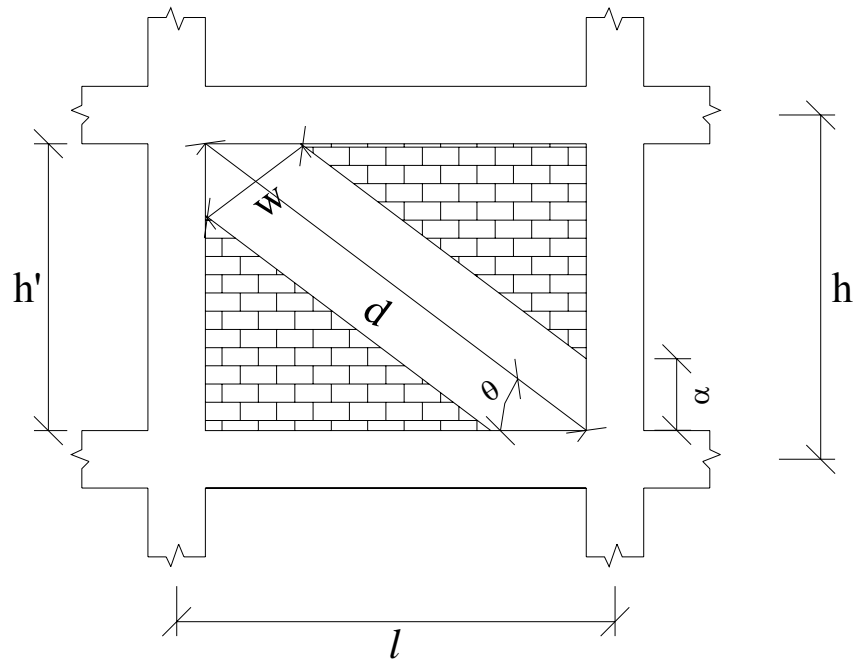
Figure 4.1 – Equivalent Strut Modeling of Infills

Once the equivalent strut width is determined, the second step of modeling the brick infills is the determination of the load-deformation curve for the compression strut. The shape of the load deformation curve given in FEMA-356 [8] and shown in Figure 4.2 represents the behavior of equivalent strut. In this curve there are four critical points (Points 1 to 4 in Figure 4.2). The first one is the point where the strut, hence the infill loses its linearity (yield point). This drift ratio (δ_y) and the axial force level (N_y) is calculated from the related expressions proposed in the equivalent strut model used. The second point is the one that the load carrying capacity of the strut decreases significantly. The amount of this decrease and the corresponding drift ratio locate the points 3 and 2 on Figure 4.2, respectively.   The last point is related to the ultimate drift ratio of the infill and designates the point where the strut loses its load carrying capacity completely.

The points 2, 3, and 4 on Figure 4.2 represent the post yield behavior of the equivalent strut and in general they are determined subjectively.
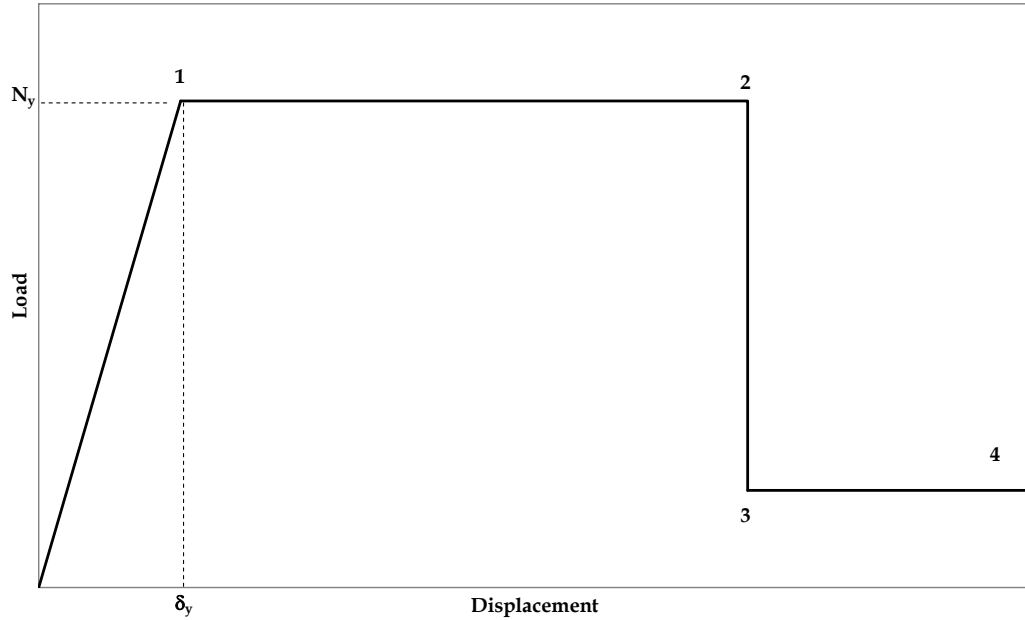
Figure 4.2 – Equivalent Strut Model for the Brick Infills

As indicated before, of the various strut models, the ones proposed by Sucuoğlu & McNiven [41] and Smith [42] were used in this study. The strut models were mainly employed to determine the initial stiffness and the yield drift ratio of the equivalent struts. In other words, the equivalent strut models are used to locate point 1 on Figure 4.2.

4.2.1 Sucuoğlu & McNiven Model [41]

The procedure proposed by Sucuoğlu and McNiven [41] to estimate the properties of the equivalent diagonal struts are summarized in the following paragraphs.

- The shear strength τ_c of a rectangular brick infill may be taken as:

$$\tau_c = \frac{f_c f_t}{1.5(f_c + f_t)} \tag{4.1}$$

where f_c and f_t are compressive and tensile strength of the brick infill panels.

- According to this model, the yield strength of the strut, N_y can be taken as the cracking strength of the panel. Thus, the yield strength of the strut element can be calculated using Equation 4.2.

$$N_y = \tau_c . A_v . \frac{d}{b} \qquad (4.2)$$

In this equation A_v is the shear area, d is the diagonal length, and b is the horizontal length of the infill panel (Figure 4.3).

- The initial stiffness of the bar element can be calculated in terms of shear modulus G, length of the panel b, height h and thickness t using Equation 4.3.

$$k = \frac{G.b.t}{h} \qquad (4.3)$$
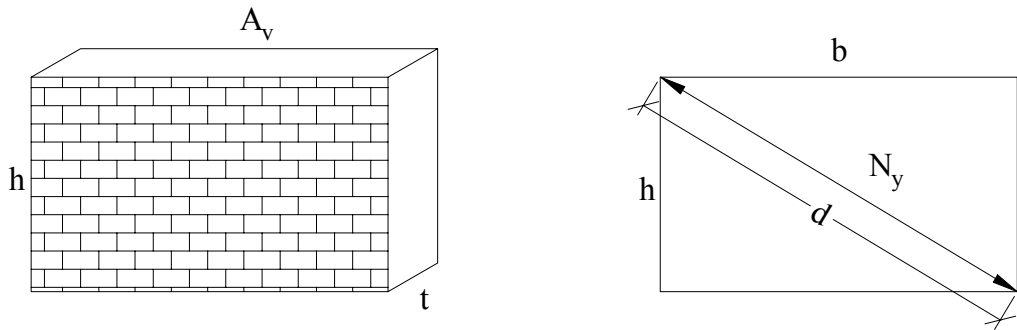
Figure 4.3 – Diagonal Strut representing the infill

- Having determined the initial stiffness and the yield strength of the panel the yield drift ratio of the panel is given as:

$$\delta_y = \frac{1}{h}(\frac{N_y}{k})\cos\theta \qquad (4.4)$$

where;

h: the height of the infill

N_y: yield strength of the infill

k: initial stiffness of the infill

θ: the angle between the direction of the strut and the horizontal.

4.2.2 Smith Model [42]

As a result of his experimental studies, Smith [42] stated that the properties of the axial strut depend not only on the physical and geometrical properties of the infill but also on the length of the contact between the infill and the surrounding frame. The contact length, in turn, depends on the relative stiffness of the infill and the frame members. Smith proposed an empirical equation for the determination of the contact length, α (Equation 4.5):

$$\frac{\alpha}{h} = \frac{\pi}{2\lambda h} \tag{4.5}$$

In this equation h is the column height (Figure 4.1) and λh is a non-dimensional parameter that represents the relative stiffness of the frame to the infill. The expression for the calculation of λ is given as:

$$\lambda = \sqrt[4]{\frac{E_I t \sin 2\theta}{4EIh'}} \tag{4.6}$$

where E_I and t are the modulus of elasticity and thickness of the infill respectively. E and I are the modulus of elasticity and the moment of inertia of the column and h′ is the clear story height.

In the original work, Smith [42] proposed empirical charts for the equivalent strut width, w for various aspect ratios (ratio of the length to the height) of infills. Later, Mainstone [43] proposed an empirical formulation for the equivalent strut width in terms of the non-dimensional parameter, λh (Equation 4.7).

$$w = 0.175(\lambda h)^{-0.4} d \tag{4.7}$$

In this equation d is the diagonal length of the infill. Later this equation was also adopted as the recommended strut width formulation in FEMA 356 [8].

Once the equivalent strut width is determined, the stiffness of the strut can readily be determined by:

$$k = \frac{E_I(tw)}{d} \tag{4.8}$$

Here t is the thickness of the infill and w is the equivalent strut width determined from Equation 4.7.

For the yield strength of the equivalent strut two different failure modes should be investigated: sliding shear failure and compression failure of the diagonal strut. Of these two failure modes, the one giving the lower strength is considered as the most probable failure mode and the strength of the equivalent strut is chosen accordingly. In 1969, Smith and Carta [44] prepared graphs for the determination of strengths of the infills in both modes for corresponding λh values. For the compressive strength Mainstone [43] proposed the formulation given in Equation 4.9.

$$N_{comp} = 0.56(\lambda h)^{-0.875} f_c ht \cot \theta \qquad (4.9)$$

where, N_{comp} is the compressive strength of the infill.

For the calculation of the diagonal shear failure force Paulay & Priestly [45] proposed the following formulation:

$$N_s = \frac{\tau_o}{1 - \mu(h/l)} dt \qquad (4.10)$$

where, N_s is the shear strength of the infill panel, τ_o is the shear strength of the infill material, μ is the coefficient of friction, l is the bay width (measured from the centerline of the columns). Paulay & Priestly [45] suggest that the shear strength of the infill material can be taken to be equal to the 3% of its compressive strength (f_c), and the coefficient of friction is equal to 0.3. Imposing these into Equation 4.10 yields:

$$N_s = \frac{0.03 f_c}{1 - 0.30(h/l)} dt \qquad (4.11)$$

The yield strength of the equivalent strut will be taken as the minimum of the compression and shear strength of the infill panel calculated from equations 4.9 and 4.10; i.e.

$$N_y = \min(N_{comp}, N_s) \qquad (4.12)$$

Once the initial stiffness and the yield strength of the equivalent strut are determined, the yield drift ratio can be determined using equation 4.4.

4.3 DEVELOPMENT OF THE DAMAGE CURVES

Brick infills are brittle materials with a limited plastic displacement capacity. The infills can be assumed to be undamaged until the formation of the first major crack which can be taken to correspond to the yield point of the equivalent strut model. Once the first major crack is formed, the stiffness of the infill panel decreases significantly and the damage level increases drastically till failure. Hence, the point at which the first major crack forms (i. e. the yield point of the equivalent strut model) can be taken as the lower limit of the heavy damage. In other words, the yield drift ratio of the equivalent strut model is assumed to correspond to a damage score of 50% according to the damage criterion used herein.

In this study, a total of 624 infill panels with different properties were modeled using both of the aforementioned models. Once the damage criterion summarized above was adopted, damage score - drift ratio data points were plotted for Sucuoğlu & McNiven [41]and Smith [42] (Figure 4.4) models. When the data set for Sucuoğlu & McNiven model was examined, it was observed that the stiffness of the infill panels was too high resulting in unrealistic equivalent strut widths. As a result, the yield drift ratios obtained using this model were too low resulting in highly conservative damage scores for a given drift ratio. Thus, it can be stated that, the data set developed using Smith Model gives more realistic results. Hence, the rest of the discussion on the damage curves for brick infill panels will be restricted to this model.

As it will be recalled, there were two expressions for the yield strength of the equivalent strut for Smith model. In the post earthquake observations carried out after the recent earthquakes occurred in Turkey, it was observed that most, if not all, of the brick infills failed in compression mode. Therefore, in developing the damage curves, the expression for the compression failure of the equivalent strut (Eq. 4.9) was used.

The closed form solution for the yield drift ratio of the brick infills can be computed using Eqs. 4.4 to 4.9 as:

$$\delta_y = 3.2(\lambda h)^{-0.475} \frac{f_m L^2}{E_I dh} \tag{4.13}$$
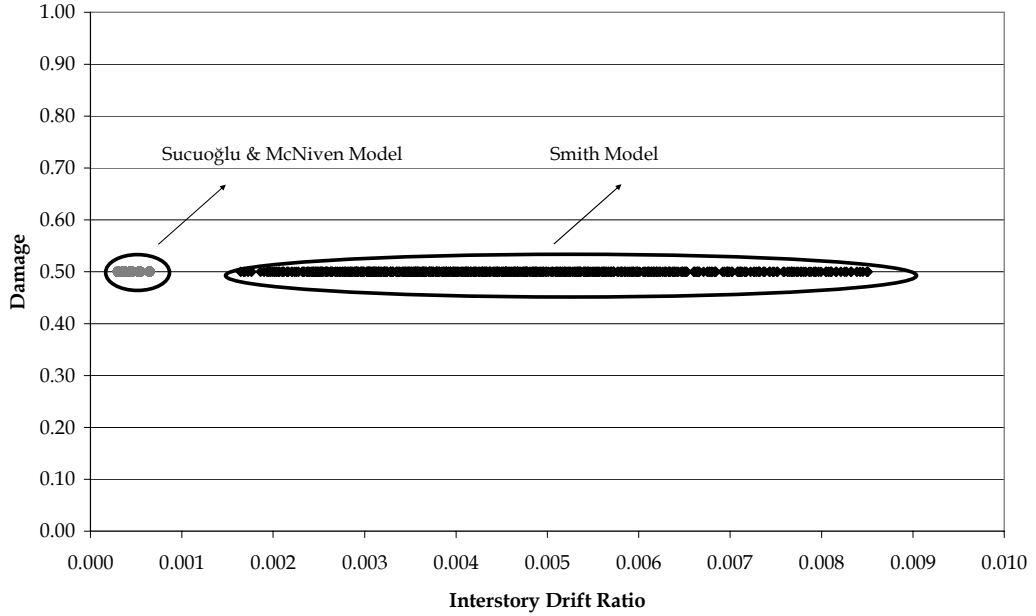
Figure 4.4 – Data Points for both Models

As it can be seen in Figure 4.4, there is a large scatter in the drift ratio vs. damage points for the brick infills analyzed. To refine the data and decrease the amount of scatter, the brick infills were grouped into four. When the closed form expression for the yield drift ratio given in Eq. 4.13 is investigated, it can be stated that, although the first part of the expression $((\lambda h)^{-0.475})$ influences the yield drift ratio of the infills to some extent, the major parameter that affects δ_y is the non-dimensional term, $\frac{f_m L^2}{E_I dh}$. Hence, the analyzed infills were grouped into four according to their $\frac{f_m L^2}{E_I dh}$ values and the classification is summarized in Table 4.1

Table 4.1 – Brick Infill Groups

Group	$\dfrac{f_m L^2}{E_I dh}$ value
1	<0.0015
2	between 0.0015 and 0.0020
3	between 0.0020 and 0.0025
4	<0.0025

Then, the data points were plotted for each group and a damage curve similar to the ones that had been developed for the columns and beams was fit for each group. The equation of the damage function is given in Equations 4.14 and 4.15 and plotted for each group in Figures 4.5 to 4.8. Figure 4.9 shows the damage curves for all 4 groups.

$$f(\delta) = 1 - e^{-\left(\frac{\delta}{a}\right)^b} \tag{4.14}$$

$$g(\delta) = 0.5\left[1 - \cos\left(\frac{\pi\delta}{c}\right)\right] \qquad \text{if } \delta \leq c$$

$$g(\delta) = 1 \qquad \text{if } \delta > c \tag{4.15}$$

In these equations δ is the drift ratio and a, b, and c are the equation parameters that are given in Table 4.3.

Table 4.2 – Values of Equation Parameters for Brick Infills

Par.	Group 1	Group 2	Group 3	Group 4
a	0.0030	0.0042	0.0055	0.0070
b	7.0	10.0	12.0	14.0
c	0.0020	0.0020	0.0020	0.0020
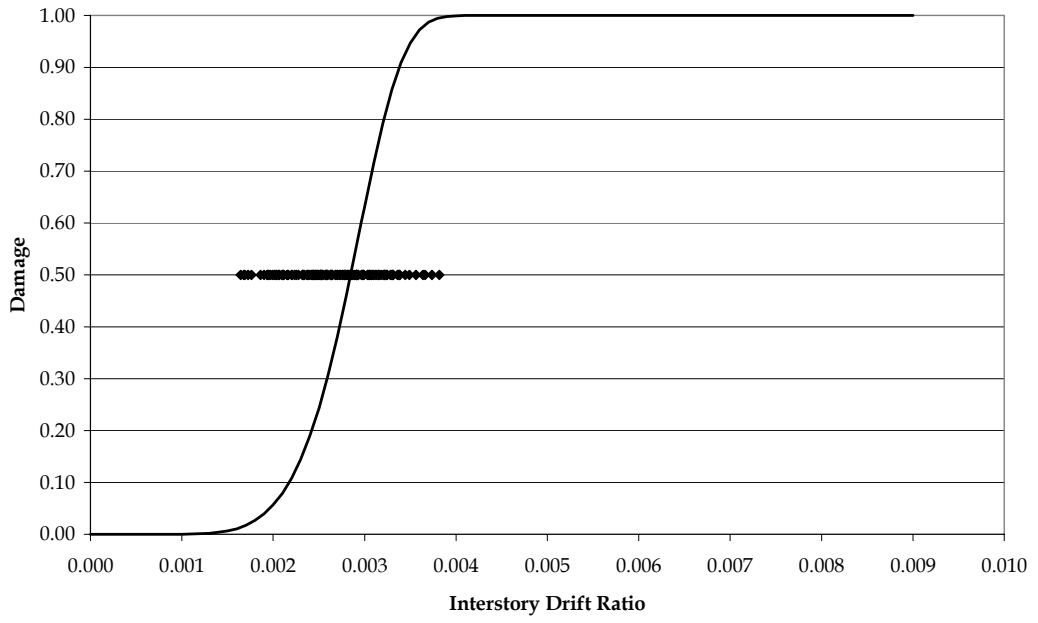
Figure 4.5 – Data Points and the Fitted Damage Curve for Group 1
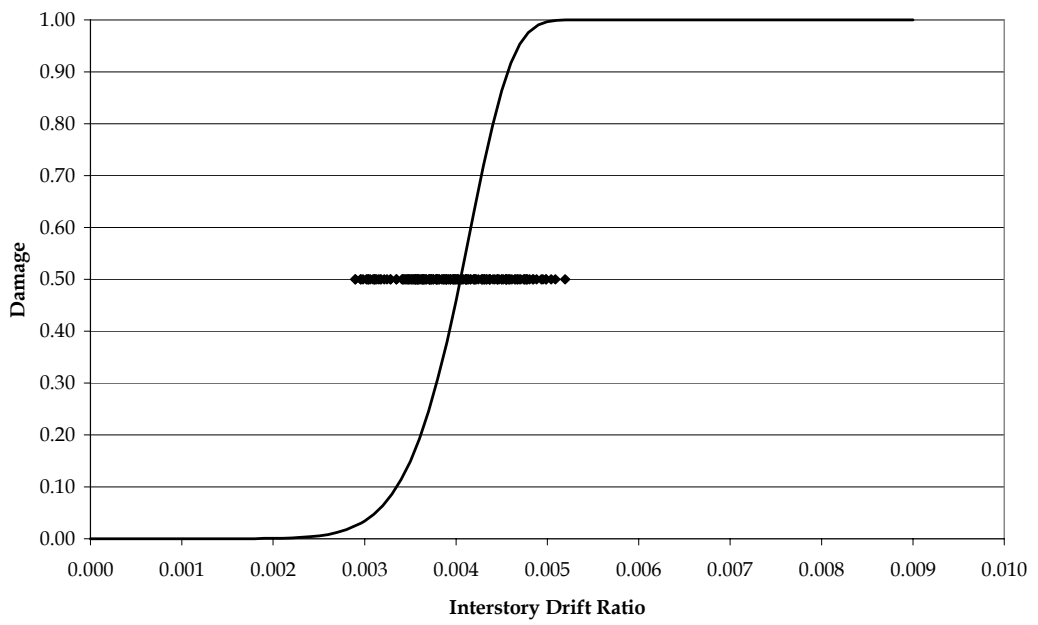
Figure 4.6 - Data Points and the Fitted Damage Curve for Group 2
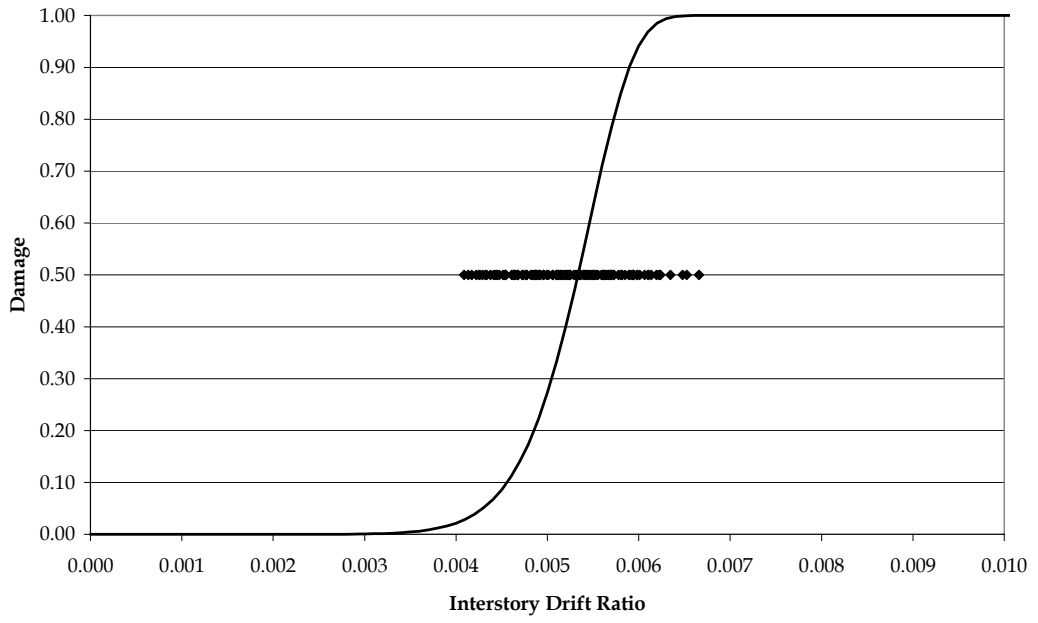
Figure 4.7 - Data Points and the Fitted Damage Curve for Group 3
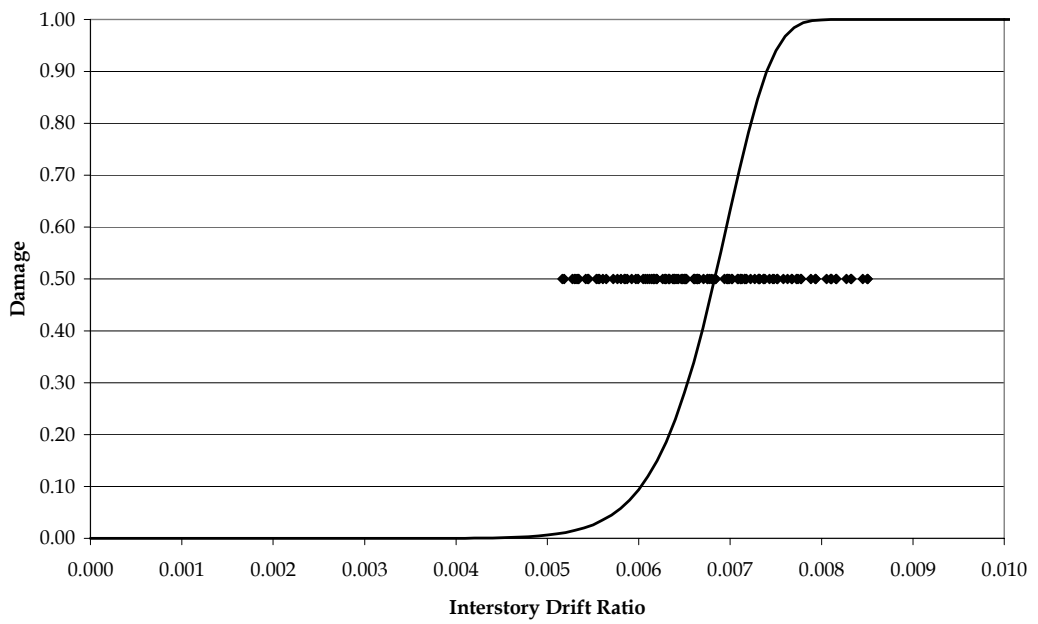
Figure 4.8 - Data Points and the Fitted Damage Curve for Group 4
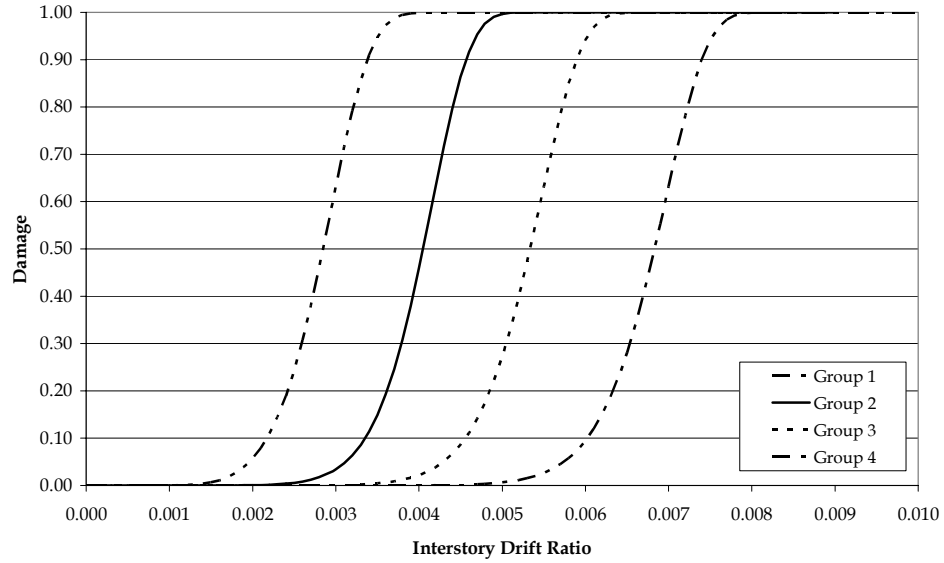
Figure 4.9 – Damage Curves Developed for all Groups of Infills

4.4 COMPARISON WITH EXPERIMENTAL DATA

The developed damage curves were compared with the observed damages in the experiments that had been carried out by several researchers. As summarized in the preceding paragraphs a damage score of 50% corresponds to the formation of the first major crack. The comparison was made at this level and the results of this comparison are given in Table 4.3 and Figure 4.10

Table 4.3 – Comparison of the Developed Damage Curves with the Experimental Data

Test Specimen	$\delta_{y\text{-obs}}$	$\dfrac{f_m L^2}{E_I dh}$	Group	$\delta_{y\text{-pred}}$	$\delta_{y\text{-obs}}/\,\delta_{y\text{-pred}}$
Mehrabi et.al [46]. SP-4	0.0063	0.0029	4	0.0068	0.93
Mehrabi et.al [46]. SP-6	0.0061	0.0030	4	0.0068	0.90
Mehrabi et.al. [46] SP-8	0.0080	0.0023	3	0.0053	1.51
Mehrabi et.al. [46] SP-10	0.0040	0.0050	4	0.0068	0.59
Baran [47] Story 2	0.0035	0.0019	2	0.0041	0.86
Baran [47] Story 1	0.0047	0.0019	2	0.0041	1.16
				Mean	0.99
				COV	0.32
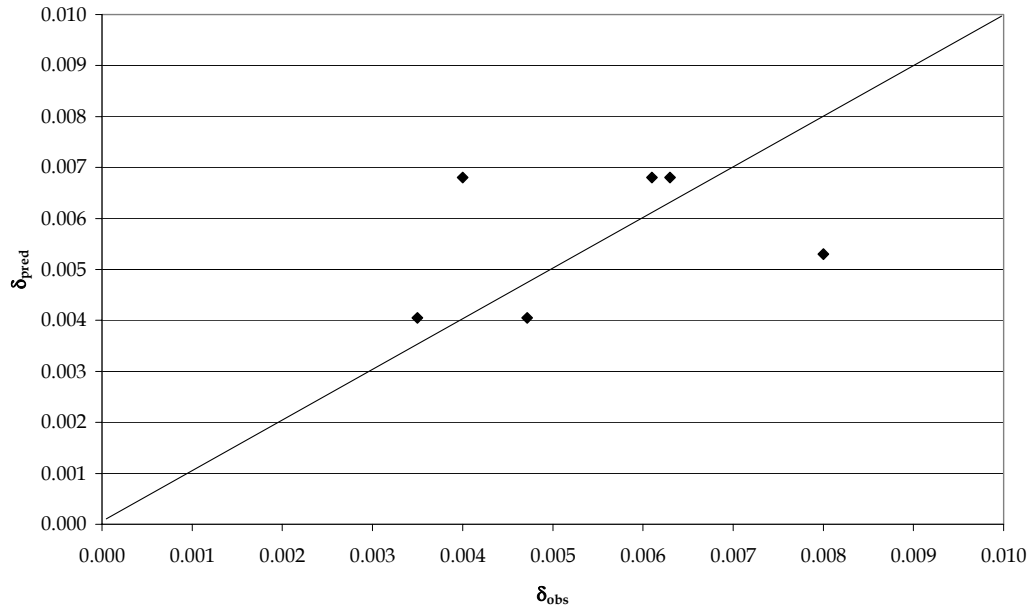
Figure 4.10 - Comparison of the Developed Curves with Experimental

Data

Figure 4.10 and Table 4.3 show that the developed damage curves can predict the behavior of the masonry infills fairly well with a certain variation, which can be seen as reasonable once the damage functions and the related data points given in Figures 4.5 to 4.8 are examined.

CHAPTER 5

DRIFT BASED DAMAGE FUNCTIONS FOR SHEAR WALLS

5.1 GENERAL

The behavior of reinforced concrete structures differs significantly depending on the existence or non-existence of shear walls. The lateral stiffness and strength of shear walls is very high compared to columns and hence they influence the system behavior significantly. Considering this fact, research was carried out to develop drift based damage functions for shear walls to be used for the assessment of reinforced concrete structures with shear walls. The development of the damage functions for shear walls is discussed in this chapter.

5.2 EXPERIMENTAL BEHAVIOR AND PREVIOUS RESEARCH

Numerous experimental and analytical studies had been carried out, in the past to understand the behavior of shear walls. In these studies, researchers tried to develop expressions to estimate the shear strength of walls and to define limit states for the displacement capacities of the walls. In this section, some of these studies will be briefly reviewed.

In the 1997 Uniform Building Code (UBC), concrete compressive strain limits were provided for the design of shear walls. In that document, a maximum compression strain limit of 0.015 was set for the extreme fiber compression strain of the concrete section. In addition to this strain limit, interstory drift ratios were also limited to a value of θ=0.02 or 0.025 depending on the period of the structure. However, in his paper Kowalsky [48] proved that the governing criteria will rarely be the extreme compression strain. Moreover, he stated that the aspect ratio

of a wall (defined as the ratio of the shear span to the depth of the wall) is a very important parameter in the behavior of the shear walls in the sense that the ductility demand of a structural wall varies from 20 for an aspect ratio of 1 to less than 1 for aspect ratios greater than 13. Based on this discussion, he stated that using a constant force reduction and hence a ductility factor does not accurately represent the behavior of walls.

Salonikos [49] stated that the confinement and the longitudinal reinforcement of the edge columns of a shear wall and the web reinforcement should not be considered separately. He observed in the experiments he conducted that, the edge columns' confinement and longitudinal reinforcement contributes to the shear strength at least for shear walls with aspect ratio less than or equal to 1.5. He also observed that the shear crack's inclination and width are considerably decreased close to the confined edge column.

Sittipunt and Wood [50] stated that, although building codes of the United States that were in force in 1995 suggested that the nominal shear strength of slender walls is directly proportional to the amount of horizontal web reinforcement, the behavior they had observed in the thirteen tests carried out by the PCA [51] is not in accordance with this and in most cases increasing only the horizontal reinforcement is not sufficient in preventing the shear failure of the walls. To defend their idea, they published the results of two of these thirteen tests. In these tests, two walls with the same material and geometric properties were tested. The only variable was the horizontal reinforcement. In one case the horizontal reinforcement was 0.63%, whereas it was 1.38% in the second case. Despite the horizontal reinforcement ratio was doubled in the second specimen, the load-deformation behaviors were exactly the same.

In their paper Lefas et. al. [52] had also stated that the horizontal web reinforcement does not have a significant effect on the shear capacity of the shear walls and the main contributor to the shear resistance was observed to be the concrete strength of the compression zone. They claimed that the high shear resistance of the compression zone must be attributed to the development of the triaxial compressive stress conditions.

In 2000, Zhang and Whang [53] stated that the shear-compression ratio ($V_{max}/f_{ck}A_g$; V_{max} is the maximum shear force attained, f_{ck} is the compressive strength of concrete and A_g is the gross cross sectional area) is an important parameter that affects the post-yield behavior of the shear walls.

The individual studies generally include limited number of tests and it was not possible to evaluate the effect of every parameter on the behavior of walls by using the results of a single study. Moreover, when all the tests available in the literature were compiled, it was observed that it was too hard to carry out a systematic study using the results of these tests since the tested walls were not systematically designed. Hence, additional numerical analyses were carried out on shear walls in order to be able to investigate the effect of certain parameters on the behavior of reinforced concrete shear walls.

5.3 NUMERICAL ANALYSES

To investigate the behavior of reinforced concrete shear walls systematically, 89 numerical analyses were carried out in the finite element program ANSYS [33]. As in the case of columns and beams, 8 node brick elements that can take the cracking and crushing of concrete into account were used in the analyses. Both the vertical and the horizontal reinforcement were modeled as smeared throughout the section. These analyses were carried out for different combinations of geometric and material properties. The main parameters that had been investigated within the scope of this dissertation were the aspect ratio of the wall (a/d) defined as the ratio of the shear span ($a=M/V$) to the depth of the cross section (d), compressive strength of concrete (f_{ck}), yield strength of reinforcement (f_{yk}), amount of vertical reinforcement (ρ_v) and the amount of horizontal reinforcement (ρ_h). Table 5.1 summarizes the range of the parameters used in the analyses of shear walls. The effect of axial load on the behavior of shear walls were not taken into account, since they are generally too low compared to the nominal axial load capacity of the wall for the low and mid rise buildings and no axial load was applied on the analyzed walls.

Table 5.1 – Range of the parameters used

f_{ck} (MPa)	a/d	f_{yk} (MPa)	ρ_v (%)	ρ_h (%)
10	1.00	220	0.25	0.00
20	1.50	330	0.45	0.25
30	2.00	420	0.80	0.50
	2.80	550		0.80
		650		1.00
				1.50

The effect of these parameters on the behavior of shear walls was mainly evaluated based on their effect on the failure mode of the shear walls. In general, it can be stated that there are three major failure modes of shear walls. The first mode is pure shear where the wall fails in shear before developing the flexural shear capacity. This type of failure is generally observed in squat walls.The second failure mode is pure flexure. In this mode, the behavior of the wall is dominated by the flexural behavior and the effect of shear on the overall behavior can be neglected. Slender shear walls generally exhibit a flexural failure. The third failure mode is a combined mode of these two modes, which is generally named as flexure-shear. In this failure mode, the behavior of the wall is affected by both the flexural and shear behavior and the element fails in shear after flexural yielding. Figure 5.1 shows the schematic view of the crack patterns of the walls failing in shear, flexure and flexure shear.
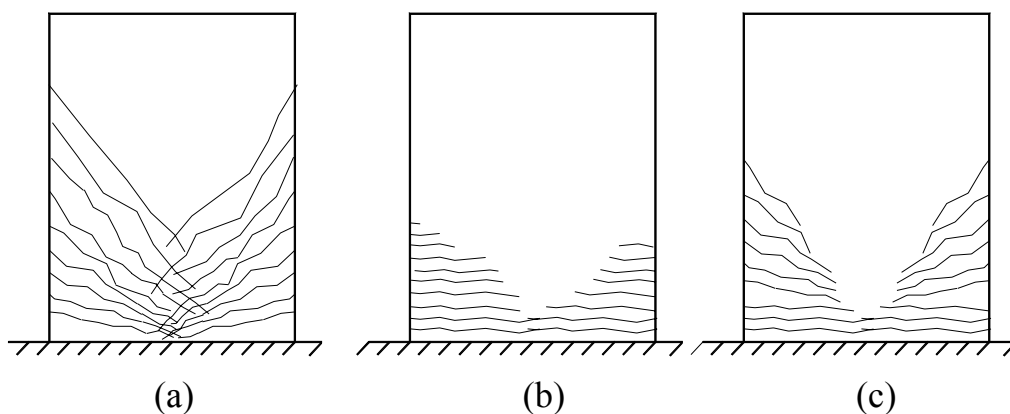
Figure 5.1 – Schematic view of the crack patterns of (a) shear critical (b) flexure critical (c) flexure shear critical walls

To distinguish the failure mode of the shear walls, FEMA 356 [8] uses a criteria based solely on the aspect ratio of the wall (a/d ratio). According to FEMA 356 [8], the walls with an aspect ratio less than 1.5 fail in shear. On the other hand, if the aspect ratio of the wall exceeds 3.0, the wall is named to be slender and the expected predominant failure mode for this type of walls is flexure. If the aspect ratio of the wall is between 1.5 and 3.0, FEMA 356 [8] states that the behavior of these walls is influenced by both shear and flexure.

In her work, Wood [54] defines a shear stress index for the identification of shear and flexural critical shear walls. The shear stress index is the ratio of the maximum attained shear stress (υ_{max}) (Eq. 5.1) to the nominal shear stress capacity of the wall computed using the formula given in ACI 318-83 [55] (υ_c) (Eq 5.2).

$$\upsilon_{max} = \frac{V_{max}}{b_w h} \tag{5.1}$$

In equation 5.1, V_{max} is the maximum shear force carried by a shear wall, b_w is the width and h is the height of the cross-section.

$$\upsilon_c = \frac{\sqrt{f_{ck}}}{6} + \rho_n f_{yk} \tag{5.2}$$

where, f_{ck} is the compressive strength of concrete, ρ_n and f_{yk} are the volumetric ratio and the yield strength of the horizontal reinforcement, respectively. Wood expressed that, 24 of the 37 shear walls she had investigated failed in shear and 20 of these had developed a shear stress index ($\upsilon_{max}/\upsilon_c$) greater than 0.75. Moreover, of the 13 walls that had failed in flexure 12 of them developed a shear stress index less than 0.75.

As a result of the numerical analyses carried out, it was observed that the criterion set by FEMA 356 [8] and Wood [54] were not very effective in distinguishing the failure modes of the analyzed walls. This observation will be discussed in more detail in the forthcoming paragraphs.

In order to identify the failure mode of the analyzed walls, the load-deformation curves of the walls were examined together with the crack patterns at the ultimate stage. If the load-deformation curve of a wall shows that the wall fails before the flexural yielding occurs and the crack pattern shows that severe inclined cracks form in the wall, then the failure mode of the wall is considered to

be shear. Figures 5.2 and 5.3 show the load-deformation curve and the crack pattern of a shear critical wall, respectively. If the load-deformation curve of the wall shows a certain ductility level (μ≥3) (Figure 5.4) and the cracks forming in the wall are limited to horizontal flexural cracks (Figure 5.5), then the predominant failure mode of the wall is stated to be flexure. If a wall fails after the flexural yielding, but the deformation capacity is low (μ<3) and the horizontal flexural cracks are accompanied by inclined cracks, then it can be stated that both the flexural and the shear effect influences the behavior of the wall and the predominant failure mode of the wall is deemed to be flexure-shear (combined). The ductility limit of 3 was assumed to distinguish the flexure and flexure shear critical walls based on the crack patterns of the walls. In general, if the ultimate ductility of a wall is greater than 3, no significant inclined cracks were observed at the ultimate stage. However, when the ultimate ductility of a wall decreases below 3, the horizontal cracks were observed to be accompanied by significant inclined cracking indicating that the behavior of the wall was influenced by both flexural and shear effects. The load-deformation curve and the crack pattern of a flexure-shear critical wall are given in Figures 5.6 and 5.7, respectively.
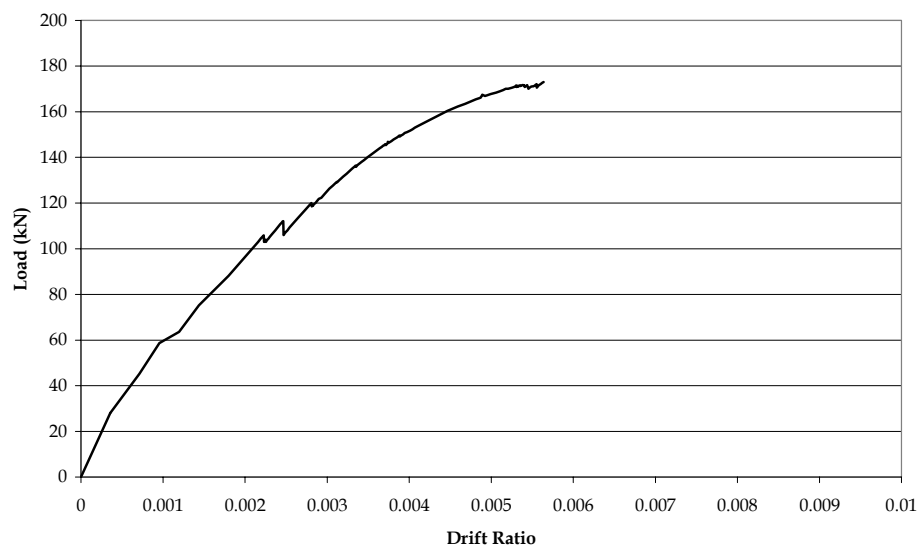
Figure 5.2 – Typical load-deformation response of a shear critical shear wall

101
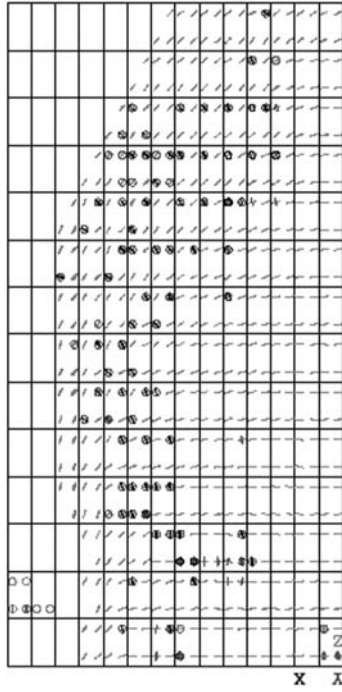
Figure 5.3 – Crack pattern of a shear critical shear wall
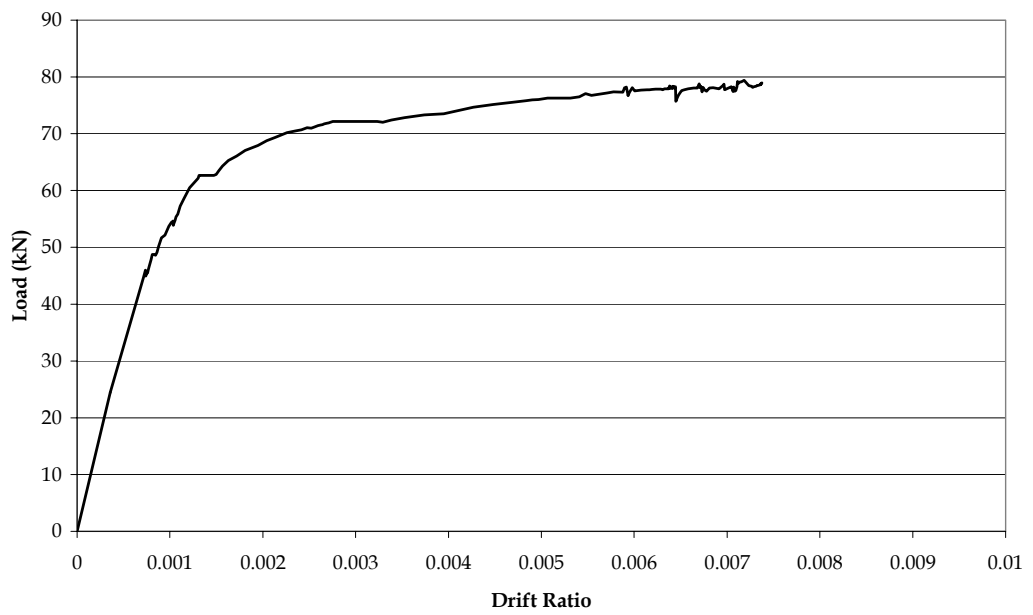
Figure 5.4 - Typical load-deformation response of a flexure critical shear wall
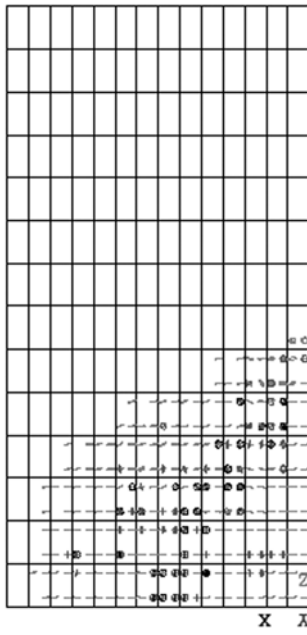
Figure 5.5 – Crack pattern of a flexure critical shear wall
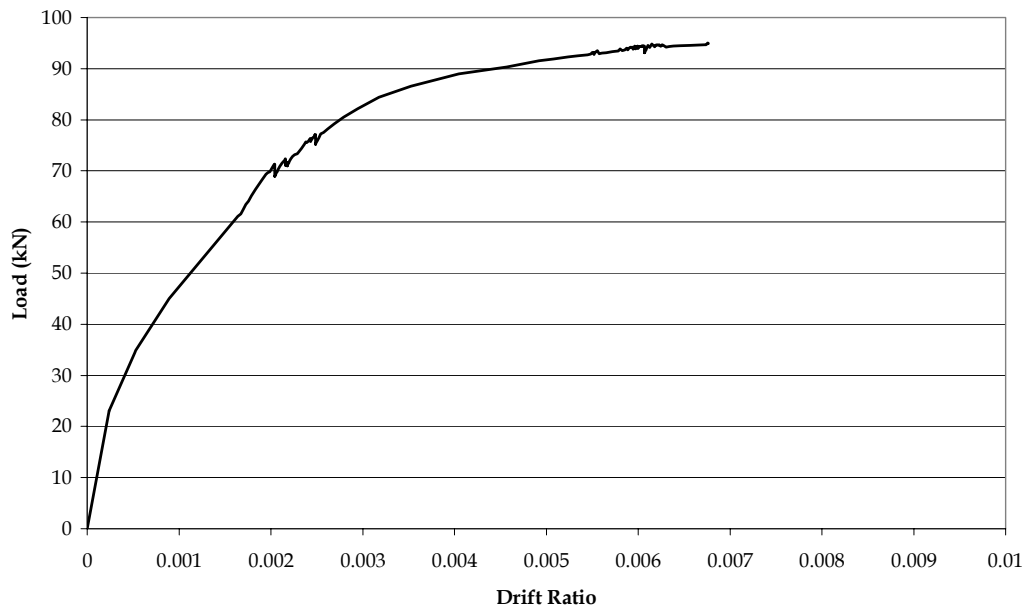
Figure 5.6 - Typical load-deformation response of a flexure-shear critical
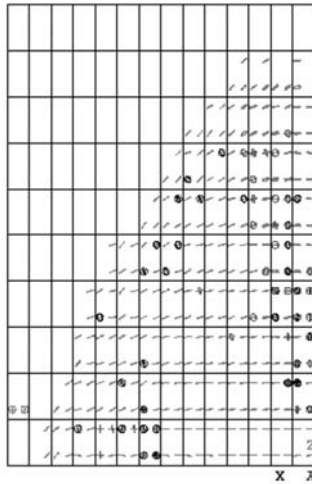
shear wall

Figure 5.7 – Crack pattern of a flexure-shear critical shear wall

In the following paragraphs, the effect of each parameter on the behavior of reinforced concrete shear walls will be discussed briefly through numerical analysis.

5.3.1 Aspect Ratio (a/d)

The aspect ratio of a shear wall is defined as the ratio of the shear span to the depth of the cross section of the wall. As mentioned in the preceding paragraphs, FEMA 356 [8] treats this parameter as the only parameter that affects the predominant failure mode of the shear walls. Figure 5.8 shows the load-deformation curves of four shear walls with different aspect ratios obtained from the numerical analyses. Figure 5.8 clearly indicates that the ductility of the shear walls increases significantly with an increase in the aspect ratio given that all other parameters are constant. Hence, looking at the capacity curves it can be stated that the failure mode of a shear wall shifts from flexure to shear as the aspect ratio of the wall decreases.
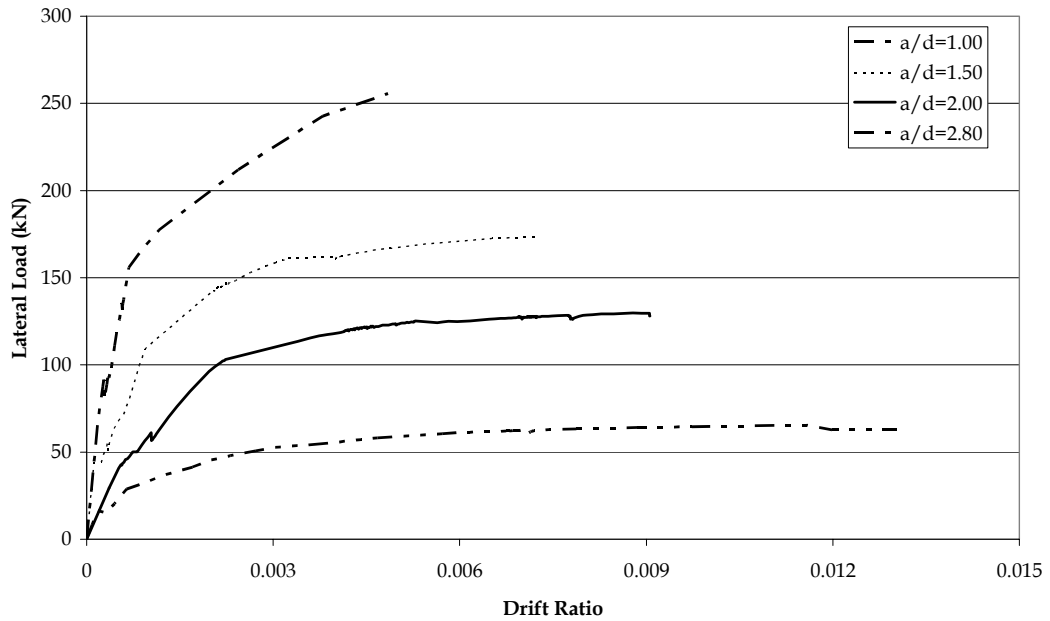
Figure 5.8 – Effect of aspect ratio on the capacity curves of shear walls

5.3.2   Compressive Strength of Concrete (f_{ck})

In order to investigate the effect of concrete strength on the behavior of shear walls, three walls with an aspect ratio of 1.5 were analyzed for different concrete strengths. The vertical and horizontal reinforcement ratios were both 0.45% for all walls. The capacity curves given in Figure 5.9 for different concrete strengths show that the ultimate ductility of the shear walls increase with the increase in f_{ck}. This increase may directly be related to the increase in the tensile strength of concrete with f_{ck} which is a major parameter that affects the nominal shear strength of shear walls.

5.3.3   Yield Strength of Reinforcement (f_{yk})

The effect of yield strength of reinforcement on the behavior of shear walls was investigated by analyzing five shear walls with f_{yk} of 220 MPa, 330 MPa, 420 MPa, 550 MPa, and 650 MPa. Figure 5.10 shows the capacity curves obtained as a result of these analyses. These curves indicate that the ductility of the walls

decreases significantly with the increase in f_{yk}. Hence, as the yield strength of reinforcement increases, the behavior of the wall shifts from flexure to shear.
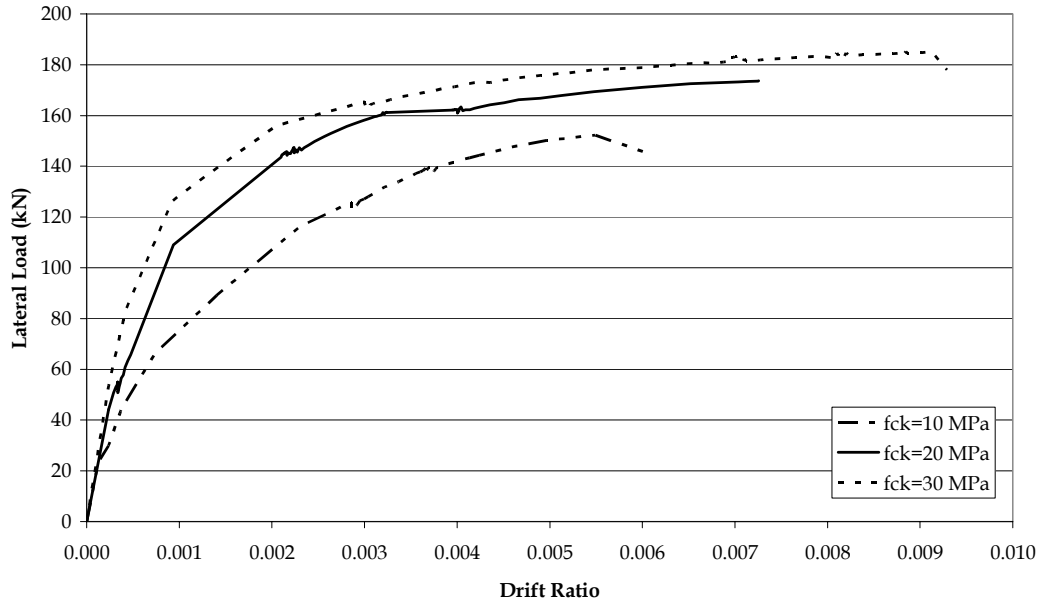
Figure 5.9 - Effect of concrete strength on the capacity curves of shear walls

5.3.4   Amount of Vertical Reinforcement (ρ_v)

To investigate the effect of amount of vertical reinforcement on the damageability of shear walls, three analyses were carried out on a shear wall with an aspect ratio of 1.5. The amount of vertical reinforcement varied between 0.25%, 0.45% and 0.80%. The capacity curves plotted in Figure 5.11 reveal that, as the amount of vertical reinforcement increases, the ductility of the wall tends to decrease since, with increasing ρ_v the flexural shear capacity of the wall increases and the predominant failure mode shifts towards shear. The crack patterns of the analyzed walls also show that the behavior of the walls tends to shift from flexure to shear as ρ_v increases.

106
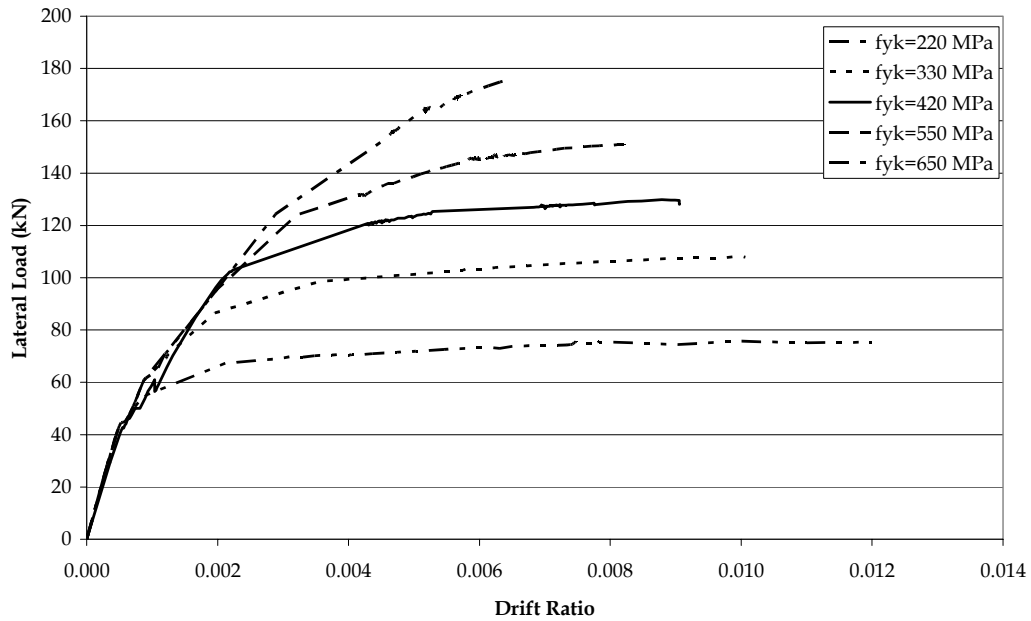
Figure 5.10 - Effect of yield strength of reinforcement on the capacity curves of shear walls

5.3.5 Amount of Horizontal Reinforcement (ρ_h)

A series of finite element analyses were carried out on a shear wall with an aspect ratio of 1.5 to study the effect of ρ_h on the behavior of shear walls. The results plotted in Figure 5.12 show that the influence of horizontal reinforcement on the behavior of shear walls is insignificant provided that all the other parameters are kept constant. This observation is in accordance with the test results of Lefas et. al. [52], who stated that the contribution of horizontal reinforcement on the nominal shear strength of shear walls is negligible and the main parameters contributing to the shear strength of a wall are the shear area and the concrete strength.
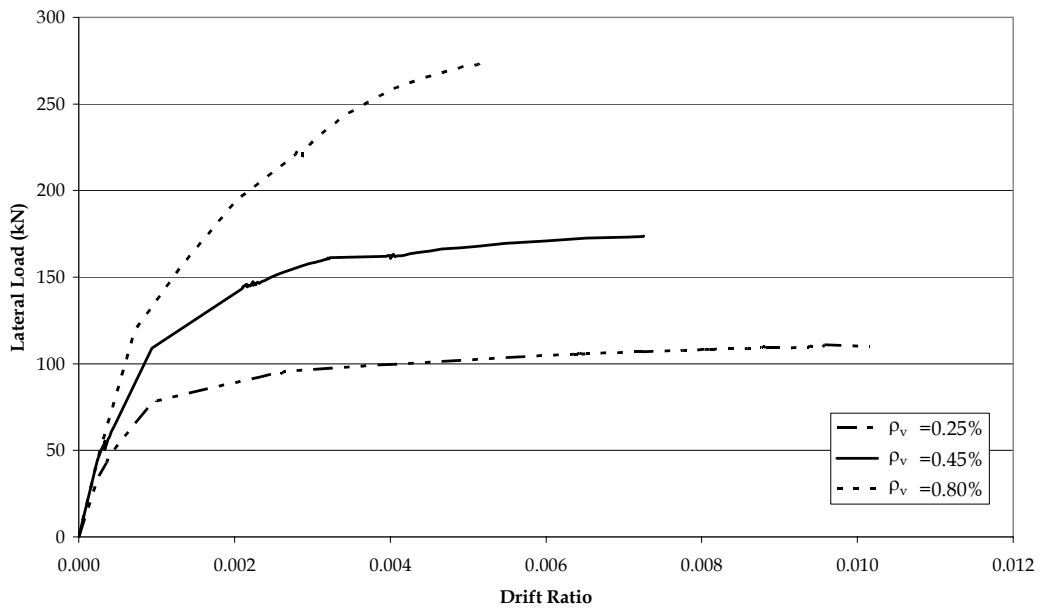
Figure 5.11 - Effect of amount of vertical reinforcement on the capacity curves of shear walls
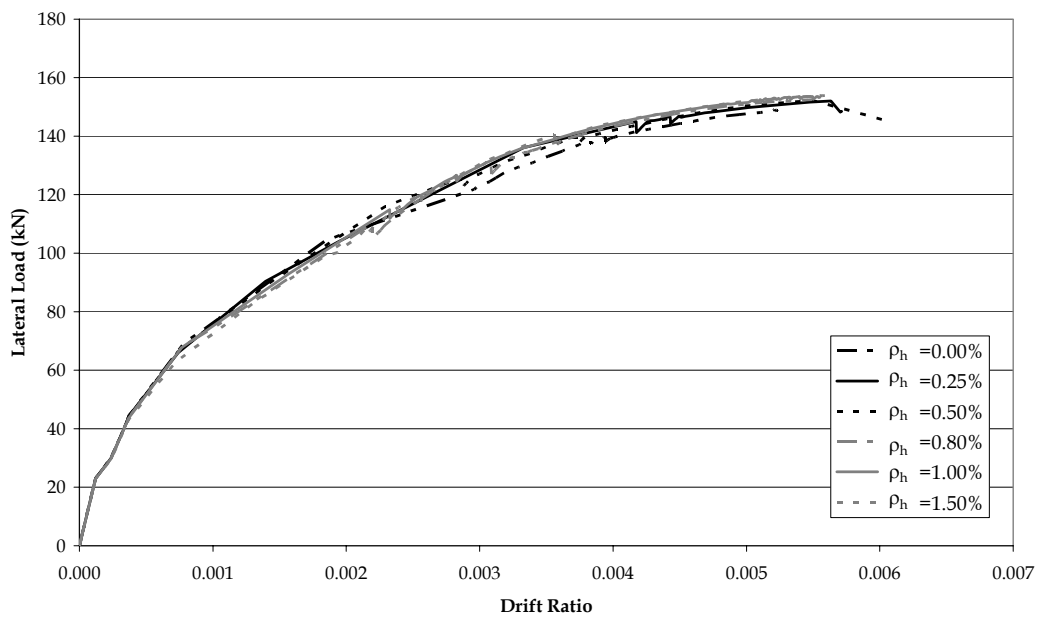
Figure 5.12 - Effect of amount of horizontal reinforcement on the capacity curves of shear walls

108

5.4 SIGNIFICANT PARAMETERS

The effect of certain parameters, namely the aspect ratio, compressive strength of concrete (f_{ck}), yield strength of reinforcement (f_{yk}), amount of vertical (ρ_v) and horizontal reinforcement (ρ_h) on the damageability of shear walls was investigated using the results of the finite element analyses carried out. Of the investigated parameters, the effect of the amount of horizontal reinforcement (ρ_h) was found to be insignificant. All the other parameters influence the behavior of the shear walls significantly. As it was summarized in the previous paragraphs, the ductility of the shear walls decreases with an increase in the amount of vertical reinforcement (ρ_v), yield strength of reinforcement (f_{yk}) and with a decrease in the aspect ratio (a/d). It is noticeable that an increase in ρ_v and f_{yk} and a decrease in a/d results in an increase in the flexural shear capacity (V_f) of the wall, which is defined as the ratio of the moment capacity to the shear span of the wall. When the flexural shear capacity of a member increases without a significant change in the nominal shear capacity (V_n) of that member, the predominant failure mode of the member starts to shift from flexure to shear.

The other parameter that affects the behavior of the shear walls is the concrete strength. With an increase in the f_{ck}, the ductility of the wall tends to increase. This may be attributed to the increase in the tensile strength and hence the shear strength of the member. The results indicate that, although the flexural shear capacity increases to some extent with the concrete strength, the increase in the nominal shear capacity due to the increase in f_{ck} is much more pronounced. Thus, the behavior of the wall starts to shift from shear to flexure with an increase in the concrete strength.

In light of this discussion, it can be stated that the ductility and the predominant failure mode of shear walls depend on the value of the flexural shear capacity of the wall with respect to the nominal shear capacity of the wall. The nominal shear capacity of a wall is directly proportional to the product of width (b_w) and depth (d) of the wall and the square root of the concrete strength ($\sqrt{f_{ck}}$). Hence, a new term, defined as the ratio of the flexural shear strength (V_f) to the product, $b_w d \sqrt{f_{ck}}$ is introduced. This term was used to identify the

expected predominant failure mode of the shear walls. In order to test the validity of this parameter, the $\dfrac{V_f}{b_w d \sqrt{f_{ck}}}$ value for all the analyzed walls were computed and plotted against the mode of failure. This plot is given in Figure 5.13. In this plot, a value of 1 corresponds to a failure mode of flexure whereas the values 2 and 3 correspond to the flexure-shear and shear modes, respectively.
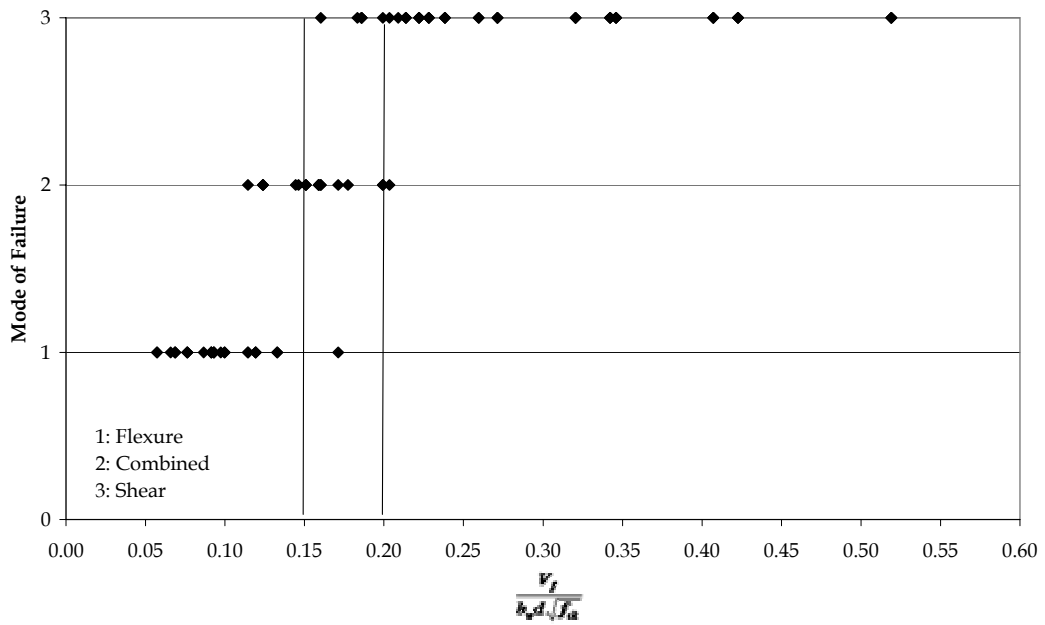
Figure 5.13 – Failure modes and the corresponding $V_f / (b_w d \sqrt{f_{ck}})$ values of the analyzed walls

When the analyses results were examined, it was observed that, of the 43 walls failed in shear, 37 of them developed a $\dfrac{V_f}{b_w d \sqrt{f_{ck}}}$ value higher than 0.20. Moreover, the $\dfrac{V_f}{b_w d \sqrt{f_{ck}}}$ value of the 26 of the 27 walls that had failed in flexure did not exceed 0.15. Finally, the $\dfrac{V_f}{b_w d \sqrt{f_{ck}}}$ value for the 12 of the 19 walls failed in combined flexure – shear mode was between 0.15 and 0.20.

110

The mode of failure of the analyzed walls was also plotted against the corresponding $\upsilon_{max}/\upsilon_c$ values, which was stated to be a possible criterion to distinguish the mode of failure of shear walls by Wood [54] (Figure 5.14).
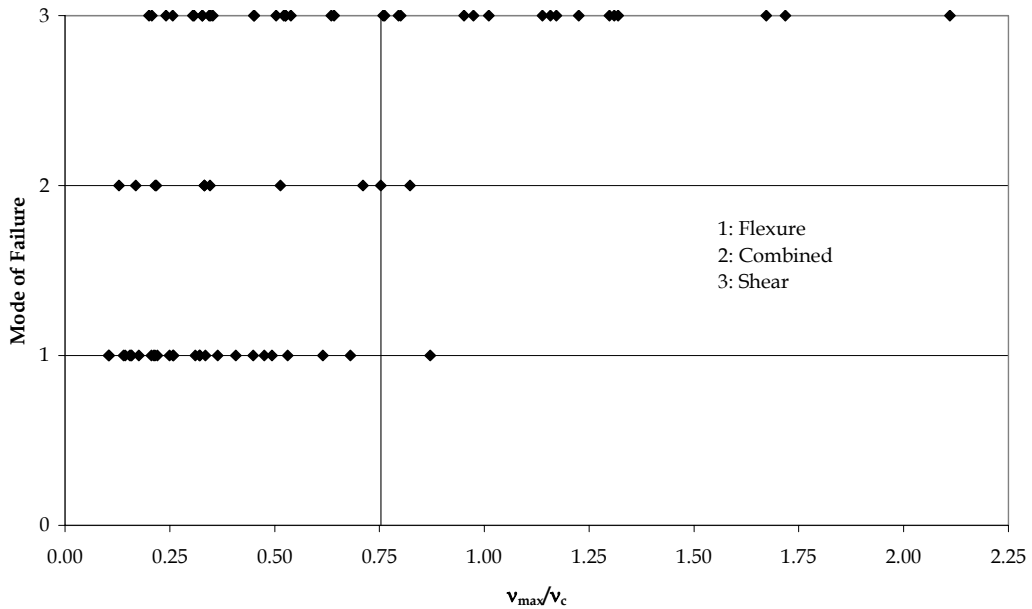
Figure 5.14 – Failure modes and the corresponding $\upsilon_{max}/\upsilon_c$ values of the analyzed walls.

When Figure 5.14 is examined, it can be seen that all but one of the walls that had failed in flexure developed a $\upsilon_{max}/\upsilon_c$ less than 0.75, which is in accordance with the observations of Wood [54]. However, in the case of walls failed in shear, the results of this study does not match with the observations of Wood [54]. The $\upsilon_{max}/\upsilon_c$ value of the 20 of the 43 shear critical walls remained below 0.75 and computed to be as low as 0.20. Considering the results of the analyses carried out, it can be stated that this deviation results from the fact that Eq. 5.2 may overestimate the nominal shear capacity of the walls since it is linearly proportional to the contribution of the horizontal reinforcement, which was found to have an insignificant effect on the behavior of walls. Moreover, using this criterion, it did not seem to be possible to distinguish the flexure-shear critical walls from the other ones.

111

When the approach proposed by FEMA-356 [8] document to distinguish the shear and flexure critical walls was employed, it was observed that this approach is a rather rough one and it could not effectively predict the predominant failure mode of the walls. For instance, all the columns that had failed in flexure had an aspect ratio less than 3.0, which is the lower bound for the flexure critical columns given in FEMA 356 [8]. Some walls with an aspect ratio of 1.5 was observed to develop a flexural failure mode, whereas some walls with an a/d ratio of 1.0 failed in a combined flexure – shear mode. The main reason of this discrepancy between the observed failure mode and the one predicted by FEMA 356 [8] is that, the criterion in this document is solely based on the aspect ratio and does not take the effect of the other parameters into account.

The behavior of the walls that Wood used in her paper [54] to develop a criterion based on $\upsilon_{max}/\upsilon_c$ were also compared with their corresponding $\dfrac{V_f}{b_w d \sqrt{f_{ck}}}$ values. Of the 32 walls (Wood had used 37 specimens but 5 of them were I section walls and they were omitted since they are not within the scope of this dissertation), 14 of them had been reported to fail in flexure. The $\dfrac{V_f}{b_w d \sqrt{f_{ck}}}$ value of the 9 of these specimens was less than 0.20 (7 of these were less than 0.15). All the specimens that had failed in shear had developed $\dfrac{V_f}{b_w d \sqrt{f_{ck}}}$ values greater than 0.20. Figure 5.15 compares the behavior of shear walls and their corresponding $\dfrac{V_f}{b_w d \sqrt{f_{ck}}}$ values.
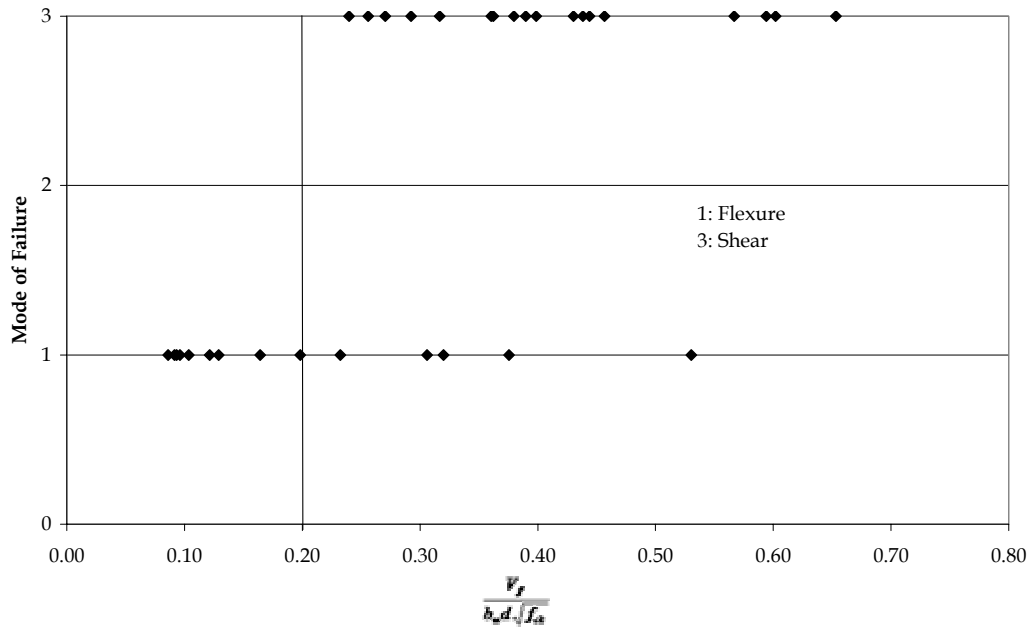
Figure 5.15 - Failure modes and the corresponding $V_f/(b_w d \sqrt{f_{ck}})$ values

of the specimens used in Wood's work

Based on these observations, it was decided to use the $\dfrac{V_f}{b_w d \sqrt{f_{ck}}}$ value of

the shear walls to estimate the predominant failure mode of the shear walls. The

proposed limits for each failure mode are given in Table 5.2.

Table 5.2 Criterion for the determination of the failure mode of the shear

walls

Predominant Failure Mode	$\dfrac{V_f}{b_w d \sqrt{f_{ck}}}$ value
Shear	>0.20
Flexure – Shear	between 0.15-0.20
Flexure	<0.15

5.5   DAMAGE FUNCTIONS

Damage functions for the shear walls were developed for the three failure

modes, separately. The functional form utilized for the damage functions for the

113

columns, beams and infills were used for the damage functions of the shear walls as repeated in Eq. 5.3 and 5.4.

$$Damage(\delta) = \left(1 - e^{-\left(\frac{\delta}{a}\right)^b}\right) g(\delta) \tag{5.3}$$

$$g(\delta) = 0.5\left[1 - \cos\left(\frac{\pi\delta}{c}\right)\right] \qquad \text{if } \delta \leq c$$

$$g(\delta) = 1 \qquad\qquad\qquad\quad \text{if } \delta > c \tag{5.4}$$

In the development of the damage functions for the shear critical walls, the ultimate drift ratio of each shear wall was assigned a damage score of 90%. For the flexure shear critical and flexure critical shear walls, the damage criterion used was based on both the yield and ultimate drift ratios. The yield drift ratio was assigned a damage score of 30% and the ultimate drift ratio was assigned a damage score of 90%.

The values of the equation parameters, a, b, and c in the equations 5.3 and 5.4 were determined by applying the least squares curve fitting technique on the database formed. These values were determined for not only the mean values for each group, but also for the upper and lower bounds. The values of the equation parameters determined are given in Table 5.3. The lower, mean and upper bound curves developed for shear critical, flexure shear critical and flexure critical walls are given in Figures 5.16 to 5.18, respectively. Figure 5.19 shows the mean damage curves for all groups.

Table 5.3 – Values of equation parameters

Par.	Shear Critical			Flexure-Shear Critical			Flexure Critical		
	Upper	Mean	Lower	Upper	Mean	Lower	Upper	Mean	Lower
a	0.0055	0.0035	0.0024	0.0058	0.0045	0.0033	0.0070	0.0058	0.0042
b	1.7	2.4	4.0	1.8	1.8	2.2	1.3	1.5	1.5
c	0.0030	0.0030	0.0030	0.0040	0.0030	0.0020	0.0035	0.0030	0.0020
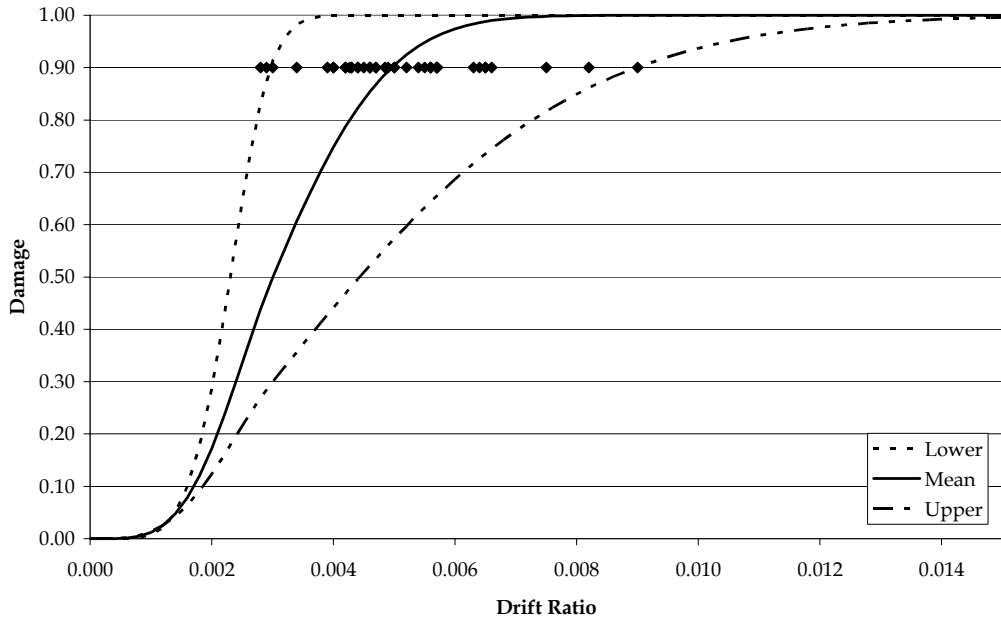
Figure 5.16 – Developed damage curves and the corresponding data points for shear critical shear walls
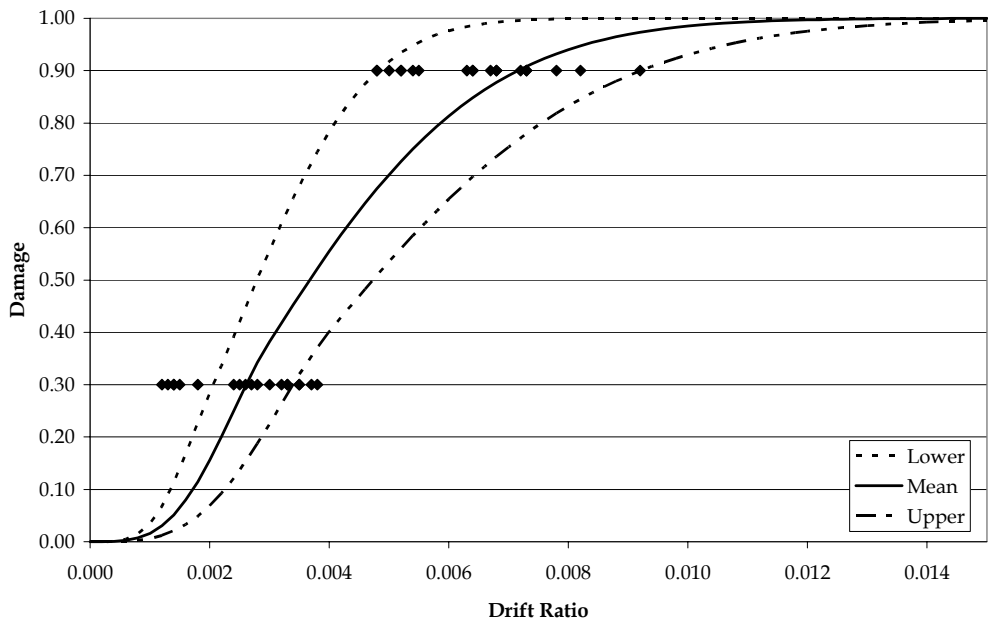
Figure 5.17 - Developed damage curves and the corresponding data points for flexure-shear critical shear walls
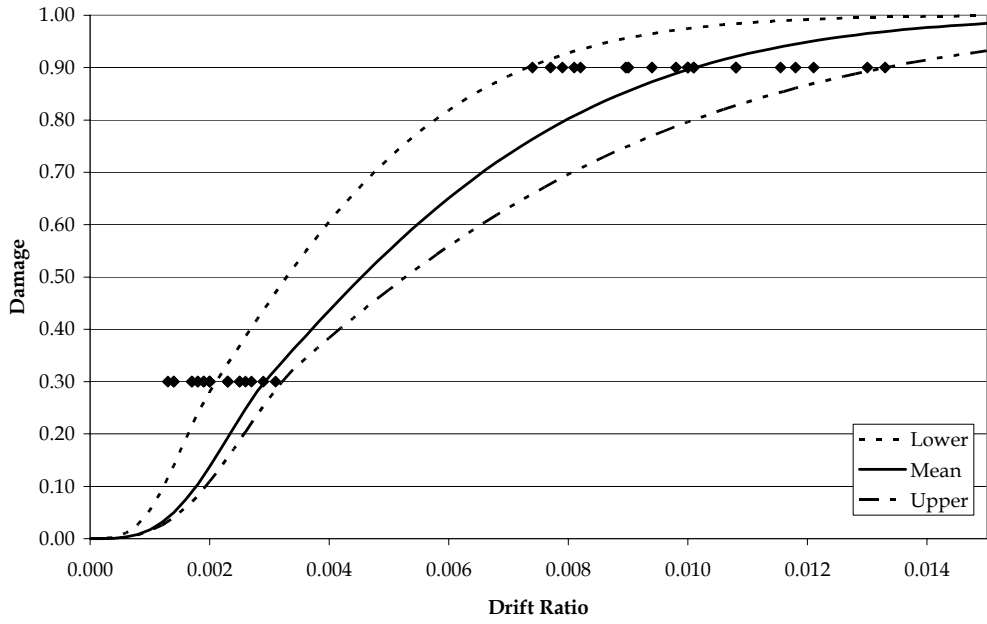
Figure 5.18 - Developed damage curves and the corresponding data points
for flexure critical shear walls
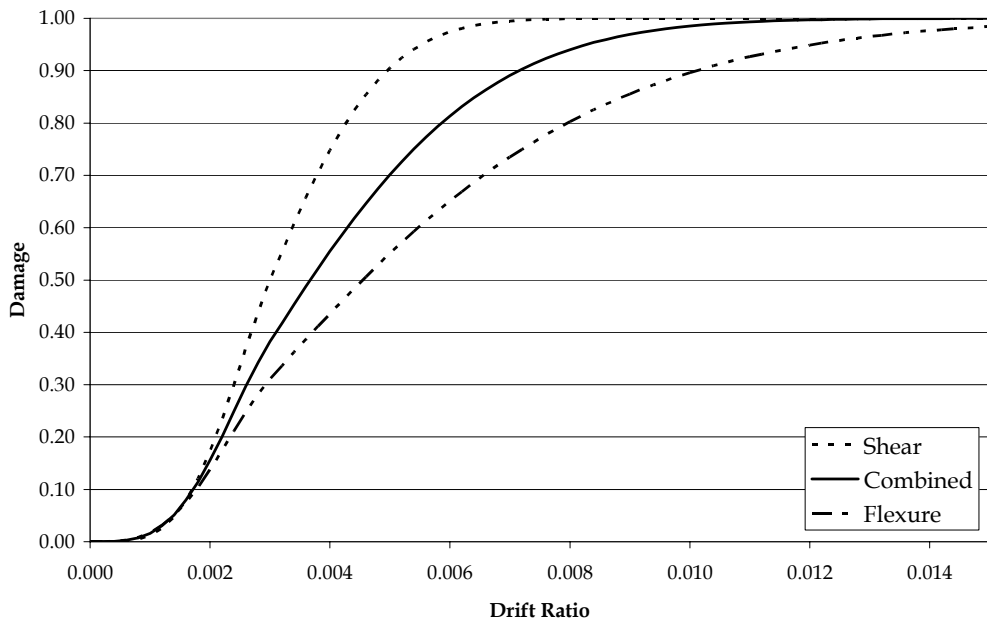
Figure 5.19 – Mean damage curves for all types of shear walls

116

5.6 COMPARISON WITH EXPERIMENTAL DATA

The developed damage curves for shear walls were compared with the 33 shear wall experiments available in the literature. The comparison could only be made at the ultimate level, since no information on the yield drift ratio of the walls could be found on the related documents. Here it must be recalled that the ultimate drift ratio corresponds to a damage score of 90% in the proposed curves. In this comparison, firstly the expected predominant failure mode of the walls was predicted according to their $\dfrac{V_f}{b_w d \sqrt{f_{ck}}}$ values. Then, the observed ultimate drift capacity of each wall was compared with the predicted ultimate drift capacity. Figure 5.20 and Table 5.4 show the comparison of the observed and predicted ultimate drift ratios of the shear walls.
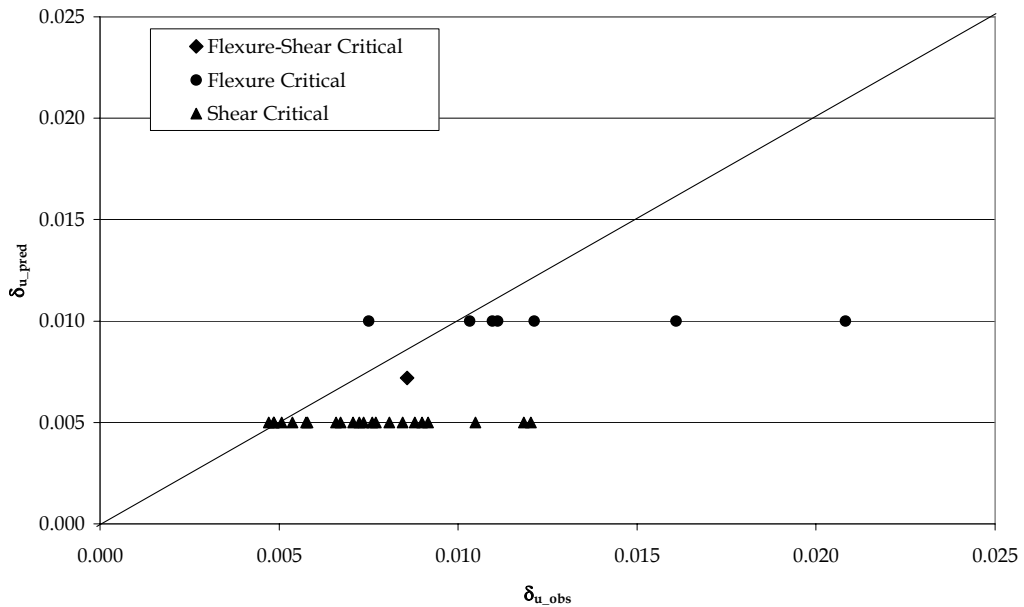
Figure 5.20 - Comparison of the Developed Curves with Experimental Data

Table 5.4 - Comparison of observed and predicted ultimate drift capacities for shear walls

	$\delta_{u\text{-}obs}/\delta_{u\_pred}$
Mean	1.43
cov	0.30

As Table 5.4 and Figure 5.18 indicate, the developed damage curves are on the conservative side since they underestimate the ultimate drift capacity of shear walls by 43%. Here, it must be stated that the ultimate drift capacity of the walls were taken as the ones stated by the authors and in most of the works there was no information on the criterion on which the ultimate drift capacity was selected. The author believes that this may be one of the reasons of the discrepancy between the predicted and observed ultimate drift capacities. However, it can still be stated that the developed damage curves can capture the behavior of shear walls in a satisfactory manner.

CHAPTER 6

COMPONENT IMPORTANCE FACTORS

6.1 GENERAL

In the component based vulnerability assessment procedures, one of the most important and challenging tasks is the combination of the damage scores obtained for different components to come up with a single damage score for the entire building. The most appropriate way for this seems to take the weighted average of the damage scores. The weighing coefficients for each component should reflect the importance of that component in resisting the seismic forces. In this part a procedure was developed for the determination of these weighing coefficients which were named as *component importance factors*. The approximate values for these component importance factors were developed and are proposed for reinforced concrete buildings.

6.2 GENERAL PROCEDURE

In the seismic performance of buildings, one of the most important points that determine the survival of the building is its energy dissipation capacity. Based on this fact, it can be stated that the importance of a component in resisting the seismic forces is directly related with its contribution to the energy dissipation capacity of the building. Hence, the energy dissipation capacity is selected as the criterion in determining the component importance factors for a given building.

The procedure developed for the determination of the component importance factors can be used for brick infilled reinforced concrete frames and reinforced concrete wall frame systems.

The procedure developed will be introduced on a sample 2D brick infilled frame structure and the modifications for wall-frame systems will be summarized in the forthcoming paragraphs. The sample frame is a five bay, five story frame. The second and fourth bays of the frame are filled with brick walls. The overview and cross-sectional properties of the frame are presented in Figure 6.1. The brick infills of this frame were modeled using the equivalent strut model developed by Smith [42], which was summarized in the fifth chapter of this dissertation.
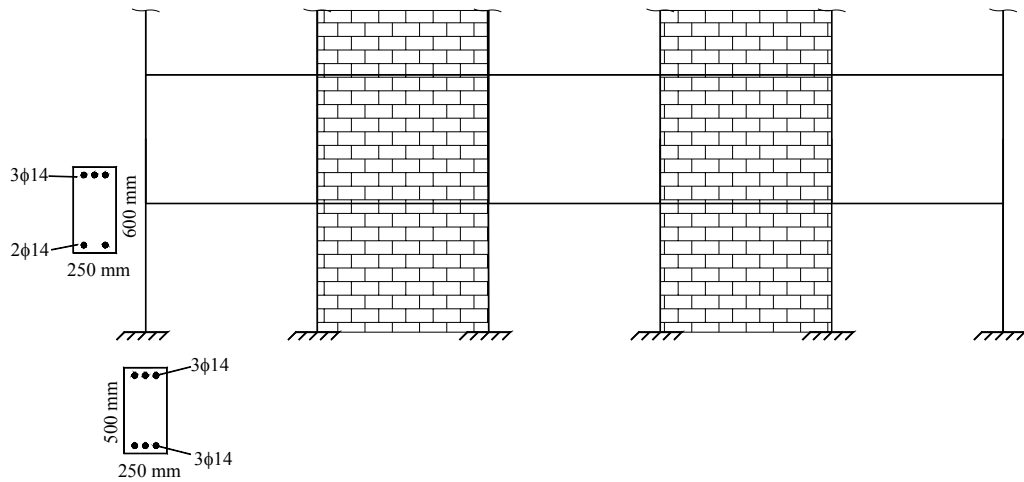
Figure 6.1 – Overview of the sample frame

As the first step, a pushover analysis was carried out on this initially undamaged frame (virgin frame). As a result of this analysis, the story displacement – story shear force curves for each story is obtained (Figure 6.2). The area under the story displacement – story shear force curve is equal to the energy dissipated by that story. The sum of the areas under these curves for each story gives the total energy dissipated by the virgin frame (E_o). The relationship for the energy dissipated by an n story frame is given by:

$$E = \sum_{i=1}^{n} A_i \qquad (6.1)$$

where, A_i is the area under the story displacement – story shear curve of the ith story and n is the total number of stories.
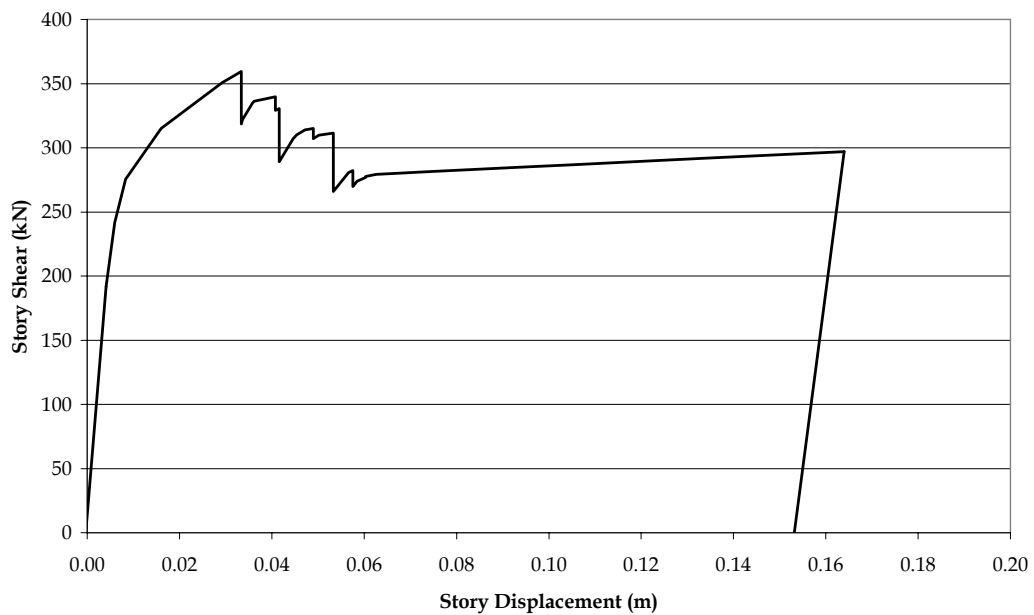
Figure 6.2 – Sample story shear vs. story displacement curve

After the computation of the dissipated energy by the virgin frame, E_o, the frame was modified through the introduction of moment releases at both ends of the first story columns. These moment releases represent the plastic hinges occurring during seismic action. Here it must be noted that the moments at the end of interior columns were released and the exterior columns were assumed to be undamaged to prevent the formation of an unstable system. Figure 6.3 shows the configuration of the frame used to represent the damaged first story columns (damage case 1).

The energy dissipated by this frame was computed via the application of Eqn. 6.1 and designated as E_1. Then, this procedure was repeated for the columns of all the stories (damage cases 2 to 5) and the energy dissipated by each case were computed (E_2 to E_5).

To represent the damage of the first story beams, the moments at both ends of all the beams of the first story were released (Figure 6.4). Then, the energy dissipated by this frame (damage case 6) was computed and named as E_6.

121

As in the case of columns, this procedure was repeated for the beams of all the stories.
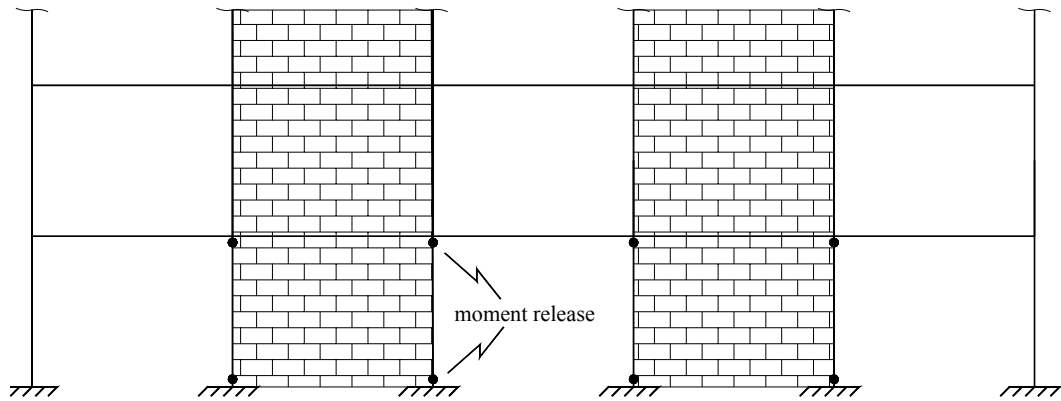
Figure 6.3 – Overview of damage case 1
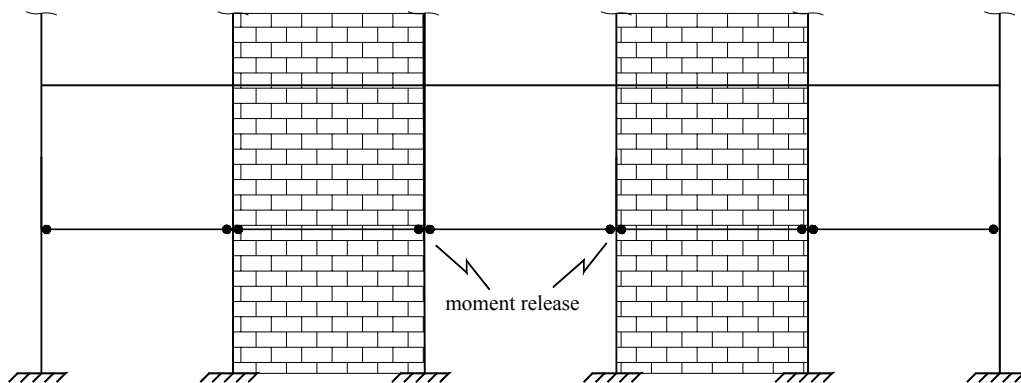
Figure 6.4 – Overview of damage case 6

In the case of infill walls, the infills of one story were deleted (Figure 6.5) for each case and once again the energy dissipated by those damaged frames was computed. As a result, for this 5 story building, the energy dissipated by the virgin frame, E_o, and by the 15 damage cases were obtained.
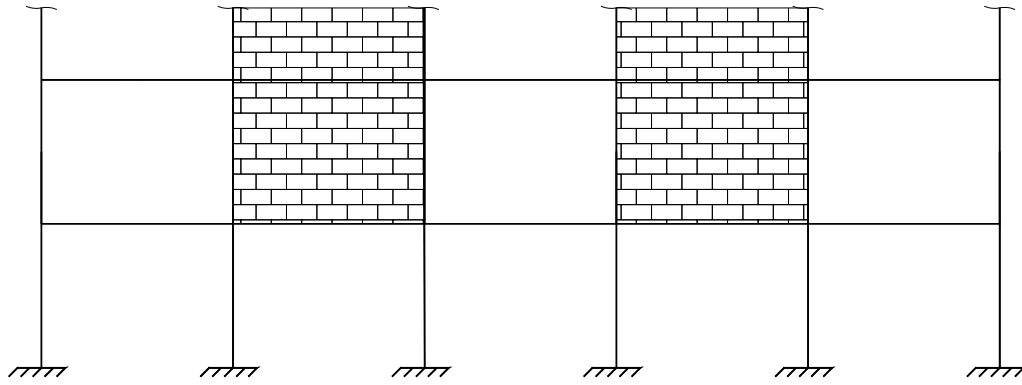
Figure 6.5 – Overview of damage case 11

The importance of a component within the frame is inversely proportional to the ratio of the energy dissipated (E_i) by the corresponding damage case to the energy dissipated by the virgin frame. The sum of the importance factors for all components within a frame must sum up to 1. For this, the E_o/E_i ratio for each damage case "i" is summed and the importance factor obtained for each component was normalized by this value. In other words, the importance factor of a component is given as:

$$IF_j = \frac{E_0 / E_j}{\sum_{i}^{3n} E_0 / E_j} \tag{6.2}$$

where j represents the damage case corresponding to the component of interest and n is the number of stories.

By this way the importance factors for the columns, beams and brick infills of a brick infilled RC moment resisting frame can be computed. The importance factors computed using the above procedure are not for a single member. Instead, they reflect the importance of all the members of the same type located in the same story. To compute the importance of each column, the weighted average of the importance factor for all of the columns of a story must be taken where the weighing coefficient is the moment of inertia of the column. Simply taking the average of the importance factor computed using the above formulation for the

beams and infills would be sufficient for determining the importance factor of a single beam or a single infill.

The procedure summarized above can also be used for reinforced concrete wall-frame systems. When the lateral load resisting system of a structure is composed of shear walls and columns, the contribution of brick infills in resisting the seismic forces becomes very limited and can be assumed to be negligible. Hence, for the wall-frame systems, the moment releases are applied at the ends of shear walls, columns and beams of each story and the energy dissipated by each damage case is computed using Eq. 6.1. Then, the importance factor of each component is computed using Eq. 6.2. As in the case of brick infilled moment resisting frames, the importance factors computed are not for a single member, but they are for all the members of the same component type located in a single story. Importance factor of each wall can be computed by taking the weighted average of the importance factor for all the walls of a story, where the weighing coefficient is the moment of inertia of the wall.

6.3 APPROXIMATE VALUES FOR REINFORCED CONCRETE BUILDINGS

The procedure developed for the determination of the component importance factors and summarized in the section 6.2 is not so simple to apply. To apply this procedure, the nonlinear static analysis of the structure must be carried out for a number of times. It requires not only time but also some expertise to carry out these analyses correctly. Hence, it may not be possible to carry out this procedure every time due to some limitations. Considering this fact, the procedure developed was applied to several frames in order to propose some approximate values for the component importance factors. However, engineers that would like to use the seismic vulnerability assessment procedure proposed in this dissertation are encouraged to apply the procedure summarized above for each and every building to determine the building specific component importance factors.

The approximate values for component importance factors were developed for moment resisting frames and wall – frame systems, separately. The ones that fit to the type of the structure of interest should be used.

6.3.1 Approximate Values for Brick Infilled Moment Resisting Frames

In the development of the approximate expressions for the component importance factors, the first step was the investigation of the influence of certain parameters on the importance factors. These parameters were the concrete strength, yield strength of longitudinal reinforcement, bay width, story height and the value of gravity load applied on the beams. For the bay width and story height, different configurations were also modeled. For instance, different widths were assigned for different bays and the height of the first story was modified to form systems with soft stories. As a result of the analyses carried out, it was observed that the concrete strength, yield strength of longitudinal reinforcement, bay width, value of gravity load and story height have no significant effect on the values of the component importance factors. This is mainly due to the fact that, the component importance factors are determined based on the energy dissipation capacity of the damage cases relative to that of the virgin frame and the parameters mentioned above are constant for the damage cases and the virgin frame for a given building. In other words, although the energy dissipated by the virgin frame with a certain concrete strength $(E_o)_1$ may differ significantly from the energy dissipated by the virgin frame with different concrete strength $(E_o)_2$ $\left[(E_o)_1 \neq (E_o)_2 \right]$, the ratio of the energy dissipated by the damage case 1 to the energy dissipated by the corresponding virgin frame does not vary significantly.

$$\left[\left(\frac{E_1}{E_o} \right)_1 \approx \left(\frac{E_1}{E_o} \right)_2 \right].$$

Number of stories alters the values of the component importance factors significantly. This is mainly due to the fact that the number of components increases with the increasing number of stories and the sum of the importance factors for all the components is 1.00. To take this effect into account, the approximate values for component importance factors were developed for different number of stories ranging from 2 to 12.

The approximate values of the component importance factors for the brick infilled reinforced concrete frames are given in Tables 6.1 to 6.3.

Table 6.1 – Approximate values for importance factors for columns of brick infilled moment resisting frames

		Number of Stories										
		2	3	4	5	6	7	8	9	10	11	12
Story Number	1	0.375	0.250	0.233	0.174	0.193	0.165	0.144	0.132	0.116	0.110	0.096
	2	0.375	0.250	0.233	0.174	0.193	0.165	0.144	0.132	0.116	0.110	0.096
	3		0.250	0.233	0.174	0.193	0.165	0.144	0.132	0.116	0.110	0.096
	4			0.053	0.174	0.058	0.165	0.144	0.132	0.116	0.110	0.096
	5				0.053	0.058	0.030	0.043	0.132	0.116	0.110	0.096
	6					0.058	0.030	0.043	0.023	0.035	0.110	0.096
	7						0.030	0.043	0.023	0.035	0.018	0.029
	8							0.043	0.023	0.035	0.018	0.029
	9								0.023	0.035	0.018	0.029
	10									0.035	0.018	0.029
	11										0.018	0.029
	12											0.029

Table 6.2 - Approximate values for importance factors for beams of brick infilled moment resisting frames

		Number of Stories										
		2	3	4	5	6	7	8	9	10	11	12
Story Number	1	0.075	0.053	0.042	0.034	0.029	0.025	0.022	0.019	0.017	0.016	0.014
	2	0.075	0.042	0.037	0.032	0.027	0.024	0.021	0.019	0.017	0.015	0.014
	3		0.031	0.032	0.029	0.026	0.023	0.020	0.018	0.016	0.015	0.014
	4			0.028	0.027	0.024	0.022	0.020	0.018	0.016	0.015	0.014
	5				0.024	0.023	0.021	0.019	0.017	0.016	0.014	0.013
	6					0.021	0.020	0.018	0.017	0.015	0.014	0.013
	7						0.019	0.018	0.016	0.015	0.014	0.013
	8							0.017	0.016	0.015	0.014	0.013
	9								0.015	0.014	0.013	0.013
	10									0.014	0.013	0.012
	11										0.013	0.012
	12											0.012

Table 6.3 - Approximate values for importance factors for brick infills of brick infilled moment resisting frames

Story Number		Number of Stories										
		2	3	4	5	6	7	8	9	10	11	12
	1	0.055	0.037	0.028	0.022	0.018	0.016	0.014	0.012	0.011	0.010	0.009
	2	0.055	0.037	0.028	0.022	0.018	0.016	0.014	0.012	0.011	0.010	0.009
	3		0.037	0.028	0.022	0.018	0.016	0.014	0.012	0.011	0.010	0.009
	4			0.028	0.022	0.018	0.016	0.014	0.012	0.011	0.010	0.009
	5				0.022	0.018	0.016	0.014	0.012	0.011	0.010	0.009
	6					0.018	0.016	0.014	0.012	0.011	0.010	0.009
	7						0.016	0.014	0.012	0.011	0.010	0.009
	8							0.014	0.012	0.011	0.010	0.009
	9								0.012	0.011	0.010	0.009
	10									0.011	0.010	0.009
	11										0.010	0.009
	12											0.009

Tables 6.1 to 6.3 show that the sum of the importance factors of the columns of all stories adds up to 0.75 while those of beams and infills are 0.14 and 0.11, respectively. In Table 6.2 it can be seen that the importance factors of beams decrease linearly with the increasing story number within a building. For the brick infills of a building, the importance factors of the infills were found to be invariant throughout the height of the building. For the 2 and 3 story buildings, the importance factors of the columns were also found to be invariant with the story number. For 4 and 5 story buildings, the importance factors of the columns were found to be constant for the first n-1 stories of an n story building. The importance factor of the nth story column is very low compared to the first n-1 stories. For higher buildings two different values for the importance factors of columns are observed when Table 6.1 is examined. For the first n/2 stories, the importance factors of columns have a constant value and for the remaining stories they take another constant value which is well below the first one.

The approximate importance factors proposed for the component importance factors of brick infilled moment resisting frames were compared with the ones proposed by Gülkan et. al., which are based on the expert opinion [56]. Gülkan et. al. proposes an importance factor of 2 for columns, whereas values of 1 and 0.5 were proposed for beams and infills respectively. When brought in the

same format (normalized by the sum to add up to 1) the importance factors for columns become 0.57, which is 76% of the value proposed in this study (0.75). For the beams and infills, the importance factor for beams and infills Gülkan et. al. proposes values of 0.29 and 0.14, respectively.

6.3.2 Approximate Values for Reinforced Concrete Wall-Frame Systems

The approximate values for the components of wall-frame systems were also developed using the procedure summarized in the previous parts. The procedure was carried out for 2D structures with a total number of stories ranging from 3 to 12. For each structure, the procedure was applied for four different material properties and the average values obtained from these analyses are given in the following parts.

In wall-frame systems, the component importance factors are affected by the variations in the wall contribution factor. In this study wall contribution factor (WCF) is defined as the ratio of the sum of the moment of inertias of the walls to the sum of the moment of inertias of walls and columns in the analysis direction (Eq. 6.3).

$$WCF = \frac{\sum I_{wall}}{\sum I_{wall} + \sum I_{column}} \tag{6.3}$$

In Eq. 6.3 WCF is the wall contribution factor, I_{wall} is the moment of inertia of a shear wall and I_{column} is the moment of inertia of a column.

To check the validity of the wall contribution factor defined, a series of elastic analyses were carried out for different WCF values. At the end of these analyses, the variation of the ratio of the base shear carried by the walls to the total base shear with the wall contribution factor was investigated. The results of these analyses given in Figure 6.6, the base shear contribution of the walls increases linearly with the increasing wall contribution factor. Hence, it can be stated that the wall contribution factor defined in Eq. 6.3 is a sound basis for the identification of the contribution of the walls to the seismic behavior.
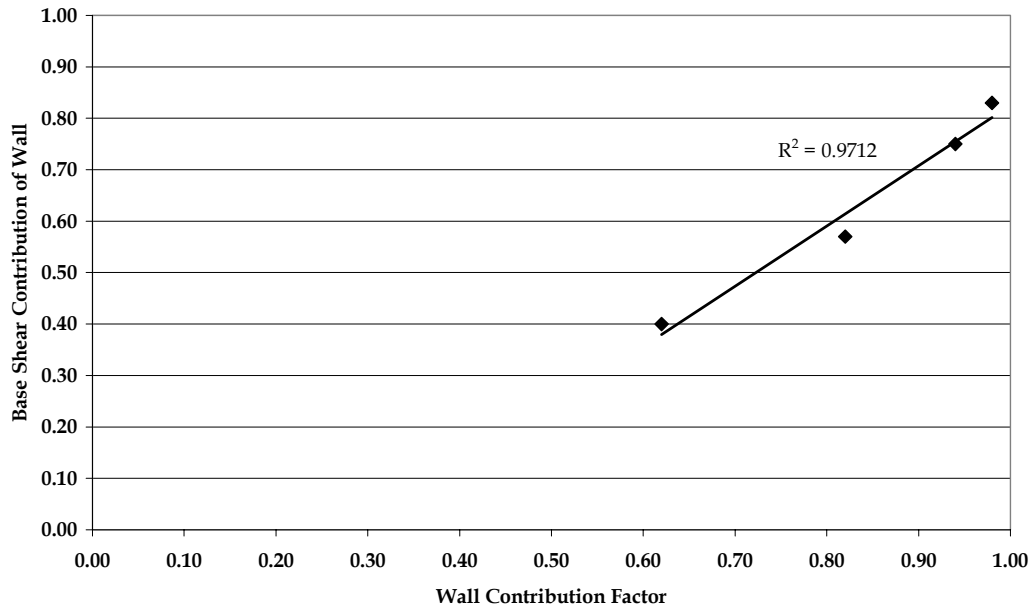
Figure 6.6 – Variation of base shear contribution of shear walls with wall contribution factor

The approximate values for the component importance factors of wall-frame systems are first computed for a certain wall contribution factor and given in tabularized form in the following paragraphs and then correction factors were developed to modify these values according to the variations in the wall contribution factor.

In order to compute the approximate values for the component importance factors, a sample structure was designed and the procedure was applied on this structure. The sample structure is a 6-bay structure consisting of 6 250 mm by 450 mm columns and a 250 mm by 1800 mm shear wall. The number of stories varies between 3 and 12. The corresponding wall contribution factor was computed to be 0.914. The overview of the sample structure is shown in Figure 6.7. Four different combinations for the material properties of the sample structure were used in the analyses. These combinations are shown in Tables 6.4 and 6.5, where the results for the 4 and 5 story frames are summarized. Tables 6.4 and 6.5 show that, the variation in the component importance factors of wall-frame systems with the variations in the material properties is insignificant as in the case of brick infilled frames. Based on this discussion, it can be stated that

129

taking the average values for the importance factors of components of wall-frame systems computed for different material properties will be adequate to represent the variations in the material properties. Tables 6.6 to 6.8 show the average approximate values obtained for the component importance factors of the wall-frame systems.
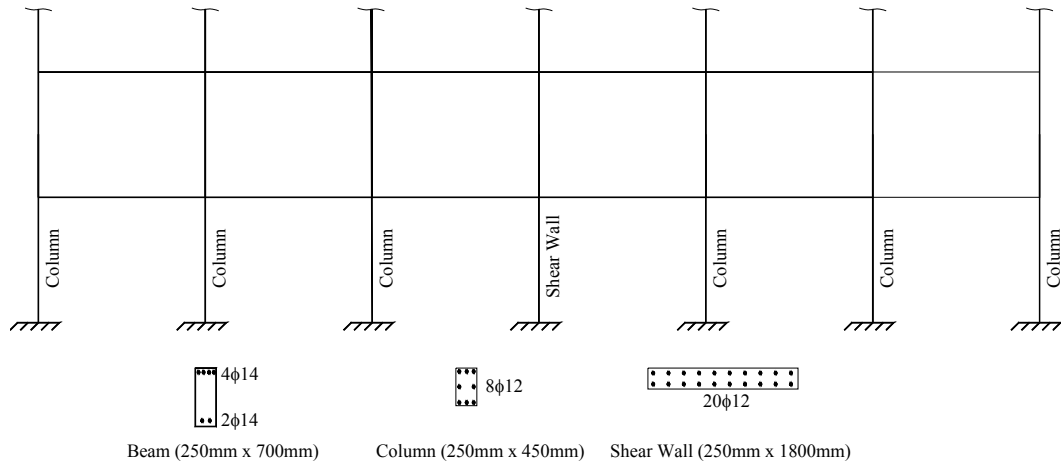
Figure 6.7 –Overview of the sample structure

Table 6.4 – Variation of component importance factors with material properties for 4 story wall-frame systems

Comp.	f_{ck}=20 MPa f_{yk}=420 MPa	f_{ck}=20 MPa f_{yk}=220 MPa	f_{ck}=10 MPa f_{yk}=420 MPa	f_{ck}=30 MPa f_{yk}=420 MPa	Mean	COV
Beam (1st)	0.054	0.058	0.061	0.053	0.057	0.06
Beam (2nd)	0.050	0.060	0.053	0.052	0.054	0.08
Beam (3rd)	0.055	0.056	0.049	0.054	0.053	0.05
Beam (4th)	0.048	0.051	0.042	0.048	0.047	0.08
Column (1st)	0.052	0.055	0.058	0.051	0.054	0.05
Column (2nd)	0.051	0.062	0.055	0.049	0.054	0.11
Column (3rd)	0.047	0.049	0.053	0.053	0.051	0.06
Column (4th)	0.049	0.055	0.046	0.052	0.050	0.07
Wall (1st)	0.183	0.169	0.182	0.180	0.179	0.04
Wall (2nd)	0.183	0.169	0.182	0.180	0.179	0.04
Wall (3rd)	0.183	0.169	0.173	0.180	0.176	0.04
Wall (4th)	0.044	0.047	0.045	0.048	0.046	0.04

Table 6.5 - Variation of component importance factors with material
properties for 5 story wall-frame systems

Comp.	f_{ck}=20 MPa f_{yk}=420 MPa	f_{ck}=20 MPa f_{yk}=220 MPa	f_{ck}=10 MPa f_{yk}=420 MPa	f_{ck}=30 MPa f_{yk}=420 MPa	Mean	COV
Beam (1st)	0.038	0.035	0.041	0.039	0.038	0.07
Beam (2nd)	0.037	0.036	0.040	0.036	0.037	0.05
Beam (3rd)	0.035	0.037	0.034	0.035	0.035	0.04
Beam (4th)	0.033	0.036	0.031	0.036	0.034	0.07
Beam (5th)	0.031	0.032	0.030	0.033	0.031	0.04
Column (1st)	0.035	0.035	0.040	0.039	0.037	0.07
Column (2nd)	0.034	0.035	0.035	0.032	0.034	0.04
Column (3rd)	0.034	0.034	0.035	0.035	0.034	0.02
Column (4th)	0.036	0.035	0.033	0.038	0.035	0.06
Column (5th)	0.030	0.037	0.034	0.036	0.034	0.09
Wall (1st)	0.159	0.154	0.160	0.154	0.157	0.02
Wall (2nd)	0.159	0.154	0.160	0.154	0.157	0.02
Wall (3rd)	0.159	0.154	0.157	0.154	0.156	0.02
Wall (4th)	0.150	0.154	0.138	0.148	0.148	0.05
Wall (5th)	0.031	0.033	0.031	0.031	0.031	0.04

Table 6.6 - Approximate values for importance factors for shear walls of
wall-frame systems for a wall contribution factor of 0.914

		Number of Stories									
		3	4	5	6	7	8	9	10	11	12
Story Number	1	0.241	0.169	0.133	0.127	0.118	0.122	0.107	0.094	0.092	0.082
	2	0.240	0.169	0.133	0.127	0.117	0.103	0.106	0.094	0.092	0.082
	3	0.069	0.167	0.132	0.127	0.115	0.100	0.100	0.094	0.092	0.082
	4		0.044	0.125	0.110	0.098	0.092	0.090	0.088	0.083	0.079
	5			0.027	0.030	0.048	0.052	0.039	0.065	0.051	0.070
	6				0.029	0.027	0.029	0.030	0.038	0.029	0.038
	7					0.026	0.027	0.027	0.022	0.024	0.027
	8						0.026	0.026	0.015	0.023	0.020
	9							0.025	0.020	0.022	0.018
	10								0.020	0.021	0.017
	11									0.022	0.017
	12										0.017

Table 6.7 - Approximate values for importance factors for columns of wall-frame systems wall contribution factor of 0.914

		Number of Stories									
		3	4	5	6	7	8	9	10	11	12
Story Number	1	0.080	0.058	0.048	0.039	0.037	0.031	0.028	0.026	0.024	0.021
	2	0.073	0.059	0.044	0.040	0.034	0.031	0.027	0.024	0.022	0.020
	3	0.072	0.055	0.044	0.040	0.033	0.030	0.027	0.024	0.021	0.020
	4		0.054	0.045	0.039	0.033	0.030	0.027	0.023	0.021	0.020
	5			0.044	0.034	0.032	0.028	0.027	0.024	0.021	0.021
	6				0.033	0.030	0.027	0.024	0.024	0.021	0.020
	7					0.028	0.024	0.024	0.022	0.021	0.020
	8						0.023	0.021	0.021	0.019	0.017
	9							0.020	0.019	0.018	0.016
	10								0.021	0.018	0.016
	11									0.019	0.016
	12										0.016

Table 6.8 - Approximate values for importance factors for beams of wall-frame systems for a wall contribution factor of 0.914

		Number of Stories									
		3	4	5	6	7	8	9	10	11	12
Story Number	1	0.080	0.060	0.049	0.042	0.037	0.031	0.029	0.026	0.024	0.022
	2	0.078	0.057	0.048	0.041	0.036	0.032	0.028	0.026	0.023	0.021
	3	0.067	0.057	0.045	0.039	0.034	0.031	0.027	0.025	0.022	0.021
	4		0.050	0.043	0.036	0.033	0.032	0.026	0.025	0.022	0.021
	5			0.040	0.035	0.029	0.027	0.025	0.024	0.022	0.021
	6				0.032	0.028	0.024	0.023	0.021	0.019	0.020
	7					0.027	0.024	0.022	0.020	0.019	0.018
	8						0.024	0.022	0.018	0.018	0.017
	9							0.022	0.019	0.018	0.016
	10								0.021	0.018	0.016
	11									0.018	0.016
	12										0.016

Tables 6.6 to 6.8 indicate that the sum of the importance factors of the shear walls in all the stories are 0.550. Gülkan et. al. [56] proposes a value of 0.667 for this. The sum of the importance factors proposed in this dissertation for columns and beams of a wall-frame system are both 0.225 whereas Gülkan et. al.

proposes 0.222 and 0.111 for the importance factors of columns and beams, respectively.

As indicated before, the approximate values given in Tables 6.6 to 6.8 are for a wall contribution factor of 0.914. To investigate the effect of the wall contribution factor on the component importance factors, additional analyses were carried out for wall densities of 0.619, 0.719, 0.818 and 0.976. Table 6.9 presents the number and dimensions of the columns and shear walls for each wall contribution factor value. These analyses were carried out for 4, 5 and 7 stories. The concrete strength was 20 MPa and the yield strength of longitudinal reinforcement was 420 MPa in these analyses. The results of the analyses were evaluated in terms of the sum of the importance factors of all stories for a component type. Figures 6.8, 6.9 and 6.10 show the variation of the sum of the importance factors with the wall contribution factor for shear walls, columns and beams, respectively. In these figures, the horizontal axis is the wall contribution factor whereas the vertical axis shows the ratio of the sum of the importance factors for all stories for the wall contribution factor of interest to that for a wall contribution factor of 0.914, which is the value of the sample frame. Figures 6.7 to 6.9 show that, the importance factors for shear walls increase linearly with the increasing wall contribution factor, whereas those for columns and beams decrease. The equations of the lines fitted to the data points of Figures 6.8 to 6.10 are given in Eqs. 6.4 to 6.6. In order to be able to take the effect of the wall contribution factor into account, the approximate component importance factors for wall-frame systems given in Tables 6.6 to 6.8 should be multiplied with the appropriate correction factors before they are used.

Table 6.9 – Number and dimensions of the columns and shear walls for different wall contribution factor values

Wall contribution factor	Columns		Shear Wall	
	#	Dimensions (mm)	#	Dimensions (mm)
0.619	6	250x700	1	250x1500
0.719	6	250x600	1	250x1500
0.818	6	250x600	1	250x1800
0.914	6	250x450	1	250x1800
0.976	6	250x400	1	250x2500
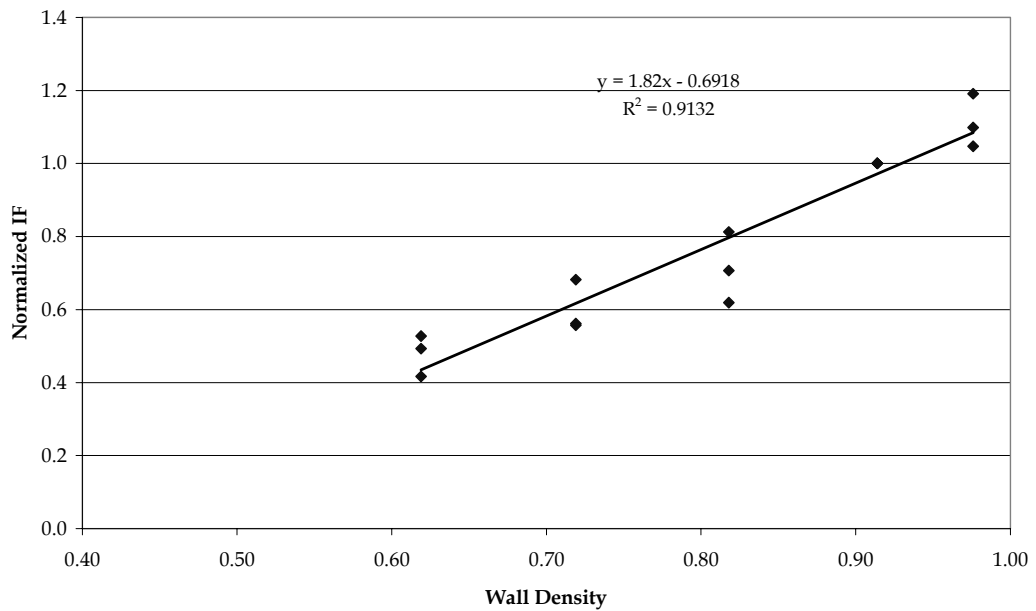
Figure 6.8 –Variation of importance factor of shear walls with wall contribution factor
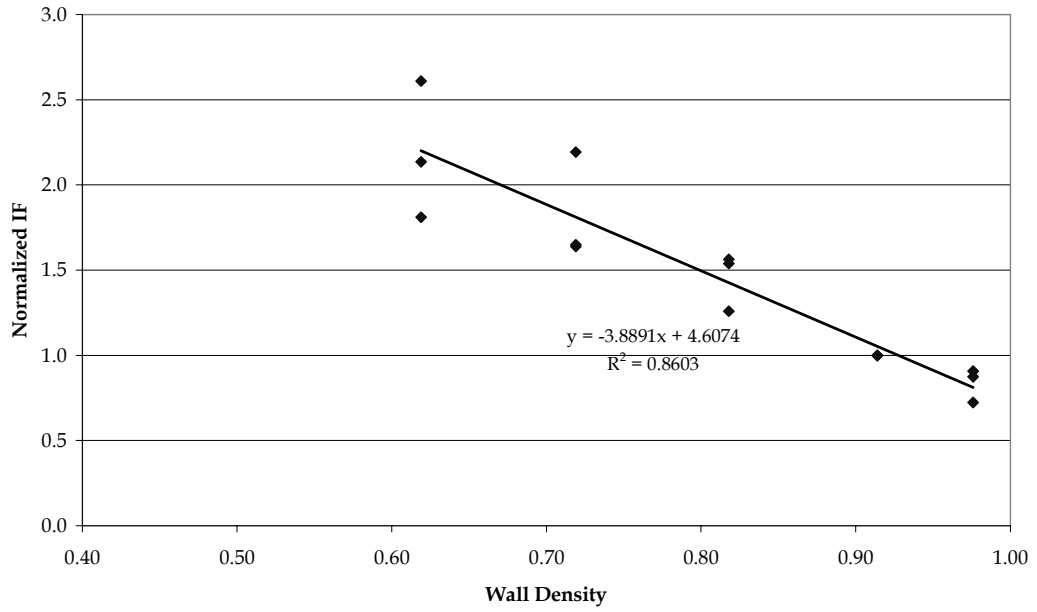
Figure 6.9–Variation of importance factor of columns with wall

contribution factor
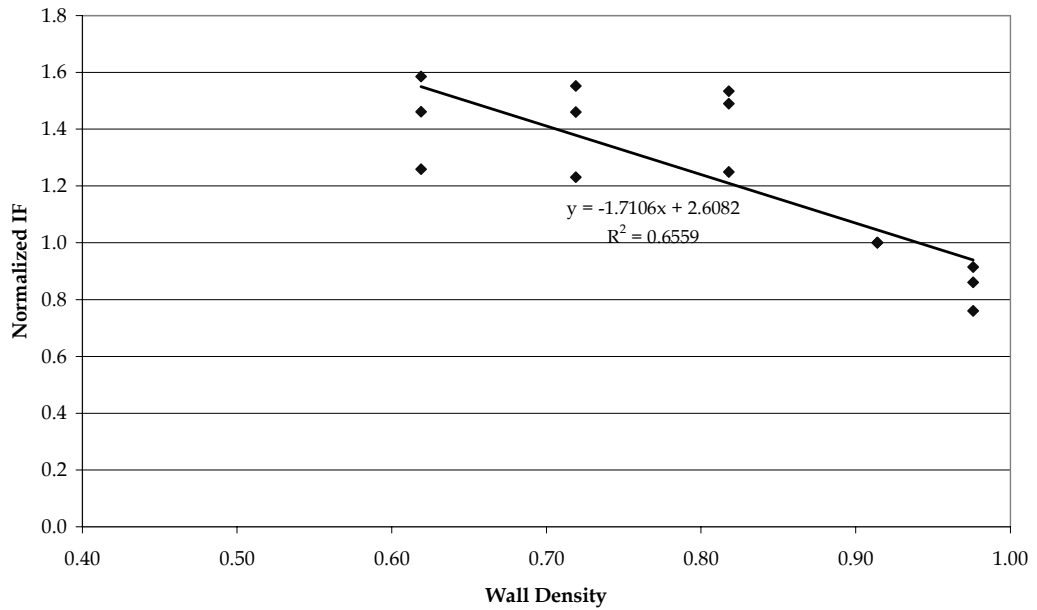
Figure 6.10 - Variation of importance factor of beams with wall

contribution factor

135

$$C_{sw} = 1.82 \times WCF - 0.69 \tag{6.4}$$

$$C_{col} = -3.89 \times WCF + 4.61 \tag{6.5}$$

$$C_{beam} = -1.71 \times WCF + 2.61 \tag{6.6}$$

In the analyses carried out so far, the number of shear walls was limited to one. To investigate the effect of number of shear walls on the component importance factors of wall-frame systems, additional analyses with systems containing two shear walls were carried out. These analyses were carried out for wall contribution factor values approximately equal to 0.818, 0.914 and 0.976. For the wall contribution factor of 0.818 two 250mmx1500mm shear walls were used instead of a single 250mmx1800 mm shear wall. For the wall densities of 0.914 and 0.976, two shear walls of 250mmx1500mm and 250mmx2000mm were used, respectively. The number of stories was 5 for the analyzed structures. The results of these analyses are given in Figures 6.11 to 6.13.
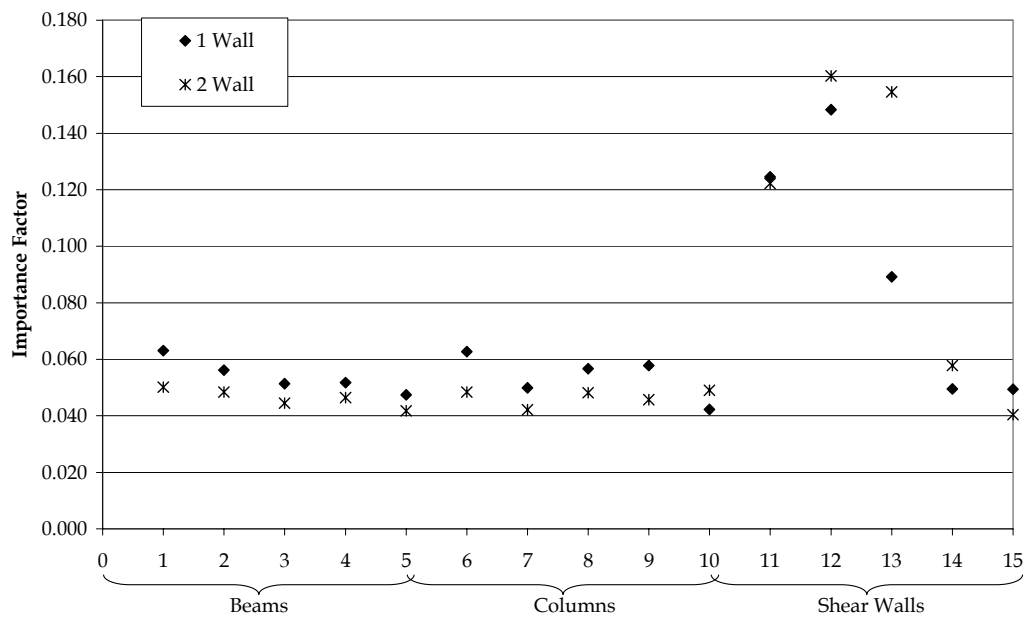
Figure 6.11 – Effect of number of walls on component importance factors for a wall contribution factor of 0.818
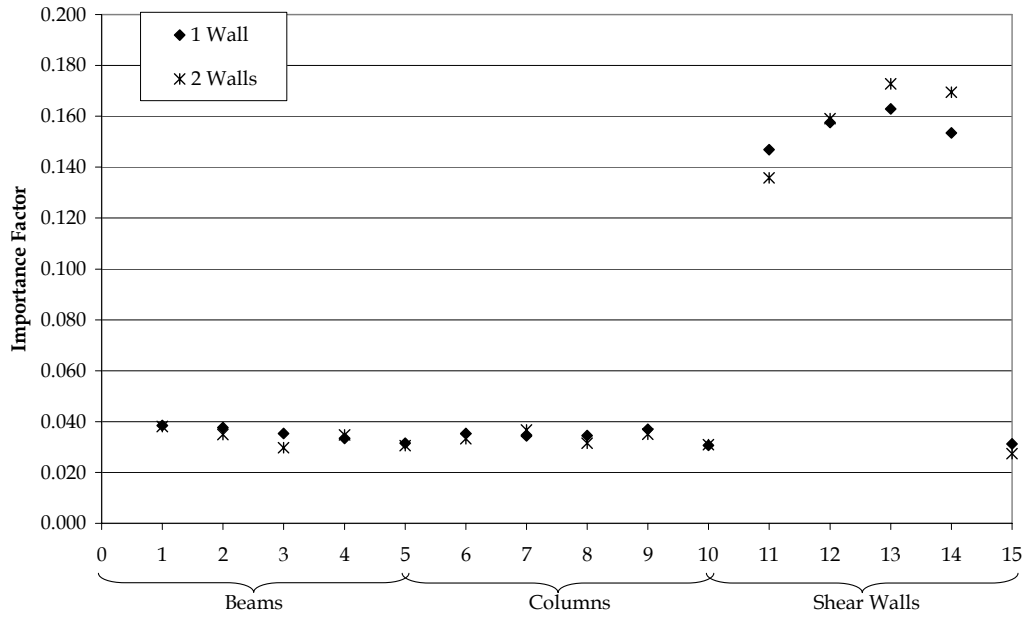
Figure 6.12 - Effect of number of walls on component importance factors
for a wall contribution factor of 0.914
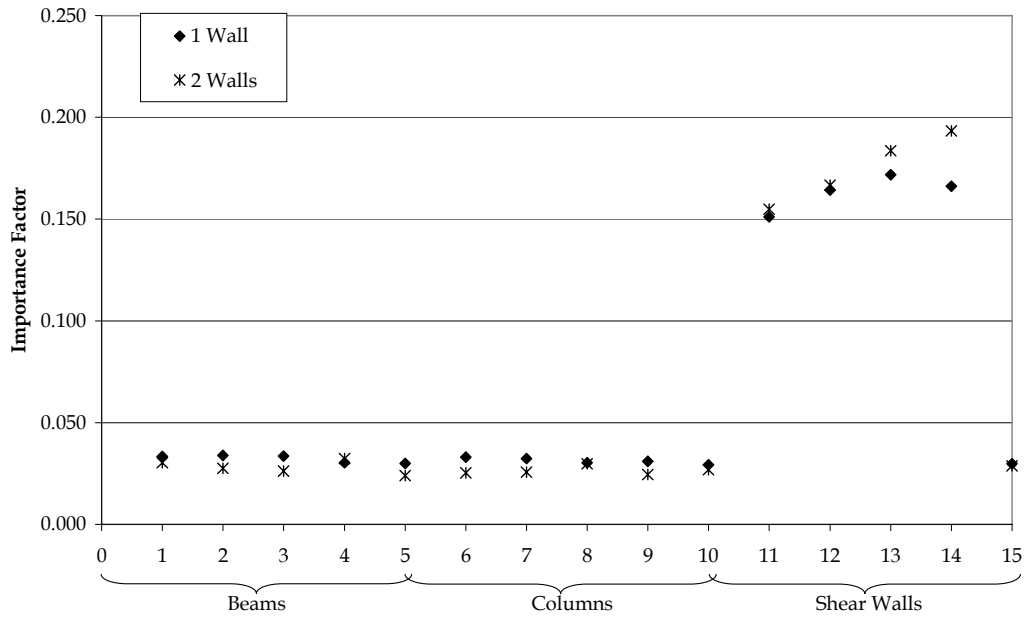
Figure 6.13 - Effect of number of walls on component importance factors
for a wall contribution factor of 0.976

137

Figures 6.11 and 6.13 show that, as far as the wall contribution factor remains constant, the number of shear walls in a system does not have a significant influence on the component importance factors of wall frame systems.

6.4 COMPUTATION OF THE STORY AND BUILDING DAMAGE SCORES

The proposed methodology is capable of assessing not only the damage of the members but also the damage levels of each story as well as the damage score of the entire building. Once the nonlinear analysis is carried out and the member end deformations under the given earthquake are computed, the damage scores of each member are computed from the associated damage curves. Then, the importance of each member is taken from the approximate values given in Tables 6.1 to 6.3 or 6.6 to 6.8 depending on the lateral load resisting system of the investigated building. The importance factor computed for a member reflects the importance of that member within the entire structure. To determine the importance of the member within its own story, the importance factor of that member is divided by the sum of the importance factors of all the members in that story. Then, the damage score of each member of a story is multiplied by the importance factor of that member within its own story and these products are summed up to compute the damage score of the given story. By this way, the damage score for each story is computed.

To determine the damage score for the entire building, the importance factor of each story is needed. This factor should also reflect the importance of the story due to its location. That is, for example, the first floor damage in a building is more crucial than other floors because it impacts all the floors above and the story importance factor of the first story should reflect this. Therefore, a linear importance is assigned to the location of the story. For this, the raw importance factor of the story (equal to the sum of the importance factors of all the members in that story) is multiplied by the number of stories above that story (including itself). For instance, for a five-story building, the raw importance factor for the first story is multiplied by 5, that of the second story is multiplied by 4 and so on. Then, these values are summed up and the value computed for each story is normalized by this sum. The values obtained at the end of this process are the

story importance factors. Finally, the damage score of each story is multiplied by its importance factor and these values are summed up to obtain the damage score of the building.

6.5 PERFORMANCE EVALUATION OF THE BUILDING

According to the damage criterion set in this study, there are mainly four damage levels: negligible, light, moderate and heavy. In addition to this, the performance of the buildings under a given earthquake is mainly grouped into three as immediate occupancy (IO), life safety (LS) and collapse prevention (CP). The first two of the damage levels used in this study correspond to the immediate occupancy performance criterion. The moderate damage state corresponds to the life safety performance criterion whereas the heavy damage level corresponds to the collapse prevention. Recalling the damage scores assigned to the four damage levels, the damage scores corresponding to the performance levels are summarized in Table 6.10.

Once the damage score of each story and the entire building is computed, their performance levels are evaluated using Table 6.10. However, to be able to take the local failures that may exist in a single story of a building such as soft story, an additional criterion was also set. According to this criterion, if the damage score of a story exceeds 70%, then the performance level of the building is accepted to be collapse prevention regardless of the damage score of the entire building.

Table 6.10 – Building damage scores and the corresponding performance levels

Damage Score	Performance
0% - 10%	Immediate Occupancy
10% - 50%	Life Safety
50% - 100%	Collapse Prevention

CHAPTER 7

CASE STUDIES

7.1 GENERAL

Several case studies were carried out on buildings which were damaged in the recent earthquakes that occurred in Turkey to calibrate and validate the proposed vulnerability assessment procedure. In these case studies, nonlinear static analyses were carried out on the selected buildings and the capacity curve of each building was obtained. These analyses were carried out using the software SAP2000. The performance point of each building under the ground motion it was exposed to was determined using the procedure summarized in the following paragraphs. Then, the performance of all the members at the performance point were assessed using the proposed methodology as well as the ATC-40, FEMA-356 and EUROCODE 8 procedures summarized in Chapter 1.

7.2 MODELING AND ANALYSIS IN SAP2000

In this study, 3D models of the buildings were analyzed in the SAP2000 software. The analysis type carried out was a nonlinear static analysis (pushover analysis) which yields a lateral force vs. lateral deformation curve (capacity curve) of the building. In the pushover analysis carried out, the load pattern used was an inverted triangle load pattern, which is the equivalent lateral load pattern given in the 1998 Turkish Earthquake Code [1] for buildings with an overall height above grade less than 25m. The load at each story level was applied at the geometric centroid of the floor plan. The story displacements were measured at the point of application of the lateral load.

In the nonlinear static analysis, one of the most crucial points is modeling of the nonlinear behavior of the structural members. In this study, the nonlinear models of the structural elements were formed using the default nonlinear hinge properties given in SAP2000. The default hinge properties of SAP2000 are mainly based on the modeling guidelines given in the FEMA 356 document [9].

The moment-rotation relationship used for reinforced concrete columns and beams is shown in Figure 7.1.

In Figure 7.1, M_y is the yield moment capacity and θ_y is the yield rotation of the section computed from the classical section analysis, respectively.

The nonlinear force-deformation relationship of the brick infill walls were obtained using the equivalent strut model proposed by Smith [42] as explained in Chapter 4.
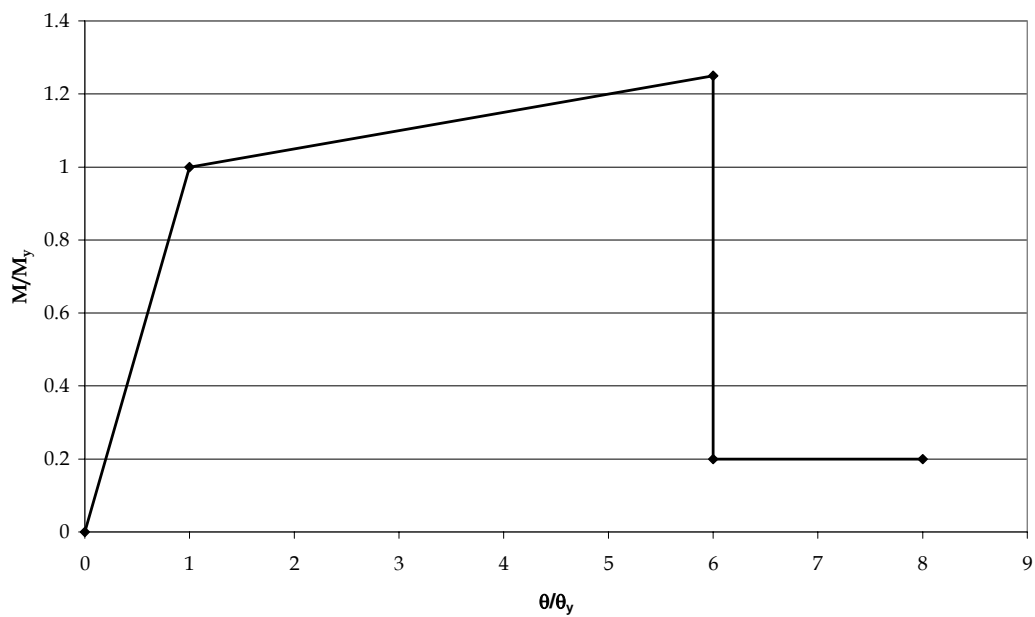
Figure 7.1 - Nonlinear Moment – Rotation Relationship used for Reinforced Concrete Columns and Beams

7.3 Procedure for Determination of the Displacement Demand of a Building under A Ground Motion

For the assessment of a building under a ground motion or design spectrum, the displacement demand of that ground motion on the building must be determined. In other words the "performance point (pp)" of the building under the given ground motion must be found. Once the capacity curve of the building is obtained, the pp can be determined using approximate procedures such as the Capacity Spectrum Method of ATC-40 [9] or the Displacement Coefficient Method proposed in FEMA 356 [8].

In this study, a nonlinear time history analysis was carried out on the equivalent single degree of freedom system of the building to determine the performance point. For this, firstly, the nonlinear force-deformation relationship of the equivalent single degree of freedom system must be established. The capacity curve of a building is expressed in terms of the base shear of the building and the corresponding roof displacement, whereas the nonlinear force deformation relationship of the equivalent single degree of freedom system is expressed in terms of the base shear force and the spectral displacement (Figure 7.2). This conversion was done using the formulations given in ATC-40. These formulations are briefly summarized in the following paragraphs.

Each mode of a multi degree of freedom (MDOF) system can be represented by an equivalent single degree of freedom (SDOF) system having a normalized mass (M^*), stiffness (K^*) and the same period, T. In Figure 7.2, the force-deformation relationships for MDOF and SDOF systems are equivalent to each other. In other words, if the roof of the building will move a distance of δ_{roof} for a certain base shear force, the displacement of the equivalent single degree of freedom system will be S_d. The ratio of δ_{roof} to S_d is, by definition, the modal participation factor for the fundamental mode at the roof level (PF_{R1}). For an n story building, PF_{R1} is given as:

$$PF_{R1} = \frac{\sum\limits_{i=1}^{n} m_i \phi_{i1}}{\sum\limits_{i=1}^{n} m_i \phi_{i1}^2} \phi_{n1}$$
(7.1)

where

i is the story number; m_i is the lumped mass at story i; ϕ_{i1} is the amplitude of mode 1 at level i.

Then,

$$\delta_{roof} = PF_{R1} S_d$$
(7.2)

The stiffness of the equivalent single degree of freedom (K*) system can be computed from:

$$T = 2\pi \sqrt{\frac{M*}{K*}}$$
(7.3)

Here, T is the period of the corresponding mode of the MDOF system and M* is the effective mass at that mode, which is equal to the product of the effective mass coefficient of the mode j (α_j) and total mass of the building, M. For the first mode, the effective mass coefficient is:

$$\alpha_1 = \frac{\left(\sum\limits_{i=1}^{n} m_i \phi_{i1}\right)^2}{\left(\sum\limits_{i:1}^{n} m_i\right)\left(\sum\limits_{i=1}^{n} m_i \phi_{i1}^2\right)}$$
(7.4)

The bilinear force-deformation curve of the multi-story building can be converted to that of an equivalent SDOF by computing the yield spectral displacement, S_{dy} using Eq. 7.1 and 7.2 and the equivalent stiffness, K*.

Then, the software NONLIN was used to carry out a nonlinear time history analysis using the nonlinear force deformation relationship obtained using Eqs 7.1 through 7.4. At the end of this analysis, the maximum spectral displacement is obtained and this spectral displacement is converted to the equivalent roof displacement using Eq. 7.2. The point corresponding to this roof displacement on the capacity curve is the performance point of the building under the given ground motion.
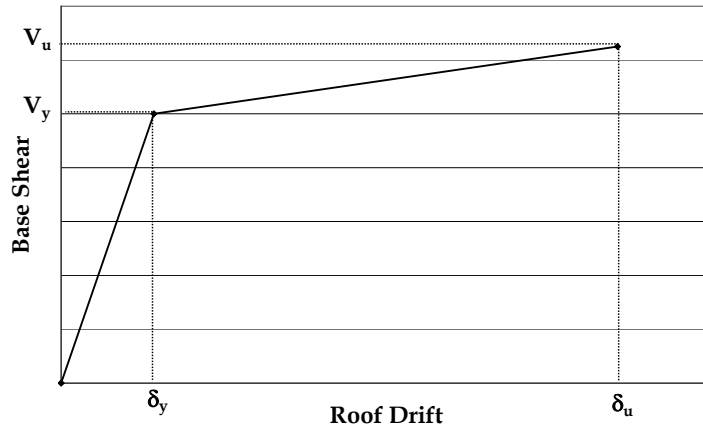
Figure 7.2 - Force – Deformation Relationships for the Building and the
Equivalent Single Degree of Freedom System

7.4   CASE STUDIES ON BUILDINGS DAMAGED IN THE RECENT EARTHQUAKES THAT OCCURRED IN TURKEY

7.4.1   Case Study Building 1

The first case study building is a five story building located in the city of Ceyhan. It had experienced the Ceyhan Earthquake, which occurred in 1998. The moment magnitude of this earthquake was 6.2 and the recorded peak ground acceleration in Ceyhan was 0.273g. The floor plan area of the building is 250 m²

and the lateral load resisting system is a moment resisting reinforced concrete frame with brick infills in certain bays of the frame. The floor system of the building is joist floor. The mean compressive strength of concrete was found to be 14 MPa and the yield strength of the reinforcement was reported to be 220 MPa.

The building had been investigated by the experts from Middle East Technical University and the damage sustained by the building was reported to be "*light*" [57]. According to the reports, damage was concentrated at the ground floor level. Seven columns and seven beams of the ground floor were lightly damaged, whereas only one column was moderately damaged. There were also 5 heavily and 12 moderately damaged brick infills. The plan view of the first story of the building is shown in Figure 7.3.
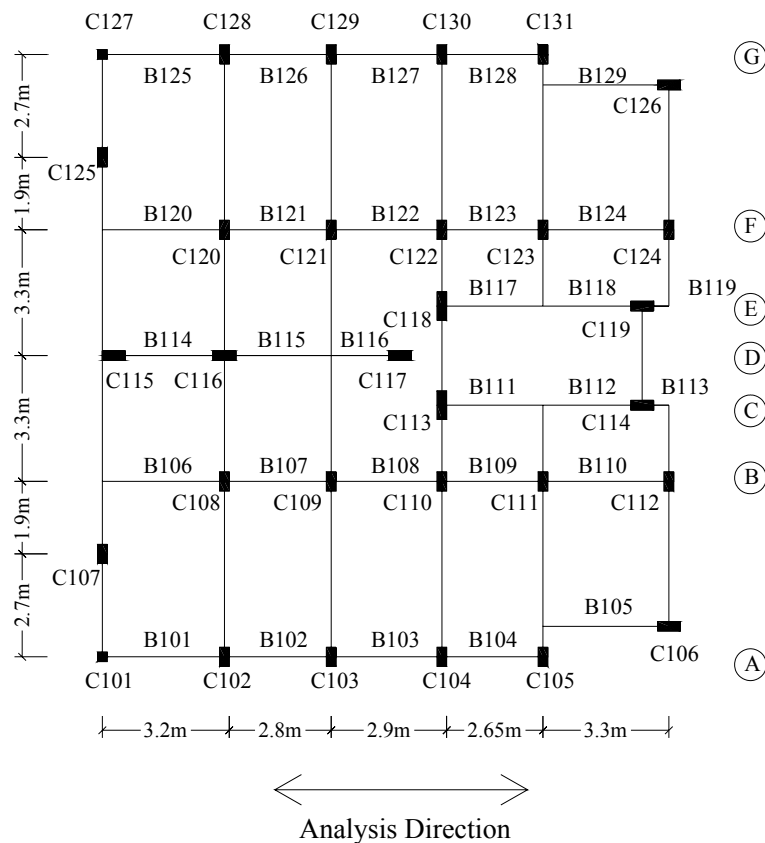
Figure 7.3 – Plan view of the Case Study Building 1

The building was investigated in the longitudinal direction and under the North-South component of the Ceyhan ground motion. The acceleration time history record of the ground motion is given in Figure 7.4 and the 5% damped response spectrum is given in Figure 7.5. In the time history analysis, it was assumed that the ground motion the building was subjected to was exactly the same as the recorded ground motion. Moreover, it was also assumed that the direction of the North-South component of the given ground motion matches exactly with the longitudinal direction of the building.
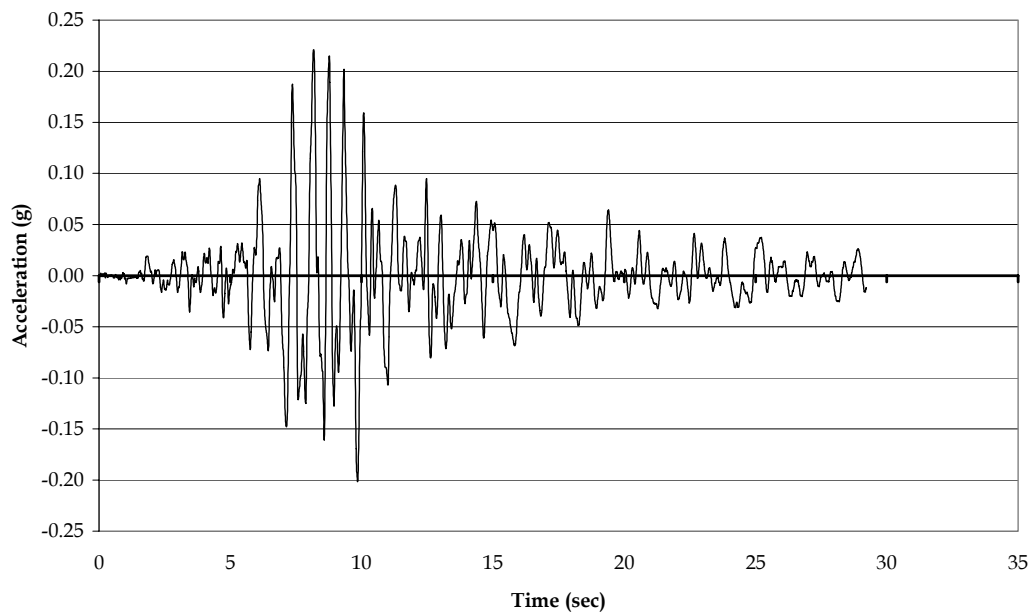
Figure 7.4 – Acceleration Time History of Ceyhan Earthquake

As the first step, the building was modeled in 3D in SAP 2000 and a modal analysis was carried out. As a result of this analysis the fundamental period of the building was computed as 0.744 seconds. The corresponding mode shape is presented in Figure 7.6 (a). Then, a pushover analysis was carried out on the building. The load-deflection curve obtained as a result of this pushover analysis is presented in Figure 7.7. The capacity curve obtained was converted to the capacity curve of an equivalent single degree of freedom system using the formulations summarized in the above paragraphs. Then, a nonlinear time

146

history analysis was carried out on the equivalent single degree of freedom system using the software NONLIN. As a result of this time history analysis, the maximum spectral displacement was computed to be 47.2 mm and the corresponding roof displacement was computed to be 62.0 mm. The performance point of the structure under the Ceyhan Earthquake is shown on the capacity curve of the building given in Figure 7.7. The displacement profile is given in Figure 7.6 (b). Figure 7.8 shows the hinge patterns at the performance point.
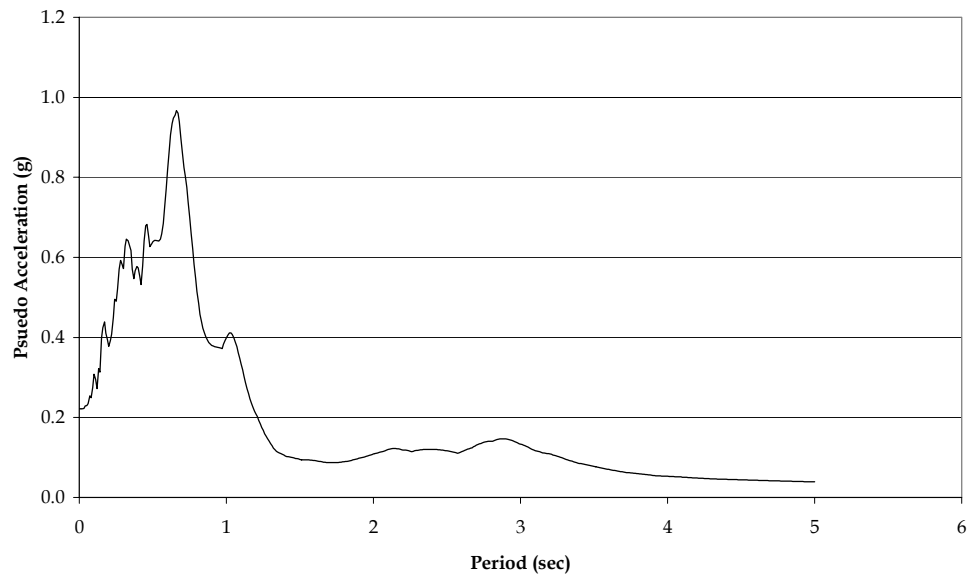
Figure 7.5 – 5% Damped Response Spectrum of Ceyhan Ground Motion

The member end deformations at the performance point were used to compute the damage score of all of the members using the proposed component damage curves. The performance of the members was also evaluated using the methods proposed by ATC 40, FEMA 356 and EUROCODE 7. The results obtained are summarized in Table 7.1 for the members of the first story together with the observed damage states.

After the computation of the member damage scores, the component and story importance factors were computed. Then, the damage score of each story and the building was computed. These computations are summarized in Table 7.2.

(a)   (b)

Figure 7.6 – (a) 1st Mode Shape of Case Study Building 1 and (b) the
displacement profile at the performance point
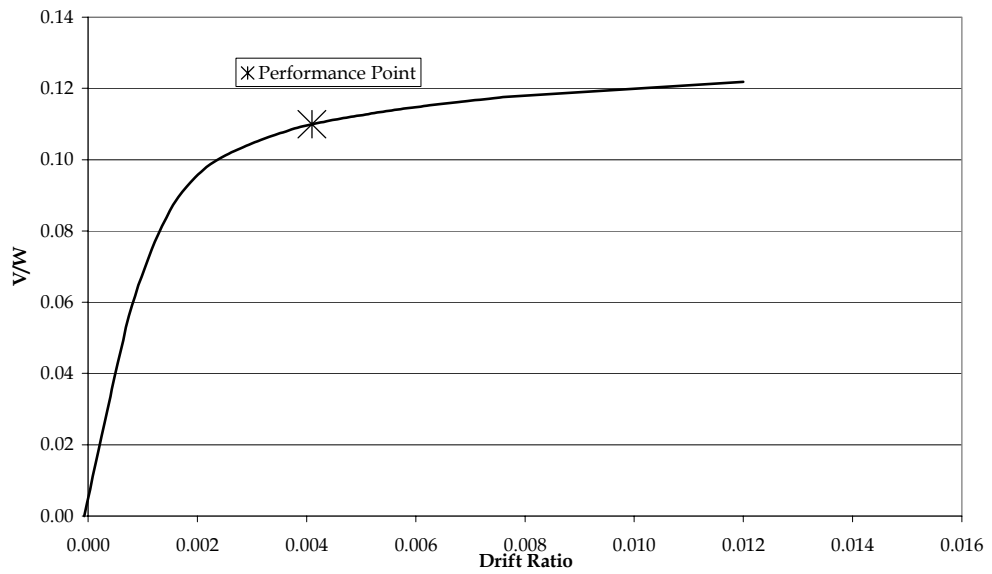
Figure 7.7 – Capacity Curve of the Case Study Building 1 and the
Performance Point under Ceyhan Ground Motion

Frame A

Frame B

Frame C

Frame D

Frame E

Frame F

Frame G
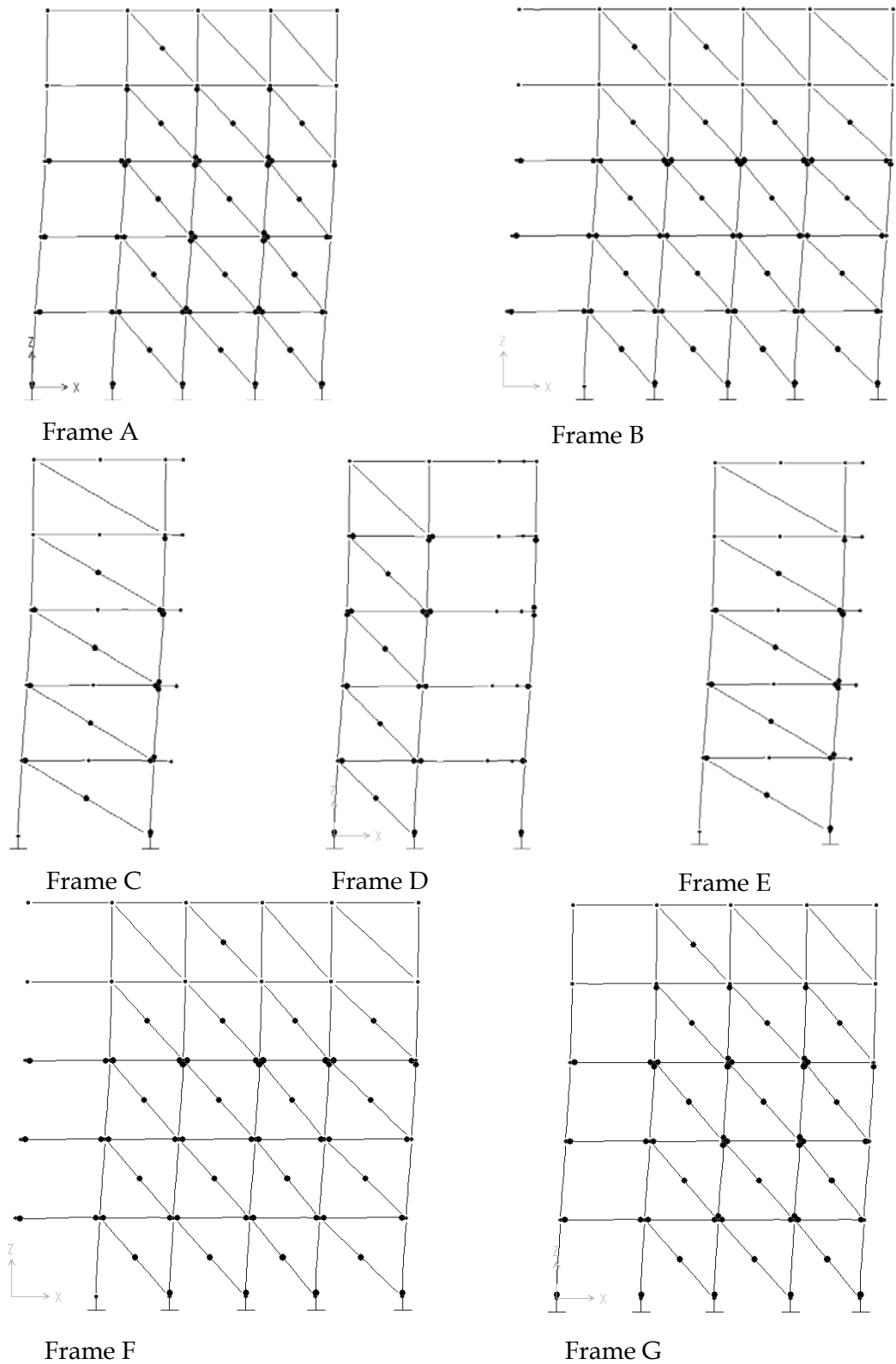
Figure 7.8 – Hinge pattern of the Case Study Building 1 at the performance point

Table 7.1 – Member Damage Scores for Case Study Building 1

Member	Observed	This Study	ATC-40	FEMA-356	EUROCODE
C101	N (None)	1.96	IO	IO	IO
C102	N	3.98	CP	IO	IO
C103	N	3.98	CP	IO	IO
C104	N	3.98	CP	IO	IO
C105	N	3.98	IO	IO	IO
C106	N	15.70	IO	IO	LS
C107	N	3.98	CP	IO	IO
C108	N	3.98	CP	IO	IO
C109	N	3.98	IO	IO	IO
C110	N	3.98	CP	IO	IO
C111	L (Light)	3.98	IO	IO	IO
C112	L	3.98	IO	IO	IO
C113	N	1.96	IO	IO	IO
C114	N	27.34	CP	IO	LS
C115	N	39.57	CP	Collapsed	LS
C116	L	39.57	CP	CP	LS
C117	L	27.34	IO	IO	LS
C118	N	1.96	IO	IO	IO
C119	N	27.34	CP	IO	LS
C120	N	3.98	CP	IO	IO
C121	N	3.98	IO	IO	IO
C122	N	3.98	CP	IO	IO
C123	N	3.98	IO	IO	IO
C124	N	3.98	IO	IO	IO
C125	N	3.98	CP	IO	IO
C126	N	15.70	IO	IO	LS
C127	N	1.96	IO	IO	IO
C128	N	3.98	CP	IO	IO
C129	N	3.98	CP	IO	IO
C130	N	3.98	CP	IO	IO
C131	M	3.98	IO	IO	IO
B101	N	0.47	LS	LS	IO
B102	N	4.54	IO	IO	LS
B103	N	0.73	IO	IO	LS
B104	N	2.64	IO	IO	LS
B105	N	0.59	IO	IO	IO
B106	N	0.56	LS	LS	IO
B107	N	0.56	LS	LS	LS
B108	N	0.34	IO	IO	IO
B109	N	0.34	IO	IO	LS
B110	N	0.52	IO	IO	IO
B111	N	21.88	IO	IO	LS

Table 7.1 (Cont'd) – Member Damage Scores for Case Study Building 1

Member	Observed	This Study	ATC-40	FEMA-356	EUROCODE
B112	N	10.88	IO	IO	LS
B113	N	3.33	IO	IO	LS
B114	L	27.13	LS	LS	LS
B115	N	24.24	LS	LS	LS
B116	N	24.24	IO	IO	LS
B117	L	21.88	IO	IO	LS
B118	N	10.88	IO	IO	LS
B119	N	3.33	IO	IO	LS
B120	N	0.56	LS	LS	IO
B121	N	0.56	LS	LS	LS
B122	N	0.34	IO	IO	IO
B123	N	0.34	IO	IO	LS
B124	N	0.52	IO	IO	IO
B125	L	0.47	LS	LS	IO
B126	L	4.54	IO	IO	LS
B127	L	0.73	IO	IO	LS
B128	N	2.64	IO	IO	LS
B129	N	0.59	IO	IO	IO

When Table 7.1 is examined, it is observed that the damage states predicted by the proposed damage curves are generally in accordance with the observed damage with certain deviances. The largest discrepancy between the observed and predicted damage states was observed for the columns C114 – C119 and the beams B114- B117. For these elements, the observed damage states were either light or none. However, the proposed damage curves predict the damage states of these members as moderate (damage scores vary between 10.88% and 39.57%). The main reason for this discrepancy seems to be the fact that the columns C114-C119 were placed in their stronger direction in the analysis direction whereas the remaining columns were placed in their weaker directions. Hence, these columns are theoretically more susceptible to damage then the other columns. In Table 7.1, it can also be seen that the other assessment methods also predict higher damages for these columns than the other ones. For the beams B-114-B118, it can be stated that these beams were found to suffer heavier damage than the others since they are connected to the columns which are placed in their stronger direction (C114-C119).

Table 7.2 – Story and Building Damage Scores for Case Study Building 1

Story #	Raw Story IF	Stories Above	Story IF	Story Damage (%)	Weighted Story Damage (%)
1	0.23	5	0.35	24.21	7.53
2	0.23	4	0.28	11.08	3.08
3	0.22	3	0.21	15.24	3.13
4	0.22	2	0.14	1.83	0.25
5	0.09	1	0.03	0.01	0.00
Building Damage Score (%)					14.99

The building damage score was computed to be equal to 14.99%. Although this damage score is in the range of the life safety performance level according to the criterion set in this study, it is just above the upper limit for the immediate occupancy and the lower limit for the life safety (10%). Hence, it can be stated that the results of the assessment of the building using the proposed procedure shows a pretty good match with the observed damage for this case study building.

7.4.2 Case Study Building 2

The second case study building is a four story commercial building in the center of the city of Dinar, which is owned by the municipality. The typical plan area is 310 m². The height of the ground floor was 3.8 m and the heights of the remaining stories were 3.5 m. The mean compressive strength of concrete was determined as 12 MPa from the core samples taken from the building. The yield strength of longitudinal reinforcement is 280 MPa.

The building was moderately damaged in the Dinar Earthquake which occurred on October 1, 1995 (M_L=5.9). The recorded peak ground acceleration of the ground motion was 0.293g. The acceleration time history of the Dinar ground motion and the 5% damped response spectrum are given in Figures 7.9 and 7.10, respectively.

The major damage in the building was reported to be concentrated at the ground floor level. There were 1 severely damaged, 3 moderately damaged and 1 lightly damaged columns at this floor. Of the 20 beams in the analyzed direction

of the building, one was moderately damaged and another one was lightly damaged. The plan view of the first story and the observed damage is shown in Figure 7.11.

After the building was modeled in 3D in SAP2000, a modal analysis was carried out and the fundamental period of the building was computed to be 0.8 sec. The corresponding mode shape is shown in Figure 7.12 (a). Then, a nonlinear static analysis was carried out and the capacity curve of the building was obtained (Figure 7.13). The capacity curve was converted to a force-deformation diagram of an equivalent single degree of freedom system and a nonlinear time history analysis was carried out on this single degree of freedom system. As a result of this analysis, the maximum spectral displacement was computed to be 46.7 mm and the corresponding roof displacement was found to be 61.2 mm. The performance point obtained is shown in Figure 7.13 on the capacity curve of the building. Figure 7.14 shows the hinge patterns of the case study building 2 at the performance point. The displacement profile at the performance point is shown in Figure 7.12 (b). The member end deformations at the performance point were used to assess the damage level of the members using the proposed curves as well as the ATC-40, FEMA-356 and Eurocode 8 procedures. The results of this analysis are presented in tabular form in Table 7.3 together with the observed damage.
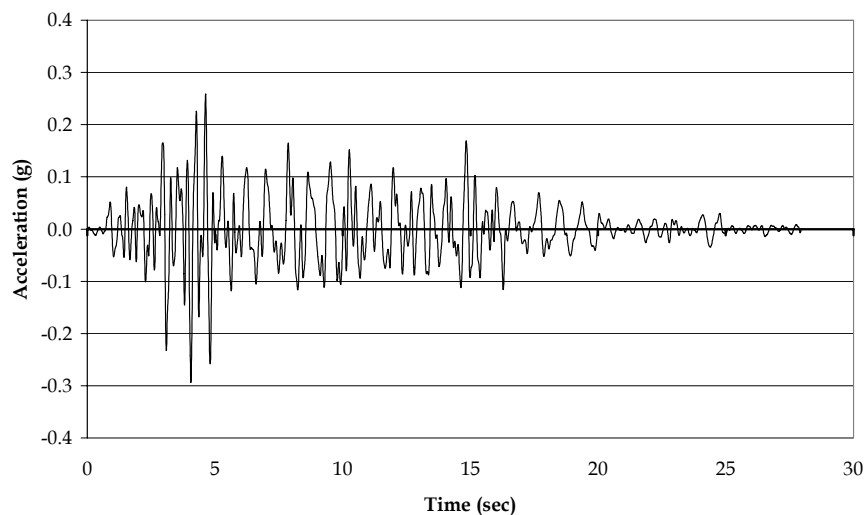
Figure 7.9 – Acceleration Time History of Dinar Earthquake

153
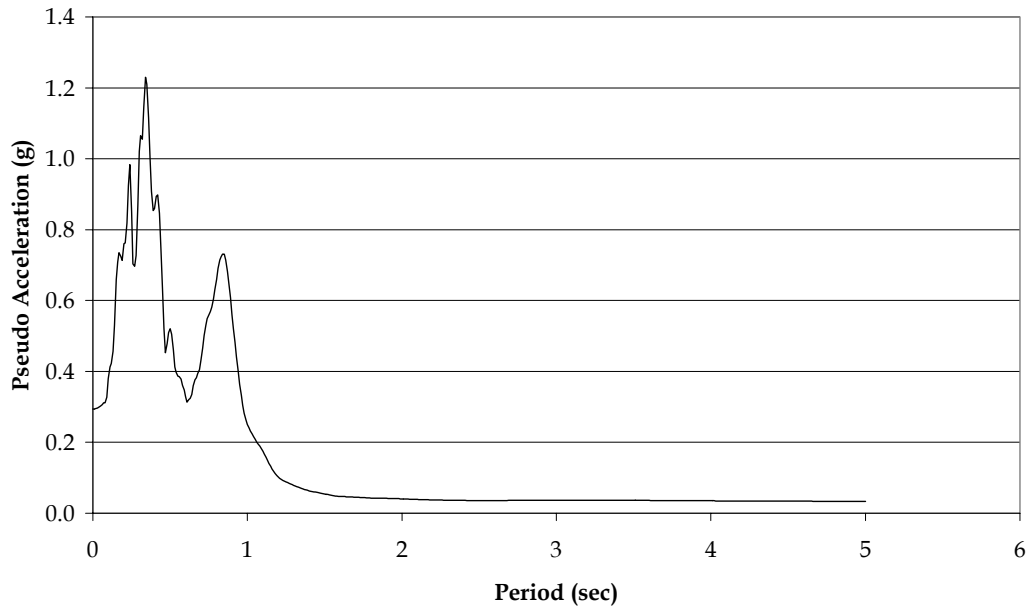
Figure 7.10 – 5% Damped Response Spectrum of Dinar Earthquake
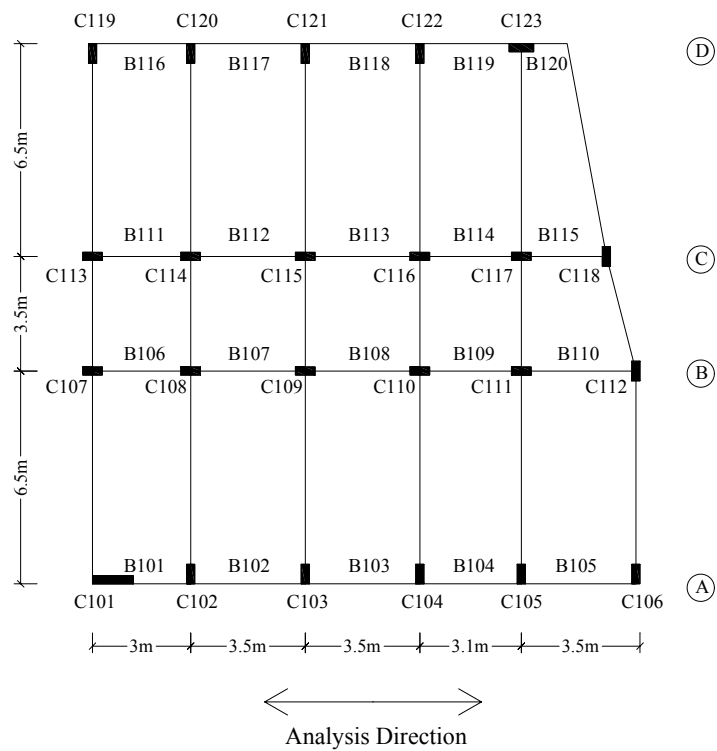
Figure 7.11 – Plan View of the Case Study Building 2

154

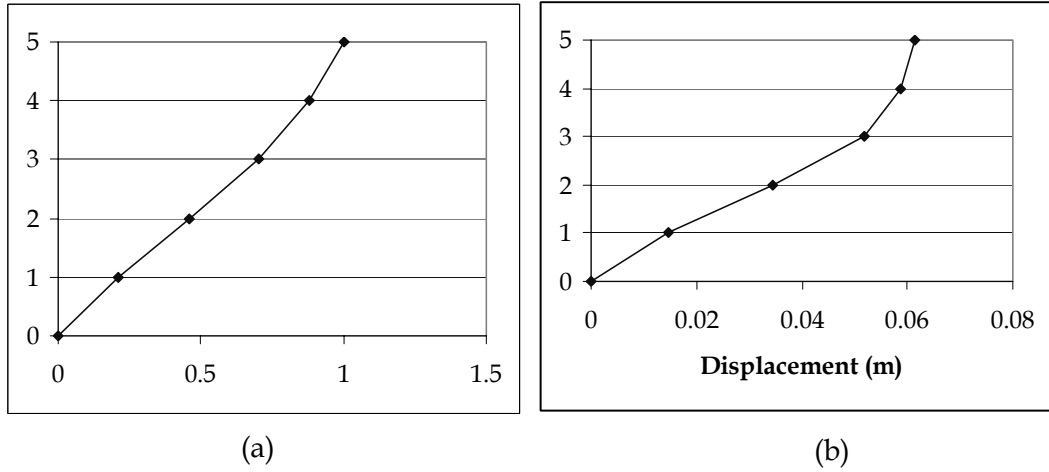(a)   (b)

Figure 7.12 – (a) 1st Mode Shape of Case Study Building 2 and (b) the
displacement profile of at the performance point

Figure 7.13 – Capacity Curve of the Case Study Building 2 and the
Performance Point under Düzce Earthquake

155

Frame A

Frame B

Frame C

Frame D
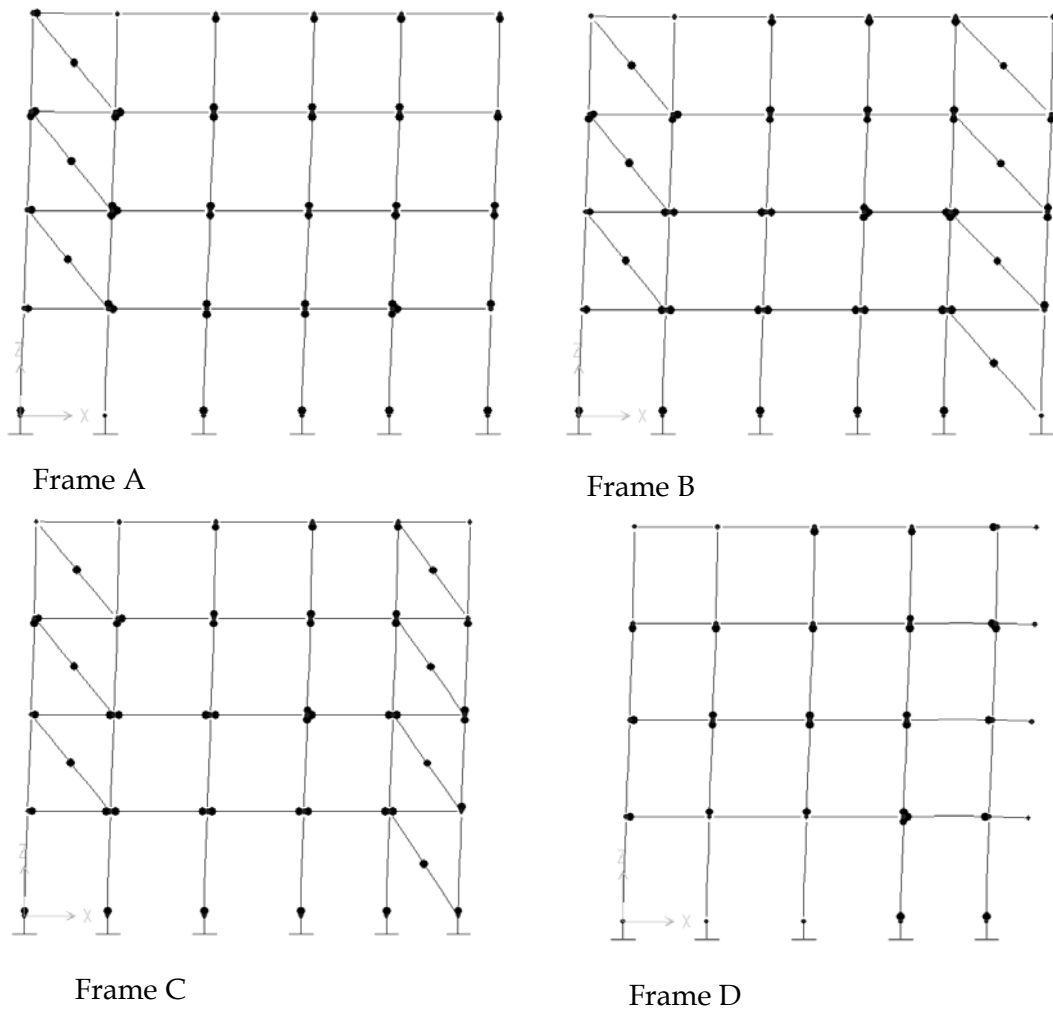
Figure 7.14 – Hinge Patterns of the Case Study Building 2 at the
performance point

Table 7.3 – Member Damage Scores for Case Study Building 2

Member	Observed	This Study	ATC-40	FEMA-356	EUROCODE
C101	M (Moderate)	59.83	IO	IO	LS
C102	N (None)	1.19	IO	IO	IO
C103	N	1.19	IO	IO	IO
C104	N	1.19	IO	IO	IO
C105	N	1.19	IO	IO	IO
C106	N	1.19	IO	IO	IO

Table 7.3 (Cont'd) – Member Damage Scores for Case Study Building 2

Member	Observed	This Study	ATC-40	FEMA-356	EUROCODE
C107	M	15.29	CP	IO	LS
C108	M	22.70	CP	CP	LS
C109	S (Severe)	15.29	CP	IO	LS
C110	N	15.29	CP	CP	LS
C111	N	22.70	CP	CP	LS
C112	N	1.05	IO	IO	IO
C113	N	14.43	CP	IO	LS
C114	L (Light)	21.54	CP	IO	LS
C115	N	14.43	CP	IO	LS
C116	N	14.43	CP	CP	LS
C117	N	21.54	CP	IO	LS
C118	N	0.98	IO	IO	IO
C119	N	0.86	IO	IO	IO
C120	N	0.86	IO	IO	IO
C121	N	0.86	IO	IO	IO
C122	N	0.86	IO	IO	IO
C123	N	41.89	CP	IO	LS
B101	M	16.54	IO	IO	LS
B102	N	0.02	IO	IO	IO
B103	N	0.00	IO	IO	IO
B104	N	0.00	IO	IO	IO
B105	N	0.01	IO	IO	IO
B106	L	14.03	IO	IO	LS
B107	N	9.10	IO	IO	LS
B108	N	7.81	IO	IO	LS
B109	N	9.52	IO	IO	LS
B110	N	9.52	IO	IO	LS
B111	N	13.49	IO	IO	LS
B112	N	7.52	IO	IO	LS
B113	N	7.29	IO	IO	LS
B114	N	9.44	IO	IO	LS
B115	N	9.44	IO	IO	LS
B116	N	3.46	IO	IO	LS
B117	N	0.00	IO	IO	IO
B118	N	0.00	IO	IO	IO
B119	N	13.28	IO	IO	LS
B120	N	13.28	IO	IO	LS

For the second case study building, the proposed damage curves could predict the damage states of the members satisfactorily, especially for beams. For the columns, some discrepancies between the observed and predicted damage

states were observed. The most interesting one of these discrepancies was observed for the columns C107, C109 and C110. These columns all have the same properties and undergo the same displacement. As a result the damage scores of these columns were computed to be same. However, the observed damage states for these columns were moderate, severe and light, respectively. The other assessment methods also predict that these three columns would suffer the same level of damage. The author believes that the difference in the observed damage for these columns is due to the local deficiencies that arose during the construction stage, which is not possible for any analytical method to capture.

After the computation of the component importance factors, the story damage scores and the story importance factors were computed and the building damage score was found to be 22.60% (Table 7.4). This damage score falls in the life safety limit state according to the damage criterion used in this study, which is in a quite good agreement with the observed damage.

Table 7.4 – Story and Building Damage Scores for Case Study Building 2

Story #	Raw Story IF	Stories Above	Story IF	Story Damage (%)	Weighted Story Damage (%)
1	0.30	4	0.43	36.76	15.90
2	0.30	3	0.32	10.76	3.43
3	0.29	2	0.21	13.86	2.91
4	0.11	1	0.04	9.44	0.36
Building Damage Score (%)					22.60

7.4.3 Case Study Building 3

The third case study was conducted on the branch office of the Ministry of the Public Works and Settlement in Bolu. The building was approximately 39 km away from the epicenter of the November 12, 1999 Duzce Earthquake.

The building was a five story reinforced concrete structure with a plan area of 230 m². It is essentially rectangular in shape with three bays in both directions. The depth of the peripheral beams was 1.2 m. The floor height was 3.8 m for the first story and 3.2 m for the remaining stories. The average concrete strength was 20 MPa, and the yield strength of longitudinal reinforcement was

220 MPa. Most of the infills of the building were not spanning from one column to another. Hence, it was assumed that the contribution of the infills in the seismic behavior of the building was negligible.

The instrument that recorded the ground acceleration history of the Duzce Earthquake (M_w=7.2) was located in the garden of this building. Hence, the ground motion that the building was exposed to was exactly known. The analyses on this building were carried out under the East-West component of this record which was assumed to correspond to the longitudinal direction of the building. The peak ground acceleration was 0.512 g for this component of the ground motion. The acceleration time history of the ground motion and the 5% damped response spectrum is given in Figures 7.15 and 7.16, respectively.
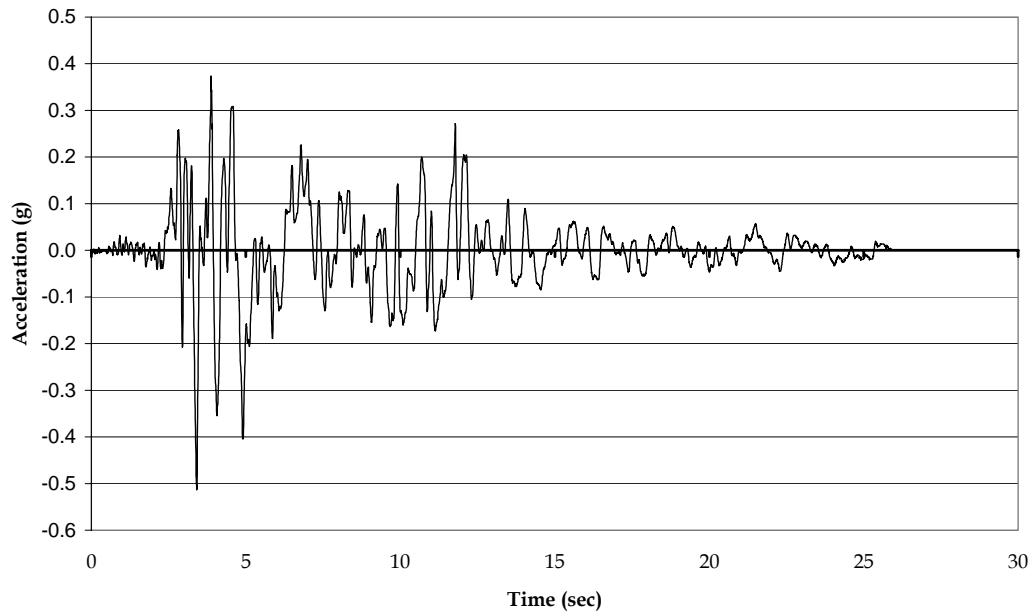
Figure 7.15 – Acceleration Time History of Düzce EQ

The building was heavily damaged during the November 12, 1999 Düzce Earthquake. Most of the damage was observed in the first story. In this story, almost all of the columns had diagonal shear cracks. Moreover, severe buckling in the longitudinal reinforcement of one of the columns was also observed. All of the beams in this story had flexural cracking and the damage level of all of them was

159

reported as moderate. Diagonal shear cracks were also observed at the second story columns. The observed damage in the first story is shown on the plan view in Figure 7.17.
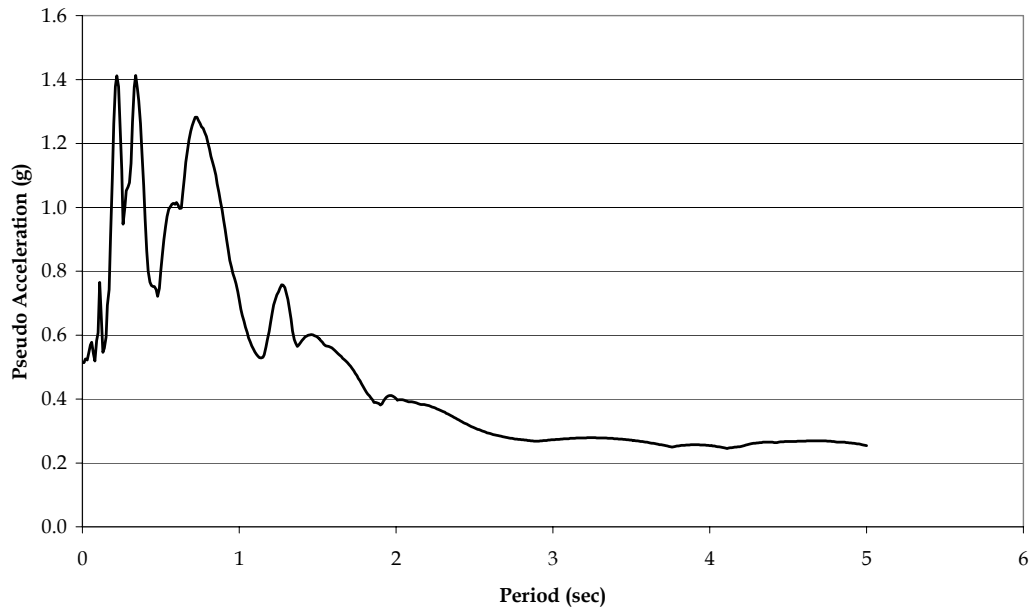
Figure 7.16 – 5% Damped Response Spectrum of Düzce Earthquake
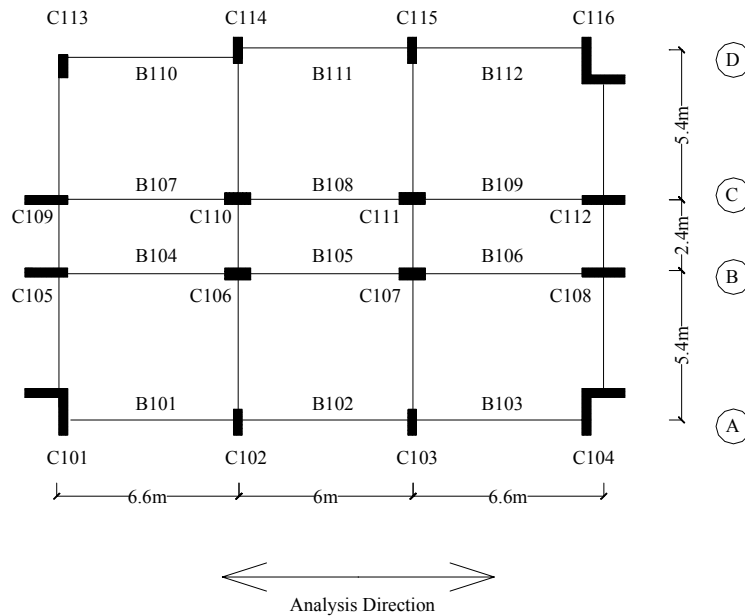
Figure 7.17 – Plan View of the Case Study Building 3

160

As in the case of the previous buildings, this building was also modeled in 3D in SAP2000. As a result of a modal analysis, the period of the structure was computed as 0.7 seconds. The mode shape of the building is shown graphically in Figure 7.18 (a). The capacity curve of the building obtained as a result of the nonlinear static analysis is shown in Figure 7.19. As a result of the nonlinear time history analysis carried out on the equivalent single degree of freedom system of the building the maximum spectral displacement was found out to be 161.7 mm which corresponds to a roof displacement of 214.9 mm. The performance point of the building under the given ground motion record is shown on the capacity curve in Figure 7.19. Figure 7.18 (b) shows the displacement profile at the performance point. The hinge patterns of the building at the performance point are shown in Figure 7.20.

The results of the damage assessment of the structural members of the first story using the methodologies developed in this study, ATC-40, FEMA-356 and EUROCODE-8 and the observed damage are shown in Table 7.5. Table 7.6 shows the story damage scores, story importance factors and the building damage score computed according to the methodology summarized before.
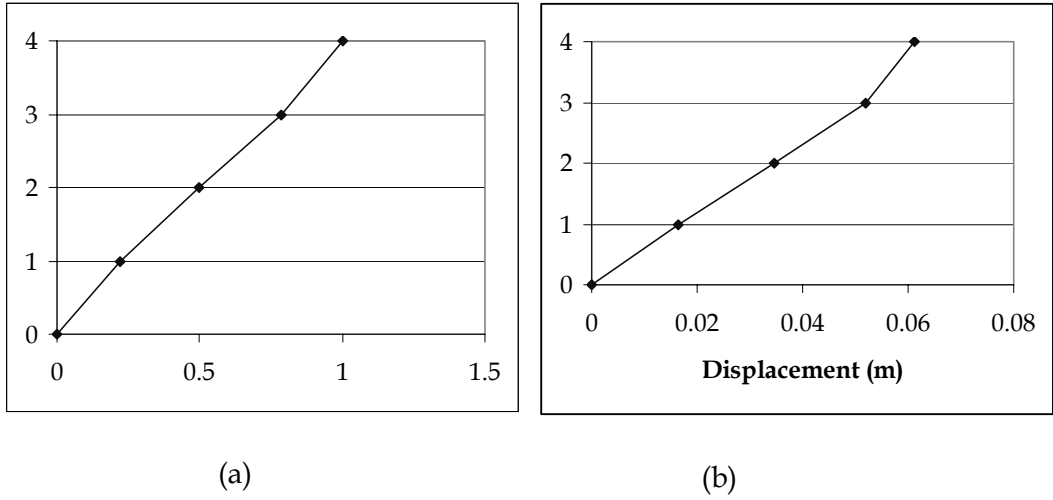

(a)   (b)

Figure 7.18 – (a) 1st Mode Shape of Case Study Building 3 and (b) the displacement profile at the performance point
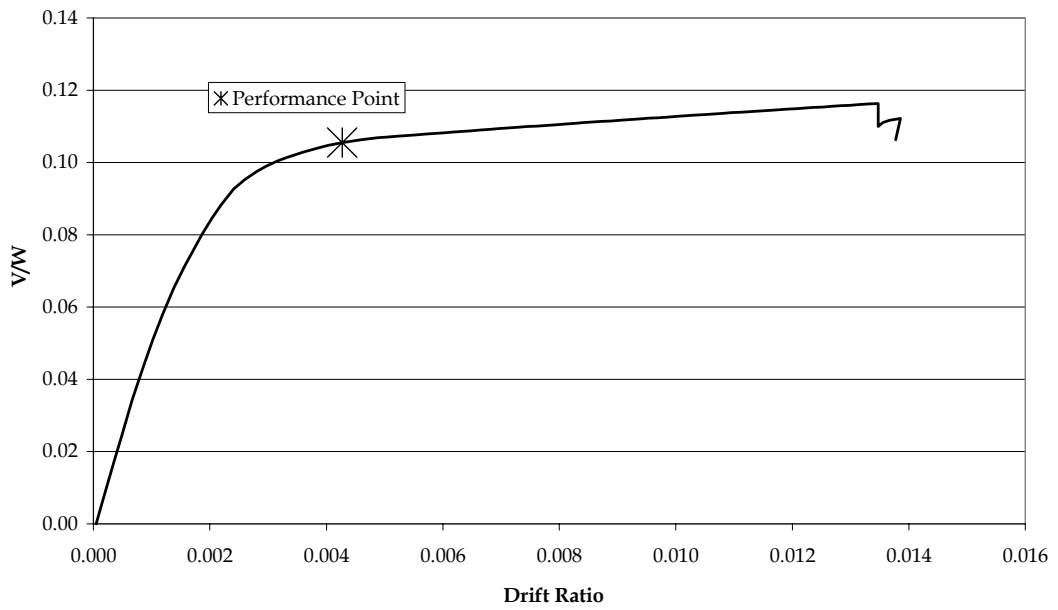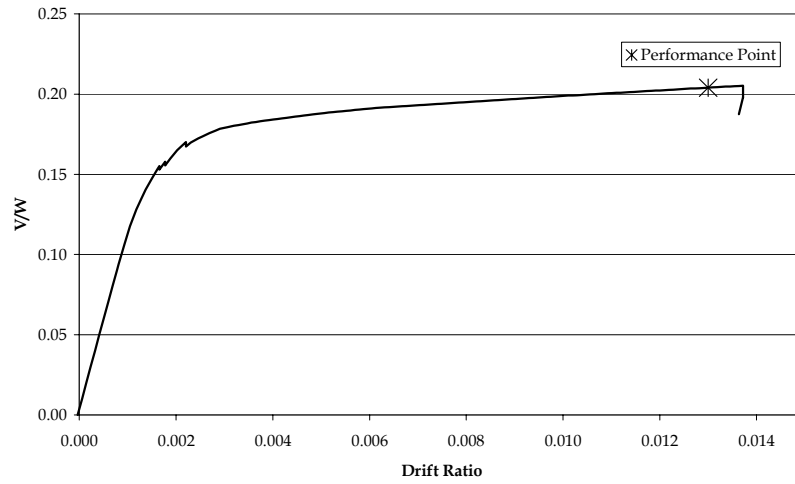
Figure 7.19 – Capacity Curve of the Case Study Building 3 and the Performance Point under Düzce Earthquake
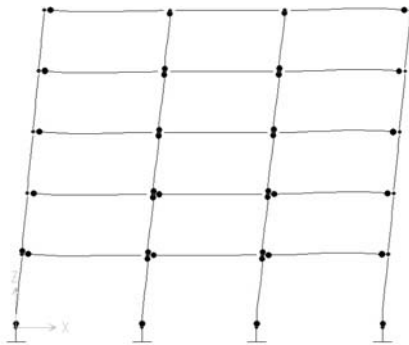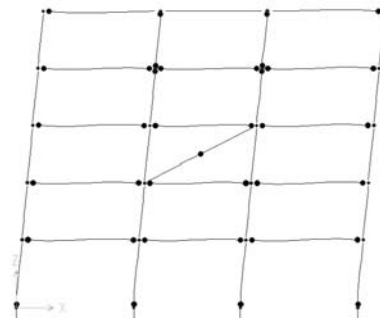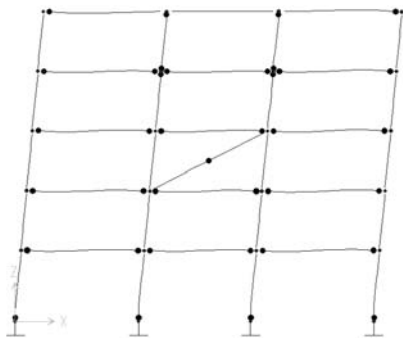
Frame A

Frame B

Frame C

Frame D

Figure 7.20 – Hinge Patterns of the Case Study Building 3 at the performance point

162

Table 7.5 – Member Damage Scores for Case Study Building 3

Member	Observed	This Study	ATC-40	FEMA-356	EUROCODE
C101	S (Shear)	100.00	Collapsed	Collapsed	LS
C102	L (Light)	35.12	CP	Collapsed	LS
C103	L	35.12	Collapsed	Collapsed	LS
C104	S (Shear)	100.00	Collapsed	Collapsed	LS
C105	S (Shear)	100.00	Collapsed	Collapsed	LS
C106	S (Shear)	100.00	Collapsed	Collapsed	CP
C107	L	100.00	Collapsed	Collapsed	CP
C108	S (Shear)	100.00	Collapsed	Collapsed	LS
C109	S (Shear)	100.00	Collapsed	Collapsed	LS
C110	S (Shear)	100.00	Collapsed	Collapsed	CP
C111	S (Shear)	100.00	Collapsed	Collapsed	CP
C112	S (Shear)	100.00	Collapsed	Collapsed	LS
C113	S (Shear)	37.58	CP	Collapsed	LS
C114	S (Shear)	37.58	Collapsed	Collapsed	CP
C115	S (Shear)	37.58	Collapsed	Collapsed	LS
C116	S (Shear)	100.00	Collapsed	Collapsed	LS
B101	S (Severe)	55.38	CP	CP	LS
B102	S	0.69	IO	IO	IO
B103	S	55.78	IO	IO	LS
B104	S	64.82	CP	CP	LS
B105	S	63.72	CP	CP	LS
B106	S	64.82	CP	CP	LS
B107	S	65.39	CP	CP	LS
B108	S	64.25	CP	CP	LS
B109	S	65.21	CP	CP	LS
B110	S	51.08	CP	CP	LS
B111	S	0.07	IO	IO	IO
B112	S	56.85	IO	IO	LS

For the case study building 3, the predicted damage states show a good match with the observed cases.

The building damage score was computed as 39.6%, which corresponds to a performance level of life safety. However, the damage score for the first story was computed to be 89.2%. According to the criterion set in this methodology, since the maximum story damage exceeds 70%, the performance of the building under the Duzce Earthquake is estimated to be collapse prevention, which is in accordance with the observed damage state.

Table 7.6 – Story and Building Damage Scores for Case Study Building 3

Story #	Raw Story IF	Stories Above	Story IF	Story Damage (%)	Weighted Story Damage (%)
1	0.24	5	0.36	89.19	31.72
2	0.23	4	0.28	15.96	4.45
3	0.23	3	0.21	9.08	1.86
4	0.22	2	0.13	7.95	1.20
5	0.09	1	0.03	15.14	0.40
Building Damage Score (%)					39.63

7.4.4   Case Study Building 4

The fourth case study building was the administrative building of a school located in the city of Düzce. The building is a two story moment resisting frame with a plan area of 407 m². The plan view of the building is given in Figure 7.21. The height of both stories was measured as 3.05 m. The Schmidt Hammer readings taken from different locations yielded an average compressive concrete strength of 17 MPa, while the yield strength of the longitudinal reinforcement was determined to be 220 MPa.

The building was lightly damaged in the Düzce Earthquake of 12 November 1999. The acceleration time history and 5% damped elastic response spectrum of the Düzce Earthquake was given in Figures 7.15 and 7.16, respectively.

The assessment of the building was carried out in the longitudinal direction which was determined as the weaker direction. The building was modeled in 3D in SAP 2000 and a free vibration analysis was carried out. As a result of this analysis the fundamental period of the structure was found out to be 0.29 seconds. The first mode shape of the building is shown in Figure 7.22 (a).
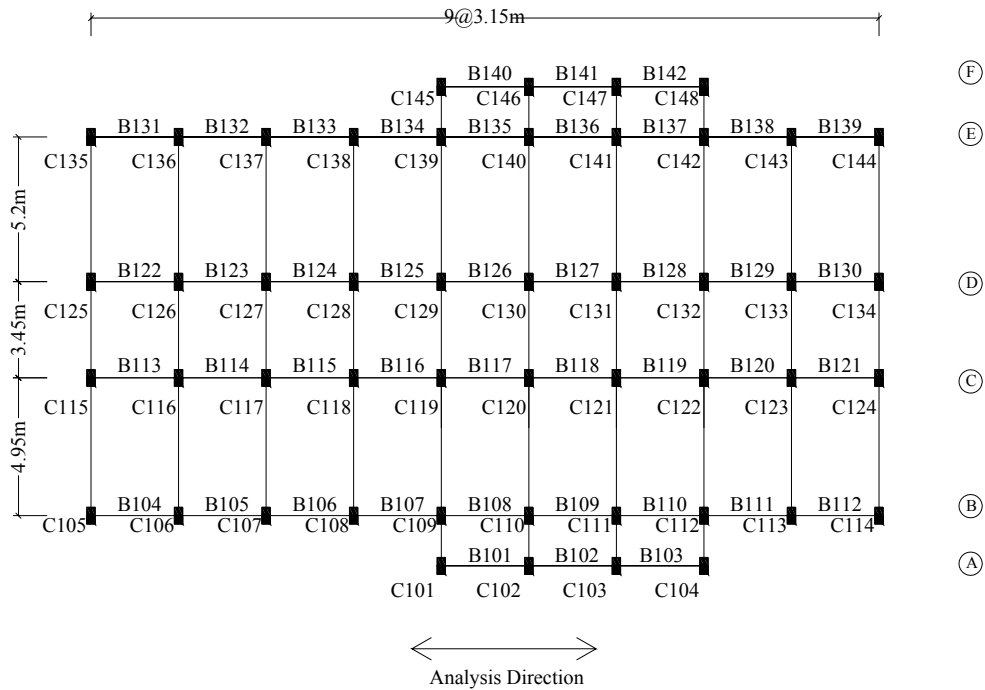
Figure 7.21 – Plan View of Case Study Building 4

After the free vibration analysis, a nonlinear static analysis was carried out on the building. The capacity curve obtained from the nonlinear static analysis is given in Figure 7.23. Then, this capacity curve was converted to the bilinear capacity curve of an equivalent single degree of freedom system. The nonlinear time history analyses carried out on the equivalent single degree of freedom system, the maximum spectral displacement was computed as 0.021 m which corresponds to a roof displacement of 0.025 m. The performance point of the building under the Düzce Earthquake is shown on the capacity curve of the building in Figure 7.23. The displacement profile of the case study building 4 at the performance point is shown in Figure 7.22 (b) Figure 7.24 designates hinge patterns of the case study building 4 at the performance point. The member end deformations at the performance point were used to assess the performance of the members using the damage curves developed in this study together with the procedures of FEMA-356 [8], ATC-40 [8] and Eurocode 8 [12]. Although, the overall damage state of the building after the 12 Düzce Earthquake is known, the

damage state of the members was not documented by the teams who investigated the building. Hence, only the member damage states of the columns of the first story of this building predicted by the aforementioned procedures are presented in Table 7.7 and no information on the observed damage can be given.

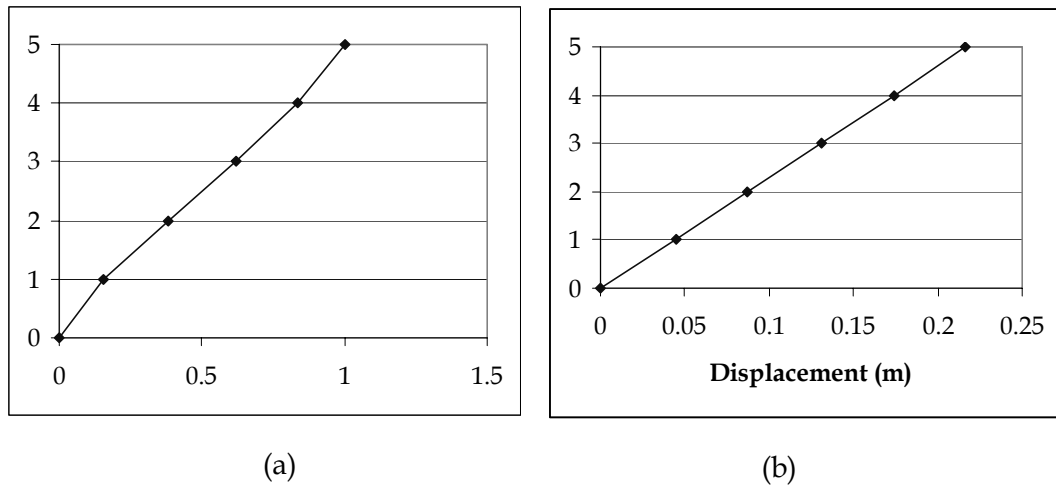(a)   (b)
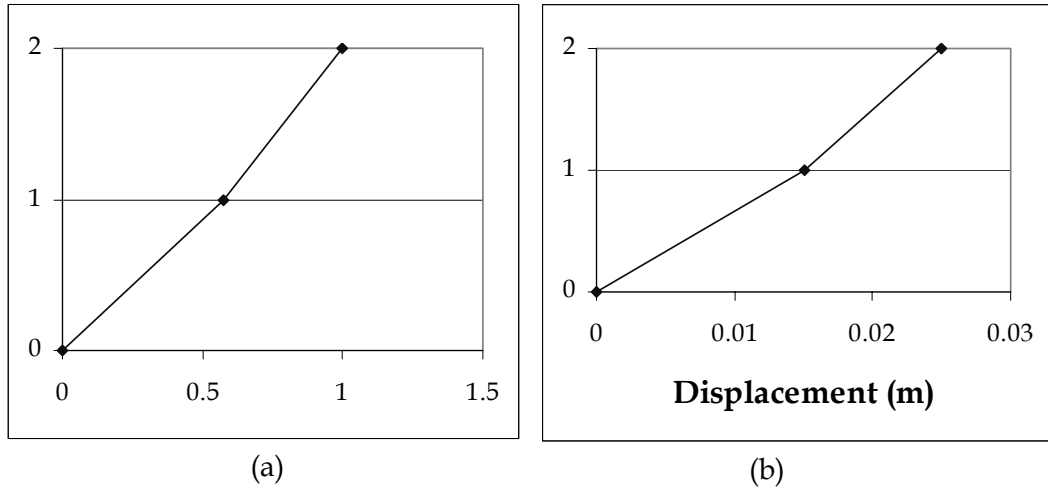
Figure 7.22 – (a) 1st Mode Shape of Case Study Building 4 and (b) the displacement profile at the performance point
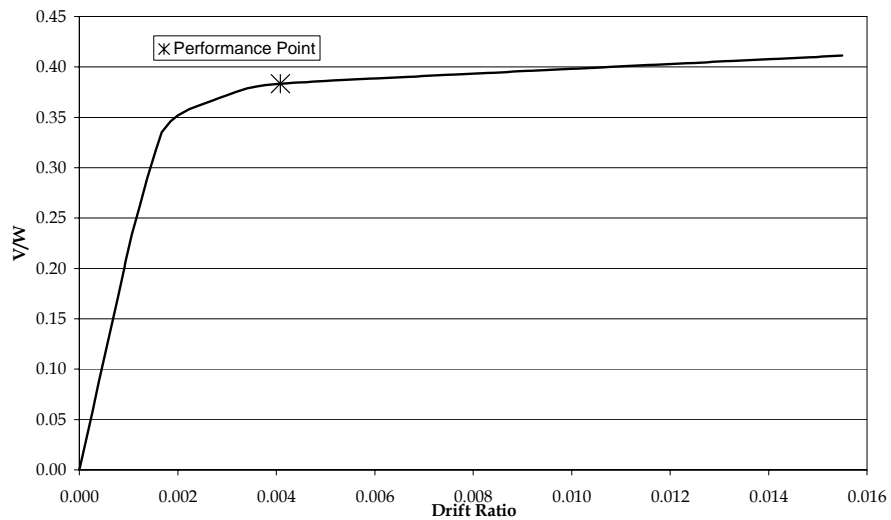


Figure 7.23 – Capacity Curve of the Case Study Building 4 and the Performance Point under Düzce Earthquake
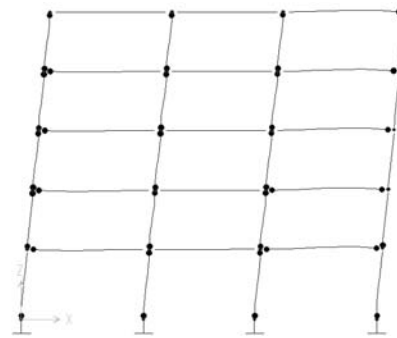
Frame A

Frame F

Frame B

Frame C

Frame D

Frame E
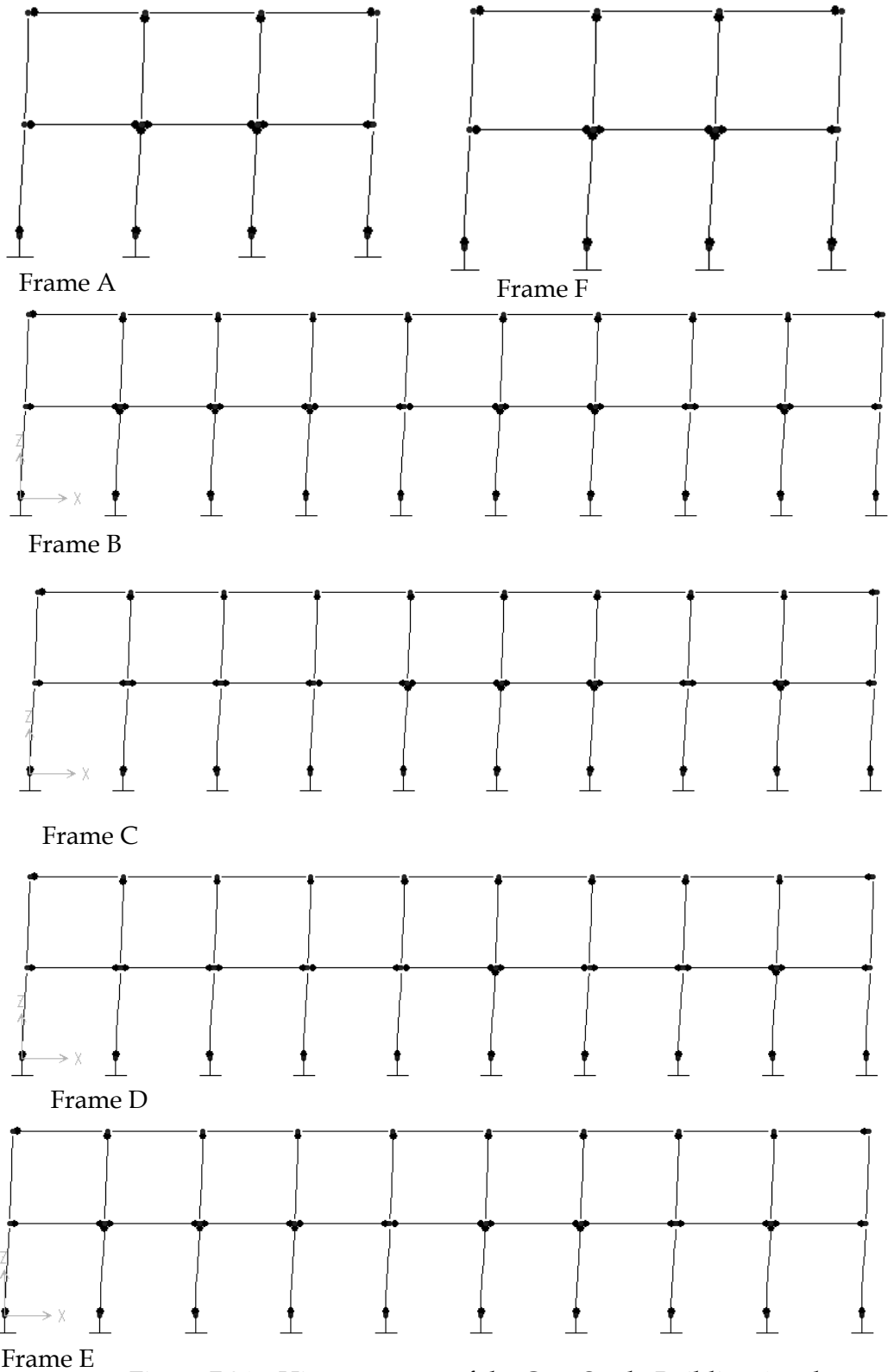
Figure 7.24 – Hinge patterns of the Case Study Building 4 at the

performance point

Table 7.7 – Member Damage States for the 1st Story Columns of the Case Study Building 4

Member	This Study	ATC-40	FEMA-356	EUROCODE
C101	4.07	IO	IO	IO
C102	4.07	IO	IO	IO
C103	4.07	IO	IO	IO
C104	4.07	IO	IO	IO
C105	4.07	IO	IO	IO
C106	6.89	IO	IO	IO
C107	6.89	IO	IO	IO
C108	6.89	IO	IO	IO
C109	6.89	IO	IO	IO
C110	6.89	IO	IO	IO
C111	6.89	IO	IO	IO
C112	6.89	IO	IO	IO
C113	6.89	IO	IO	IO
C114	4.07	IO	IO	IO
C115	6.89	IO	IO	IO
C116	6.89	IO	IO	IO
C117	6.89	IO	IO	IO
C118	6.89	IO	IO	IO
C119	6.89	IO	IO	IO
C120	6.89	IO	IO	IO
C121	6.89	IO	IO	IO
C122	6.89	IO	IO	IO
C123	6.89	IO	IO	IO
C124	6.89	IO	IO	IO
C125	6.89	IO	IO	IO
C126	6.89	IO	IO	IO
C127	6.89	IO	IO	IO
C128	6.89	IO	IO	IO
C129	6.89	IO	IO	IO
C130	6.89	IO	IO	IO
C131	6.89	IO	IO	IO
C132	6.89	IO	IO	IO
C133	6.89	IO	IO	IO
C134	6.89	IO	IO	IO
C135	4.07	IO	IO	IO
C136	6.89	IO	IO	IO
C137	6.89	IO	IO	IO
C138	6.89	IO	IO	IO
C139	6.89	IO	IO	IO
C140	6.89	IO	IO	IO
C141	6.89	IO	IO	IO

Table 7.7 (Cont'd) – Member Damage States for the 1st Story Columns of the Case Study Building 4

Member	This Study	ATC-40	FEMA-356	EUROCODE
C141	6.89	IO	IO	IO
C142	6.89	IO	IO	IO
C143	6.89	IO	IO	IO
C144	4.07	IO	IO	IO
C145	4.07	IO	IO	IO
C146	4.07	IO	IO	IO
C147	4.07	IO	IO	IO
C148	4.07	IO	IO	IO

Table 7.8 shows the story and building level damage scores which were computed using the member damage scores and the component importance factors. The maximum story damage score was computed as 5.39% and the overall building damage score was computed as 3.81% which corresponds to the immediate occupancy performance level. The reported damage after the Düzce Earthquake was light, which is in accordance with the predicted performance.

Table 7.8 – Story and Building Damage Scores for Case Study Building 4

Story #	Raw Story IF	Stories Above	Story IF	Story Damage (%)	Weighted Story Damage (%)
1	0.50	2	0.67	5.39	3.59
2	0.50	1	0.33	0.66	0.22
Building Damage Score (%)					3.81

7.4.5 Case Study Building 5

Another case study building is a five story residential building located in Düzce. The plan area of the building is 163.5 m² (Figure 7.25) and the story height is 2.9 m for all stories. The average compressive strength of concrete was reported to be 22 MPa and the yield strength of longitudinal reinforcement was 220 MPa.

The building was moderately damaged in the Düzce Earthquake that occurred on 12 November 1999 (Figures 7.15 and 7.16).
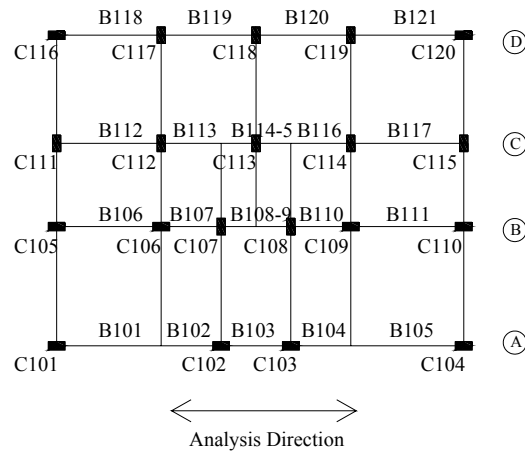
Figure 7.25 – Plan View of the Case Study Building 5

As a result of the modal analysis carried out on the building, the fundamental period of the building was computed as 0.477 seconds. The mode shape of the first mode is Figure 7.26 (a). The capacity curve of the building, obtained as a result of the nonlinear static analysis carried out is shown in Figure 7.27. The performance point of the building under the Düzce Earthquake was determined using the procedure summarized in part 7.3 of this dissertation and it is shown on the capacity curve of the building in Figure 7.27. Figure 7.26 (b) designates the displacement profile at the performance point. In Figure 7.28, the hinge patterns at the performance are shown.

(a)

(b)
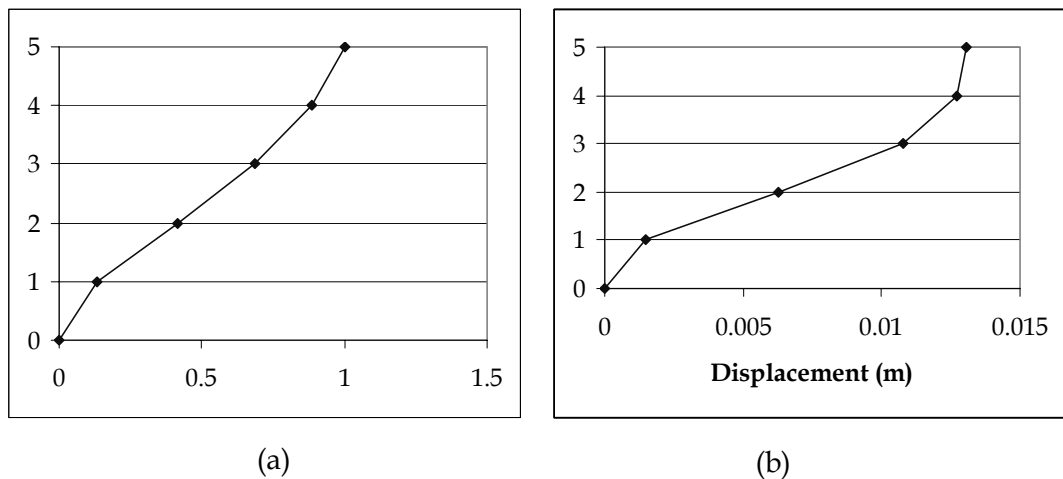
Figure 7.26 – (a) 1st Mode Shape of Case Study Building 4 and (b) displacement profile at the performance point

170
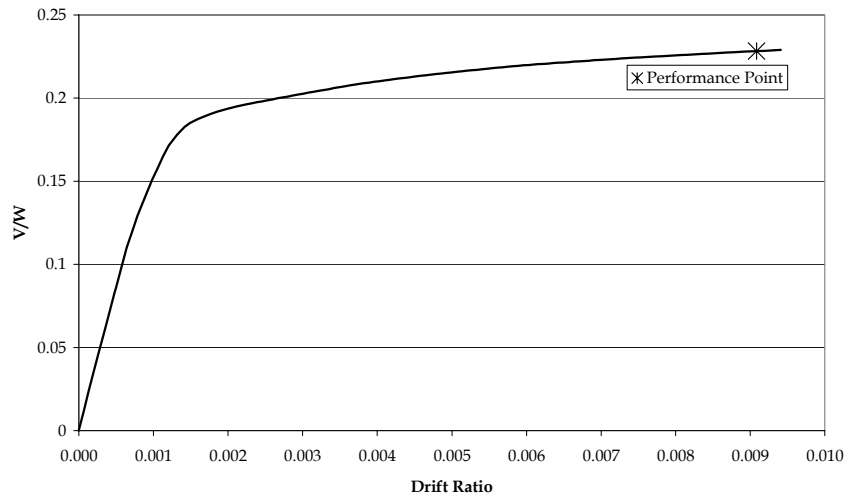
Figure 7.27 – Capacity Curve of the Case Study Building 5 and the Performance Point under Düzce Earthquake

Frame A

Frame B

Frame C

Frame D
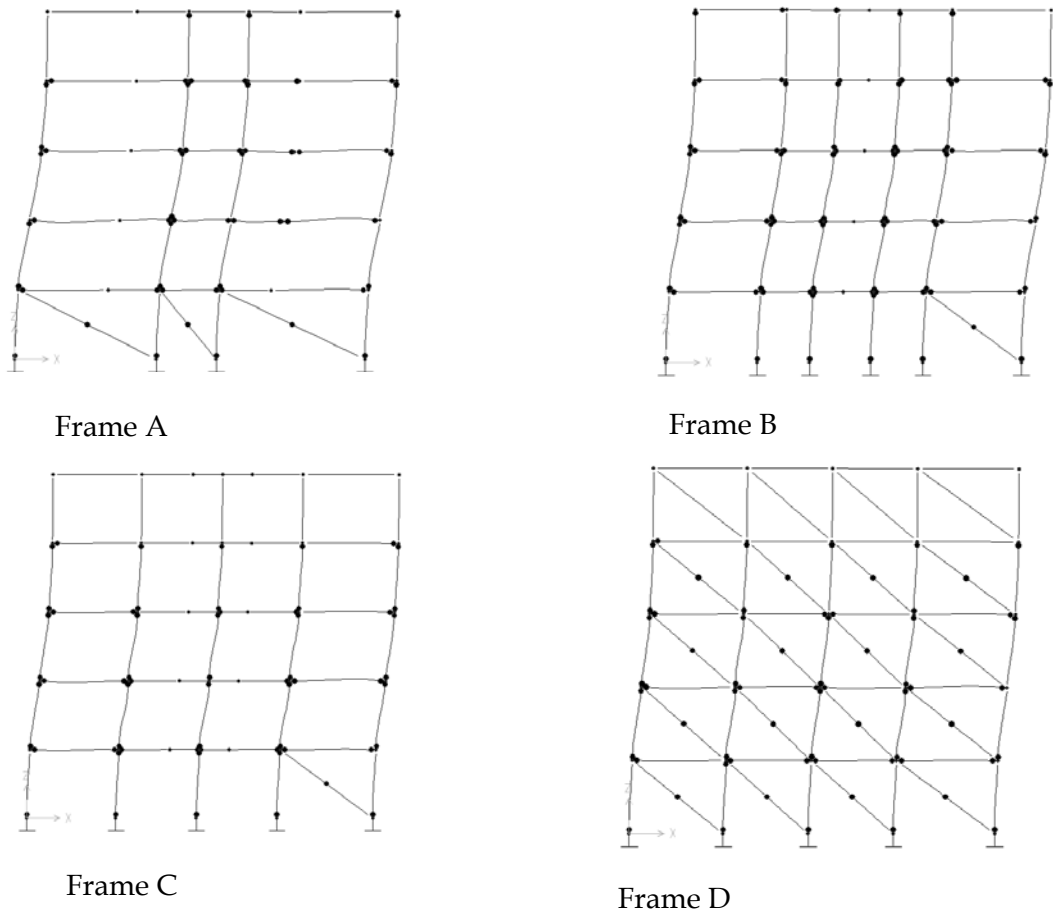
Figure 7.28 – Hinge Patterns of the Case Study Building 5 at the performance point

The damage state of the members of the building was assessed using the member end deformations at the performance point and the procedures used for the previous case study buildings. The results of the member damage assessment are presented in Table 7.9 for the columns and beams of the second story, which was found to suffer the heaviest damage.

Table 7.9 - Member Damage States for the 2nd Story Columns and Beams of the Case Study Building 5

Member	This Study	EUROCODE	FEMA-356	ATC-40
C201	63.46	LS	Collapsed	Collapsed
C202	64.90	LS	Collapsed	Collapsed
C203	64.07	LS	Collapsed	Collapsed
C204	63.16	LS	Collapsed	Collapsed
C205	57.37	LS	Collapsed	Collapsed
C206	61.27	LS	Collapsed	Collapsed
C207	43.23	LS	Collapsed	Collapsed
C208	41.08	LS	Collapsed	Collapsed
C209	60.01	LS	Collapsed	Collapsed
C210	55.96	LS	Collapsed	Collapsed
C211	7.59	LS	Collapsed	Collapsed
C212	37.20	LS	Collapsed	Collapsed
C213	41.43	LS	Collapsed	Collapsed
C214	41.02	LS	Collapsed	Collapsed
C215	12.38	LS	Collapsed	CP
C216	22.83	LS	Collapsed	CP
C217	35.57	LS	Collapsed	Collapsed
C218	51.43	LS	Collapsed	CP
C219	32.50	LS	Collapsed	CP
C220	34.50	LS	Collapsed	CP
B201	97.29	LS	CP	CP
B202	95.66	LS	CP	CP
B203	96.52	LS	CP	CP
B204	96.52	LS	CP	CP
B205	97.22	LS	CP	CP
B206	93.48	LS	CP	CP
B207	86.24	LS	CP	CP
B208	5.48	LS	CP	CP
B209	10.21	LS	CP	CP
B210	0.02	IO	LS	LS
B211	93.91	LS	CP	CP
B212	81.96	LS	CP	CP

Table 7.9 (Cont'd) - Member Damage States for the 2nd Story Columns and
Beams of the Case Study Building 5

Member	This Study	EUROCODE	FEMA-356	ATC-40
B213	0.01	IO	CP	CP
B214	0.00	IO	LS	LS
B215	0.00	IO	LS	LS
B216	0.00	IO	CP	CP
B217	84.99	LS	LS	LS
B218	0.00	IO	LS	LS
B219	0.00	IO	LS	LS
B220	66.72	LS	CP	CP

Table 7.10 shows the story and building damage scores for the case study building under the Düzce Earthquake.

As a result of the assessment carried out, the maximum story damage score was computed to be 55.63% and the overall damage score turned out to be 37.01%. According to these damage scores and the damage criterion set in this dissertation, the performance level of the case study building 5 was determined as *life safety*, which is in accordance with the observed damage.

Table 7.10 – Story and Building Damage Scores for Case Study Building 5

Story #	Raw Story IF	Stories Above	Story IF	Story Damage (%)	Weighted Story Damage (%)
1	0.23	5	0.35	30.58	10.77
2	0.23	4	0.28	55.63	15.46
3	0.22	3	0.21	43.05	7.85
4	0.22	2	0.14	21.67	2.93
5	0.10	1	0.03	0.06	0.00
Building Damage Score (%)					37.01

7.4.6 Case Study Building 6

The sixth case study building was a 4 story residential building located in Düzce. The plan area of the building is 640 m² (Figure 7.29). The height of the

ground story is 3.5 m while that of the remaining stories was 2.7 m. The average concrete strength was determined to be 18 MPa, while the yield strength of longitudinal reinforcement was 220 MPa.

The building was heavily damaged in the Düzce Earthquake of 12 November 1999. Figures 7.15 and 7.16 show the acceleration time history and 5% damped elastic response spectrum of the Düzce Earthquake, respectively.

As a result of the modal analysis the fundamental period of the building was computed to be 0.36 seconds. The first mode shape of the building is given in Figure 7.30 (a). The nonlinear analysis carried out yielded the capacity curve given in Figure 7.31. The performance point of the building under the Düzce Earthquake is also shown in Figure 7.31 on the capacity curve of the structure. Figure 7.30 (b) shows the displacement profile of the case study building 6 at the performance point. Figure 7.32 shows the hinge patterns of the building at the performance point.
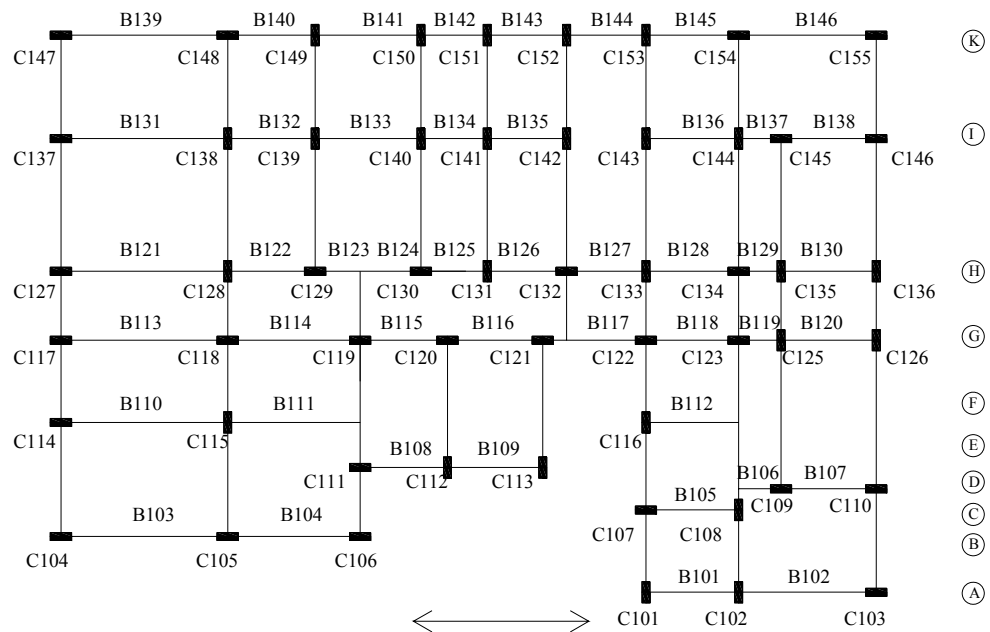
Figure 7.29 – Plan View of the Case Study Building 6
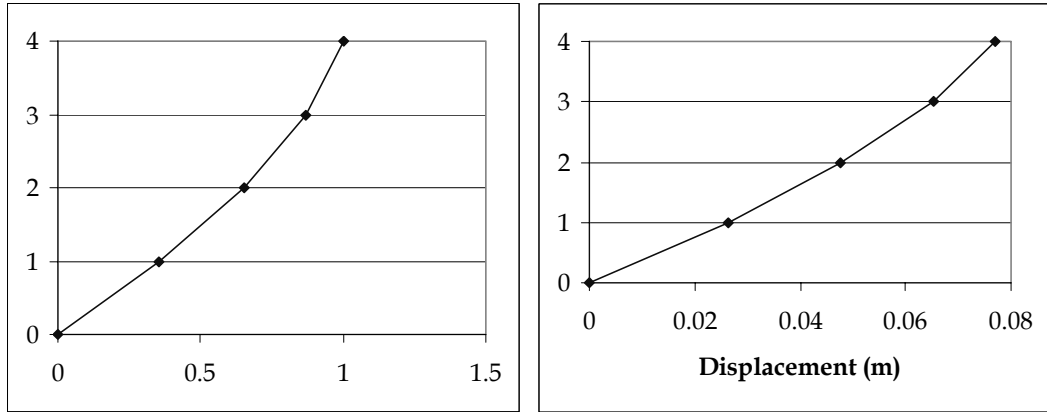
(a)   (b)

Figure 7.30 – (a) 1st Mode Shape of Case Study Building 6 and (b) the
displacement profile at the performance point

Figure 7.31 – Capacity Curve of Case Study Building 6 and the
Performance Point under Düzce Earthquake
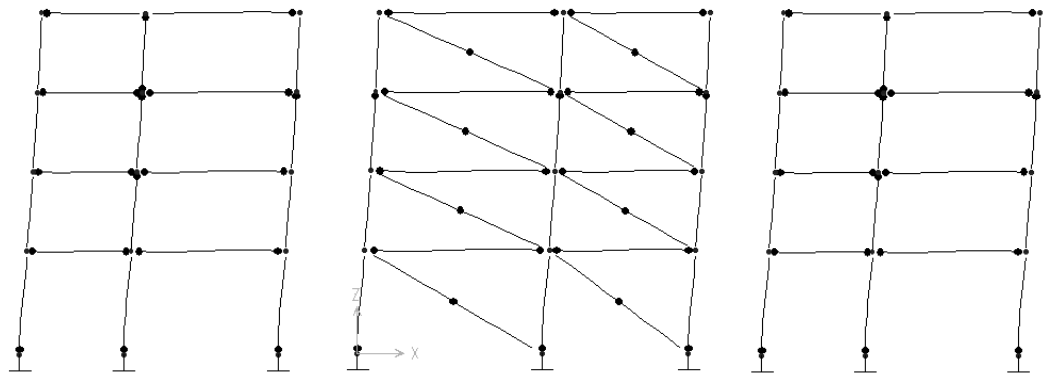
Frame A   Frame B   Frame C
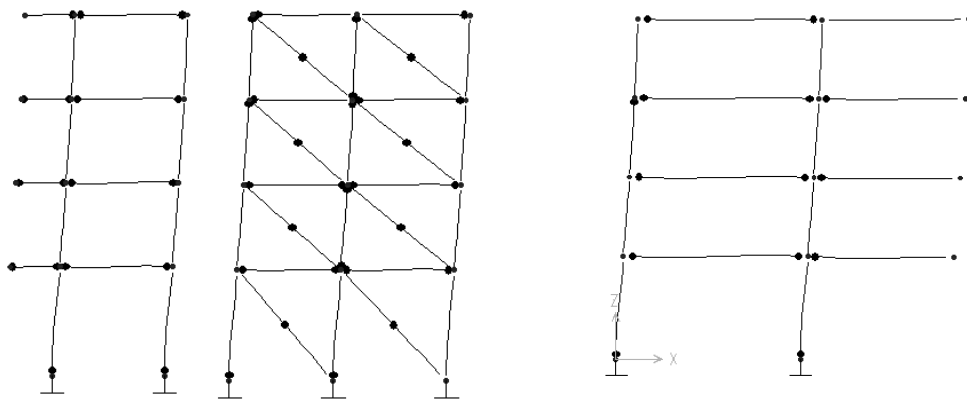
Frame D   Frame E   Frame F

Frame G

Figure 7.32 – Hinge Patterns of the Case Study Building 6

Frame H

Frame I
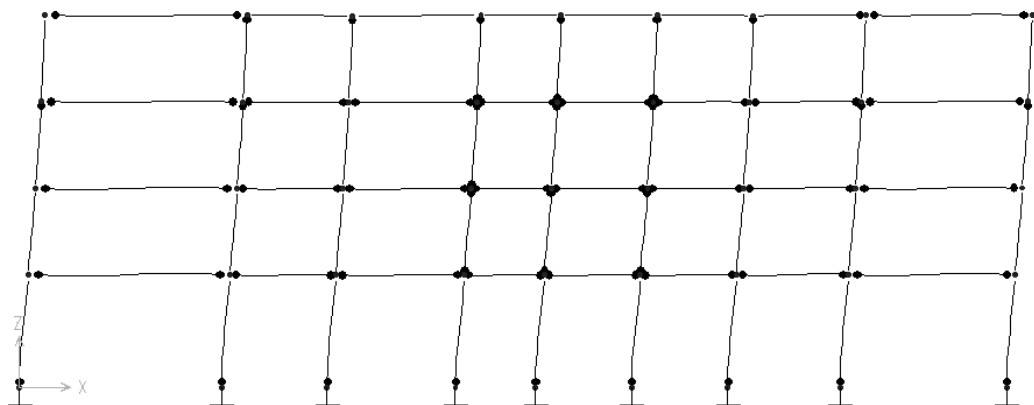
Frame K

Figure 7.32 (Cont'd)– Hinge Patterns of the Case Study Building 6

177

The member end deformations at the performance point were used to assess the damage state of the building at the component level, story level and the building as a whole. Table 7.11 presents the damage states of the first story columns predicted by the procedure developed herein, FEMA 356, ATC-40 and Eurocode 8 procedures.

Table 7.11 - Member Damage States for the 1st Story Columns of the Case Study Building 6

Member	This Study	ATC-40	FEMA-356	EUROCODE
C101	7.09	IO	IO	IO
C102	7.09	IO	IO	IO
C103	74.42	CP	CP	LS
C104	74.89	CP	Collapsed	LS
C105	61.98	CP	Collapsed	LS
C106	57.12	CP	CP	LS
C107	54.26	CP	Collapsed	LS
C108	7.44	IO	IO	LS
C109	62.41	CP	Collapsed	LS
C110	62.41	CP	CP	LS
C111	54.61	CP	Collapsed	LS
C112	7.61	IO	IO	IO
C113	7.61	IO	IO	LS
C114	75.85	CP	Collapsed	LS
C115	14.71	CP	IO	IO
C116	7.81	IO	IO	IO
C117	79.07	CP	Collapsed	LS
C118	76.50	CP	Collapsed	LS
C119	100.00	Collapsed	Collapsed	LS
C120	63.70	CP	Collapsed	LS
C121	90.07	CP	Collapsed	LS
C122	63.70	CP	Collapsed	LS
C123	55.70	CP	Collapsed	LS
C125	9.16	IO	IO	IO
C126	9.16	IO	IO	IO
C127	81.90	CP	Collapsed	LS
C128	15.73	CP	CP	IO
C129	77.05	CP	Collapsed	LS
C130	64.29	CP	Collapsed	LS
C131	9.46	CP	IO	IO
C132	64.29	CP	Collapsed	LS
C133	23.30	CP	CP	IO
C134	56.28	CP	Collapsed	LS
C135	9.46	IO	IO	IO

Table 7.11 (Cont'd) - Member Damage States for the 1st Story Columns of the Case Study Building 6

Member	This Study	ATC-40	FEMA-356	EUROCODE
C136	9.46	IO	IO	IO
C137	77.08	CP	Collapsed	LS
C138	10.07	IO	IO	IO
C139	10.07	IO	IO	IO
C140	10.07	IO	IO	IO
C141	10.07	IO	IO	IO
C142	10.07	IO	IO	LS
C143	10.07	IO	IO	IO
C144	10.07	IO	IO	LS
C145	65.42	CP	Collapsed	LS
C146	65.42	CP	Collapsed	LS
C147	57.24	CP	Collapsed	LS
C148	57.24	CP	Collapsed	LS
C149	10.56	IO	IO	IO
C150	10.56	CP	IO	IO
C151	10.56	IO	IO	IO
C152	10.56	IO	IO	IO
C153	10.56	IO	IO	IO
C154	66.28	CP	Collapsed	LS
C155	77.85	CP	Collapsed	LS

Table 7.12 shows the damage scores computed for each story of the building and for the overall building.

Table 7.12 - Story and Building Damage Scores for Case Study Building 6

Story #	Raw Story IF	Stories Above	Story IF	Story Damage (%)	Weighted Story Damage (%)
1	0.30	4	0.43	72.98	31.53
2	0.30	3	0.32	16.32	5.20
3	0.29	2	0.21	34.20	7.16
4	0.11	1	0.04	25.95	1.03
Building Damage Score (%)					44.92

Although the overall building damage score was computed as 44.92%, which corresponds to life safety performance level, the maximum story damage

was found out to be 72.98% and thus, the performance level of the building under the Düzce Earthquake was evaluated to be collapse prevention, which is in a good agreement with the observed damage.

7.4.7 Case Study Building 7

The last case study building was a 5 story, independent, residential building located in the city of Düzce. The lateral load resisting system of the building is a wall-frame system (Figure 7.33). The building has no basements. The building is rectangular in plan and the floor area is 433 m².
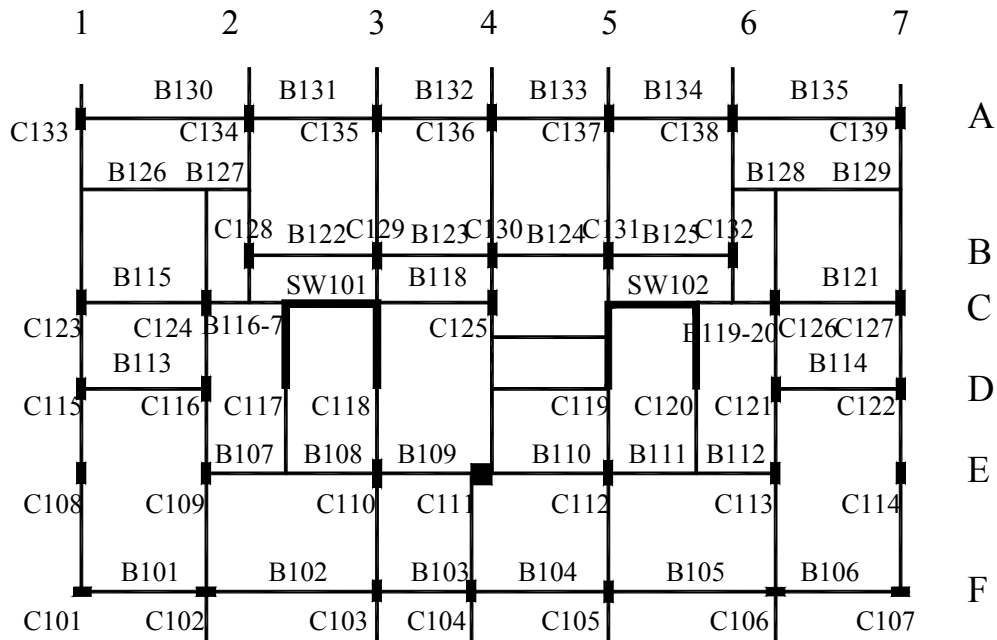
Figure 7.33 – Plan View of the Case Study Building 7

The building was investigated in the summer of 2000, approximately 8 months after the 12 November 1999 Düzce Earthquake. The mean compressive strength of concrete was determined to be 12 MPa from the samples taken building. Plain bars with yield strength of 220 MPa were used as both longitudinal and transverse reinforcement.

Bayılı [58] stated that the structure's lateral load resistance had been obviously reduced after the earthquake. However, he also added that the seismic

performance of the building during the Düzce Earthquake was good enough to permit immediate use. However, the building had been repaired before it was back in service.

The acceleration time history and 5% damped elastic response spectrum of the Düzce Earthquake were given in Figures 7.15 and 7.16, respectively.

The assessment of this building was carried out in the longitudinal direction of the building which is the weaker direction. In this direction, the wall contribution factor of the building was computed as 0.93 using the expression given in Eq. 7.3.

As a result of the modal analysis carried out, the fundamental period of the building was computed to be 0.440 seconds. The first mode shape of the building is shown in Figure 7.34 (a). After the modal analysis, a nonlinear static analysis was carried out on the building to obtain the capacity curve. Then, this capacity curve was used to determine the performance point of the building under the Düzce Earthquake. The capacity curve of the building and the performance point under the Düzce Earthquake is shown in Figure 7.35. The displacement pattern of the case study building 7 is given in Figure 7.34 (b). The hinge patterns of the case study building 7 at the performance point are shown in Figure 7.36.

(a)   (b)
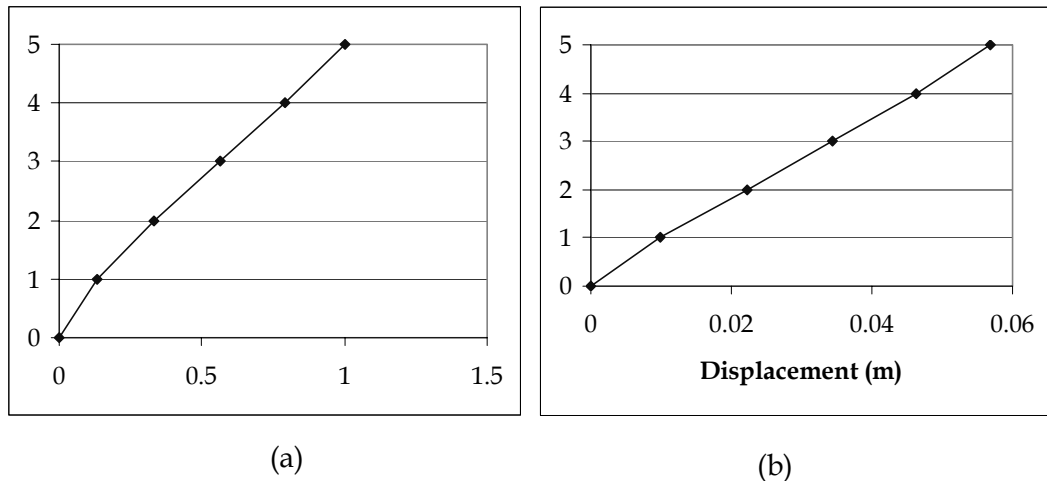
Figure 7.34 –(a) 1st Mode Shape of Case Study Building 7 and (b) the displacement profile at the performance point
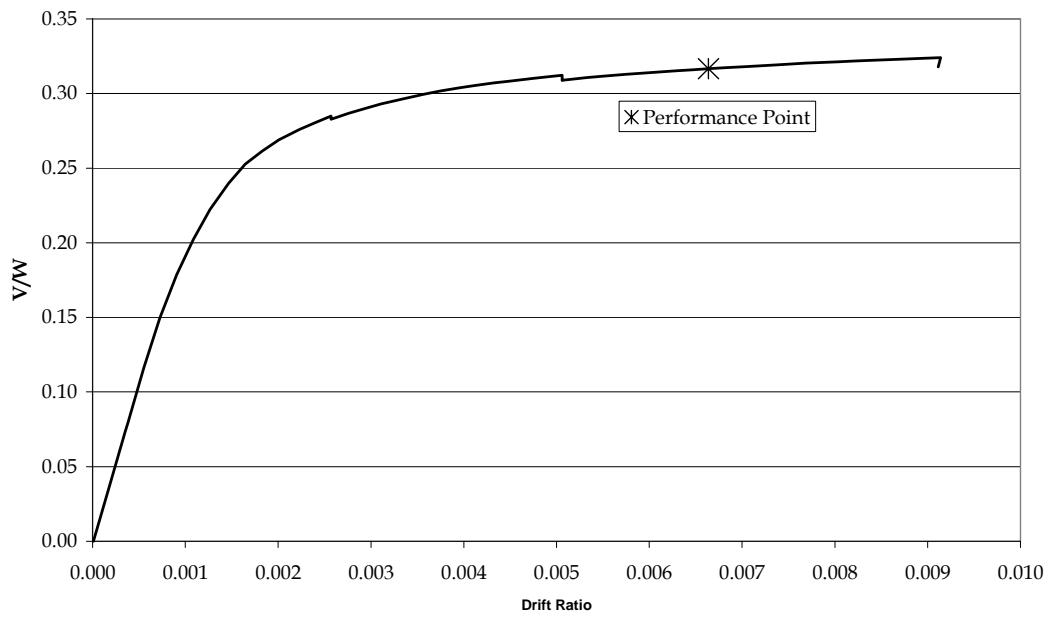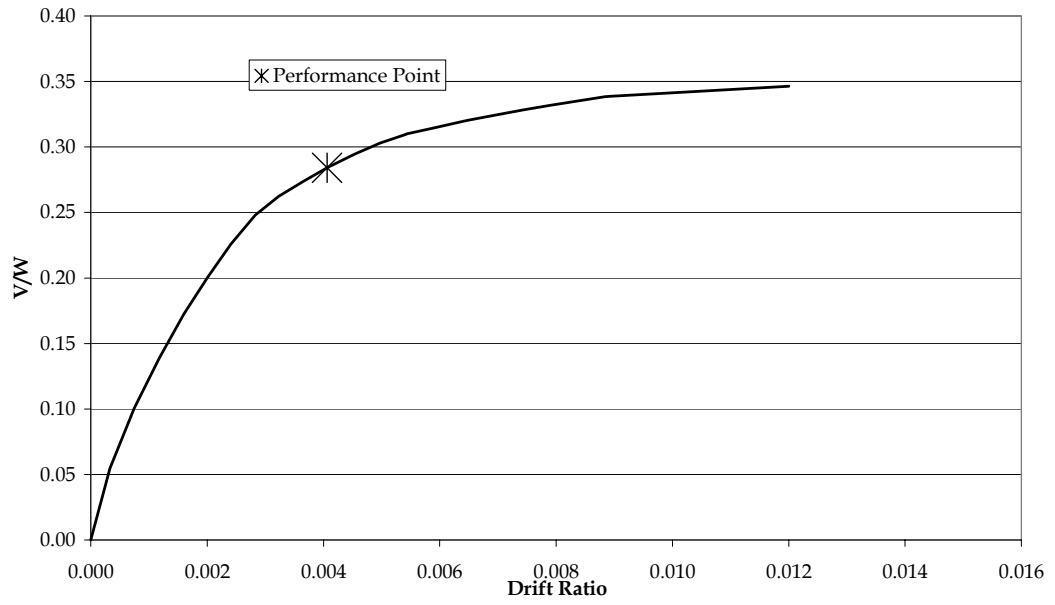
Figure 7.35 - Capacity Curve of Case Study Building 7 and the

Performance Point under Düzce Earthquake
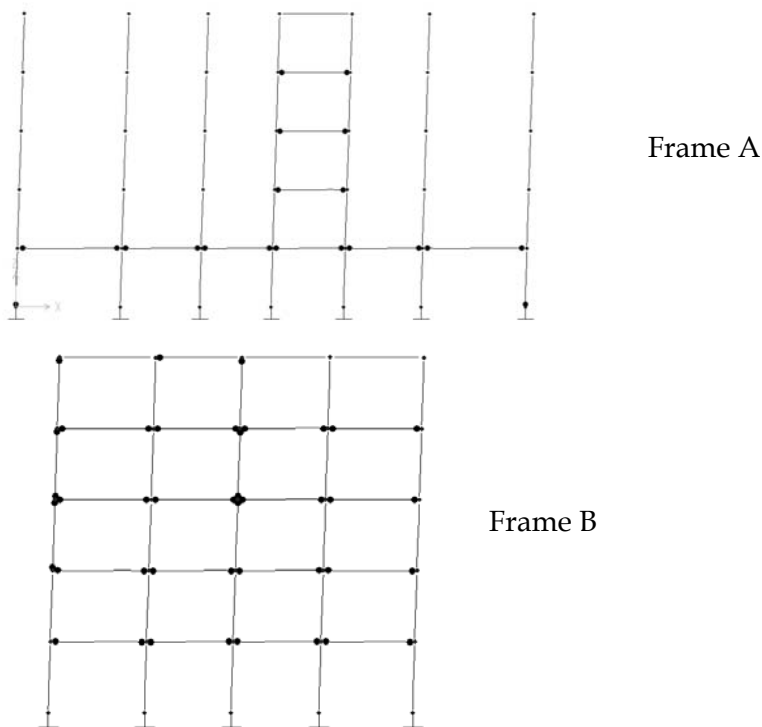
Frame A

Frame B

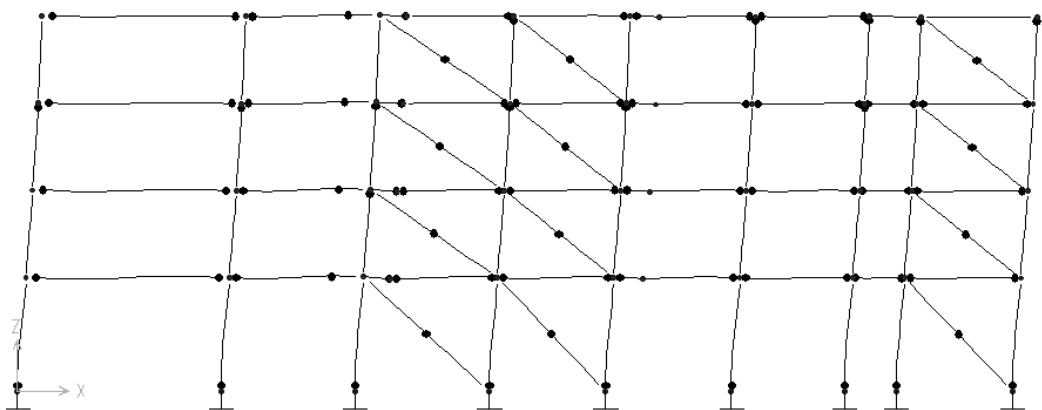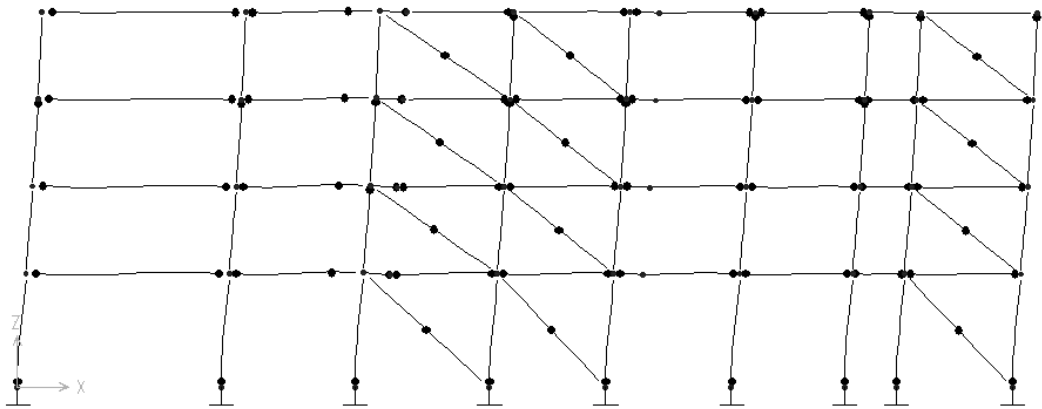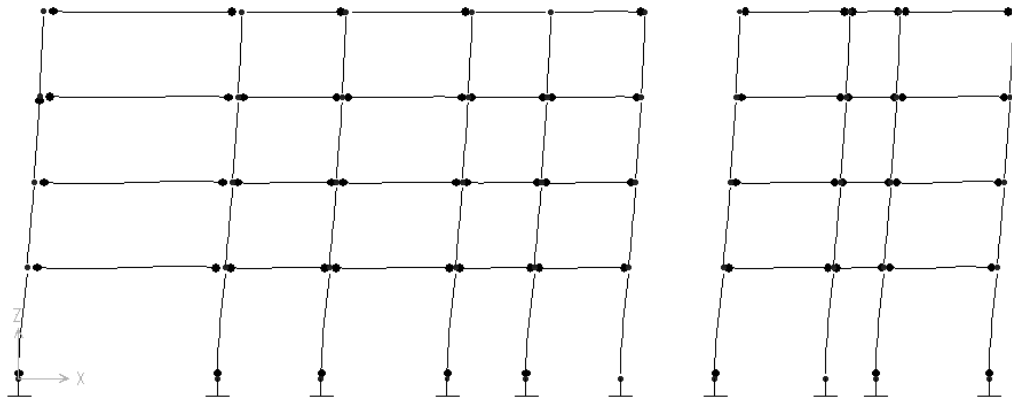Figure 7.36 – Hinge Patterns of the Case Study Building 7 at the
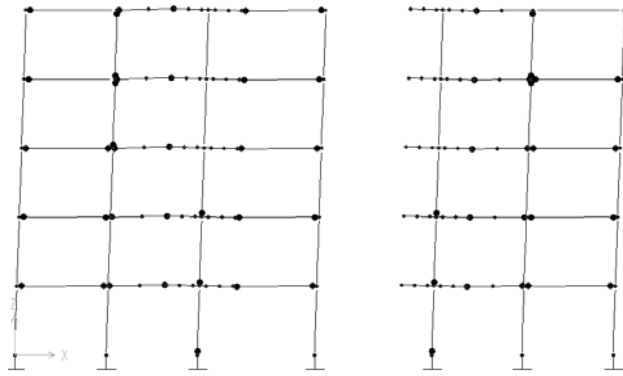
performance point

Frame C
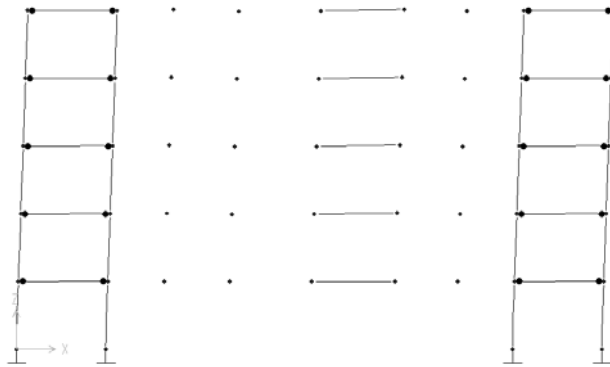
Frame D
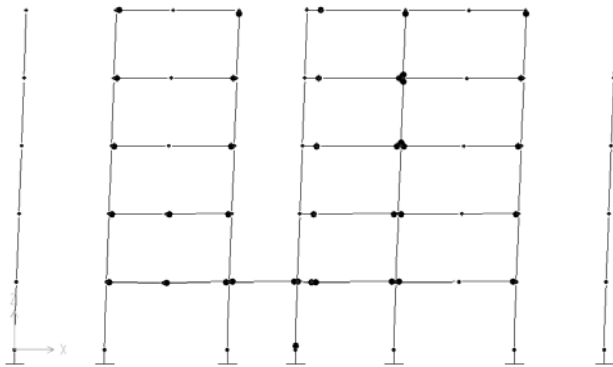
Frame E
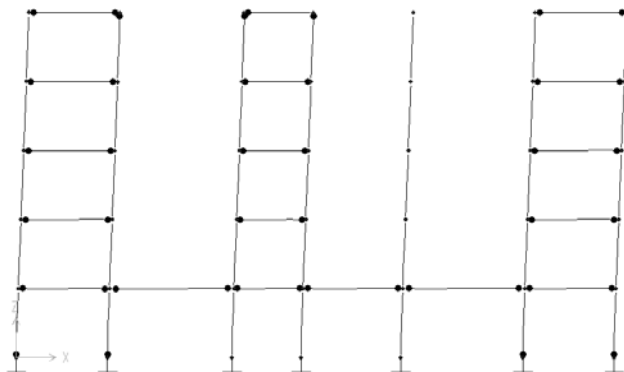
Frame F

Figure 7.36 (Cont'd) – Hinge Patterns of the Case Study Building 7 at the performance point

The member end deformations at the performance point were used to assess the damage state of the building at the component level, story level and the building as a whole. Table 7.13 presents the damage states of the first story columns and beams predicted by the procedure developed herein, FEMA 356, ATC-40 and Eurocode 8 procedures together with the observed damage. Table 7.14 shows the observed and predicted damage states of the shear walls of the building.

Table 7.13 – Observed and Predicted Damage States of the 1st Story Beams and Columns of the Case Study Building 7

Member	Observed	This Study	ATC-40	FEMA-356	EUROCODE
C101	N/L (None/Light)	17.30	IO	IO	IO
C102	N/L	22.04	CP	IO	IO
C103	N/L	2.21	IO	IO	IO
C104	N/L	2.21	IO	IO	IO
C105	N/L	2.21	IO	IO	IO
C106	M (Moderate)	22.04	CP	IO	IO
C107	N/L	17.30	IO	IO	IO
C108	N/L	2.01	IO	IO	IO
C109	N/L	2.01	IO	IO	IO
C110	N/L	2.01	IO	IO	IO
C111	N/L	25.34	IO	IO	IO
C112	N/L	2.01	IO	IO	IO
C113	N/L	2.01	IO	IO	IO
C114	N/L	2.01	IO	IO	IO
C115	N/L	1.88	IO	IO	IO
C116	N/L	1.88	IO	IO	IO
C117	N/L	1.88	IO	IO	IO
C118	N/L	1.88	IO	IO	IO
C119	N/L	0.87	IO	IO	IO
C120	N/L	0.87	IO	IO	IO
C121	N/L	0.87	IO	IO	IO
C122	N/L	0.87	IO	IO	IO
C123	N/L	1.74	IO	IO	IO
C124	N/L	1.74	IO	IO	IO
C126	N/L	1.74	IO	IO	IO
C128	N/L	1.74	IO	IO	IO
C129	N/L	1.74	IO	IO	IO
C130	N/L	1.68	IO	IO	IO

Table 7.13 (Cont'd)– Observed and Predicted Damage States of the 1st
Story Beams and Columns of the Case Study Building 7

Member	Observed	This Study	ATC-40	FEMA-356	EUROCODE
C131	N/L	1.68	IO	IO	IO
C132	N/L	1.68	IO	IO	IO
C133	N/L	1.68	IO	IO	IO
C134	N/L	1.68	IO	IO	IO
C136	N/L	1.49	IO	IO	IO
C137	N/L	1.49	IO	IO	IO
C138	N/L	1.49	IO	IO	IO
C139	N/L	1.49	IO	IO	IO
C140	N/L	1.49	IO	IO	IO
C141	N/L	1.49	IO	IO	IO
C142	N/L	1.49	IO	IO	IO
B101	N/L	6.71	IO	IO	IO
B102	N/L	4.20	IO	IO	IO
B103	N/L	0.54	IO	IO	IO
B104	N/L	0.54	IO	IO	IO
B105	N/L	3.51	IO	IO	IO
B106	N/L	4.93	IO	IO	IO
B107	N/L	5.69	IO	IO	LS
B108	N/L	0.84	IO	IO	IO
B109	N/L	4.12	IO	IO	IO
B110	N/L	4.12	IO	IO	IO
B111	N/L	0.33	IO	IO	IO
B112	N/L	1.80	IO	IO	IO
B113	N/L	0.28	IO	IO	IO
B114	N/L	0.00	IO	IO	IO
B115	N/L	0.22	IO	IO	IO
B116	N/L	0.13	IO	IO	IO
B117	N/L	3.18	IO	IO	IO
B118	N/L	0.39	IO	IO	IO
B119	N/L	0.93	IO	IO	IO
B120	N/L	0.06	IO	IO	IO
B121	N/L	0.72	IO	IO	IO
B122	N/L	0.42	IO	IO	IO
B123	N/L	0.94	IO	IO	IO
B124	N/L	0.96	IO	IO	IO
B125	N/L	0.39	IO	IO	IO
B126	N/L	0.44	IO	IO	IO
B127	N/L	0.38	IO	IO	IO
B128	N/L	0.00	IO	IO	IO
B129	N/L	0.00	IO	IO	IO
B130	N/L	0.01	IO	IO	IO

Table 7.13 (Cont'd)– Observed and Predicted Damage States of the 1st
Story Beams and Columns of the Case Study Building 7

Member	Observed	This Study	ATC-40	FEMA-356	EUROCODE
B131	N/L	0.00	IO	IO	IO
B132	N/L	1.25	IO	IO	IO
B133	N/L	0.03	IO	IO	IO
B134	N/L	0.06	IO	IO	IO
B135	N/L	0.10	IO	IO	IO
B136	N/L	0.10	IO	IO	IO
B137	N/L	0.11	IO	IO	IO

The damage states of the members of the last case study building could be predicted satisfactorily except a few columns (C101, C102, C107 and C110). The damage scores of these columns were computed to be higher than the other ones since their stronger direction coincides with the analysis direction.

Table 7.14 – Observed and Predicted Damage States of the Shear Walls of
the Case Study Building 7

Member	Observed	This Study	ATC-40	FEMA-356	EUROCODE
SW101	M	47.02	IO	IO	IO
SW102	M	47.02	IO	IO	IO
SW201	N/L	2.96	IO	IO	IO
SW202	N/L	2.79	IO	IO	IO
SW301	N/L	0.26	IO	IO	IO
SW302	N/L	0.25	IO	IO	IO
SW401	N/L	0.04	IO	IO	IO
SW402	N/L	0.04	IO	IO	IO
SW501	N/L	0.00	IO	IO	IO
SW502	N/L	0.00	IO	IO	IO

After the computation of the member damage scores, the story and building damage scores were computed using the component importance factors and the methodology summarized in Chapter 7. For the component importance factors, the values given Tables 7.6 to 7.8 were directly used since the correction factors for the wall contribution factor given in equations 7.4 to 7.6 were all

computed to be 1.00 for a wall contribution factor of 0.930. The story and building level damage scores are given in Table 7.15.

Table 7.15 - Story and Building Damage Scores for Case Study Building 7

Story #	Raw Story IF	Stories Above	Story IF	Story Damage (%)	Weighted Story Damage (%)
1	0.23	5	0.35	33.62	11.90
2	0.23	4	0.28	2.24	0.62
3	0.23	3	0.21	0.37	0.08
4	0.22	2	0.13	0.19	0.03
5	0.10	1	0.03	0.29	0.01
Building Damage Score (%)					12.64

The maximum story damage score was computed as 33.62% and the overall building damage score was found to be 12.64%. The limiting value between the immediate occupancy and life safety performance levels was set as 10% indicating that the expected performance of this building under the Düzce earthquake is just above the immediate occupancy level which is in accordance with the observed damage after the Düzce earthquake.

7.5 DISCUSSION OF RESULTS OF THE CASE STUDIES

The results of the case studies show that the proposed vulnerability assessment procedure can estimate the observed global damage state satisfactorily. The results also show that, the observed damage level of each component can also be predicted by the associated damage curves. Of the 220 members assessed, the developed damage curves were able to predict the observed damage state of the 176 of these members (80%). The damage curves overestimated the damage state of the 37 (17%) of these members, while the damage state of 7 (3%) members were underestimated. For most of the members whose damage state could not be predicted, it was observed that the other assessment procedures give parallel results with the damage curves.

7.6 APPLICATION OF THE DEVELOPED PROCEDURE TO THE SELECTED BUILDINGS IN ZEYTINBURNU

The developed procedure was applied to several buildings damaged from past earthquakes for verification and calibration purposes. It has been shown that the observed seismic performances of the case study buildings have been predicted satisfactorily. The procedure has also been used for assessment of several RC frame buildings located in Zeytinburnu district of İstanbul and surveyed under the pilot project initiated to determine expected performance of the buildings in Zeytinburnu.

In the assessment of the buildings located in the Zeytinburnu district, the elastic response spectrum proposed in the National Earthquake Hazards Reduction Program (NEHRP) document published in 2001 [59] was used to represent a ground motion with a probability of exceedance of 50% in 50 years. Figure 7.37 shows the response spectrum used in this study. The major parameters in this response spectrum are the spectral acceleration at short periods (S_{DS}) and the spectral acceleration at the period of 1 sec (S_{D1}). The response spectrum given in Figure 7.37 can be fully defined for each ground motion and site once these two values are known. The S_{DS} and S_{D1} values that define the ground motion each building will be exposed to under a certain scenario earthquake were taken from the study carried out by Bosphorus University.
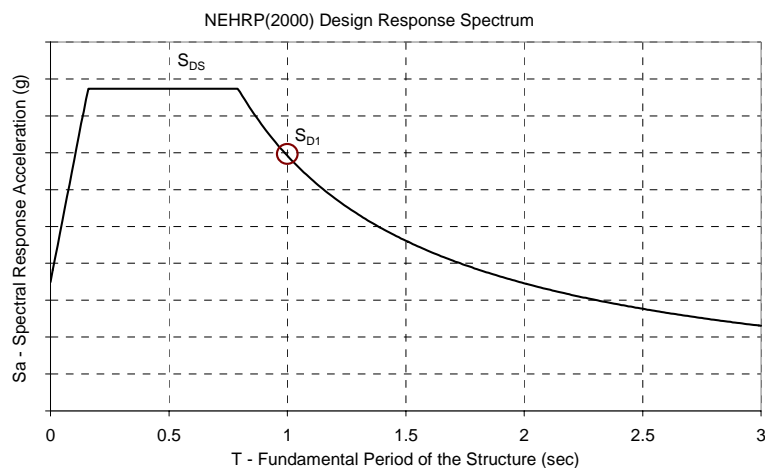
Figure 7.37 – NEHRP Elastic Spectrum

188

Within the scope of this study, the detailed assessment of 10 mid-rise buildings (3-6 stories) with variable material properties was carried out. Table 7.16 presents the properties of the buildings assessed together with the S_{DS} and S_{D1} values for each building.

Table 7.16 - Properties of the assessed buildings in Zeytinburnu district

Building ID	Plan Area (m²)	# of Stories	f_{ck} (MPa)	Weight (kN)	Height (m)	f_{yk} (MPa)	S_{DS} (g)	S_{D1} (g)
BLD 1	165	6	27	11070	17.95	420	0.767	0.454
BLD 2	100	4	9	4050	10.80	220	0.692	0.412
BLD 3	70	5	16	3766	13.90	220	0.698	0.417
BLD 4	98	5	8	5941	14.25	220	0.729	0.432
BLD 5	80	5	10	5900	13.75	220	0.873	0.692
BLD 6	91	4	15	4438	10.80	220	0.873	0.692
BLD 7	147	5	11	5182	14.25	220	0.699	0.416
BLD 8	269	3	16	5987	8.95	420	0.698	0.417
BLD 9	83	6	13	5142	17.30	220	0.735	0.435
BLD 10	145	4	15	4326	11.95	220	0.714	0.424

All of the buildings were modeled in 3D in SAP2000 and nonlinear static analysis was carried out to determine the capacity curve of the buildings together with the modal analysis. Then, these capacity curves were bilinearized to determine the yield base shear force (V_y), yield roof drift ratio (δ_y), ultimate base shear force (V_u) and the ultimate drift ratio of (δ_u) of the buildings. The target displacement of each building under the specified ground motion was computed using the displacement coefficient method summarized in FEMA 356 [8]. Once the displacement demand is determined, the assessment procedure developed was applied on each building to determine expected performance of each member, each story and the entire building under the given ground motion. Table 7.17 summarizes the bilinear capacity curve, target roof drift ratio under the given elastic spectrum (δ_t), maximum story damage score, building damage score and the expected performance of each building.

Table 7.17 - Results of the assessment of the buildings in Zeytinburnu district

Building ID	T (sec)	$\dfrac{V_y}{W}$	δ_y (%)	$\dfrac{V_u}{W}$	δ_u (%)	δ_t (%)	Max Story Damage (%)	Building Damage Score (%)	Expected Perf.
BLD 1	0.627	0.32	0.14	0.49	1.32	0.58	10.85	5.60	IO
BLD 2	0.644	0.11	0.17	0.13	1.24	0.94	27.22	22.06	LS
BLD 3	0.921	0.06	0.19	0.07	1.29	1.01	54.20	25.16	LS
BLD 4	1.430	0.04	0.25	0.06	1.51	1.51	90.05	42.67	CP
BLD 5	0.996	0.03	0.13	0.04	1.24	1.24	77.12	40.88	CP
BLD 6	0.672	0.10	0.23	0.11	1.85	1.75	87.41	52.16	CP
BLD 7	0.798	0.09	0.14	0.13	1.28	0.95	63.09	27.77	LS
BLD 8	0.519	0.25	0.34	0.29	1.68	0.85	33.71	19.27	LS
BLD 9	1.340	0.05	0.29	0.08	2.02	1.36	67.49	31.99	LS
BLD 10	0.792	0.11	0.15	0.13	1.04	1.03	71.86	46.01	CP

As shown in Table 7.17 one of the ten buildings assessed was found to be immediately occupiable under the given ground motion. 5 buildings were found to suffer moderate damage and the remaining 4 were found to suffer either heavy damage or collapse. The results of the assessment shows that the buildings with favorable material properties will probably not suffer heavy damage or collapse, while the ones with poor material properties are highly vulnerable to devastating earthquakes.

CHAPTER 8

CONCLUSION AND RECOMMENDATIONS

8.1 SUMMARY

Research had been undertaken to develop a component based vulnerability assessment procedure for reinforced concrete structures.

For this, firstly damage functions for the components of reinforced concrete structures have been developed. These damage functions were defined in terms of the interstory drift ratio for columns, shear walls, and brick infills, whereas the chord rotation was the independent parameter for the damage functions of reinforced concrete beams. In the development of the damage functions for these components, firstly, the effect of several parameters on the behavior of each component was investigated and the effective parameters were determined. Then, for each component certain criteria was set in terms of the effective parameters to distinguish the ductility level and/or failure type of the components. Finally, regression analyses were carried out to develop the damage functions for each component type.

As the next step, a procedure for the determination of component importance factors which are used to combine the damage scores of the components was developed. This procedure is based on the energy dissipation capacity of the reinforced concrete structures, which is a vital criterion that determines the survival of a building during a severe earthquake. Then, this procedure was applied on several generic frames to propose approximate values for the component importance factors of brick infilled reinforced concrete frames and wall frame systems.

Finally, the developed vulnerability assessment procedure was validated by applying the procedure on seven buildings that had been damaged in the recent earthquakes occurred in Turkey. The damage level of each building had been assessed by METU teams and the component damage data, as-built dimensions and material properties were all known. After the validation of the developed procedure, it had been applied on 10 buildings located in the Zeytinburnu district of Istanbul.

8.2   DISCUSSION OF RESULTS AND CONCLUSIONS

In the following paragraphs, the results of this study will be briefly discussed and the conclusions of the study will be drawn. These conclusions were drawn based on the numerical analyses and literature survey carried out in this study.

- The main parameters affecting the deformation capacity of reinforced concrete columns were determined as the slenderness ratio (L/i), yield strength of longitudinal reinforcement (f_{yk}), axial load level (N/N_o) and the amount of confinement (ρ_s). The first of these parameters affect the yield drift ratio of the columns while the latter two affect the ultimate ductility of the columns.

- Damage curves for reinforced concrete columns for three ductility levels were developed by carrying out regression analyses on the data points obtained as a result of the numerical analyses. These damage curves have been validated by comparison with the available experimental data.

- The comparison of the damage curves with the ATC-40 limits showed that, for very ductile columns, plastic rotation limits given are too high and need to be revised.

- For the reinforced concrete beams, the most significant parameters affecting the behavior were found to be the depth of the beam (d), amount and yield strength of longitudinal reinforcement (ρ and f_{yk}), concrete strength (f_{ck}), amount of transverse reinforcement (ρ_s) and amount of compression reinforcement (ρ'/ρ).

192

- As in the case of columns the damage curves developed for reinforced concrete beams were also validated via comparison with the experimental data.

- The damage curves for the brick infills were developed using the equivalent strut model developed by Smith [42]. The drift ratio corresponding to the yielding of the equivalent strut model was chosen as an indicator of the heavy damage. To be able to refine the data and group the infills, the closed form solution for the yield drift ratio of the equivalent strut model was derived (Eq. 4.13). As a result, it was observed that the main parameter influencing the yield drift ratio of the equivalent strut model was $\dfrac{f_m L^2}{E_I dh}$.

- The main parameters affecting the behavior of shear walls were determined as the aspect ratio (a/d), amount and yield strength of vertical reinforcement (ρ_v and f_{yk}) and concrete strength (f_{ck}). To distinguish the failure mode of the shear walls, a new term which is an indicator of the ratio of flexural shear capacity of the wall to its nominal shear capacity ($\dfrac{V_f}{b_w d \sqrt{f_{ck}}}$) was set. The ability of this term in distinguishing the failure mode of the walls was validated through the application of this term on available test data.

- The procedure allows the evaluation of the building components with different failure modes and ductility levels.

- The vulnerability assessment procedure has been calibrated and verified on a number of case study buildings that have suffered various degrees of damage during some recent earthquakes, showing quite satisfactory predictions.

- The main strength and central point of the developed procedure is to provide a way to combine the component damage scores to come up with story level and global damage scores. By this way, the developed procedure also resolves the drawbacks of ATC-40

[9], FEMA-356 [8] and Eurocode 8 [12] procedures, which only provides acceptance criteria at the component level

8.3 RECOMMENDATIONS FOR FUTURE STUDIES

- The main objective of this study was to develop a vulnerability assessment procedure for reinforced concrete buildings The procedure for the determination of component importance factors was developed as a tool for this procedure. Although the results obtained show that the procedure developed gives logical results, it should be better to concentrate on the component importance factors in the future studies, since it is the most difficult part of the component based vulnerability assessment procedures and the studies carried out on this subject in this study and in literature are limited.

- The slippage of reinforcement was not taken into account in the damage curves for the reinforced concrete components. The damage curves may be enhanced by carrying out further analyses in which the slippage of reinforcement is taken into account.

- The damage curves developed for shear walls are only valid for walls with rectangular cross sections. Additional analyses should be carried out to develop damage functions for walls with barbell cross sections.

- Limited experimental data on the behavior of brick infill walls and shear walls was available in literature. The developed damage curves for these components can be calibrated using more detailed experimental data.

- As the new earthquakes occur and new damage data is obtained, the developed procedure may be applied on these buildings for calibration purposes.

- Implementation of the developed procedure in computer software can be very useful, since it would enable the assessment of the buildings in a much shorter time.

194

REFERENCES

[1].   Ministry of Public Works and Settlement, Government of Republic of Turkey, (1998) "Specifications for Structures to be Built in Disaster Areas", Ankara

[2].   Federal Emergency Management Agency (FEMA) (1988), "Rapid visual screening of buildings for potential seismic hazards: a handbook", FEMA-154, Washington, DC

[3].   Federal Emergency Management Agency (FEMA) (1998), "Handbook for the seismic evaluation of buildings-a prestandard", FEMA-310, Washington, DC

[4].   Sucuoğlu H. and Yazgan U. (2003), "Simple survey procedures for seismic risk assessment in urban building stocks" In: Wasti T. and Özcebe G., editors. Seismic assessment and rehabilitation of existing buildings. Earth and environmental sciences, Vol. 29, Kluwer Academic Publishers, London

[5].   Özcebe G., Yücemen M. S. and Aydogan V., (2004), "Statistical seismic vulnerability assessment of existing reinforced concrete buildings in Turkey on a regional scale", Journal of Earthquake Engineering, 8(5), 749-773

[6].   Yücemen M. S., Özcebe G. and Pay A. C., (2004), "Prediction of potential damage due to severe earthquakes", Structural Safety, 26, 349-366

[7].   Yakut A. (2004), "Preliminary seismic assessment procedure for RC buildings", Engineering Structures, 26, 1447-1461

[8].   Federal Emergency Management Agency (FEMA) (2000), "Prestandard and commentary for the seismic rehabilitation of buildings", FEMA-356, Washington, DC

[9].   Applied Technology Council (ATC). (1996), "Seismic evaluation and retrofit of concrete buildings" ATC-40, California

[10].   Sucuoğlu et. al. (2004), "Performance based seismic rehabilitation of damaged reinforced concrete buildings", ASCE Structural Journal, 130(10), 1475-1486

[11].   Park Y. and Ang A. H. (1985), "Mechanistic seismic damage model for reinforced concrete", J. Struct. Eng., 111(4), 722-739

[12].   European Committee for Standardization (2003) "Eurocode 8: Design of structures for earthquake resistance Part 3: Strengthening and repair of buildings – Draft No:4" Eurocode 8, Brussels

[13].   Williams M. S. and Sexsmith R. G. (1995). "Seismic Damage Indices for Concrete Structures: A State-of-the-Art Review", Earthquake Spectra, 11(2), 319-349.

[14].   Banon et. al. (1981), "Seismic damage in reinforced concrete frames", ASCE Journal of Structural Engineering, 107(9), 1713-1729

[15].   Chung et. al. (1987), "Seismic damage assessment of RC members", Technical Report NCEER-87-002, National Center for Earthquake Engineering Research, State University of New York, Buffalo, NY

[16].   Bracci et. al. (1989), "Deterministic model for seismic damage evaluation of RC structures", Technical Report NCEER-89-0033, National Center for Earthquake Engineering Research, State University of New York, Buffalo, NY

[17].   Roufaiel M. S. L. and Meyer C. (1987), "Reliability of concrete frames damaged by earthquakes", J. Struct. Eng., 113(3), 445-457

[18].   DiPasquale E. and Cakmak A. S. "Detection and assessment of seismic structural damage", Technical Report NCEER-87-0015, National Center for Earthquake Engineering Research, State University of New York, Buffalo NY

[19].   Park Y., Ang, A. H. S., Wen K., "Seismic damage analysis of reinforced concrete buildings" J. Struct. Eng., 111(4), 740-757

[20].   Panagiotakos T. B. and Fardis M. N. (2001), "Deformations of reinforced concrete members at yielding and ultimate", ACI Struct. J., 98(2), 138-148

[21].   Chopra A. K. and Goel R. K. (1999)"Capacity-demand-diagram methods for estimating seismic deformation of inelastic structures:

SDF systems", Technical Report PEER-1999/02, Pacific Earthquake Engineering Research Center, University of California at Berkeley, Berkeley, California

[22]. Azizinamini et al. (1992) "Effects of transverse reinforcement on seismic performance of columns", ACI Struct. J., 89(4), 442-450

[23]. Priestly, M. J. N., Kowalsky, M. J. (1998), "Aspects of drift and ductility capacity of rectangular cantilever structural walls", Bulletin of the New Zealand National Society for Earthquake Engineering, 31(6): 73-85

[24]. Paulay T. (2002), "An estimation of displacement limits for ductile systems", Earthquake Engineering and Structural Dynamics, 31, 583-599

[25]. Taylor et al. (2002). "A summary of cyclic lateral load tests on rectangular concrete columns", National Technical Information Service Report NISTIR-5984, Gaithersburg

[26]. Barbosa, A. F., Ribeiro, G. O. (1998), "Analysis reinforced concrete structures using ANSYS nonlinear concrete model", Computational Mechanics: New Trends and Applications, Barcelona, Spain

[27]. Kent, D.C., Park, R. (1971), "Flexural members with confined concrete", ASCE Journal of the Structural Division; 97:ST 7

[28]. Ohkubo M. (1991), "Current Japanese system on seismic capacity and retrofit techniques for existing reinforced concrete buildings and post-earthquake damage inspection and restoration techniques" Report No. SSRP-91/02, University of California, San Diego

[29]. Frosch R. J. (1999). "Another look at cracking and crack control in reinforced concrete", ACI Struct. J., 96(3), 437-442

[30]. Priestly M. J. N. (1998), "Displacement based approaches to rational limit states design of new structures" Proc. 11th European Conference on Earthquake Engineering, Balkema, Rotterdam, 317-335

[31]. Sozen, M (1980)., "Review of Earthquake Response of R.C. Buildings with a view to Drift Control, State-of-the-art in Earthquake Engineering", 7th WCEE, pp. 383-418, Istanbul.

[32]. Turkish Standards (2000), "Requirements for design and construction of reinforced concrete structures", TS 500, Ankara

[33]. ANSYS Engineering Analysis System. User and Theoretical Manual, ANSYS, Inc, South Pointe, Canonsburg, Pennsylvania, Release 7.9 UO20021010, 2002

[34]. Lynn A. C., (2001)"Seismic evaluation of reinforced concrete building columns", PhD Thesis, University of California at Berkeley

[35]. Arakawa et. al. (1984), "Effects of the rate of cyclic loading on the load-carrying capacity and inelastic behavior of reinforced concrete columns," Transactions of the Japan Concrete Institute, Vol. 4

199

[36]. Scribner, C.F., and Wight, J.K., (1978) "Delaying Shear Strength Decay in Reinforced Concrete Flexural Members Under Large Load Reversals", Department of Civil Engineering, University of Michigan, Ann Arbor, Michigan

[37]. Nmai, C.K. and Darwin, D., (1986), "Lightly Reinforced Concrete Beams Under Cyclic Load", ACI Structural Journal, 83, 777-783.

[38]. Xie et. al. (1994) "Shear ductility of reinforced concrete beams of normal and high strength concrete" ACI Structural Journal, 91(2), 149-149

[39]. Holmes M., (1961), "Steel frames with brickwork and concrete infilling" Proceedings of Institute of Civil Engineers, London, 73, 473-478

[40]. Saneinejad A. and Hobbs B. (1995). "Inelastic design of infilled frames" J. Struct. Eng., 121(4), 634-650

[41]. Sucuoğlu, H. and McNiven, H. D. (1991), "Seismic shear capacity of reinforced masonry piers" Journal of Structural Engineering, 117, 2166-2186

[42]. Smith S. B. (1967) "Methods for predicting the lateral stiffness and strength of multi-storey infilled frames" Building Science, 2, 247-257

[43]. Mainstone R. J. "On the stiffness and strength of infilled frames", Proceeding of Institute of Civil Engineers, Paper 7360

200

[44]. Smith, B. S. and Carta C. (1969), "A method of analysis of infilled frames" Proceedings of the Institute of Civil Engineers, 44

[45]. Paulay T., Priestly M. J. N., (1992), "Seismic design of reinforced concrete and masonry buildings", John Wiley and Sons Inc, 744.

[46]. Mehrabi et. al. (1996), "Experimental evaluation of masonry infilled RC frames" Journal of Structural Engineering, 122(3), 228-237

[47]. Baran M. (2005), "Precast concrete panel reinforced infill walls for seismic strengthening of reinforced concrete frames structures" PhD. Thesis, Middle East Technical University

[48]. Kowalsky, M. J., (2001), "RC structural walls designed according to UBC and displacement based methods", Journal of Structural Engineering, 127(5), 506-516

[49]. Salonikos, T. N., (2002), "Shear strength and deformation patterns of RC walls with aspect ratio 1.0 and 1.5 designed according to Eurocode 8", Engineering Structures, 24, 39-49

[50]. Sittipunt C. and Wood S. L., (1995), "Influence of web reinforcement on the cyclic response of structural walls", ACI Structural Journal, 92(6), 1-11

[51]. Oesterle et. al (1976), "Earthquake resistant structural walls – tests of isolated walls" Report to the National Science Foundation, Portland Cement Association, Illinois

[52]. Lefas et. al. (1990), "Behavior of reinforced concrete structural walls: strength, deformation characteristics, and failure mechanism", ACI Structural Journal, 87(1), 21-31

[53]. Zhang Y. and Wang Z. (2000), "Seismic behavior of reinforced concrete shear walls subjected to high axial loading", ACI Structural Journal, 97(5), 739-750

[54]. Wood S. L. (1989), "Minimum tensile reinforcement requirements in walls", ACI Structural Journal, 86(4), 582-591

[55]. American Concrete Institute (ACI). (1983), "Building code requirements for structural concrete", *ACI Committee 318*, Farmington Hills, Mich.

[56]. Gülkan et. al., (1994) "Preparation of a damage assessment form for engineered buildings", Earthquake Engineering Center Report No. 94-01, Middle East Technical University (in Turkish)

[57]. Gür T. and Sucuoğlu H. (2000), Seismic rehabilitation of 108 RC buildings in Ceyhan after the 27 June 1998 Adana-Ceyhan earthquake" Earthquake Engineering Center Report No. 2000-01, Middle East Technical University

[58]. Bayili S., (2002), "Seismic performance assessment of a residential building in Düzce after the 12 November 1999 Düzce Earthquake" M.S. Thesis, Middle East Technical University

[59]. Building Seismic Safety Council for the Federal Emergency Management Agency, (2001), "NEHRP recommendations for seismic regulations for new buildings and other structures", Washington DC

APPENDIX A

Table A.1 – Data for the columns used in the regression analyses for the relationship between ultimate ductility and $\rho_s/(N/N_o)$

Specimen	N/N_o	ρ_s	$\dfrac{\rho_s}{N/N_o}$	δ_y (mm)	δ_u (mm)	μ
Soesianawati et al. 1986, No. 4	0.29	0.01	0.02	17.50	42.70	2.44
Soesianawati et al. 1986, No. 3	0.30	0.01	0.03	14.50	45.10	3.11
Soesianawati et al. 1986, No. 2	0.30	0.01	0.04	16.20	50.20	3.10
Galeota et al. 1996, BA2	0.32	0.02	0.06	12.80	36.10	2.82
Galeota et al. 1996, BA3	0.32	0.02	0.06	12.90	32.90	2.55
Bayrak and Sheikh 1996, AS-3HT	0.49	0.03	0.06	7.02	32.01	4.56
Bayrak and Sheikh 1996, AS-7HT	0.46	0.03	0.06	9.63	33.90	3.52
Bayrak and Sheikh 1996, ES-1HT	0.49	0.03	0.06	6.39	28.50	4.46
Galeota et al. 1996, AB1	0.17	0.01	0.07	12.80	36.10	2.82
Galeota et al. 1996, BB4	0.26	0.02	0.07	17.86	63.50	3.56
Tanaka and Park 1990, No. 8	0.29	0.02	0.07	13.20	55.80	4.23
Bayrak and Sheikh 1996, AS-2HT	0.35	0.03	0.08	10.70	44.10	4.12
Galeota et al. 1996, BA4	0.21	0.02	0.09	13.65	40.60	2.97
Soesianawati et al. 1986, No. 1	0.10	0.01	0.09	16.20	97.80	6.04
Bayrak and Sheikh 1996, AS-5HT	0.46	0.04	0.09	5.76	22.00	3.82
Bayrak and Sheikh 1996, ES-8HT	0.48	0.04	0.09	7.82	24.10	3.08
Bayrak and Sheikh 1996, AS-4HT	0.49	0.05	0.10	9.72	51.60	5.31
Galeota et al. 1996, BB	0.17	0.02	0.11	17.80	69.30	3.89
Galeota et al. 1996, BB1	0.17	0.02	0.11	15.80	55.80	3.53
Galeota et al. 1996, CA2	0.32	0.04	0.11	12.62	44.63	3.54
Galeota et al. 1996, CA4	0.32	0.04	0.11	15.42	60.65	3.93
Bayrak and Sheikh 1996, AS-6HT	0.47	0.07	0.14	10.22	55.70	5.45
Galeota et al. 1996, CB3	0.26	0.04	0.14	20.50	95.42	4.65
Tanaka and Park 1990, No. 1	0.18	0.03	0.15	15.50	86.00	5.55
Tanaka and Park 1990, No. 2	0.18	0.03	0.15	15.80	85.50	5.41

Table A.1 (Cont'd)– Data for the columns used in the regression analyses
for the relationship between ultimate ductility and $\rho_s/(N/N_o)$

Specimen	N/N_o	ρ_s	$\dfrac{\rho_s}{N/N_o}$	δ_y (mm)	δ_u (mm)	μ
Tanaka and Park 1990, No. 3	0.18	0.03	0.15	14.10	75.00	5.32
Tanaka and Park 1990, No. 4	0.18	0.03	0.15	15.90	77.80	4.89
Galeota et al. 1996, CA3	0.21	0.04	0.17	13.82	56.67	4.10
Tanaka and Park 1990, No. 5	0.10	0.02	0.18	15.40	74.00	4.81
Tanaka and Park 1990, No. 6	0.10	0.02	0.18	16.40	111.17	6.78
Galeota et al. 1996, CB1	0.17	0.04	0.21	17.97	92.39	5.14
Galeota et al. 1996, CB2	0.17	0.04	0.21	18.51	89.54	4.84

CURRICULUM VITAE

PERSONAL INFORMATION

Surname, Name: Erduran, Emrah

Nationality: T.C.

Date and Place of Birth: 30.03.1978, Burdur

Phone: +90 (312) 210 5465

Fax: + 90 (312) 210 1193

E-mail: eerduran@metu.edu.tr

EDUCATION

Degree	Institution	Year of Graduation
PhD	METU Civil Engineering	2005
MS	METU Civil Engineering	2002
BS	METU Civil Engineering	2000
High School	Bornova Anatolian High School, İzmir	1996

WORK EXPERINCE

Year	Place	Enrollment
2000- Present	METU Department of Civil Engineering	Research Assistant

PUBLICATIONS

1. Erduran E. and Yakut A., "Drift Based Damage Functions for Reinforced Concrete Columns", *Computers and Structures*, Vol 82: 121 – 130

2. Erduran E. and Yakut A., "Parameters Affecting Damageability of Reinforced Concrete Members", *Seismic Assessment and Rehabilitation of Existing Buildings (eds. Wasti, S. T. and Ozcebe, G.)*, Kluwer Academic Publishers, Dotrecht, 2003

3. Ersoy U, Ozcebe G., Tankut T., Akyuz U., Erduran E., Erdem I., "Strengthening of Infill Walls with CFRP fabrics", *Seismic Assessment and Rehabilitation of Existing Buildings (eds. Wasti, S. T. and Ozcebe, G.)*, "Kluwer Academic Publishers", Dotrecht, 2003

4. Erduran E. and Yakut A., "Component Based Vulnerability Assessment of Brick Infilled RC Structures", *5th International PhD Symposium in Civil Engineering,* Delft, 2004

5. Erduran E. and Yakut A., "Drift Based Damage Functions for Components of RC Structures" *13th World Conference on Earthquake Engineering,* Vancouver, 2004

6. Ozcebe G., Ersoy U., Tankut T., Akyuz U., Erduran E., "Rehabilitation of Existing Reinforced Concrete Structures using CFRP Fabrics" *13th World Conference on Earthquake Engineering,* Vancouver, 2004

7. Erduran E. and Yakut A., "Development of Component Importance Factors for RC Buildings" *6th International Conference on Advances in Civil Engineering,* Istanbul, 2004.

8. Erduran E., "Behavior of Brick Infilled Reinforced Concrete Frames Strengthened by CFRP Reinforcement: Phase II", *MSc. Thesis, Middle East Technical University,* Ankara, 2002

9. Ozcebe G., Ersoy U., Tankut T., Erduran E., Keskin S., Mertol C., "Strengthening of Brick-Infilled RC Frames with CFRP", *SERU Report No: 2003/1*, 2003

10. Ozcebe G., Ersoy U., Tankut T., Akyuz U., Erduran E., Keskin S., Mertol C., "Seismic Rehabilitation of Existing Reinforced Concrete Buildings", *Memorial Symposium for Ergin Citipitoglu*, Ankara, 2002 (*In Turkish*)